UC San Diego
Research Theses and Dissertations

Title

Offshore Structural System Reliability: Wave-Load Modeling, System Behavior, and Analysis

Permalink

Author

De, Rabi S.

Publication Date

1990

Peer reviewed

INFORMATION TO USERS

The most advanced technology has been used to photograph and reproduce this manuscript from the microfilm master. UMI films the text directly from the original or copy submitted. Thus, some thesis and dissertation copies are in typewriter face, while others may be from any type of computer printer.

The quality of this reproduction is dependent upon the quality of the copy submitted. Broken or indistinct print, colored or poor quality illustrations and photographs, print bleedthrough, substandard margins, and improper alignment can adversely affect reproduction.

In the unlikely event that the author did not send UMI a complete manuscript and there are missing pages, these will be noted. Also, if unauthorized copyright material had to be removed, a note will indicate the deletion.

Oversize materials (e.g., maps, drawings, charts) are reproduced by sectioning the original, beginning at the upper left-hand corner and continuing from left to right in equal sections with small overlaps. Each original is also photographed in one exposure and is included in reduced form at the back of the book.

Photographs included in the original manuscript have been reproduced xerographically in this copy. Higher quality 6" x 9" black and white photographic prints are available for any photographs or illustrations appearing in this copy for an additional charge. Contact UMI directly to order.

U·M·I

University Microfilms International
A Bell & Howell Information Company
300 North Zeeb Road, Ann Arbor, MI 48106-1346 USA
313/761-4700   800/521-0600

Offshore structural system reliability: Wave-load modeling, system behavior, and analysis

De, Rabi Sankar, Ph.D.

University of California, Berkeley, 1990

U·M·I

300 N. Zeeb Rd.
Ann Arbor, MI 48106

Offshore Structural System Reliability:
Wave-Load Modeling, System Behavior, and Analysis

By

Rabi Sankar De

B. Tech. (Hons.) (Indian Institute of Technology at Kharagpur) 1980
M.S. (University of California) 1982

DISSERTATION

Submitted in partial satisfaction of the requirements for the degree of

DOCTOR OF PHILOSOPHY

in

ENGINEERING
NAVAL ARCHITECTURE AND OFFSHORE ENGINEERING

in the

GRADUATE DIVISION

of the

UNIVERSITY OF CALIFORNIA at BERKELEY

Approved:

co-Chair .... March 8, 1990

co-Chair .... Date March 21, 1990

.... Mar. 14, 1990

.... March 15, 1990

DOCTORAL DEGREE CONFERRED
MAY 22, 1990
****

Offshore Structural System Reliability:
Wave-Load Modeling, System Behavior, and Analysis

by

Rabi Sankar De

ABSTRACT

The application of system reliability methodology for offshore structural problems is investigated. The emphasis is on wave-load modeling and its implications with respect to system reliability analysis of fixed offshore structures. In addition, probabilistic and deterministic measures of "system effects" are proposed.

The wave loading in system reliability analysis is usually modeled as a fixed spatial pattern of nodal forces scaled by a random intensity factor. In this work, the change of spatial pattern of the mean nodal wave forces with increasing wave height is accounted for by using the so-called "fragility approach" to systems analysis. The change of the relative importance of different member-failure sequences with wave loads corresponding to different wave heights is studied for a fixed offshore jacket in 140 feet of water. Results from simplified "fixed-pattern" analyses are calibrated against the "fragility" analysis.

The nodal wave forces are implicitly assumed to be fully correlated in both the "fixed pattern" and the "fragility" analysis. In response, a framework is developed that allows modeling of a general correlation structure of nodal wave forces. Using this framework the effects of less than perfect spatial correlation among nodal wave forces on the system reliability of a fixed offshore structure are investigated.

The reliability of near-ideal parallel structural systems is studied in order to understand and quantify the probabilistic and deterministic "system factors" influencing the overload capacity and redundancy of realistic statically indeterminate structures. Efficient use of reduced space Monte Carlo simulation techniques in system reliability analysis is

1

demonstrated. Application of these findings in accelerated system reliability assessment of a fixed offshore jacket structure under wave-loading is demonstrated.

In view of the importance of the load variability in system reliability assessment, a new model for short-term extreme (storm) sea-states for static structural reliability problems is presented. The model is based on a "multivariate" random variable characterization of the observed irregular process suitable for use in efficient reliability computation, e.g., FORM / SORM, and in general purpose methods such as Monte Carlo simulation. Although the model is restricted to at least semi-narrow banded time histories, it does not make any a priori assumption regarding the Gaussianity of the time series. Hence it is attractive for characterizing the skewed wave elevation processes observed in shallow water and / or in extreme (storm) sea-states. The application of the proposed model is demonstrated by analyzing a 34.13 min. long wave-elevation record collected during hurricane Camille. Calculation of response statistics such as the probability distribution of extreme base shear of a pile, the spatial correlation of sets of drag forces at different locations, etc., is demonstrated.

C. Allin Cornell, co-Chair

Alaa E. Mansour, co-Chair

2

ACKNOWLEDGEMENTS

I wish to express my deepest gratitude to Professor C. Allin Cornell for his guidance during the course of this research. His challenging ideas, breadth of experience, and insight into reliability problems have influenced my work in many ways. His professionalism and integrity as a researcher will always be a source of inspiration.

The support and encouragement of Professor Alaa E. Mansour have also been invaluable. It was through his lectures on Ship Structures that I was first exposed to reliability concepts. I am grateful to Professor Armen Der Kiureghian for the excellent course he taught on Structural Reliability and for the numerous stimulating discussions we have had on the subject over the years. Professor J. Randolph Paulling has been helpful in answering whatever questions I have had on wave kinematics and loading. I also thank him for his interesting lectures on the art and science of Offshore Engineering.

Other faculty members of the department have contributed to my education in a variety of ways. Professor William C. Webster has always been extra helpful both in academic and administrative matters. I have been fortunate to have Professor John V. Wehausen as a teacher and advisor. I thank Professor Robert G. Bea for his constant encouragement and for generously sharing his industrial experience and up-to-date information.

Dr. Steven R. Winterstein has made many valuable contributions to my research. Dr. Peter Bjerager has generously shared his insights on System Reliability. I have also benefited from my discussions with a number of other researchers in the field, most notably, Dr. Sverre Haver and Professor Daniele Veneziano. For data, technical support, discussion, and review of my work, I thank Dr. Hugh Banon, Mr. Jeff Geyer, Dr. Charles Petrauskas, and Dr. Bernhard Stahl.

Discussions with fellow researchers at Berkeley, including Espen Cramer, Colin Moore, Maria Ximenes, and Arnt Olufsen (visiting scholar) have helped me to clarify my thinking. During the last few years of "tele-commuting", the friendship and social support

i

TABLE OF CONTENTS

iii

CHAPTER 1

INTRODUCTION AND OVERVIEW

1.0 INTRODUCTION

Structural design has long been dominated by deterministic analysis. However, uncertainties in the loads, variability in the strength of structures, and the uncertainties from the use of idealized models in analyzing structural behavior contribute to a small but finite probability of failure. Reliability methods attempt to quantify the risk by providing a probabilistic framework for treating these uncertainties in a rational way. Offshore structures call for more attention than others. They are placed in a random environment and have large failure consequences. In response, structural reliability is rapidly gaining acceptance in design and analysis of offshore structures (e.g., *Freudenthal and Gaither, 1969; Marshall, 1969; Marshall and Bea, 1976; Moses and Stahl, 1978; Guenard, 1984; Murotsu et al., 1987; Nordal et al., 1987; Paliou et al., 1987; Cornell et al., 1988; Madsen, 1989; Harding and Banon, 1989; etc.*).

1.0.1 Why System Reliability?

System reliability deals with the uncertainties influencing the overall reliability of a structure as opposed to that of individual components. Offshore structures are, in general, highly indeterminant structures. Failure of an individual member does not imply system failure, and the ultimate capacity of the structure is usually larger than the load at which first-member failure occurs. In structural reliability redundancy is often defined as the conditional probability of system failure given first failure of any member (*Cornell, 1987; Nordal et al., 1987; Paliou et al., 1987*). An alternative probabilistic measure of redundancy has also proposed in this work. Deterministically redundancy can be measured by the ratio of the ultimate load capacity of the structure to the load capacity at first member

1

failure. While consequences of redundancy are much desired "system effects", not all aspects of the multi-member situation are beneficial. In particular, in a multi-member system more than one member may initiate failure resulting in an adverse system effect due to the presence of many members (*Ditlevsen et al., 1986; Cornell, 1987*). This effect is most clearly seen in a statically determinate structure where failure of any member causes global collapse. Because in this case, the system failure event is the union of individual component failure events, the system failure probability is greater than (or equal to) the failure probability of individual components. Because such "system effects" differ from design to design, structures with the same member-level reliability may manifest widely varying overall structural reliability.

Current reliability based codes, e.g., the Load and Resistance Factor Design format (*Ravindra and Galambos, 1978; API RP2A - LRFD Draft, 1989*), entail, in effect, designing each member (or members within a group, e.g., braces, piles) to a target reliability. What is still needed is the "system factor" for each component (or group of components) that indicates the importance of the component for the survival of the structure as a system, not just in the initial intact condition but in various potential damaged states. The ability of the structure to survive the demand in various damaged scenarios has been referred to as "robustness" in recent literature (e.g., *Cornell, 1987*). For example, in a fixed offshore jacket structure the horizontal braces are lightly stressed in the inplace wave-load condition because of the symmetry of the structure. However, accidental damage due to collision from a ship or a falling object may result in the loss of one or more members producing asymmetry in the structure. The structural survival in such a damaged condition depends on the ability of the horizontal braces to provide alternate load paths to prevent progressive failure. Even though the operational experience of survival of offshore jackets is substantial, often such robustness is implicitly produced as a result of the diverse design demands on the structure. Strengthening required for loadout, transportation, and installation of the jacket structure produces both redundancy and robustness not explicitly

2

designed for with respect to the intact inplace load condition. Such "system effects" (e.g., redundancy, robustness) need to be quantified in order to design alternate novel structures with the same overall structural safety. For example, limited operational experience exists for tension leg platforms (TLP). Moreover, the loadout, transportation, and installation requirements are different from that of conventional fixed offshore structures. In addition, TLP has a totally different structural configuration, namely, hulls made of stiffened shell plating and moored by tendons held under tension. While system reliability techniques for such continuous structures such as TLP or semisubmersible hulls (pontoons and columns) are currently under development, existing methodology can still be applied to study the gross system behaviors, such as that of the frame model of hull or of the tendon system (e.g., *Murotsu et al., 1986; Lee, S.-J., 1988; Stahl and Geyer, 1985*; etc.). System reliability methods have found ready application in the analysis of space frame / truss type structures (e.g., *Moses and Stahl, 1978; Rashedi and Moses, 1983; Guenard, 1984; Bjerager et al., 1987; Chan et al., 1987; Nordal et al., 1987; Paliou et al., 1987; Wu and Moan, 1989;* etc.). Structural system reliability analysis is expected to have application in code development and design of both conventional and novel structural concepts through qualitative and quantitative understanding of "system effects". In addition, system reliability analysis has potential for application in safety reassessment and economic requalification of existing structures nearing the end of their design lives. Because of updated design requirements, some of the aging structures do not meet the current standards of member-level reliability. It may be justified to requalify structures which manifest adequate system reliability in spite of their member level deficiency. It is also expected that system reliability will find application in designing optimum strategies for inspection and repair.

3

1.1 OVERVIEW: BACKGROUND AND SCOPE OF WORK

The work carried out in this thesis spans three inter-related areas: study of system behavior, application of system reliability analysis techniques to fixed offshore structures, and wave-load modeling. The organization of the thesis reflects the inter-relation of the three areas. The emphasis has been on wave-load modeling with a view to its implication on system reliability analysis. In order to introduce the necessary terminology and put the present work in perspective, a critical overview of the background is presented below.

1.1.1 System Behavior

The study of multi-component structural systems began early in the history of structural reliability (e.g., *Shinozuka and Itagaki; 1966; Cornell, 1967; Ang and Amin, 1968*). These studies were mostly restricted to rather idealized systems, because until recently efficient reliability computation techniques (or faster computers for simulations) were not available. Some of the early studies are based on the assumption of deterministic loading. It is recognized today that load variability plays a crucial role in system reliability (e.g., *Cornell, 1987*). In structural failure from overloads, all the components are exposed to the common variability of the load environment which in turn makes the component failure events dependent on each other. This happens even in the case where member capacities may be considered independent random variables. The dependence among individual component-failure events affects the system failure event and its probability of occurrence.

Recent reliability studies of ideal parallel systems have considered the dependence of failure events due to the variability of the common load. However, parallel system studies have been restricted to balanced systems (e.g., *Hohenbichler and Rackwitz, 1983a; Guenard, 1984; Stahl and Geyer, 1985; Cornell, 1987; Rackwitz and Gollwitzer, 1988;* etc.). In balanced parallel systems the ratio of mean member capacity to mean member force, i.e., the mean safety factor, is the same for all the members in both the intact and in the damaged states of the structure. Useful insights have been gained from these ideal

4

system studies that have put in perspective some common beliefs about structural redundancy. For example, static indeterminancy (while necessary) is not sufficient to assure redundancy as measured by the ability of the structure to withstand the load after the first-member failure (e.g., *Moses and Yao, 1983; Furuta et al., 1985; Frangopol et al., 1987;* etc.). In addition to the obvious dependence on the reliability of individual components, reliability of the structural system depends on the postfailure behavior (e.g., ductile, brittle, residual capacity of buckling members, etc.) of individual members, number of members, relative variability of load and capacity variables, and correlation among the member-capacity variables.

Balanced structures represent behavior of real structures that are well optimized (i.e., perfectly proportioned) under a single load case, e.g., lateral inplace load on a structure from one direction only. Study of real systems (e.g., offshore jackets, jackups, etc.) has showed that even deterministic design differences causes unbalance. For example, the diagonals of an X- braced subsystem will have equal member size if designed to withstand lateral loads from either direction in the plane of the diagonals. However, while under the action of a lateral load from a given direction the compression member fails before the tension member (deterministically), because the compression capacity is less than the tension capacity of slender braces of same size. Moreover, diverse design requirements such as, launching, etc., require strengthening of certain members beyond that required by the inplace load condition. This in turn leads to mean safety factors that vary from member to member. Often this implicitly provided unbalance has more pronounced "system effects" than an idealization of the balanced type might suggest. In particular, much better redundancy is achieved because capacity is available "elsewhere". Accordingly unbalanced parallel systems have been studied in the present work (Chapter 4) to suggest meaningful understanding of redundancy of real structures.

5

1.1.2 System Reliability Framework

The computation of failure probability for components as well as systems requires probabilistic characterization of the governing variables describing load and capacity. Complete characterization of the variables in the probability space requires the joint distribution of all the variables which is seldom available. Second moment characterization (mean and standard deviation) is usually insufficient to describe the tail of probability distribution which is important in reliability analysis. A framework that incorporates various levels of incomplete probability information, e.g., marginal probability distributions and pair-wise correlation between the random variables, is also available (*Der Kiureghian and Liu, 1986*). A joint distribution function consistent with the available (incomplete) information is implicitly assigned. This framework has been extended to treat higher marginal moment descriptions (e.g., skewness and kurtosis) and pair-wise correlation structure of the random variables using univariate Hermite transformations and a correlation mapping based on a power series involving Hermite polynomials (Appendix IV; *Winterstein, De, and Bjerager, 1989*).

The next step in failure probability estimation requires dividing the sample space of the governing random variables into two states, the failure domain and the safe domain. The general form of the equation for probability of failure is:

$$P_f = \int\int_{g(\underline{x}) \le 0} \int\int f_{\underline{X}}(\underline{x})\, d\underline{x} \tag{1.1}$$

in which $f_{\underline{X}}(\underline{x})$ is the joint probability density function of the basic / physical random variable vector $\underline{X} = [X_1, X_2, \ldots\ldots, X_n]^T$, and $g(\underline{x}) = 0$ denotes the limit state surface, i.e., the boundary between the failure ($g(\underline{x}) \le 0$) and safe ($g(\underline{x}) > 0$) sets. The limit state function $g(\underline{x})$, also known as failure function or performance function, is a deterministic function either explicitly defined in terms of the basic / physical variables $\underline{x}$, or implicitly

6

defined through other variables which are functions of the basic variables (e.g., limit state surface can be obtained through a finite element formulation of static or dynamic response such as, stress or deflection at one or more points, and equating the value of the response to a threshold value).

The main difference between a system and a component reliability problem is in the complexity of their failure surfaces. In structural reliability theory, the notions of components and systems do not necessarily correspond to physical components (e.g., beams, braces, diagonals, etc.) and systems (structures). The component reliability deals with failures involving a single "mode" defined by a single limit state (performance / failure) function. If the failure of an entire structure can be described by a single equation (e.g., single plastic mechanism equation) the problem essentially is one of component reliability. On the other hand, a structural element may fail in flexure or shear or buckling, or combinations thereof, and is to be considered a system for reliability analysis. Similarly, for a multicomponent structural system, failures of different sets of components may constitute different "failure modes" requiring system reliability techniques for analysis. The difference becomes subtle, however, if general purpose methods (to be described later) are adopted for probability computation where it is convenient to think of the existence of a "system" or "global" or "big" g-function whose negativity denotes system failure (e.g., *Bjerager, 1987; Cornell,1987; Der Kiureghian, 1988; Lin and Der Kiureghian, 1989*). For example, the system failure criteria for the fixed offshore structure can be specified in terms of some response (e.g., stress at a point in the structure or deflection at the top of the structure) exceeding a threshold value. However, the specified system failure criterion may be arrived at by different modes of failure (e.g., different groups and sequences of member failure events in a truss, etc.), and system failures by different "modes" need to be accounted for.

7
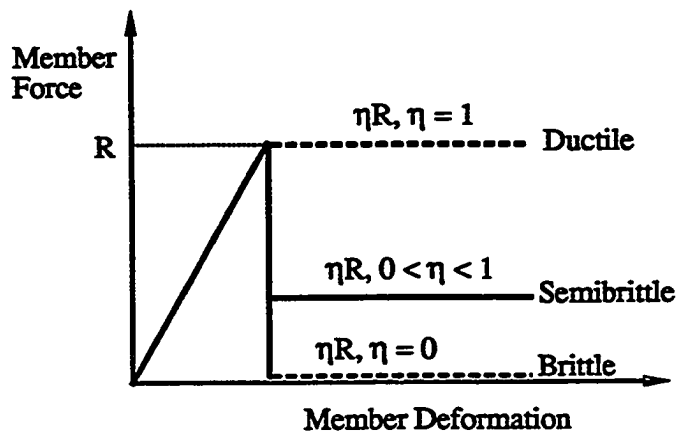
Fig. 1.1 Two-State Model for General Semibrittle Members
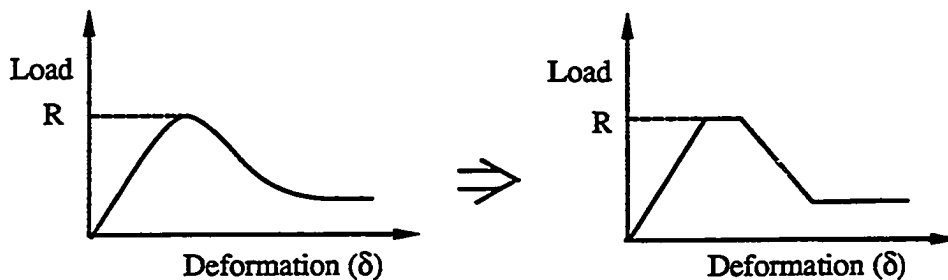
Fig. 1.2 Non-Linear and Piece-Wise Linear (Multi-State) Models of a Member-Force Deformation Function

Formulation of the g-function requires the choice of a mechanical model for the structural behavior, a methodology to analyze the behavior, and finally deciding on one or more failure criteria (see *Moses and Rashedi, 1983; Bjerager, Karamchandani, and Cornell, 1987; Karamchandani, 1987 ; Melchers, 1987; Der Kiureghian, 1988*). The choice of the mechanical model (e.g., postfailure behavior model of truss elements) and the analysis technique (e.g., static or dynamic, finite element / matrix analysis of truss / frame

8

structures) is restricted depending on the approach selected for probability computations. For the present work, the offshore jacket is modeled as a space truss with "two-state" (semibrittle) members. These members are at first linear elastic and then upon first yield continue to carry a fraction of the load at failure (Fig. 1.1). This postfailure model is particularly suitable for efficient system reliability analysis. In the present work an "event-to-event" strategy (e.g., *Simons and Powell, 1982*) has been used for structural analysis, where at each event (any member state change) the deformations, capacities, forces, and stiffnesses for analysis of the next linear segment are updated. For a structure with two-state members a convenient way to carry out postfailure structural analysis using linear structural analysis programs is to use the so-called "member replacement method", wherein upon failure the member is simply removed from the structure and replaced in the analysis by a fixed force equal to the residual strength of the failed member. Post-yield strain reversal of the two-state member used in the member replacement method implies simply retention of the constant force associated with the residual strength. A more realistic "multi-state" (piece-wise linear approximation of a non-linear force-deformation diagram) member model (Fig. 1.2) can be used in efficient system reliability analysis (*Cornell, De, Karamchandani, and Bjerager, 1988*). Multi-state member force deformation model may in general include "unloading" and or "load shedding". By "unloading" we mean here the reduction of force associated with a reversal of strain. "Load shedding" refers to the reduction of force with a continuing strain direction (e.g., Fig. 1.2). "Load shedding" behavior is important in modeling buckling compressive braces.

A space frame model could have been adopted; however, in addition to the difficulties in modeling the nonlinear interaction of axial force and moment in beam-column elements, little is known (even deterministically) about the postfailure behavior of beam-column elements especially for buckling failures. Current work is restricted to linear interaction curves and plasticity based postfailure behavior (e.g., *Thoft-Christensen and Murotsu, 1986*). The actual postfailure behavior of structural members in an offshore jacket is of

9

hysteretic nature with progressive stiffness and capacity degradation under repeated (static or dynamic) load reversals. In principle, any mechanical model for which deterministic analysis procedure exists can be incorporated in the system reliability analysis at least through the use of "general purpose methods" such as simulations (to be discussed later). However, computational costs may be prohibitive. For the purposes of the present work the truss model (with semibrittle members) is considered adequate. Its adequacy has been confirmed by comparison with multi-state members in *Cornell, De, Karamchandani, and Bjerager, 1988.*

The final step in system failure probability estimation is evaluating the multi-dimensional integral described in Equation 1.1. For a general review the reader is referred to *Karamchandani, 1987; Melchers, 1987; and Bjerager, 1989a.* A brief discussion of the important features is presented here.

1.1.2.1 General Purpose Methods

General purpose methods such as numerical integration and simulation techniques are equally applicable to system and component reliability problems. Numerical integration of Equation 1.1 is inefficient unless the problem can be formulated in terms of two or three random variables. Consider a problem with ten random variables where each variable space is discretized into ten intervals; then 10^{10} evaluations of the performance function will be necessary to evaluate the integral.

Monte Carlo simulation is a powerful numerical integration technique suitable for interfacing with structural analysis packages of any sophistication. Moreover its implementation is straightforward and requires little knowledge of specialized system reliability analysis techniques. In its original form, a large number of independent samples of the vector of random variables are generated from the prescribed joint distribution. For each realization, $\underline{x}^{(i)}$, it is checked if failure has occurred (i.e., $g(\underline{x}^{(i)}) \leq 0$). The g-function may be evaluated using a standard structural analysis computer program or from a

10

simple analytical formulation, as the problem demands. The ratio of the number of failures to the total number of simulations is an estimate of the probability of failure. The results may include member failure events, sequence of member failures (if such discretization is meaningful for the system) or just the system failure event. Sensitivities of failure probability with respect to governing variables and parameters of the problem can also be obtained with little extra computational effort (*Karamchandani et al., 1988; Karamchandani, 1990*). Monte Carlo simulation is conceptually simple but because the failure probabilities of structural systems are very low, the number of simulations required (and the associated checks for failure through evaluation of the performance function) for reliable estimates of failure probability is very high. For example, if the failure probability being estimated is of the order 10^{-3}, then roughly 10^4 simulations are required for a reliable estimate (coefficient of variation of estimation ≈ 0.3). However, several variance reduction techniques and rapidly developing hybrid methods, where at least part of the probability computation is done analytically, are increasingly being used in system reliability analysis (e.g., *Shinozuka, 1983; Harbitz, 1983; Augusti et al., 1984; Ang and Tang, 1984; Melchers, 1987; Karamchandani 1987; Cornell, 1987; Bjerager, 1989; Karamchandani, 1990;* etc.). A "Reduced Space Monte Carlo" simulation technique proved very efficient (i.e., the probability of failure could be estimated from only a few simulations) for the study of unbalanced systems in the present work, and this was then successfully applied for estimating the system failure probability of an offshore jacket structure (see Chapter 4). Efficient use of such techniques usually requires taking advantage of the specific situation of the problem at hand (e.g., load modeled by a single variable, load variability higher than the capacity variability, and the load variable independent of the capacity variables).

1.1.2.2 FORM / SORM and Failure Path Approach

A major thrust in system reliability research has been in developing special purpose approximate analytic methods. They are, in general, computationally more efficient but are

11

applicable only to a comparatively less general class of structural reliability problems, and they require several idealizations in the mechanical model, limit state, load model, response and probability calculations. In general, these methods are applicable when the system failure can be expressed as a combination of relatively simple component-failure events. The computation techniques are aimed at approximating the probability of failure of the system, given the probabilities of failure of the individual components of the system. These techniques are based on first - and second order reliability methods (FORM / SORM) (see *Madsen et al., 1986; Melchers, 1987; Bjerager, 1989a)*. FORM and SORM are essentially fast integration techniques where the problem is first mapped in the multi-dimensional standard Gaussian space using a probability preserving transformation (*Rosenblatt, 1952; Hohenbichler and Rackwitz, 1981)*. The problem of multi-dimensional integral is avoided by solving a constrained optimization problem to locate the point on the failure surface ($g(\underline{x}) = 0$) closest to the origin in the standard Gaussian space called the "design point" and then approximating the failure surface in the Gaussian space by a linear or quadratic hyper-surface around the "design point". In addition to an approximate estimate of the failure probability for the approximated failure domain, measures of sensitivities of the failure probability with respect to the variables and parameters of the distribution function and those of the g- function are easily obtained. FORM and SORM are accurate especially in the range of small probabilities (10^{-3} to 10^{-8}) suitable for structural reliability, and the computation time is not sensitive to the level of failure probability (unlike the Monte Carlo simulation). With recently developed "exact" SORM accurate prediction for component reliability problems are possible for all probability ranges (*Tvedt, 1988)*.

The use of FORM / SORM in system reliability usually requires that the system g-function be specified as a combination of simple component g-functions. There have been recent attempts to use FORM / SORM with global (or system) g-function directly, as computed from general purpose structural analysis programs, such as, non-linear finite

12

element analysis programs (e.g., *Liu and Der Kiureghian, 1988; Lin and Der Kiureghian, 1989; Holm, 1990*). Even though the finite element reliability methods (FERM) has the appeal of being able to use any state of the art structural analysis method, further development is needed to identify and treat multiple "failure modes" (e.g., by selecting different starting points in the optimization procedure to arrive at the system failure through different modes of failure). The problem of identifying the failure modes can be avoided if the system g-function defined by a suitable global response measure turns out to be sufficiently smooth, implying dominance of a single failure mode, in which case the results from straightforward component FORM / SORM analysis would suffice. Other challenges in FERM include the efficient gradient computation needed for solving the constrained optimization problem in FORM /SORM analysis; this is presently being addressed (e.g., *Liu and Der Kiureghian, 1988; Lin and Der Kiureghian, 1989*).

Usually the system g-function is constructed using the basic concepts of classical reliability theory (e.g., *Barlow and Prochan, 1975; Madsen et al., 1986*). The basic system representations are series systems, parallel systems, series systems of parallel subsystems, and parallel systems of series subsystems. These idealizations refer to the failure interaction and not to the structural topology. For example, consider a tension leg platform with eight tendons in a physically parallel arrangement. The system failure may, however, be defined as any (i.e., at least one) first tendon failure, because even though the structure could possibly survive with one or more tendons removed, it is not known what level of damage a tendon falling to the ocean floor would create either to the adjacent tendons, to the risers, or to the foundation well template (*Harding and Banon, 1989*). The "any first-failure" event is a "series system" of individual tendon failure events in the sense that any failure in the chain of events would imply system failure. In contrast, in a parallel system all the individual components need to fail to cause failure of the system. For example, in a fixed offshore structure the system may fail (according to one or more system failure criteria) as a result of a number of different member-failure sequences. Each

13

sequence of member failures which leads to the system failure is known as a "failure path". Each failure path event is a parallel system, because all the members within the sequence need to fail to cause failure of the system. Because there are many such possible failure paths (distinguished by individual member-failure events and the order in which the members fail within a sequence) any of which could cause system failure, the system failure event can be modeled as a series of such parallel subsystems. This is the so-called "cut set" representation of a general system. The system g-function is expressed as:

$$g(\underline{x}) = \bigcup_{k} \bigcap_{i \in C_k} (g_{ki}(\underline{x}) \leq 0) \tag{1.2}$$

in which $g_{ki}(\underline{x})$ is the failure function for the i th component in the k th cut set, C_k. Unlike classical reliability theory, however, the component performance functions are not represented by simple, independent, zero-one indicator variables. General stochastic dependence between component failure events is modeled through the multivariate distribution of the basic random variables and / or through the presence of common basic variables to different components. This is an important characteristic of the structural system reliability problem, where among other things the common dependence on the global load variables makes the component failure events (typically) highly dependent on each other even if the capacity variables are independent. Several approximate methods are available for the probability calculation of the system failure event as represented by Equation 1.2, using FORM / SORM (e.g., *Ditlevsen, 1979; Hohenbichler and Rackwitz, 1983b; Hohenbichler et al., 1987;* etc.). For a general review the reader is referred to *Madsen et al., 1986.*

14

$$P_f = P\{(F_1^0 \cap F_2^1) \cup (F_2^0 \cap F_1^2)\}$$
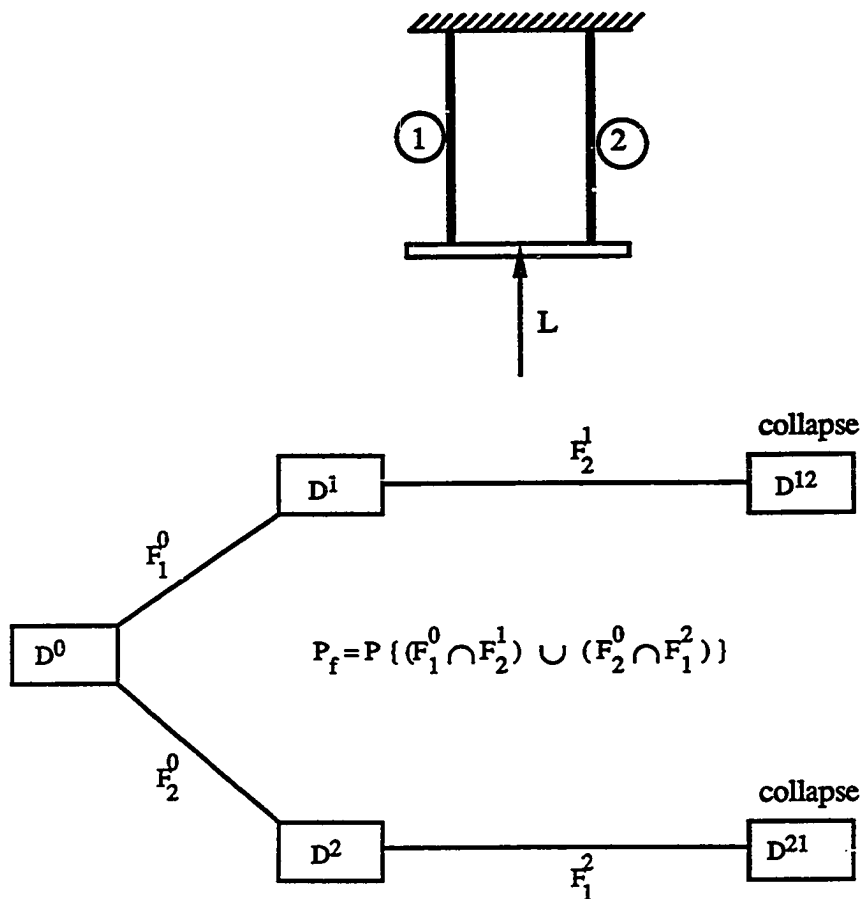
Fig. 1.3 Failure Tree for the Two-Member System

The cut set representation, where available, can be graphically represented by failure trees, also known as event trees. The associated system reliability methodology that takes advantage of the discrete representation of the system in terms of component failure events is known as the "failure path approach". Fig. 1.3 shows a failure tree for a two member (semibrittle) system under compression. Each node (e.g., D^0 or D^1, D^{21}, etc.; the superscript 0 refers to the intact state) represents a particular state (intact and all possible damaged states) of the structure, and each branch represents a member failure event (e.g.,

15

F_2^0 represents the failure event of member 2 in the intact state, F_1^2 represents the failure event of member 1 in the damaged state where member 2 has failed, etc.). While it is visually simple to represent each branch as a "member-failure event", a closer inspection would reveal that each "branch" is not a single component failure event that can be represented by a simple failure equation. Strictly speaking, a "branch" describing the failure of member i is also a "system event" that requires not only that member i fails in the state of the structure specified by the preceding node, but that all other previously undamaged members survive at the load level at which member i fails. This requires calculation of an intersection of a low probability (failure) event with several high probability (survival) events, and this is neither computationally expedient nor accurate in the context of FORM / SORM. It is therefore assumed in the "failure path approach" that the survival events are certain. This permits treating the failure function (g_{ki} in Equation 1.2) of each "branch" as a simple component failure function corresponding to the failure of the member i in the given state of the structure. The price to be paid for this simplification (besides the introduction of a small error of usually unknown magnitude) is that the cut set events (i.e., the failure path events) are no longer disjoint, and hence their union is no longer a sum of failure probabilities of the individual cut set events. The other feature of the failure tree representation is that it captures the order in which members fail within a cutset and not just the members that belong to individual cut sets. The ordering is necessary for structural systems because the load redistribution (at least for non-ductile members) and the change of stiffness at each damaged state of the structure affects subsequent member-failure events.

For typical structures, there exists a large number of failure sequences because of the nonlinear post-failure member behavior and high redundancy. Fortunately, only a few sequences contribute significantly to the overall probability of system failure (*Ang and Ma, 1981; Murotsu et al., 1981; Rashedi and Moses, 1983; Murotsu et al., 1983; Bjerager,*

16

1984; Guenard,1984; Melchers and Tang, 1984; Thoft-Christensen and Murotsu, 1986).
At present there is no way of ascertaining a priori which sequences are most significant. A
"branch and bound" algorithm (e.g., *Guenard,1984)* can be used to identify the most
likely to occur sequences, but they are often highly "overlapping" (e.g., made up of the
same member failure events but in different order) adding little contribution to the system
failure (union) event. In view of this difficulty, a modified "branch and bound" algorithm
is used in the present work (Chapters 2 and 3) in which key members in "the most likely
sequence" are systematically excluded in the subsequent searches for the "next most likely
to occur sequences". As a result, the identified sequences are less likely (compared to
those obtained by the regular "branch and bound" algorithm) but are less "overlapped" and
hence may contribute more to the union event of system failure.

1.1.3 Wave-Load Modeling

Based on an investigation of system behavior of idealized "parallel" systems (Chapter
4), it was concluded that the "effective redundancy" of the structure strongly depends on
the variability of the load. In general, it was noted that the wave-load variability (due to
inherent randomness of the wave-elevation process, statistical uncertainty in estimating sea-
state parameters, and uncertainties in prediction of wave forces given a sea-state
description, e.g., *Olufsen and Bea, 1989)* is significantly greater than the variability of the
capacity parameters, at least in the case of truss type behavior of offshore jackets.
Therefore it is necessary to study and represent loads as well as possible to assure accurate
reliability assessments. Offshore structures are exposed to several environmental loads
acting simultaneously. Loads from waves, currents, and wind are of random nature and
tend to be highly correlated because of the common generating and driving mechanisms.

17

1.1.3.1 "Fixed-Pattern" Approach

Wave loads are often the most dominating of all environmental loads. For offshore structural design several different approaches to wave-load modeling are available. The simplest approach is a deterministic "pseudo-static" method, where the maximum loads corresponding to a "design" regular wave are applied to a static analysis of the structure (see *Sarpkaya and Isaacson, 1981*). While other more sophisticated wave-load models, e.g., "time dependent", "stochastic", etc., are available for offshore structural analysis, the wave-load models for efficient system reliability computation have largely been restricted to a probabilistic variation of the "pseudo-static" approach (e.g., *Moses and Stahl, 1978; Chan and Melchers, 1987; Nordal et al., 1987; Bjerager et al., 1987; Paliou et al., 1987*, etc.). In this approach (henceforth referred to as "fixed-pattern approach") the wave load is modeled as a fixed spatial pattern of nodal forces scaled by a random intensity factor. For example, the spatial pattern may correspond to the relative forces produced by the "design wave" at its "worst location" with respect to the structure. The "worst location" is usually characterized by the position of the wave (during its passage through the structure) where some global load effect, e.g., base shear is maximum. The random (load) intensity factor for a fixed offshore structure may be base shear, the total lateral load, whose probability distribution can be derived from that of the wave height using a simple functional relationship between the base shear and the wave height. The variability of the wave-load magnitude (e.g., base shear) depends on the variability of the wave height and the uncertainty in predicting the wave forces given a wave height. The implicit assumption in the "fixed-pattern approach" is that the load pattern is independent of the wave height; only the load magnitude is a function of the wave height. Gravity loads are modeled by a deterministic spatial pattern with random (scalar) magnitude. System reliability is estimated under the assumption of "static monotonic" application of the load pattern with random magnitude (i.e., the nodal loads are gradually increased from zero to their final magnitude in a monotonic fashion always maintaining the same relative nodal-force pattern).

18

The requirement for the nodal loads to be raised proportionally from the zero level to their final random magnitudes constitutes the specification of a "load path". This path specification refers to the relative rates by which the various loads are raised to their final random values, and may often involve multiple load systems, such as wave loads and gravity loads. For example, the gravity loads are applied first and then the wave loads, or both the loads are applied to the structure at the same relative rate, etc. In general failure of each member (and hence the system) depends not only on the final magnitude of the load vector, but also on the specification of the load path (*Bjerager, 1984; Wen and Chen, 1986; Karamchandani, 1987, Cornell, 1987*). The "proportional load path" is the simplest to deal with in the failure path approach, but it may not always be representative of all possible load paths. In this work the assumption of the proportional load path is retained in the system reliability analyses with more refined wave-load models.

In Chapter 4, several simulation based accelerated system reliability analysis techniques are investigated where the wave load is also modeled by a fixed load pattern scaled by a scalar random variable.

1.1.3.2 "Wave-Fragility" Approach

The choice of the wave-load pattern corresponding to the "design wave" (e.g., the 100-year wave) in the "fixed-pattern approach" is arbitrary. The load pattern changes significantly with wave height due to the change in fluid kinematics. In particular, because of the air gap (vertical separation of the deck from the mean water level) provided in design, waves reaching the deck of the platform produce slamming forces that cannot be modeled realistically by the 100-year-wave pattern. In Chapter 2, a more rigorous approach, referred to as **wave-fragility**, has been used to estimate the system failure probability. In this approach the system failure probability is obtained for each of a set of wave heights. These probabilities are conditional on the wave height, and hence the load variability in each of these system reliability analyses depends only on the uncertainty in

19

estimating the wave-load magnitude given a wave height. The conditional system failure probabilities are multiplied by the (discrete) probability levels of the wave heights, and the products are summed to obtain the (total) system failure probability. The "wave-fragility" approach provides insight into the mechanism of failure at each wave height. This approach also provides a basis for calibration of simpler fixed (single) pattern approaches for estimating system reliability.

1.1.3.3 Spatial Correlation of Nodal Wave Forces

The wave-load patterns adopted for both the "fixed-pattern" and the "wave-fragility" approaches are deterministic. The randomness of the wave load is modeled by a single random variable, namely, the load intensity factor (e.g., the base shear). The nodal wave forces are fully correlated, i.e., if the force is known at one node, the forces at all other nodes are also known. Common functional dependence of the nodal wave forces on the wave height results in a high level of correlation among the nodal wave forces. However, local variations due to the irregular wave elevation, uneven marine growth on the structure, and local uncertainties in wave kinematics and force prediction result in less than perfect correlation among the nodal wave forces. Given the importance of the load aspects of the problem the question arises as to what effects this more realistic correlation have on system reliability assessments.

In Chapter 3, an analytical form is assumed for the spatial distribution of correlation between nodal wave forces. The parameters of the correlation model include a base (non-ergodic level) correlation and rates of decay in each of the three dimensions in space. A framework is developed for the probabilistic description of nodal wave forces, consistent with the prescribed correlation structure and the available information on the base shear probability distribution. A parametric study is carried out to investigate the effects of variation of the correlation model parameters on both the member-level and the system-level (system failure and "any-first-member failure") failure probabilities including changes in

20

potential failure sequences. The correlation model is calibrated based on the published wave-loading results from the Ocean Test Structure (*Dean et al., 1979; Haring et al., 1979; Heideman et al., 1979*).

Calibration from limited published data indicates that wave-load representation by a deterministic pattern scaled by a scalar random variable can be satisfactorily used in system reliability analysis for global truss type behavior of jacket structures. The investigation clarifies issues dealing with spatial averaging involved in the base shear, the chosen global load intensity random variable, and suggests when the commonly adopted estimates of load variability have to be be reduced (or increased in some cases) in system reliability calculations.

1.1.3.4 Random Variable vs. Random Field Model

The wave-load models described above are characterized in terms of random variables. A random variable (as opposed to random process or random field) model of the governing parameters of the problem is necessary for efficient system reliability computation. For example, if the instantaneous distribution of the load and capacity variables is known and the failure surface is time independent, then instantaneous probability of failure can be evaluated by the failure path approach using FORM / SORM.

The usual quantity of interest, however, is the lifetime reliability of the system. More generally, the actual wave load, $F(q, t)$, acting on an offshore structure can be represented by a random field, i.e., a vector F varying both in space (q, the spatial coordinates) and time (t). A random field can be thought of as a collection of random variables for each point in time and space (see *Vanmarcke, 1984*). A random process is a special case of a random field with collection of random variables over only one parameter set, such as time. Spatial and temporal correlation of the underlying family of random variables of a random field can theoretically be described by a joint probability distribution function of the underlying collection of random variables. However, an efficient reliability

21

framework to treat such general characterization of the random field is not yet available. Limited capability exists to treat Gaussian random processes, and to a more limited extent non-Gaussian processes also, in mostly component reliability problems, where the time dependent reliability is estimated from the first "outcrossing" probability (e.g., *Veneziano et al., 1977; Madsen et al., 1986; Melchers, 1987; Wen, 1987; Wen and Chen, 1987; Bjerager et al. 1988a;* etc.). The "outcrossing" probability for system reliability problems is only recently being addressed (e.g., *Guers et al., 1988; Wen and Chen, 1989).*

In the present work, the random field is discretized in space and time, so that a random variable representation of the lifetime reliability problem is possible. Space discretization is simple and can be done with a relatively few random variables or processes corresponding to the locations of interest (e.g., E_j (t), wave load at node j; $j = 1, 2, 3$, etc.). In Chapter 3, nodal wave loads are modeled by such a random variable vector with a further assumption that wave forces at a node in three directions of space are fully correlated, i.e., they can be modeled by just one random variable for each node. The modeling of the time dependence of the nodal wave forces is explained next.

1.1.3.5 "Time-Integrated" Approach

Usually in structural reliability of overload problems, the capacity variables are assumed to be time independent random variables (i.e., degradation due to aging is neglected). The time dependence of the wave height or the wave-load process can be taken into account by the "time-integrated approach". In this approach statistical parameters of all the random variables must relate to the entire lifetime $(0, t_L)$ of the structure (e.g., *Guenard, 1984; Melchers, 1987).* The probability distribution of the lifetime maximum / extreme load may, in principle, be obtained directly by fitting an appropriate probability distribution to the observed extreme value data of past observations. Usually extreme value records are available for much shorter period of time (e.g., a year or even shorter durations such as a storm or the duration of assumed stationarity in the sea-state data base). The

22

extreme value distribution corresponding to the lifetime is derived from the distribution of the shorter period under the assumption of finite number (number of years or storms, which may be a random variable itself, or the number of stationary sea states in the lifetiime, as the case may be) of independent applications of the load processes (e.g., Chapter 2). If the number of applications is very large, one of the standard extreme value distributions such as Weibull or Gumbel is often used.

The "time-integrated approach" can be applied in a straightforward manner provided that the load can be modeled by one (scalar) random variable (as in the "fixed-pattern" or "wave-fragility" approaches, see Chapter 2). In Chapter 2, the distribution of the lifetime extreme wave height and that of the corresponding base shear were derived from the annual extreme wave height whose "long-term" (i.e., sea state to sea state) statistics were available. The calculation of the distribution of the annual extreme wave height (wave load or other load effect) usually involves solving the "short-term" (e.g., the duration of the storm or of the period of assumed stationarity of the sea states in the wave data base, etc.) random process problem to obtain the probability distribution of the extreme wave height (or response) within the "short-term". Usually the "long-term" descriptions of sea states are available in terms of a joint probability distribution of some slowly varying (every 3 to 6 hours) sea-state characteristics, such as the significant wave height and some characteristic time period, e.g., the spectral peak period (e.g., *Haver and Nyhus, 1986*). The "short-term" sea state is usually defined by some characteristic spectral density function of the wave elevation process in terms of the sea-state characteristics, such as the significant wave height and the spectral peak period, for which the "long-term" joint distribution is available. The wave elevation (also the response, i.e., the load / load-effect) process is assumed to be a zero mean Gaussian process for which solution of the "outcrossing" problem is available. Various alternative approaches (e.g., "long-term" or "(short-term) extreme design storm", etc., see *Guenard, 1984; Haver and Nyhus, 1986; Haver, 1989)*, including one based on FORM / SORM and system reliability techniques

23

(Bjerager et al., 1988b; Holm et al., 1988), are available to estimate the lifetime extreme wave-height, wave-load, or load-effect statistics for use in the "time-integrated" reliability analysis. The "long-term / short-term" analysis methods are further discussed later.

A New Short-Term Model for Extreme Sea States

In view of the importance of the load variability in system reliability analysis, a new framework for modeling short-term extreme (storm) sea states is proposed in Chapter 5. Unlike the common frequency domain (i.e., spectral) representation of the wave elevation process, the proposed model is based on a "multivariate" random variable characterization of the random process suitable for use in efficient reliability computation, e.g., FORM / SORM and in general purpose methods such as Monte Carlo simulation. This model does not make any a priori assumption regarding, for example, the Gaussianity of the time series. Hence it is attractive for characterizing the skewed wave elevation process in extreme (storm) sea states. Moreover, the response of nonlinear systems (e.g., the drag force) becomes non-Gaussian, even if the input wave process is Gaussian. Calculation of response statistics such as the probability distribution of extreme base shear of a pile, the spatial correlation of sets of drag forces at different locations, etc., have been demonstrated.

The focus in this work is on the maximum static response prediction, but the model might also be used to simulate elevation and forces for dynamic response prediction (at least for lower frequency effects). It is expected that in the future through analysis of similar extreme sea-state data, parameters of this multivariate-sequence model of a short-term sea state can be functionally related to the long-term sea-state distribution parameters such as, significant wave height, average zero-up crossing periods, etc. At present, this idea is presented as a research tool for better understanding and characterization of load processes. The methodology also demonstrates diverse application of both the component and the system FORM / SORM reliability techniques.

24

The Load Combination Problem

The extension of the "time-integrated approach" to the multiple load system is not straightforward. For example, the wave load, the wind load, and the current load at each node may not be fully correlated. Even if the loads are highly correlated, their lifetime peaks need not coincide unless they are perfectly positively correlated. In the "time-integrated" approach, it is conservative to assume an extreme value distribution for each loading separately. For a restricted class of problems, "load combination" can be treated more realistically (e.g., *Borges and Castenhata, 1972; Wen, 1977; Larabee and Cornell, 1979*, etc.). For example, for a component behaving linearly until failure under the action of multiple load Gaussian processes, the maximum scalar load effect is characterized by its probability distribution (using outcrossing rate / first-passage probability of the Gaussian load-effect process).

In a multi-member situation load combination problems arise even for one load system, such as due to waves only. Consider a multi-member jacket structure under the action of time varying nodal wave forces, e.g., E_j (t), wave load at node j; $j = 1, 2, 3$, etc. The scalar load effect of each member (e.g., axial stress of a truss element) is a function of multiple (i.e., vector) random processes whose peaks, in general, occur at different points in time. Moreover, the maximum lifetime load effects of different members need not coincide at the same point in time. The problem is usually treated in a manner similar to the long-term / short-term analysis of environmental events (e.g., *Guenard, 1984; Cornell, 1987*). In this framework, the short-term extreme events are associated with a vector describing major characteristics of the loading event, e.g., the significant wave height, wave direction , and current velocity during the event (perhaps a storm). The long-term distribution of these major characteristics in principle should be available. The structural reliability of the system within the short-term event, conditional on a given description of the major sea-state characteristics, can be carried out using time-integrated random variable

description of the loads, provided the damage accumulation from event to event is ignored. The long-term structural system reliability may be obtained by unconditioning the system reliability results with respect to the major sea-state characteristics whose long-term joint distribution is available. To a first approximation extreme environmental events may be considered independent from (short-term) event to event (see *Bjerager et al., 1988b*), and hence their lifetime distribution may be derived under the assumption of repeated independent occurrence (occurring according to the long-term distribution). The system failure events in different independent environmental events will, however, be dependent because the structural capacity random variables are common in all these failure events. The lifetime reliability estimated from that of short-term events under the assumption of independence can be justified if the structural capacity variability is much smaller than the load variability.

Alternatively, an approach similar to the previously alluded to "(short-term) extreme design storm" approach may be used. In particular, in the case of an individual wave-load process at each node (e.g., F_j (t) wave load at node j; $j = 1, 2, 3$, etc.), the lifetime maximum nodal forces are assumed to be related to a the lifetime maximum global load intensity variable (e.g., base shear, the total lateral load) characterizing the extreme event, i.e., $(F_j)_{max} (0, t_L) = C_j (F_0)_{max} (0, t_L)$, where C_j is a time independent vector of random variables modeling the spatial load variation during the extreme event specified by $(F_0)_{max}(0, t_L)$, the lifetime maximum of the global load intensity variable. If the spatial patterns are deterministic (e.g., "fixed-pattern" or "wave-fragility" approach) then C_j is deterministic, and the nodal forces are perfectly correlated (e.g., Chapter 2). In Chapter 3 less than perfect correlation of the nodal forces is assumed to model the local uncertainties, and a vector of random variables is used to model the load. The lifetime maximum global load intensity, $(F_0)_{max} (0, t_L)$, is assumed to be functionally dependent on the lifetime maximum wave height. Because of this common functional dependence, the nodal load

26

forces $[(F_j)_{max} (0, t_L); j = 1, 2, 3,...]$ are highly correlated in spite of the local spatial variation of the kinematic and force-prediction related uncertainties.

In this work random variable wave-load models have been used for lifetime system reliability analysis through the "time-integrated" approach. Such models are adequate for shallow water offshore jacket structures where the static response dominates. However, even for static behavior, more refined wave-load models, member postfailure behavior models, and efficient system reliability methods are needed to treat cyclic load reversals. For deep water structures, where dynamic response is important, further developments in load modeling and system reliability framework are required.

27

CHAPTER 2

SYSTEM RELIABILITY UNDER
CHANGING LOAD PATTERN

This chapter considers structural system reliability analysis when the spatial force pattern changes as the load increases, specifically when the nodal forces on a steel offshore jacket structure change as the base shear increases under increasing wave height. This section demonstrates the so-called "fragility approach" to systems analysis, wherein the reliability of the system is obtained for each of a set of increasing wave heights. These probabilities are conditional on the wave height. These results are multiplied by the (discrete) probability levels of these wave heights, and the products are summed to obtain the (total) system reliability. The method is applied to analyze a fixed offshore jacket in 140 feet of water and designed for a 100-year (63 foot) wave. The change of the relative importance of different member-failure sequences with wave loads corresponding to different wave heights is studied. In this case study, the inclusion of wave slamming forces on the deck at higher wave heights led to an increase of the failure probability by an order of magnitude. The use of an improved fixed wave-load pattern treatment is explored. A comparison of the member level and system level failure probabilities is presented in terms of factors measuring different system effects.

2.1 INTRODUCTION

Structural safety of offshore structures with respect to overloads has always been a topic of interest. Ultimate capacity of an offshore structure depends not only on design conservatism but also on "system effects" beyond the first member failure. For a redundant structure, failure of an individual member does not imply system failure and usually the ultimate capacity is larger than the load at which first failure occurs. *Lloyd and*

28

Clawson, 1983, quantified these effects deterministically, for the example structure studied in this chapter, through static pushover analysis. In this method of analysis lateral wave loading on the structure is increased proportionally beyond the failure of first element until the structure is unable to resist the next load increment. Reserve strength, according to *Lloyd and Clawson, 1983,* is measured by the ratio of ultimate or collapse strength to the strength necessary to resist design loads.

Recently system reliability methods (e.g., *Stahl and Moses, 1978; Guenard, 1984; Chan and Melchers, 1977; Nordal et al., 1987, Paliou et al., 1987; Bjerager et al., 1987;* etc.) have been used to study the probabilistic aspects of system failure. In addition to the aspect of conservatism and redundancy seen in the deterministic analysis the number of potential failure modes in the structure is also an important factor. For a structure with many members stressed near their respective capacities the probability that any (i.e., at least one) of the members fail may be significantly higher than the failure probability of each individual member. In contrast to redundancy, this property of a structural system, referred to here as *complexity,* has a negative impact on the reliability of the system. These aspects will be addressed later in more detail in Chapter 4. The example structure studied here has also been the focus of a previous reliability study by *Nordal, Cornell, and Karamchandani, 1987.* In that study both the load and the structural capacity are modeled as random variables. The wave load is modeled as having a fixed spatial pattern (corresponding to a 100-year wave of height 63 ft.) that is scaled by a factor. The (load) factor is treated as a random variable whose distribution is derived from the distribution of wave height using an empirical relationship between the base shear and the wave height.

However, the load pattern changes significantly with wave height due to the change in fluid kinematics. In particular, waves reaching the deck of the platform produce slamming forces that cannot be modeled realistically by the 100-year-wave pattern. In the present work a more rigorous approach, referred to as **wave-fragility**, has been used to estimate the probability of system failure from the conditional probability of system failure given

29

each wave height. The true wave-load pattern, including slamming forces on the deck, when appropriate, is used to calculate the conditional probability at each wave height. The wave-fragility approach provides insight into the mechanism of failure at each wave height. It also provides a basis for calibration of simpler single pattern approaches for estimating system reliability.

2.2. STRUCTURAL MODEL

The structure analyzed is an eight-leg (four bents by two rows) steel offshore jacket in 140 feet of water (Fig. 2.1). It was designed for a 63 foot wave with a period of 11.4 seconds, which has a return period of 100 years in the Gulf of Mexico. The design is idealized in the sense that it was designed for the inplace condition only. Forces due to loadout, transportation, and installation were not considered in the design. The importance of this should be kept in mind while generalizing specific numerical results of this study.

The jacket was modeled as a space truss. The deck level horizontal members (including bracings) were sized to provide the same level of stiffness as the deck (*Lloyd and Clawson, 1983*). Failure of these members were not considered in this study. The remaining members were sized according to the API guidelines (including API recommended values for buckling factors (K) and equivalent lengths (l)). The member capacities as specified in the codes include material safety factors. However for the reliability analysis we estimated member capacities more realistically, i.e., without a built in factor of safety, (e.g., using less conservative buckling factors and equivalent lengths) as outlined in *Nordal et al., 1987*.

The mean compression capacities of the members were reduced by 15% to compensate for the neglected moments due to frame action (*Nordal et al., 1987*). The member resistances were assumed to be lognormally distributed, with a coefficient of variation of 10% for the tension capacity, and 13% for the compression capacity (*Nordal et al., 1987*). The postfailure behavior of truss members was modeled by semibrittle elements with

30

ductile tensile failure, and an instantaneous drop to 40% of the original capacity when failing in compression (Fig. 2.2).
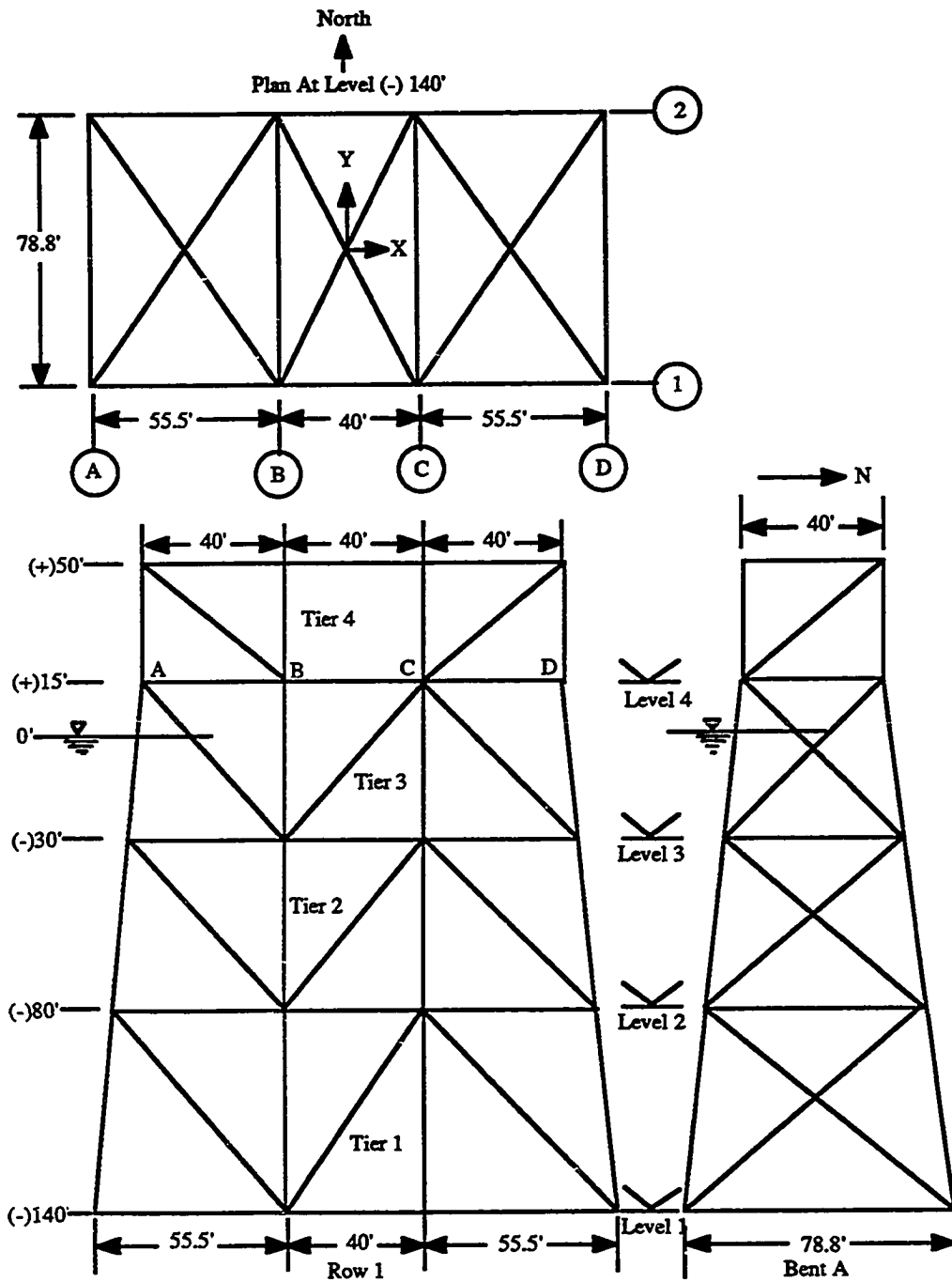
Fig. 2.1 Offshore Jacket Structure

31
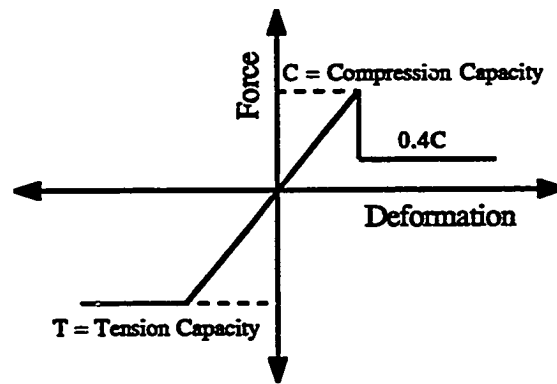
Fig. 2.2 Postfailure Behavior Model of Truss Elements

2.3 LOAD MODEL

The structure was analyzed under the action of gravity and wave loads. The wave loads were arbitrarily increased by 60% to account for the effects of wind, current, unmodeled appurtenances and conductors (*Lloyd and Clawson, 1983*). The wave loads for a number of different wave heights (63 ft., 75 ft., 85 ft., 92 ft., 96 ft., and 98 ft.) were obtained as lumped nodal loads through standard Morison-equation type formulation. In the previous study by *Lloyd and Clawson, 1983*, it was found that the load due to the wave from the south was critical compared to waves from other directions. Hence in our analysis, for all wave heights only the broadside wave (from the south), producing maximum base shear, was considered. The probability distribution of the lifetime extreme wave from the south was used in the reliability analysis. A rigorous reliability computation should include the contribution to the structure failure probability due to lifetime extreme waves from all directions. However, because the structure is relatively much stronger for waves from directions other than the south, inclusion of failure events from these other waves is not expected to affect (increase) the system failure probability calculated using only the wave from the south.

32

Based on an analysis using Stokes 5th-order wave-kinematic theory, it was concluded that waves higher than 75 ft. would reach the deck level (+50 ft. level). Rise of mean water level due to storm surge and astronomical tide was neglected. The 100-year (63 ft.) wave has a crest elevation 9.7 feet below the deck level (+50 ft. level). Due to slamming, a jump in wave force was assumed to occur at a wave height of 75 feet. Accurate prediction of the deck slamming loads was considered beyond the scope of this work. The slamming loads were approximated as the force on a broadside deck girder (3 ft. deep and 150 ft. wide) due to the stagnation pressure from a Stokes-5th-order wave of given height (Table 2.1).

Table 2.1 Wave Slamming Forces on Deck

Wave Height (Feet)	Wave Slamming Loads (Kips)
75	673
85	825
92	925
96	976
98	1009

The slamming loads were equally distributed among the nodes on deck level and superposed on nodal wave loads obtained earlier. Figure 2.3 shows the vertical distribution of lateral wave loads (sum of horizontal, y-direction, nodal wave loads at each level with loads at nodes between two levels distributed equally between adjacent levels) for three typical wave-load pattern. The wave loads at each level have been normalized with respect to the base shear of the corresponding cases.

33
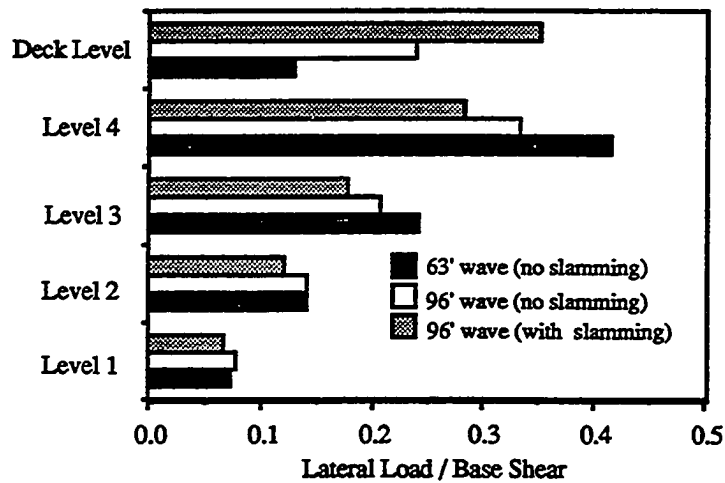
Fig. 2.3 Vertical Distribution of Lateral Wave Load

In all cases of reliability analyses, the dead loads were considered to have fixed pattern (design load) scaled by a randomly varying load factor. The load factor was assumed to be lognormally distributed with a mean = 1.0 and coefficient of variation = 0.1. The probabilistic modeling of the wave load is described below.

2.4 SYSTEM RELIABILITY FRAMEWORK

System reliability analysis consists of analyzing failure events that are expressed as combination of single component failure events. Failure is defined for each component (truss member in our system) by a performance function describing a limit state. The limit state used for the truss members of the example jacket is the condition that the axial member force is equal to its elastic resistance. When a member fails it offers zero stiffness but continues to carry a constant load equal to its post-failure capacity (Fig. 2.2). Recent studies (*Cornell, De, Karamchandani, and Bjerager, 1988*) have verified the adequacy of this simple member model.

A system may fail (according to one or more system failure criteria) as a result of a number of different member-failure sequences. Each sequence of member failures which

34

leads to the system failure is known as a "failure path". Each failure path event can be seen as an intersection of individual component failure events leading to the system failure. Since any failure path leads to the failure of the structure, the system failure event is the union of all failure path events.

2.4.1 Modified "Branch-and-Bound" Algorithm.

For most realistic structures, there exist a large number of possible failure paths. Hence, it becomes necessary to identify and include only the critical failure paths which contribute the most to the probability of occurrence of the union of failure path events. A technique to identify the failure paths which individually have a high probability of occurrence has been developed and implemented in the computer program, "FAILUR" (*Guenard, 1984*). The search technique, a "branch-and-bound" algorithm, has been described in (*Nordal et al., 1987 and Guenard, 1984*). Application of this search technique to the jacket structure under study tended to identify failure path events that involved more or less the same member failures (in different orders). Hence these failure paths represent events that are highly "overlapping", i.e., the probability of occurrence of the union of these failure path events is not significantly larger than that for any individual failure path event even though each of these events has a relatively high probability of occurrence. However, we are interested in identifying critical failure path events such that the probability of occurrence of their union is a maximum, and as yet, there is no optimal procedure to do this. A modified branch-and-bound procedure which identifies failure paths with less overlapping has been proposed and used in this study. The procedure is as follows: after identifying a few failure paths by the branch-and-bound algorithm, one or more key members that often appear in previously generated failure paths are ignored (i.e., the members are modified to be not failable by specifying artificially large capacities). The branch-and-bound algorithm is then again used to identify failure paths which now do not include these key members. Note that the artificial strengthening is used only to identify

35

important sequences (i.e., those likely to contribute significantly to the union event of system failure) which will not otherwise be identified by the branch-and-bound algorithm as important sequences because their individual probabilities of occurrence are lower than some of the most-likely-to-occur but "overlapping" sequences. When computing the probabilities of failure for the individual sequences and the union event of system failure the actual capacities of the members are used. In the case study to follow, the new failure paths / sequences generated by the modified branch-and-bound algorithm were also found to be quite important, i.e., their inclusion contributed significantly to the probability of occurrence of the union event of system failure. However, in some cases the magnitude of probability of failure for these new paths (identified by using a restricted set of members) were much smaller than that of the most important failure path event, and hence, including these paths does not significantly increase the probability of occurrence of the union. In such cases these new failure path events were ignored.

In this study, the probability of system failure is approximated as the union of a finite number (between six and eight for this study) of critical failure path events. Since other paths are neglected, the resulting estimate is a lower bound of the probability of system failure.

2.4.2 Probability Computation

The probability of component failure was obtained by first-order full-distribution method. The probability computations of intersections and unions were done using a computer program developed by *Dr. Rackwitz* and his colleagues at the Technical University of Munich. The program uses the *Hohenbichler* approximation to the multinormal integral and the equivalent hyperplane concept due to Rackwitz. The program, its strengths and limitations are described in *Karamchandani et al., 1986*. Comparison with simulation results is given in Chapter 4.

36

2.4.3 System Failure Criterion

The formal criterion of system failure, as used in this study, is a major loss (50% reduction) of the global stiffness. The global stiffness is measured by the increase in deflection at the center of the deck due to an unit increase in load. It was observed that usually, there was little change in stiffness during the first few member failures but after failure of four to six members, a large change in stiffness often occurred. This large change in stiffness was used to detect system failure. The only exception to requiring failure of four to six members for system failure was in certain failure paths involving diagonals in the top tier when the structural system failure (a large drop of stiffness) occurred after the failure of just two diagonals. It was also observed that after the occurrence of the major loss of stiffness subsequent member failure events had a high probability of occurrence and their inclusion in the failure path did not significantly decrease the probability of occurrence of the failure path. This further validates the use of major loss of stiffness as a system failure criterion for this type of system reliability analysis.

2.5 LIFETIME EXTREME WAVE HEIGHT DISTRIBUTION

The jacket structure in the case study is designed for a hypothetical location in the Gulf of Mexico with a water depth of 140 ft. and a 100-year design wave of 63 ft. (*Lloyd and Clawson, 1983*). The observed values of the coefficient of variation, V_{H_1}, of the annual extreme wave height (i.e., the height of the largest wave in a year, H_1) in the Gulf of Mexico range from 0.12 to 0.55 (*Moses, 1986*). In this study, a representative value of $V_{H_1} = 0.25$ was chosen. Assuming a lognormal form for the annual extreme wave height, and using the value of the 99th percentile equal to the 100 year wave height (i.e., $P\{H_1 < 63\} = 0.99$), the median, m_{H_1}, is calculated to be 35.6 ft., i.e., annual extreme wave height, H_1, is lognormal with $m_{H_1} = 35.6$ ft. and $V_{H_1} = 0.25$.

37

The statistics of the annual extreme wave height can now be used to determine the parameters of the lifetime extreme wave height. The lifetime of the jacket structure is assumed to be 20 years. The lifetime extreme wave height (H_{20}) is the maximum of 20 individual annual extreme waves. If we assume that the annual extremes are independent from year to year (e.g., this year's extreme has no effect on next year's extreme), then we can use simple order statistics to obtain the cumulative distribution function of H_{20} at any point h, i.e., $P\{H_{20} < h\} = (P\{H_1 < h\})^{20}$. Therefore the probability distribution of H_{20} can be estimated from that of H_1. Since the annual extreme wave height, H_1, is lognormal, the lifetime extreme wave height (which is the maximum of 20 annual extremes) will not be lognormal. However, it is common practice (see *Moses, 1986*) to assume a lognormal distribution model for the lifetime extreme wave height as well. For a lognormal model of the extreme lifetime wave height, the extreme lifetime base shear is also lognormal (to be shown later in Equation 2.3) and this simplifies certain calculations (e.g., cov of the extreme base shear can be calculated in closed form from those of the lognormal extreme wave height and the lognormal analysis uncertainty factor, and the reliability index for components can be calculated in closed form for certain simplifying assumptions). *Moses, 1986* shows that the change in reliability index is small between using the "exact" extreme distribution of the base shear and a corresponding lognormal with the same mean and cov. Strictly speaking, the choice of the distribution model for the lifetime extreme will influence the estimated value of its mean and cov. In this study we fit a lognormal distribution to the upper tail (90th and 99th percentile) of the "exact" distribution, i.e., the distribution obtained from order statistics. Because the distribution is fitted in the region of interest (i.e., in the upper tail), the errors introduced by the lognormal approximation are expected to be insignificant. The effect of using extreme value (type 1) distribution model for the extreme wave height has also been investigated in this work.

In any case, using simple order statistics, we can determine the wave height h* which has a 10% chance of being exceeded (i.e., 90th percentile value) in the lifetime of the

38

structure (i.e., $P\{H_{20} < h^*\} = 0.9$ and hence $P\{H_1 < h^*\} = 0.9^{(1/20)}$. Similarly, we can determine the wave height h^{**} which has a 1% chance of being exceeded (i.e., 99th percentile value) in the lifetime of the structure. For our example, $h^* = 66.8$ ft. and $h^{**} = 80.0$ ft.. Hence we have two points on the cumulative distribution function of the lifetime extreme wave height, H_{20}.

The distribution of the lifetime extreme wave height H_{20} is approximated by the lognormal distribution. Using the two points on the cumulative distribution function (i.e., $P\{H_{20} < 66.8\} = 0.9$ and $P\{H_{20} < 80.0\} = 0.99$), the median is calculated to be 53.55 ft. and the coefficient of variation is 0.174, i.e., the lifetime extreme wave height, H_{20}, is assumed lognormal with $m_{H_{20}} = 53.55$ ft and $V_{H_{20}} = 0.174$.

For the structure geometry under consideration, previous studies (*Lloyd and Clawson, 1983*) have shown that broadside waves from the south direction are most critical. Hence in the study we are interested in focusing on the height of the lifetime extreme wave from the south direction, H_{20}^s. *Moses, 1981* suggests that the height of the extreme wave in any specific direction should be 85% of the height of the extreme waves measured over all directions. More work is needed to quantify accurately the directional reduction of the extreme wave height. To understand the distribution of H_{20}^s, we can develop a model similar to the one used to obtain the lifetime extreme from the annual extreme. That is, we divide the compass into sectors, n of which are likely to contain the severe waves. Assume one of the n sectors is the south sector (Fig. 2.4). For each important sector i (i = 1, n), we have a distribution of lifetime extreme wave height H_{20}^i. The lifetime extreme wave height (independent of direction) is the largest of these sector extremes (i.e., $H_{20} = \{$max. H_{20}^i; i = 1, n$\}$). If the number of sectors are large the extreme wave heights from neighboring sectors will be correlated; however no such correlation data are readily available. Hence in order to provide a model for the 15% reduction we consider a small number of sectors so that the extreme wave heights will be independent from sector to sector. Assuming that the heights of waves from all n sectors have the same distribution

39

and are independent, we have, $P\{H_{20} < h\} = (P\{H_{20}^i < h\})^n$. Since the distribution in each sector is the same, we can replace H_{20}^i by H_{20}^s, the lifetime extreme wave height from the south. For a given value of n and a wave height h, this relation can be used to determine the probability that a wave from the south will exceed this value from the distribution of H_{20}. This is done for two values of h, h* and h** (h* = 66.90 ft. and h** = 80.17 ft. respectively correspond to 0.1 and 0.01 probabilities of exceedance for the lifetime extreme H_{20}). With these two points on the cumulative distribution function of H_{20}^s determined from the simple order statistics and assuming that H_{20}^s is lognormal, we can calculate its median and the coefficient of variation .
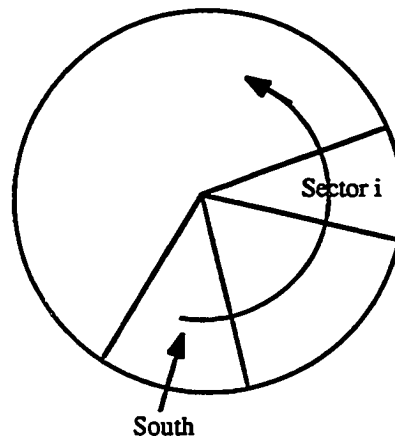
Fig. 2.4 Division of Sea into Sectors (i.e., directions)

Assuming n = 3, we get the median = 46.2 ft. and coefficient of variation = 0.205 for H_{20}^s. The value of n is chosen as 3 because this results in a ratio of medians for H_{20}^s and

H_{20} of 0.86, which is close to the reduction for direction effects suggested by *Moses, 1981*. The above analysis to account for directional effects on the extreme wave height has been presented to serve as a model; future calibration of the model with real directional distribution of wave heights is necessary to quantify directional effects on the extreme wave height accurately.

40

Hence the wave height distribution used in the reliability analysis is the one corresponding to the lifetime extreme wave height from the south, H_{20}^s, i.e., lognormal with median = 46.2 ft. and coefficient of variation = 0.205.

To study the effect of assuming the lognormal form for the extreme wave heights, an extreme value distribution (Type 1) was also developed. The process is similar to the case for the lognormal and is briefly described below. The annual extreme wave height H_1 (with 99 percentile height of 63 ft. and coefficient of variation of 0.25) under the assumed extreme value (Type 1) distribution form has a mean of 35.31 ft., $V_{H_1} = 0.25$ and $\alpha = 0.145$. The lifetime extreme wave height H_{20} is also extreme value distributed (assuming H_{20} is the maximum of 20 independent annual extremes) and has a mean of 55.93 ft., $V_{H_{20}} = 0.158$ and $\alpha = 0.145$. Following the same steps as in the earlier lognormal case and requiring a 15% reduction in the mean for the lifetime extreme wave height from the south, H_{20}^s, we get a mean value of 47.54 ft., $V = 0.186$ and $\alpha = 0.145$, i.e., H_{20}^s:

Extreme value (Type 1) with mean = 47.54 ft. and $V = 0.186$.

2.6 "WAVE-FRAGILITY" ANALYSIS

The "wave-fragility" approach takes into account the correct spatial distribution of nodal wave loads (including slamming forces on deck) as a function of wave height. Lumped nodal wave loads were obtained for regular broadside waves with heights 63 ft., 75 ft., 85 ft., 92 ft., 96 ft., and 98 ft. Deck slamming forces for waves with heights greater than or equal to 75 ft. were distributed equally among the broadside deck level nodes, as described earlier.

The probabilistic wave load model for each wave height (h) is expressed as follows:
$$\Gamma_a \, \underline{l}(h) = \Gamma_a \, \{ \, l_1 \, (h), \quad l_2 \, (h), \quad l_3 \, (h), \, .., \, l_i \, (h), \, ...\}$$
in which Γ_a is a random scale factor representing analysis (Morison's equation, wave kinematics, assumption of regular wave, etc.) uncertainties only, i.e., the inaccuracies in

41

the force given a wave height; and l_i = lumped wave load at joint i. The wave load vector $\underline{l}$ is obtained using Morison's equation. Γ_a is assumed to be lognormally distributed with a unit median and coefficient of variation = 0.25 (*Moses, 1981*). The basic steps in arriving at the probability of system failure are as follows.
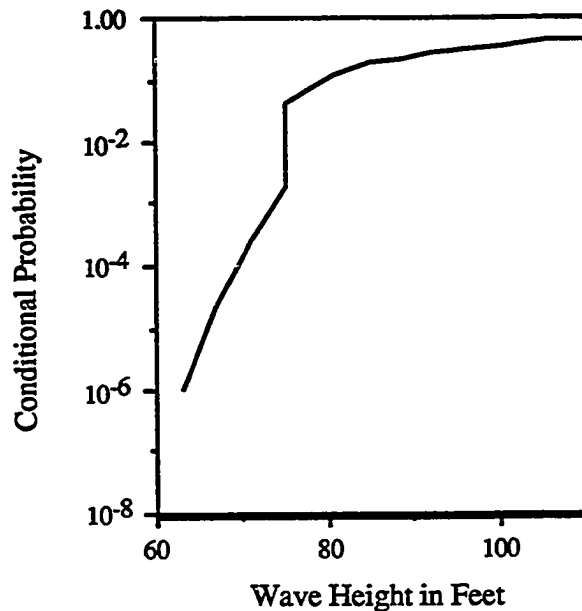
Fig. 2.5.1 Conditional Probability of System Failure Given Wave Height; Case C

Step a): For each wave height, h, at which the vector of nodal loads is available, the conditional probability of system failure, P{system failure I H=h}, is obtained. The graph of conditional probability plotted against wave height is known as the system fragility curve (Fig. 2.5.1) The conditional probabilities of system failure given wave height were calculated at a finite number of wave heights. For this study, lognormal probability distribution curve was fitted piecewise between the calculated values of conditional probabilities. The curve was extrapolated using the conditional probabilities at 85 and 96 foot wave heights to obtain the parameters of the tail. In this case the wave reaches the deck when the wave height is greater than 75 ft.; the additional slamming forces on deck

42

are responsible for the discrete jump in conditional system failure probability at the 75 ft. wave height (Fig. 2.5.1). The case (Case C) corresponding to the fragility curve shown in Fig. 2.5.1 will be described later.
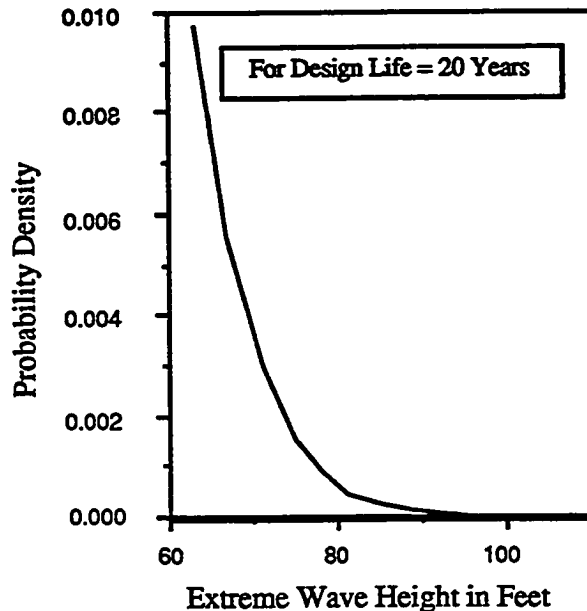
Fig. 2.5.2 Extreme Wave Height Probability Density

Step b): The distribution of extreme wave height (for waves from the south side of the jacket) for the jacket lifetime, 20 years, was assumed to be lognormal (Fig. 2.5.2). The parameters of the distribution were derived from the annual extreme wave height distribution which was modeled as lognormally distributed with a coefficient of variation = 0.25 and a 99-percentile value equal to the 100-year-wave height (63 ft.). The procedure used to calculate the parameters of the distribution for the extreme wave height in 20 years is as outlined in previous section.

43
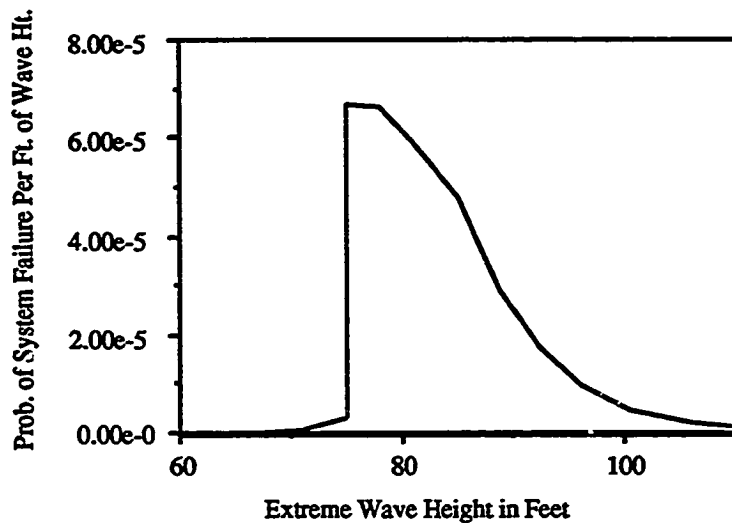
Fig. 2.5.3 System Failure Probability Density; Case C

Step c): The total probability of system failure over the entire range of extreme wave height is computed by removing the conditioning of system failure on wave height [step (a)] by using the extreme wave height distribution [step (b)]. This can be expressed as follows:

$$P\{\text{sys. failure}\} = \int_{h=0}^{\infty} P\{\text{system failure} \mid H=h\} \, f_H(h) \, dh \tag{2.1}$$

where the conditional probability, $P\{\text{system failure} \mid H = h\}$ is shown in Fig. 2.5.1, and the probability density function of the lifetime extreme wave height, $f_H(h)$, is shown in Fig. 2.5.2. The integrand in the Equation 2.1 represents the system failure probability density (i.e., probability of system failure per foot of wave height) as a function of wave height, and is shown in Fig. 2.5.3. The area under the system failure probability density curve gives the total probability of system failure over the entire range of wave height. The system failure probability density curve also graphically demonstrates the relative contribution of each wave height to the system failure. It is clear in this case that the contribution to system failure probability comes exclusively from waves equal to or greater than 75 ft. in height.

44

2.6.1 Results from "Wave-Fragility" Analysis

Three different cases were studied using wave-fragility approach. In the first case, slamming forces on the deck, and failure of the diagonals and the horizontal braces in the top tier were ignored. In other words these members were considered very strong, much above the current code requirements. In the second case, the slamming forces were included but failures in the top tier braces and diagonals were still not considered. In the third case, slamming forces were included and the strengths of the top tier braces and diagonals were based on currently recommended code design values. The phenomenon of these top tier diagonal members being critical became apparent only for load patterns of waves with larger heights, and could not be observed when a fixed load pattern based on the 100 year (63 ft.) design wave was used as in previous studies (e.g., *Nordal et al., 1987 and Guenard, 1984*). These effects were further accentuated by the inclusion of slamming forces. The case descriptions are given in Table 2.2.

Table 2.2 Fragility Analysis Cases

Case #	Wave Slamming Forces on Deck	Top Tier Braces and Diagonals Failable
A	No	No
B	Yes	No
C	Yes	Yes

Case A

The conditional probabilities of system failure are shown in Table 2.3.1 for six wave heights at which load patterns were computed. The total probability of system failure is 4.6 x 10^{-5}. To investigate the sensitivity of the total probability of system failure to the assumed shape of extreme wave height distribution, the computations were also carried out

45

assuming an "Extreme Value Type-I" distribution for the extreme wave height. The parameters of the distribution were calculated from the annual extreme wave height distribution as described in Section 2.5. It resulted in a value of total probability of system failure = 7.2×10^{-5} which is similar to the value of 4.6×10^{-5} in the lognormal distribution case.

In order to reduce the computational effort in the subsequent cases, fragility analysis for Case A was carried out using the conditional failure probability results for only four wave heights, 63, 75, 85 and 96 feet. The computed value of system failure probability, 4.8×10^{-5}, agreed well with the result obtained from using fragility results for all six available wave heights. Therefore, in all the other cases, only these four wave heights were used in the fragility analysis.

Table 2.3.1 System Fragility Results; Case A

Wave Height, H (ft.)	Prob.{System Failure⏐H}
63	9.7×10^{-7}
75	1.0×10^{-3}
85	8.9×10^{-3}
92	1.7×10^{-2}
96	2.5×10^{-2}
98	2.7×10^{-2}
Total Probability of System Failure = 4.6×10^{-5}	

Case B

The conditional probabilities of system failure are shown in Table 2.3.2. The total probability of system failure is 3.3×10^{-4}. Inclusion of slamming forces increased the probability of system failure by an order of magnitude. The contribution to the increase in system failure probability came from the wave heights at which slamming occurred.

46

Table 2.3.2 System Fragility Results; Case B

Wave Height, H (ft.)	Prob.{System Failure|H}
63 (no slam)	9.7×10^{-7}
75 (no slam)	1.0×10^{-3}
75 (with slam)	2.0×10^{-2}
85 (with slam)	5.2×10^{-2}
96 (with slam)	1.1×10^{-1}
Total Probability of System Failure = 3.3×10^{-4}	

Case C

The conditional probabilities of system failure are shown in Table 2.3.3. The total probability of system failure is 9.5×10^{-4}. As mentioned before, in the reliability analysis the search is restricted to a small set of critical members . In both Cases A and B, failure of the horizontal braces and vertical diagonals in the top tier (Tier 4) were ignored based on earlier studies using the fixed pattern (100-year wave) approach (e.g., *Nordal et al., 1987*). However, it became evident during the analyses with higher wave heights (especially with slamming forces) that the top tier braces and diagonals may be very important with respect to the system failure. They were considered failable in Case C. Comparison between results of Case C and that of Case B gives an opportunity to compare the gain in reliability if those members are strengthened beyond their current design values (as in Case B). There is about a factor of 3 reduction in the probability of failure if the top tier braces and diagonals are strengthened so that they are not likely to fail.

47

Table 2.3.3 System Fragility Results; Case C

Wave Height, H (ft.)	Prob.{System Failure|H}
63 (no slam)	9.7×10^{-7}
75 (no slam)	1.9×10^{-3}
75 (with slam)	4.4×10^{-2}
85 (with slam)	1.9×10^{-1}
96 (with slam)	3.1×10^{-1}
Total Probability of System Failure = 9.5×10^{-4}	

Failure Sequence Comparison (Case C)

To investigate the relative importance of typical failure sequences at different wave heights, the following sequences were studied. These particular sequences were chosen to represent failures in different tiers of the structure. Table 2.4.1 describes the composition of these sequences, i.e., the order in which particular members failed and whether the member failed in tension or in compression. Refer to Appendix I for member numbering.

Table 2.4.1 Description of Sequences

Sequence	Member Sequence Description[1]	
1	47, 41, -45[2], -49, -43;	(Tier 1)
2	99, 103, -101, -97, 93;	(Tier 2)
3	151, 141, 145, -147, -143;	(Tier 3)
4	194, -193;	(Tier 4)
5	141, 160, 151, 192, 167;	(Tier 3 and 4)

For Case C, Table 2.4.2 shows the fragility analyses results for each of the typical sequences described above. In general, the sequence failure probability increases with the

---

[1]Refer to Appendix I for details of the structural model
[2]Minus sign denotes failure of the member in tension.

48

wave height, as expected, due to the increased lateral load magnitude. To get a feel for the change in the relative importances of the different failure sequences due to the variation of spatial pattern at each wave height, the conditional probabilities of occurrences of the sequences, normalized by the conditional probability of system failure at each wave height are presented in Table 2.4.2. The results are graphically presented in Fig. 2.6. Note that these normalized values represent the relative importance of the sequences but do not represent the actual relative contribution of each sequence (this is because the sequences are not disjoint and hence the probability of system failure, which is the union of the sequence events, is not simply the sum of the probabilities of occurrence of individual sequences).

The results clearly demonstrate that failure sequences involving top tier members play an increasingly important role at higher wave heights, and contribute most to the total probability of system failure (Table 2.4.3). This effect cannot be captured by approaches that are based on a 100-year wave pattern over the entire range of wave height (e.g., *Nordal et al., 1987*).

Table 2.4.2 Comparison of Conditional Failure Probabilities of Typical Sequences at Each Wave Height; Case C

Wave Ht., H (ft.)	P{sys.Failure I H} = Normalizing Factor	Prob.{Sequence Failure I H}: (Normalized Results)				
		Seq.1	Seq.2	Seq.3	Seq.4	Seq.5
63 (no slam)	9.7e-7	7.2e-8 (0.07)	4.8e-7 (0.50)	1.3e-7 (0.14)	3.1e-15 (0.00)	7.2e-10 (0.00)
75 (no slam)	1.9e-3	1.0e-4 (0.05)	5.0e-4 (0.26)	6.0e-4 (0.31)	6.7e-5 (0.03)	1.0e-3 (0.54)
75 (with slam)	4.4e-2	5.6e-4 (0.01)	3.1e-3 (0.07)	7.0e-3 (0.16)	2.2e-2 (0.51)	2.7e-2 (0.63)
85 (with slam)	1.9e-1	4.9e-3 (0.03)	1.9e-2 (0.10)	3.6e-2 (0.19)	1.1e-1 (0.58)	1.1e-1 (0.61)
96 (with slam)	3.1e-1	2.2e-3 (0.07)	5.5e-2 (0.18)	7.8e-2 (0.25)	2.0e-1 (0.64)	2.0e-1 (0.65)

49

Table 2.4.3 Comparison of Total Failure Probabilities of Typical Sequences; Case C

Wave Ht., H (ft.)	P{sys.Failure} = Normalizing Factor	Prob.{Sequence Failure}: (Normalized Results)				
		Seq.1	Seq.2	Seq.3	Seq.4	Seq.5
All	9.5e-4	2.9e-5 (0.03)	1.0e-4 (0.11)	1.8e-4 (0.19)	5.3e-4 (0.56)	5.9e-4 (0.62)
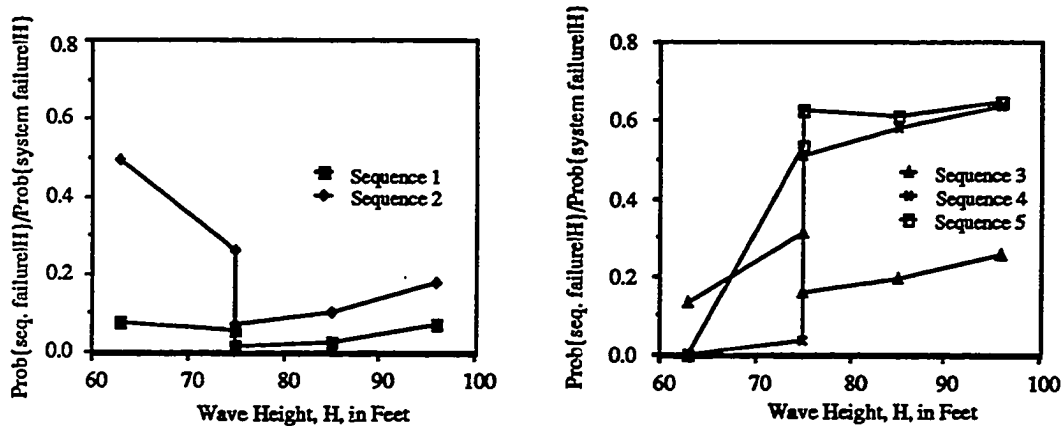
Fig. 2.6 Comparison of Normalized Conditional Failure Probabilities of Typical Failure Sequences at Each Wave Height

2.7 "FIXED-PATTERN" APPROACH

In previous studies (e.g., *Nordal et al., 1987; Guenard, 1984*; etc.), the system reliability estimate is obtained by a single analysis based on a spatial load pattern obtained from one wave height, e.g., the 100-year design wave. One of the aims of wave-fragility analysis in this study is to evaluate results from such simplified fixed-pattern approaches. In the fixed-pattern approach, the vector of wave loads is modeled as a constant, unit magnitude, nodal force pattern scaled by the base shear (the total lateral wave load

50

magnitude) which is considered random. The nodal force pattern is based on the vector of nodal wave forces due to the 100-year design wave. The base shear, f, is assumed to have an empirical relationship with wave height, h, of the form:

$$f = ch^\alpha \tag{2.2}$$

where, the constants c and α are obtained from the base shear values calculated for different wave heights. If wave load and hence base shear is available only for one wave height, e.g., the 100-year wave, then it is necessary to assume a value of α (usually ≈ 2) and calculate c using Equation 2.2. Alternatively if wave load (including slamming forces on deck) are available for a number of wave heights then c and α can be estimated by linear regression in log space.

Once c and α are determined, a probabilistic model of the base shear can be described as follows:

$$F_{20}^S = \Gamma_a c (H_{20}^S)^\alpha \tag{2.3}$$

where, F_{20}^S = base shear corresponding to the life time (20 years) extreme wave from the south.

c, α = constants estimated from wave load values at different wave heights using Equation 2.2.

Γ_a = analysis uncertainty factor in estimating the force given a wave height (e.g., Morison's equation, wave kinematics etc.); as in the fragility analysis, this is assumed to be lognormal with unit median and coefficient of variation = 0.25 (*Moses, 1986*).

H_{20}^S = height of the lifetime extreme wave from the south; lognormal with median = 46.2 ft. and coefficient of variation = 0.20. See Section 2.5 for details.

51

Because H_{20}^s and Γ_a are lognormal and are assumed to be independent, F_{20}^s is also lognormal and the parameters of the distribution of F_{20}^s can be easily obtained from that of H_{20}^s and Γ_a. The uncertainty due to the empirical nature of Equation 2.2 is neglected. Also implicit in Equation 2.3 is the assumption that the lifetime extreme base shear, F_{20}^s, occurs under the lifetime extreme wave height, H_{20}^s. Note that the cov of the analysis uncertainty factor, Γ_a, used in this study is not based on uncertainties specifically applicable to wave heights close to the extreme value (*Moses, 1986*). Alternatively, one could apply Γ_a independently to each wave to obtain the base shear for each wave and then develop an annual or lifetime extreme base shear distribution using simple order statistics.

2.7.1 Results from "Fixed-Pattern" Approach

The accuracy of the results depends on the constants c and α, and the spatial distribution of the fixed pattern. Both the previously used approach (i.e., $\alpha = 2$, pattern and c based on 100-year wave load) and suggested improvements are discussed below.

Case D

This case is analogous to the standard design practice in which only the wave load corresponding to the 100-year design-wave height is used. α was assumed to be equal to 2.0, and $c = 0.666$ was obtained from Equation 2.2, knowing that the base shear for the 100 year (63 ft.) wave was 2641.9 kips. The normalized wave pattern corresponding to the 100-year-wave height (63 ft.) was used. Hence, the method takes into account neither the effects of increased load magnitude nor the changed lateral wave-load distribution patterns (Fig. 2.3) due to the slamming forces acting on deck at higher wave heights. This approach has been used in most previous system reliability studies.

52

Case E

This case represents the approach taken when wave loads are available for a number of different wave heights higher than the 100-year wave. The constants, $\alpha = 2.02$ and $c = 0.677$ were obtained from a linear regression analysis of Equation 2.2 in log space with base shear values at 63, 75, 85, 92, 96, and 98 feet. Slamming loads on deck are included in base-shear calculations. However, the fixed pattern used for this analysis is that of the 100-year design wave, which does not include slamming forces.

Case F

In this case, an attempt is made to use a wave load pattern which is similar to the waves that contribute the most to system failure probability. Because it is not known a priori (i.e., without carrying out a full-scale fragility analysis) which wave heights contribute the most to system failure probability, this procedure involves a two-stage analysis. In the first stage, a preliminary analysis (based on the 100-year wave results, i.e., similar to Case D above) is used to approximately estimate the wave height (h*) at which system failure is "most likely to occur" (see Section 2.8). From the available base shear results, the base shears corresponding to the wave heights closest to h* (one larger height, and one smaller) are used in Equation 2.2 to determine the constants, α and c. The pattern corresponding to the height that is closest to h* is selected for use in the next stage of analysis. With these values of α and c and the fixed pattern, a second reliability analysis is done. The results of the second analysis are used as the estimate of system failure probability. The critical wave height h* was found to lie between 75 and 85 ft. The constants, α and c, (fitted at these two points) were found to be 1.447 and 9.229, respectively. The 75 ft. pattern was used in this analysis. The results are expected to be similar if the 85 ft. pattern is used. Note that this procedure includes a more accurate representation of the wave load with respect to both the constants α and c and the wave pattern.

53

In all three Cases, D, E, and F, all the members are considered failable including the top-tier diagonals and bracing members. However, since Cases D and E use the 100-year-wave pattern the diagonals and braces in the top tier are not part of the critical failure paths. The results of the analysis (along with those of Case C of the wave-fragility analysis as reference) are presented below.

The system failure probabilities for the three fixed-pattern approaches (and the fragility approach, Case C, as reference) are given in Table 2.5.1. The estimates based on the 100-year wave (Cases D and E) underestimate the probability by roughly an order of magnitude compared to the reference value (Case C). The use of more base shear values spanning the wave height range in estimating constants c and α, as in Case E, gives a better estimate of the failure probability than Case D; but is still unsatisfactory. In contrast, the results from Case F, in which the constants c and α and the wave pattern are based on the wave height which is estimated to contribute most to the system failure, agree well with the reference value. It should be pointed out that the close agreement of the system failure probabilities between Case D and Case A (fragility analysis with no slamming load, see Table 2.3.1) is purely coincidental. The choice of design wave-load pattern and the use of $\alpha = 2$ in Case D is arbitrary.

Table 2.5.1 Comparison of System Failure Probability between Wave Fragility Analysis and Fixed-pattern Approaches

Case	Description	P{Sys.Fail.}
C	Fragility approach; with slamming; top diagonals failable	9.5×10^{-4}
D	Fixed (63 ft.) pattern; no slamming; $\alpha = 2$	0.4×10^{-4}
E	Fixed (63 ft.) pattern; α and c from regression	0.8×10^{-4}
F	Fixed (75 ft.) pattern; α and c from 75 and 85 ft. wave base shear	12.9×10^{-4}

54

Failure Sequence Comparison (Fixed-pattern vs. Fragility)

Table 2.5.2 below shows the relative importance of different failure sequences (described in Table 2.4.1) for Cases C, E, and F. As expected, the fixed-pattern approach, Case F (using the wave pattern corresponding to the estimate of wave height at which failure is most likely to occur) ranks the sequences with respect to probability of failure in the same order as the more accurate fragility approach of Case C. Also as expected, the sequences involving the diagonals and braces in the top tier are relatively unimportant in Case E which uses the 100-year wave pattern.

Table 2.5.2 Comparison of Total Failure Probability of Typical Sequences between Wave-Fragility Analysis and Fixed-pattern Approaches

Case	Probability {Sequence Failure}				
	Seq.1	Seq.2	Seq.3	Seq.4	Seq.5
C	2.9e-5	1.0e-4	1.8e-4	5.3e-4	5.9e-4
E	2.6e-5	5.0e-5	3.0e-5	3.0e-8	2.4e-6
F	2.8e-5	1.1e-4	2.2e-4	6.6e-4	7.9e-4

2.8 ESTIMATING THE WAVE HEIGHT AT WHICH SYSTEM FAILURE IS "MOST LIKELY TO OCCUR" (WITH REFERENCE TO CASE D)

In the fixed-pattern approach, the load is defined as $F_{20}^s\{1\}$, where $\{1\}$ is a fixed spatial pattern of unit magnitude and F_{20}^s is the base shear. The base shear is a function of the wave height, H_{20}^s, the analysis uncertainty factor Γ_a and constants α and c (per Equation 2.3). Using the "fixed pattern approach", for a given pattern $\{1\}$ (e.g., wave-load pattern corresponding to the 100 year design wave) and constants α and c, we can determine the probability of system failure (e.g., Case D). However, the accuracy of system reliability estimation by this simple one-step fixed pattern approach can be significantly improved if a more appropriate.load pattern corresponding to the wave height at which system failure is

55

most likely to occur is used (e.g., Case F). An accurate estimation of the wave height at which system failure is most likely to occur would require using the more rigorous fragility approach (see Fig. 2.5.3). Because the objective here is to improve system reliability assessments using the simpler fixed pattern approach, an approximate method to estimate the critical wave height (at which system failure is most likely to occur) has been developed. This procedure and an example application (Case D in the study) are described below.
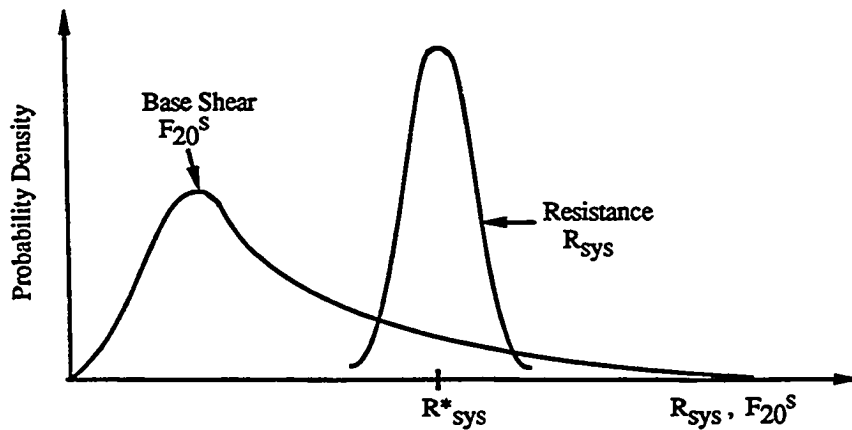
Fig. 2.7 Probability Density Functions for R_{sys} and F_{20}^s

Since the load pattern is fixed, the load can be represented by a scalar random variable (e.g., base shear) and we can think of the structure as having a scalar but random system capacity R_{sys} in load units (also see Chapter 4), i.e., R_{sys} {!} is the largest load the structure can sustain without system failure. The value of R_{sys} depends on the capacities of the members in the system. The system failure criteria can be written in terms of R_{sys} (i.e., $F_{20}^s > R_{sys}$ and probability of system failure, $P_f = P\{F_{20}^s > R_{sys}\}$) (see Fig. 2.7). In

Chapter 4 it will be shown that because the coefficients of variation of the individual member capacities are small (compared to the load cov), the coefficient of variation of R_{sys} is also small. In this reliability problem the variability in the wave load (due to

56

uncertainties in H_{20}^s and Γ_a) dominates over that of the system capacity. Hence, for the analysis to follow we approximate the random system capacity, R_{sys}, by a deterministic constant R_{sys}^* (but the value R_{sys}^* is difficult to estimate). Given the distribution of F_{20}^s (lognormal, median = 1420 kips and V = 0.506), the probability of system failure, (P_f = 0.4 x 10^{-4}), we can approximate the value of R_{sys}^* to match the system failure probability (i.e., $R_{sys}^* = F^{-1}$ (1 - P_f) = 9407, where F($\cdot$) is the cumulative distribution function of the base shear F_{20}^s). Hence in Case D, the system failure event can be written approximately as $\{F_{20}^s > 9407\}$.

This can be rewritten as $\{\ln F_{20}^s > \ln 9407\}$ or, $\{\ln \Gamma_a + \ln C + \alpha \ln H_{20}^s > 9.149\}$ (using Equation 2.3). Substituting the values of c and α, we get $\{\ln \Gamma_a + 2 \ln F_{20}^s > 9.556\}$. The next step is to transform the problem into standard normal space, i.e., using appropriate probability preserving transformation (see *Madsen et al., 1986*):

$$U_1 = \frac{\ln \Gamma_a - \ln m_{\Gamma_a}}{\sigma_{\ln \Gamma_a}} \quad \text{and} \quad U_2 = \frac{\ln H_{20}^s - \ln m_{H_{20}^s}}{\sigma_{\ln H_{20}^s}},$$

i.e., $(\sigma_{\ln \Gamma_a} U_1 + \ln m_{\Gamma_a}) + 2(\sigma_{\ln H_{20}^s} U_2 + \ln m_{H_{20}^s}) > 9.9556$

Substituting values of $\sigma_{\ln \Gamma_a}$, m_{Γ_a}, $\sigma_{\ln H_{20}^s}$, and $m_{H_{20}^s}$, we get the system failure event as:

$$\{0.246 U_1 + 0.4067 U_2 - 1.89 > 0\} \tag{2.4}$$

57
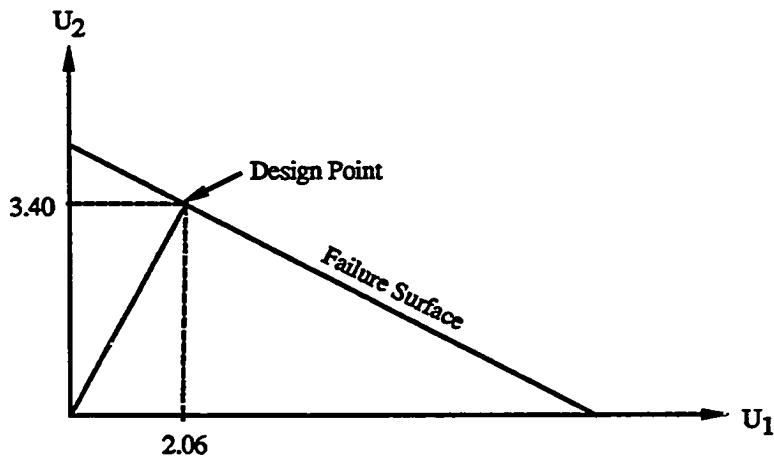
Fig. 2.8 Failure Surface (approx.) in Standard Normal Space

Fig. 2.8 shows the failure surface (which is a straight line given by Equation 2.4) in the standard normal space (i.e., U_1 - U_2 plane) for the approximate system failure event given by Equation 2.4. The design point in the standard normal space, i.e., the point on the failure surface nearest to the origin ($u_1 = 2.06$, $u_2 = 3.40$ in Fig. 2.8) is the point at which failure is most likely to occur (in $\underline{u}$-space, see *Madsen et al., 1986*) and the wave height corresponding to this point is 92 ft.. The corresponding base shear, c $(H_{20}^s)^\alpha =$

5637 kips. However, due to slamming forces, it is seen from the calculation that a base shear of 5637 kips occurs for a wave which is in the 75-85 foot range. Hence for further fixed-pattern analysis, the two base shear values at 75 ft. and 85 ft. wave height can be used to determine the constants c and α. Also it should be noted that the real problem has more random variables (e.g., random member capacities) and hence the projection on the U_2 axis at the design point will be smaller (i.e., the true critical height is smaller than that determined in the approximate analysis) and hence in our study (Case F), we chose the wave load pattern corresponding to the wave height 75 ft. as the fixed pattern.

58

2.9 SYSTEM EFFECTS: COMPARISON BETWEEN FIRST-MEMBER AND SYSTEM-LEVEL FAILURE PROBABILITIES

In this section, failure probabilities for single members, i.e., first-member failure probabilities are presented. Also included is a discussion on "complexity" and "redundancy" factors (also see Chapter 4) in light of the results of system-level and first-member failures.

For each member, the probability that it fails in the intact structure is calculated. The member with the largest probability is called the *most-likely-to-fail (MLM)* member. We also compute the probability that *any-first (member) failure (AFF)*, i.e., at least one member failure, occurs. This is the probability of occurrence of the event corresponding to the union of all first member failures. In practice only about eight members contributed to the probability of the union.

Table 2.6.1 System Fragility Results Conditional on Wave Height; Case C

Wave Height, H (ft.)	P{Sys.Fail|H}	P{MLM|H}	P{#192 FF|H}	P{AFF|H}
63 (no slam)	9.7e-7	3.0e-5	negligible	7.2e-5
75 (no slam)	1.9e-3	1.5e-2	8.5e-5	2.3e-2
75 (with slam)	4.4e-2	8.1e-2	2.7e-2	1.3e-1
85 (with slam)	1.9e-1	2.2e-1	1.2e-1	3.4e-1
96 (with slam)	3.1e-1	3.3e-1	2.1e-1	4.7e-1

Table 2.6.2 Comparison of Total Probability of Failure Between Fragility and Fixed-Pattern Approaches

Case	P{Sys.Fail}	P{MLM}	P{#192 FF}	P{AFF}
C	9.5e-4	13.6e-4	6.1e-4	21.2e-4
E	0.8e-4	2.3e-4	negligible	5.4e-4
F	12.9e-4	27.2e-4	8.7e-4	46.6e-4

59

Tables 2.6.1 and 2.6.2 summarize the results of intact structure and system-level failure probabilities for the fragility and fixed-pattern approaches. The intact structure results include the failure probabilities for the MLM member (which was always member 151 for the cases studied), for member 192, and the probability of any first member failure. Member 192 is a diagonal member in the top tier that has a much lower probability of failure (than the MLM, member 151) in the intact structure for wave load patterns without slamming, but the failure probability of member 191 is comparable to that of the MLM (member 151) for larger waves with slamming. Also for wave patterns with slamming, the conditional probability of system failure given the failure of one of the top tier diagonals is very high. This behavior is reflected at the system level where the critical sequences do not include the diagonals in the top tier for waves without slamming, but do for waves with slamming (see Tables 2.4.1, 2.4.2 and 2.4.3).

Complexity and Redundancy Factors

The system effects are expressed through the following factors (see *Cornell, 1987* and Chapter 4):

$$\text{Complexity Factor } (C_o) = \frac{P\{AFF\}}{P\{MLM\}}$$

$$\text{Redundancy Factor } (R_o) = \frac{P\{\text{System Failure}\}}{P\{AFF\}}$$

$$\text{System Factor} = \frac{P\{\text{System Failure}\}}{P\{MLM\}} = C_o R_o$$

60

Table 2.7.1 Complexity and Redundancy Factors Conditional on Wave Height;
Fragility Analysis, Case C

Wave Height, H (ft.)	Complexity Factor (C_o)	Redundancy Factor (R_o)	System Factor (C_oR_o)
63 (no slam)	2.4	0.01	0.03
75 (no slam)	1.56	0.09	0.1
75 (with slam)	1.6	0.3	0.5
85 (with slam)	1.5	0.6	0.8
96 (with slam)	1.4	0.7	0.9

Table 2.7.2 Comparison of Complexity and Redundancy Factors Between Fragility
and Fixed-Pattern Approaches

Case	Description	Comp. Fac. (C_o)	Red. Fac. (R_o)	Sys. Fac. (C_oR_o)
C	Fragility; with slamming; top diagonals failable	1.6	0.5	0.7
E	Fixed (63 ft.) pattern; α and c from regression	2.3	0.2	0.4
F	Fixed (75 ft.) pattern; α and c from 75 and 85 ft. wave base shear	1.7	0.3	0.5

Tables 2.7.1 and 2.7.2 show the system factors calculated for different cases. It is interesting to note that the complexity factors decrease with increasing wave heights while the redundancy factors increase. These trends can be explained. Wave patterns corresponding to higher wave heights, especially due to slamming forces, induce relatively higher stresses in only a few members near the top. In contrast, the stresses due to the design (100-year, 63 ft.) wave-load pattern are more evenly distributed, and hence the number of critical members is large. The larger number of critical members implies that there are more members that are potential first member failures. Hence the increase in the probability of any (i.e, at least one) first member failure relative to the probability of the

61

MLM member is relatively larger for the wave loads corresponding to lower wave heights, and this explains the increase in complexity factor for the lower wave heights.

At higher wave heights, with slamming forces acting, the critical sequences include top tier diagonal members which (unlike the lower tier diagonals) are not X-braced. Hence failure of a bent at the top tier requires only one member failure, while at a lower tier it requires two failures. Also the X-configuration requires both a compression and a tension failure, and because the tension failures are less likely, the probability of failure for the complete X-brace is much smaller than that for its first member failure in compression. The postfailure capacity of the X-brace is also higher than that of the single diagonal in compression. Hence, there is a greater post-first failure strength in the lower X-braced tiers compared to the single-member-tier configuration. This additional overload capacity of X-braced tiers explains the decrease in redundancy (i.e., increase in redundancy factor, R_o) at higher wave heights. Results in Table 2.7.2 can be similarly explained because Case E uses the 100-year (63 ft.) wave-load pattern and consequently has the lowest redundancy factor. However the change in redundancy factors reported in Table 2.7.2 (where failure is not conditional on any wave height) with wave pattern is not as significant as in the case of redundancy factors conditional on wave height (Table 2.7.1). Small values of redundancy factors conditional on lower wave heights can be explained by the combination of lower mean (because of lower wave height) and lower cov (because of conditioning on the wave height) of the wave load compared to the other load cases.

Even though the probability of system failure for Case E is different from that of Cases C or F (where slamming forces are included in the load pattern) the system factors are in the same order of magnitude. Hence, in this case the same general system effects can be observed although the extent varies with load pattern.

62

An Approximate Measure of Redundancy Factor : Some Observations

The system redundancy factor is defined as the ratio of the probability of system failure to the probability of any first (member) failure. The ratio of the failure probability of a single critical sequence to the failure probability of most-likely-to-fail member in that sequence is also a function of the system redundancy. The following study was carried out to see if the latter ratio can be used as an approximation for the redundancy factor, R_o, i.e.,

$$\text{Approx. } R_o = \frac{\text{Prob.\{Failure of a critical sequence\}}}{\text{Prob.\{Most-likely-to-fail member belonging to the critical sequence\}}}$$

Such an approximation, if accurate, would make it possible to approximate the system failure probability from the failure probability of a single critical sequence (e.g., the most-likely-to-fail sequence) which is easier to calculate. To test the hypothesis the approximations based on two sequences, sequence 3 and sequence 5, are presented in Tables 2.8.1 and 2.8.2 below. These sequences were chosen because they are critical, i.e., have high probability of occurrence, for two different types of wave patterns. In particular, sequence 5 is the most-likely-to-occur sequence for the load patterns involving slamming and / or higher wave heights, and sequence 3 is the most-likely-to-occur sequence due to a wave pattern corresponding to a wave height of 75 ft. without slamming (see Tables 2.4.2, 2.4.3, and 2.5.2). For the case of 63 ft. wave height and no slamming, sequence 3 ranks a close second to sequence 2 in probability of occurrence (see Tables 2.4.2 and 2.5.2). Sequence 3 was chosen because unlike sequence 2 it includes the most-likely-to-fail member (member 151) for the overall structure (see Table 2.4.1). Among all the members in both sequence 3 and sequence 5, member 151 is the most-likely-to-fail member (in the intact structure)

63

Table 2.8.1 Exact and Approximate Redundancy Factors Conditional on Wave Height; Fragility Analysis, Case C

Wave Height, H (ft.)	P{Sys.Fail|H} (Red. Fac., R_o)	P{AF|H}	P{#151 FF|H}	P{seq 3 Fail|H} (Approx. R_o)	P{seq 5 Fail|H} (Approx. R_o)
63 (no slam)	9.7e-7(0.01)	7.2e-5	3.0e-5	1.3e-7(0.004)	7.2e-10(0.2e-4)
75 (no slam)	1.9e-3(0.09)	2.3e-2	1.5e-2	6.0e-4(0.04)	1.0e-3(0.07)
75 (with slam)	4.4e-2(0.3)	1.3e-1	8.1e-2	7.0e-3(0.09)	2.7e-2(0.3)
85 (with slam)	1.9e-1(0.6)	3.4e-1	2.2e-1	3.6e-2(0.2)	1.1e-1(0.5)
96 (with slam)	3.1e-1(0.7)	4.7e-1	3.3e-1	7.8e-2(0.2)	2.0e-1(0.6)

Table 2.8.2 Exact and Approximate Redundancy Factors for Fragility and Fixed-Pattern Approaches

Case	P{Sys.Fail} (Red. Fac., R_o)	P{AFF}	P{# 151 FF}	P{seq 3 Fail} (Approx. R_o)	P{seq 5 Fail} (Approx. R_o)
C	9.5e-4(0.5)	21.2e-4	13.6e-4	1.8e-7(0.1e-3)	5.9e-4(0.4)
E	0.8e-4(0.2)	5.4e-4	2.3e-4	3.0e-5(0.1)	0.02e-4(0.01)
F	12.9e-4(0.3)	46.6e-4	27.2e-4	2.2e-4(0.1)	7.9e-4(0.3)

For cases involving load patterns of higher waves including slamming, sequence 5 is the most-likely-to-occur and the approximate redundancy factors calculated from failure probabilities of sequence 5 are in close agreement with the exact values. For cases involving load pattern of the 100-year wave and load patten of 75 ft. wave without slamming, sequence 3 has higher probability of occurrence than sequence 5 (see Tables 2.4.2 and 2.5.2) and the approximate redundancy factors calculated from its failure probabilities are in close agreement with the exact values.

Based on numerical evidence from the structure under study it appears that such an approximation is feasible if the proper critical sequence is chosen. Note that, member 151 is the most-likely-to-fail member in both sequences, even though 151 is not the first

64

member failure in sequence 5 (see Table 2.4.1). The agreements above may be simply coincidental patterns in the results. Further investigation is required before the conclusion can be generalized for other structures.

2.10 SUMMARY

The study has demonstrated the use of the **wave-fragility** approach in system reliability analysis for a typical fixed offshore jacket structure. The relative importance of different failure sequences has been found to change with load patterns corresponding to different wave heights. Inclusion of slamming forces on deck was found to be critical. In this example, it increases the probability of system failure by an order of magnitude and changes the relative importance of failure sequences (i.e., different members are part of the critical sequences when slamming is included). The system failure probability was not found to be sensitive to the assumed shape of the annual extreme wave height distribution (given the fitting procedure outlined in Section 2.5). Results from simplified fixed-pattern analyses were calibrated against fragility analysis. While computationally much simpler, the fixed-pattern approach can work well only if the "appropriate" wave pattern is used. An approximate procedure to obtain the "appropriate" wave load pattern is outlined in Section 2.8. Results for single member failures and comparison with the results for system failure (i.e., complexity and redundancy factors) are presented in Section 2.9.

65

CHAPTER 3

SPATIAL CORRELATION OF NODAL WAVE FORCES IN SYSTEM RELIABILITY ANALYSIS OF OFFSHORE STRUCTURES

The current practice of wave-load modeling for failure path based system reliability analysis consists of using a deterministic wave-load pattern (corresponding to the position of a regular design wave with respect to the structure when the base shear is maximum) scaled by the total lateral load (base shear) which is considered random. Realistically, however, local variations due to uneven marine growth and local uncertainties in modeling wave kinematics, forces, etc., result in less than this implied perfect correlation among the nodal wave forces. Given the importance of the load aspects of the problem (see Section 2.8) the question arises as to what the effects of the typical (fully correlated) nodal force assumption are on system reliability assessments.

In the present work, an analytical form is assumed for the spatial distribution of correlation between nodal wave forces. The parameters of the model include a base (non-ergodic level) correlation and rates of decay in each of the three dimensions in space. A framework is developed for the probabilistic description of nodal wave forces, consistent with the prescribed correlation structure and the available information on the base shear distribution. The structure analyzed is the same space truss model of the eight-leg steel offshore jacket in 140 feet of water analyzed in Chapter 2. The postfailure model of the truss elements and the system failure criterion used in this study are as described in Chapter 2. Also as in Chapter 2, "failure path approach" has been used in probability computation.

A parametric study is carried out to investigate the effects of variation of the correlation model parameters on both the member level and system level failure probabilities including changes in potential failure sequences.

66

Finally the correlation model is calibrated based on the published wave-loading results from the Ocean Test Structure (*Dean et al., 1979; Haring et al., 1979; and Heideman et al., 1979*).

3.1 INTRODUCTION AND BACKGROUND

The deterministic approach of calculating wave loadings on fixed offshore jackets in shallow to moderate water depths involves the following steps:

i) selecting a design wave height and period (usually with 100 year mean return period) through extreme value analysis;

ii) selecting an appropriate regular wave theory (e.g., Airy wave, Stokes Vth order, etc.) to calculate fluid kinematics for the design wave;

iii) calculating the wave forces on the structure from the calculated fluid kinematics using the Morison equation with appropriate values of drag and inertia coefficients, C_D and C_M.

A number of wave-load conditions are generated corresponding to the various positions of the design wave relative to the structure, and the structural members are designed to withstand them.

The wave forces acting on an offshore structure can truly be represented only by a random field varying both in time and space. In addition to the inherent randomness of the waves, considerable uncertainties are introduced in the reliability problem due to modeling errors. When modeled by a regular wave theory uncertainty in fluid kinematics may be due to the irregularity, directional spread, and because of the shielding effects due to the presence of the structural members. A second set of uncertainties are involved in using a standard set of drag and inertia coefficients in force prediction due to changes in local flow parameters and uneven marine growth.

Due to limitations in our capability of analyzing nonlinear structural behavior and difficulty in subsequent probability computations, a simplified probabilistic description of

67

the wave loading is typically used in current system reliability analysis of offshore structures (e.g., *Cornell et al., 1988; Nordal et al., 1987; Chan et al., 1987; Guenard, 1984; Wu and Moan, 1989*). The entire wave-load pattern is considered deterministic while its magnitude is considered random. It is also assumed that for most of the critical members the maximum load effects are reached when the base shear (i.e., the total lateral load) is maximum. The system reliability can then be evaluated using the load pattern corresponding to the position of the design wave producing maximum base shear. While the practice of modeling the entire wave loading by a single random variable produces much desired computational ease, the wave loads acting on different members are far from perfectly correlated due to local randomness and modeling uncertainties (irregular surface wave elevation, local variations in fluid kinematics, drag and inertia coefficients, uneven marine growth, etc.) even though they may arise from the same wave characterized by a given height and period. In response, *Bjerager et al., 1987*, have modeled the drag and inertia coefficients and the excess thickness due to marine growth as spatial Gaussian white noise processes over the structure. In this work we have assume a more general spatial correlation model among the nodal wave forces and calibrate the model from available information on spatial correlation among parameters influencing the wave kinematics and the subsequent wave-force prediction.

3.2 WAVE-FORCE MODEL

In Chapter 2 the randomness of the wave loads was represented by a single random variable (the random base shear) for both the "fixed pattern" and "fragility" analyses. Hence, the nodal forces were assumed to be fully correlated, i.e., if forces were known at one node, the forces at all other nodes were also known. In contrast the wave forces in this chapter are modeled by a random vector, $\underline{F}$, whose components are F_i , the lateral nodal wave force in the y-direction (see Fig. 2.1) at node i ($i = 1, 2, 3, ..., n_n$ the number of nodes). It is further assumed that the nodal wave forces in x, y, and z directions (see Fig.

68

2.1) at each node are fully correlated and hence can be fully characterized by F_i, the y-direction nodal wave force at that node. The nodal wave-force vector, F, is characterized by its second moment, i.e., mean and covariance matrix.

In order to reduce computational efforts in this sensitivity study we neglect the variation of mean wave-load pattern with wave height. That is, we use the "fixed pattern" approach instead of the more rigorous "fragility" approach. In view of the study in Chapter 2, we adopt as the mean wave-load pattern the fixed wave-load pattern corresponding to the 75 ft. wave height at which the "system failure is most likely to occur". Accordingly the mean y-direction nodal wave force at node i, $E(F_i) = k f_i$, where f_i is the y-direction nodal force at node i due to a wave of height 75 ft. and k is a scale factor to ensure that the mean base shear is equal to the sum of the mean lateral (y-direction) nodal wave loads (see Equation 3.1 below). That is, if B is the random base shear (i.e., $B = F_{20}^S$, base shear due to the 20 year extreme wave from the south, see Equation 2.3) we have, $B = \sum_i F_i$; then the mean base shear is given by:

$$E(B) = \sum_i E(F_i) = k \sum_i f_i = k \, b_{75} \tag{3.1}$$

where, b_{75} is the base shear for the load pattern corresponding to the 75 ft. wave height. E(B), the mean base shear due to the extreme lifetime wave from the south is, in principle, given by: $E\left[\Gamma_a c (H_{20}^S)^\alpha\right]$ (see Equation 2.3). However for general probability distributions of Γ_a and H_{20}^S, no closed form solution for $E(B)$ exists. In order to approximately obtain an estimate of the mean base shear for the purpose of this "spatial correlation sensitivity study", we assume as in Chapter 2 that Γ_a, H_{20}^S, and hence, the base shear B are lognormal. Then the median and cov of the base shear, B, and hence the mean base shear, $E(B)$, can be conveniently estimated in close form. In any case, a first order approximation for the second moment is given by:

$$\delta_B^2 = \delta_{\Gamma_a}^2 + \alpha^2 \delta_H^2 \tag{3.2}$$

69

where δ_B, δ_{Γ_a}, and δ_H are the coefficients of variation of the base shear B, the analysis uncertainty factor Γ_a, and the wave height H_{20}^S respectively.

The spatial correlation between nodal wave forces is modeled as follows:

$$\rho_{ij} = \rho_c + (1 - \rho_c) \left[\exp\left\{ - \left(\frac{x_i - x_j}{r_x}\right)^2 - \left(\frac{y_i - y_j}{r_y}\right)^2 - \left(\frac{z_i - z_j}{r_z}\right)^2 \right\} \right] \qquad (3.3)$$

where, ρ_{ij} = correlation between y-direction lateral nodal wave forces F_i at node i

         (x_i, y_i, z_i) and F_j at node j (x_j, y_j, z_j)

         ρ_c = base level (non ergodic) correlation arising from the fact that all nodal

         wave forces arise from the same wave characterized by its height and period.

         r_x, r_y, r_z = correlation lengths in x, y, and z directions respectively.

Lacking definitive spatial correlation data, the form of the correlation function has been chosen on the basis of reasonableness and convenience. An alternate model might have been of the simple exponential decay type instead of the squared exponential form.

In the absence of any information to the contrary, we further assumed that the covs of the individual nodal wave forces have the same value. The accuracy of the assumption of common nodal wave-force cov has been checked by calibration of published results later in this work. Our approach in the parametric study was to vary the correlation parameter values while simultaneously adjusting the (common) cov of the nodal wave forces in such a way as to keep the cov of the base shear a constant. The base shear cov has been measured empirically in several field studies (e.g., *Bea et al., 1988*)

70

$$\text{Var (B)} = \sum_i \text{Var (F}_i) + \sum_i \sum_{i \neq j} \rho_{ij} \sqrt{\text{Var (F}_i)} \sqrt{\text{Var (F}_j)} \qquad (3.4)$$

To maintain the same cov of the base shear, $\delta_B = \dfrac{\sqrt{\text{Var (B)}}}{E(B)}$, the cov of each of the individual nodal wave forces in y-direction, $\delta = \dfrac{\sqrt{\text{Var (F}_i)}}{E(F_i)}$, can be calculated to be:

$$\delta = \delta_B \frac{\displaystyle\sum_i E(F_i)}{\sqrt{\displaystyle\sum_{i \neq j} \sum \rho_{ij} E(F_i) E(F_j) + \sum_i \{E(F_i)\}^2}} \qquad (3.5)$$

Having established the framework for determining the second moment characteristics of the nodal wave forces we now describe their probability distributions. For the purpose of the spatial correlation sensitivity study, in the simplest case the individual nodal forces are considered jointly normal with mean vector M and covariance matrix $C = [\rho_{ij} \sigma_i \sigma_j]$. The mean and the covariance matrix are calculated using Equations 3.1, 3.2, 3.3, and 3.5. The transformation from correlated normal space X to the standard normal uncorrelated space U is given by:

$$U = L^{-1}D^{-1}(X-M) \qquad (3.6.1)$$

or,
$$X = DLU + M \qquad (3.6.2)$$

in which $D = \text{diag } [\sigma_i = \delta E(F_i)]$ = the diagonal matrix of the standard deviations, and $L =$ a lower triangular matrix obtained from Cholesky decomposition of the correlation matrix $R = [\rho_{ij}] = L L^{-1}$.

If, however, a non-normal distribution function is used to characterize the nodal wave forces in the original X space a two-step transformation is recommended (*Der Kiureghian and Liu, 1986*). The nodal force can first be mapped into correlated Gaussian space Z, using marginal univariate transformation of the form: $Z_i = \Phi^{-1}[F_{X_i}(X_i)]$; i=1, 2, 3,···.

71

The correlation structure calculated in X space (Equation 3.3) can also be related to the correlation in the Gaussian space (correlation between Z_i and Z_j, i ≠j) using a power series involving Hermite polynomials (*Winterstein, De, and Bjerager, 1989;* see Appendix IV). This series can often be truncated with good accuracy after cubic terms, leading to closed form estimation of the underlying Gaussian correlation. In particular, if the distribution functions are lognormal, an exact closed form solution to map correlation is available. Finally, the transformation from Z to U space is similar to the step described by Equation 3.6.1. In this work we also explore the effects of modeling individual nodal forces as lognormal.

It should be pointed out that for the joint normal model of the nodal wave forces, $\underline{F}$, the base shear, B, (sum of correlated normal variables) is normal. For the jointly lognormal nodal forces the base shear (sum of correlated lognormal variables) is not lognormal for less than perfectly correlated nodal wave forces. However, for the purpose of this sensitivity study, we merely match the mean and the cov of the base shear due to the nodal forces with general spatial correlation to the reference mean and cov values of the base shear for Case F (fixed pattern analysis corresponding to the load pattern of the 75 ft. wave height, see Chapter 2) which were calculated on the basis of lognormal assumption of the base shear.

3.3 PARAMETRIC STUDY

Table 3.1 shows examples of correlation values generated by Equation 3.3[1] for various choices of the parameter values. Variation is shown across different horizontal levels (due to variation of z-coordinate only), and across different vertical bents (due to variation of x-coordinate only). Even though changes in correlation level in the y-direction were modeled

---

[1] In order to insure that the correlation matrix generated by Equation 3.3 remains positive definite under all parametric variations, we rewrote the Equation 3.3 with the multiplier $(1 - \rho_c)$ of the second term replaced by $(0.999 - \rho_c)$.

in Equation 3.3, we did not expect the changes to be significant. This is because the forces considered in this study are from a regular wave travelling in the y-direction, and the wave length is large compared to the jacket dimension in the y-direction.

Table 3.1 Example Correlations Generated by Equation 3.3

r_x (ft.)	r_z (ft.)	$|x_i-x_j|$ (ft.)	$|z_i-z_j|$ (ft.)	ρ_{ij} ρ_c=0.6	ρ_c=0.4	ρ_c=0.2
-	1000	0	190	0.986	0.979	0.971
-	500	0	190	0.946	0.919	0.919
-	100	0	190	0.611	0.416	0.221
-	50	0	190	0.6	0.4	0.2
-	1	0	190	0.6	0.4	0.4
-	100	0	130	0.674	0.551	0.348
-	100	0	80	0.811	0.716	0.621
-	100	0	35	0.954	0.931	0.908
-	1	0	35	0.6	0.4	0.2
100	-	40	0	0.941	0.911	0.882
100	-	80	0	0.811	0.761	0.621
100	-	120	0	0.694	0.542	0.390
60	-	40	0	0.856	0.785	0.712
60	-	80	0	0.668	0.501	0.335
60	-	120	0	0.607	0.411	0.215

For the parametric study we determined the moments of the base shear following an earlier investigation of the same jacket structure (Chapter 2). We assumed the constants α = 1.45 and c = 9.23 (evaluated from an analysis of wave loads near the wave height 75 ft., at which the system failure is most likely to occur, Chapter 2) to calculate the mean and cov of the base shear. The <u>mean</u> value of life time maximum wave from the south is 47.1 ft. with coefficient of variation = 0.20. The lifetime maximum base shear <u>mean</u> is 2379 kips with coefficient of variation = 0.40.

For the jointly normal model of the nodal wave forces, the results of the system reliability analyses are presented in terms of the following probability of failures. For each member, the probability that it fails in the intact structure was calculated, and the member with the largest probability is called the most-likely-to-fail (MLM) member. We also computed the probability that any-first (member) failure (AFF) occurs which is the probability of occurrence of the event corresponding to the union of all first member failures (in practice, about six members contributed significantly to the probability of the union). Also included are probabilities of occurrence of the most likely to fail sequence (MLS). In most of the cases studied, the same member and the same sequence remained most likely to fail, except in cases involving low levels of correlation among nodal forces. An asterisk (*) sign against the failure probabilities denotes that the most likely to fail member or sequence is different from that in the usually assumed case of perfectly correlated nodal forces. The system factor is defined as the ratio of probability of system failure and probability of most likely to fail member (MLM). It is an overall measure of system effects including probabilistic and deterministic redundancies of the system.

Table 3.2 summarizes results from system reliability analyses for parametric variations in ρ_c, r_x, r_y and r_z in Equation 3.3. In all cases the base shear cov is kept constant at a value of 0.4 (by an adjustment of the common nodal force cov). In the usual perfectly correlated case this cov value includes, recall, (see Chapter 2) uncertainty due to the extreme lifetime wave height and an additional uncertainty associated with observed variations in base shear given the wave height.

Table 3.2 Summary of System Reliability Analyses with Parametric Variation in Spatial Correlation between Nodal Wave Forces. MLM is the most-likely-to-fail member, AFF is the event that at least one member fails, and MLS is the most-likely-to-fail sequence.

Case #	ρ_c	r_x (ft.)	r_y (ft.)	r_z (ft.)	Nodal Force cov(δ)	P(MLM)	P(AFF)	P(MLS)	P(Sys. Failure)	System Factor
A.1	1.00	1	1	1	0.40	9.84e-4	1.89e-3	2.91e-5	5.01e-5	0.05
A.2	0.90	1	1	1	0.42	9.98e-4	1.94e-3	3.10e-5	5.44e-5	0.054
A.3	0.60	1	1	1	0.51	1.07e-3	2.20e-3	4.16e-5	7.88e-5	0.07
A.4	0.40	1	1	1	0.62	1.20e-3	2.63e-3	6.08e-5	1.28e-4	0.11
A.5	0.20	1	1	1	0.85	1.55e-3	4.22e-3	1.71e-4*	3.87e-4	0.25
A.6	0.10	1	1	1	1.13	2.70e-3*	8.31e-3	7.57e-4*	1.36e-3	0.50
A.7	0.00	1	1	1	2.34	4.19e-2*	8.35e-2	2.39e-2*	3.80e-2	0.91
B.I.1	0.60	1000	1000	100	0.43	1.31e-3	2.53e-3	5.33e-3	9.62e-5	0.07
B.I.2	0.40	1000	1000	100	0.44	1.52e-3	2.99e-3	7.41e-5	1.37e-4	0.09
B.I.3	0.02	1000	1000	100	0.46	1.80e-3	3.57e-3	1.04e-4	2.00e-4	0.11
B.II.1	0.90	1000	1000	1	0.416	1.05e-3	2.08e-3	3.50e-5	6.65e-5	0.06
B.II.2	0.60	1000	1000	1	0.48	1.36e-3	2.73e-3	8.65e-5*	2.02e-4	0.15
B.II.3	0.40	1000	1000	1	0.54	1.78e-3	4.81e-3	2.80e-4*	5.38e-4	0.30
B.II.4	0.20	1000	1000	1	0.63	2.65e-3	9.06e-3	1.07e-3*	1.90e-3	0.72
C.I.1	0.60	60	1000	1000	0.44	1.09e-3	2.40e-3	5.51e-5	9.39e-5	0.09
C.I.2	0.40	60	1000	1000	0.47	1.16e-3	2.85e-3	8.00e-5	1.36e-4	0.12
C.I.3	0.20	60	1000	1000	0.505	1.26e-3	3.54e-3	1.22e-4	2.14e-4	0.17
C.II.1	0.79	1	1000	1000	0.44	1.03e-3	2.12e-3	4.09e-5	6.92e-5	0.06
C.II.2	0.60	1	1000	1000	0.49	1.10e-3	2.47e-3	6.18e-5	1.05e-4	0.10
C.II.3	0.40	1	1000	1000	0.56	1.23e-3	3.22e-3	1.13e-3	1.84e-4	0.15
C.II.4	0.20	1	1000	1000	0.69	1.51e-3	5.25e-3	2.83e-4	4.60e-4	0.30
D.1	0.40	1000	20	1000	0.495	1.18e-3	2.26e-3	4.43e-5	7.47e-5	0.06
E.1	0.4	60	1000	100	0.505	1.57e-3	3.87e-3	1.41e-4	2.55e-4	0.16
E.2	0.4	100	1000	100	0.474	1.58e-3	3.57e-3	1.17e-4	2.13e-4	0.14
F.1	0.4	100	100	100	0.48	1.59e-3	3.56e-3	1.17e-4	2.13e-4	0.14
F.2	0.2	100	100	1000	0.525	2.02e-3	4.90e-3	2.13e-4	4.01e-4	0.02

* most likely to fail member or sequence is different from the base case

75

Case A.1 represents the base case where all the nodal wave forces are perfectly correlated; consequently individual nodal wave forces have the same cov as that of the base shear, 0.4. This case is similar to Case F in Chapter 2 except that the base shear in Case A.1 is normal whereas the base shear in Case F is lognormal. The effects of modeling the correlation are compared against Case A.1. Case A.7 represents the other extreme when the nodal forces are independent; it is only of theoretical interest. Other cases in this set, Cases A.2 through A.6, describe results if the nodal wave nodal forces are equicorrelated ($\rho_{ij} = \rho_c$, for $i \neq j$). This set is of interest because it can easily be incorporated into existing system reliability software with only minor modification[1]. Within this set, we clearly observe several trends which are also present within other sets. A reduction in correlation among nodal forces results in a higher nodal force coefficient of variation, because the base shear coefficient of variation (Equation 3.5) was kept constant. With the decrease in correlation level (and the associated increase in nodal force cov) both the member level and system level failure probabilities increase, but not to the same extent, as can be seen by the large increase in the system factor. A careful inspection of the sensitivity vectors revealed that for this set of results where the normal distribution is assumed for the nodal forces, the system failure probabilities are more sensitive to the variability in load vectors than are first member failures. For example, in Case A.1 the effective squared sensitivity[2], α_L^2, of the

nodal wave forces is 0.52 for the most likely to fail member, whereas for the system failure the squared load sensitivity is 0.87. Hence a decrease in correlation level affects the

---

[1]Each of the equicorrelated nodal loads, F_i, can be written as a sum of two random variables X_0 and Y_i, where X_0 is a normal variable common to all the F_i s and where the Y_i s are independent normal variables (independent of X_0). The common correlation is given by the ratio of the variance of X_0 and the sum of the variances of X_0 and Y_i.

[2]The sensitivity, α, is given by the negative gradient vector of the failure surface at the 'design point', normalized to have a unit length. It represents one measure of the relative importance of the standard variates.

76

system failure probabilities more even though more load averaging is involved in the failure of multiple components.

Cases B.I.1 through B.II.4 represent correlation variation of nodal forces with vertical (z-direction) separation of the nodes only. Cases B.I.1 through B.I.3 represent the case when the variation is gradual, whereas Cases B.II.1 through B.II.4 represent cases with a sharp drop in correlation level (see Table 3.1) over distance.

Cases C.I.1 through C.II.4 represent correlation variation in x-direction (horizontal direction orthogonal to the direction of wave travel, and the broad side of the structure, Fig. 2.1) only. The variation is gradual (see Table 3.1) in Cases C.I.1 through C.I.3, and sharp in Cases C.II.1 through C.II.4.

Only y-direction variation of correlation has been allowed in Case D.1. Comparison with the perfectly correlated case (Case A.1) confirms our earlier intuition that such variations do not affect the results.

In Cases E.1 and E.2, correlation levels vary with both x and z-direction separation distance of the nodes for two different correlation lengths, $r_x = 60$ and 100. In Cases F.1 and F.2 correlation between nodal forces were allowed to vary with all three (x, y and z) directional separation between nodes. Comparison of Cases F.1 and E.2 again shows that the effect of variation of r_y is insignificant.

Taken together the above results show that the failure probabilities cannot be ranked according to the coefficient of variation of the nodal forces, and the correlation pattern influences both the failure probabilities and system factor. The most important single conclusion is that for Gaussian variables, the correlation level has to drop appreciably (below $\rho_c = 0.6$) before it starts affecting significantly, either the failure probabilities or the system effects.

77

Failure of Sequences and System Effects

In order to demonstrate the effect of correlation on the probability of failure of sequences we present in Table 3.3 the results from equicorrelated Cases A.1, A.3, and A.5. Sequence 1 comprises of members that are primarily in Tier 3 (one member is in Tier 4), whereas Sequence 2 comprises entirely of members in Tier 4, the topmost tier of the jacket.

Table 3.3 Effect of Correlation of Nodal Forces on Sequence Failure Probability

Case #	ρ_c	Sequence 1 (Tier 3 and 4)		Sequence 2 (Tier 4)		P(System Failure)
		P(1st. mem.)	P(seq.)	P(1st. mem.)	P(seq.)	
A.1	1.0	5.01e-4	2.91e-5	1.31e-4	1.16e-5	5.01e-5
A.3	0.6	5.98e-4	4.16e-5	2.08e-4	2.16e-5	7.88e-5
A.5	0.2	12.2e-4	14.3e-5	8.86e-4	17.1e-5	38.7e-5

Results presented in Table 3.3 indicate that the changes in failure probability are larger for Sequence 2, both for the sequence and for the first member in the sequence. The reason for this is as follows: as we decrease the correlation between the nodal forces (keeping the base shear cov constant), the cov of the individual nodal forces increases. Correspondingly, the cov of the internal member forces also increases, but the increase is less because each internal member force is caused by multiple nodal forces. The larger the number of nodal forces contributing to the internal force in a member, the greater is the averaging effect and the smaller is the increase in the internal force cov. In our structure, the internal force in a member is influenced by all the nodal forces acting at the vertical level of the member as well as by those at the levels above. Therefore, there are more nodal forces influencing the internal force in a member in Tier 3 than in a member in Tier 4. This difference leads to a smaller increase in the cov of the internal force in a member in Tier 3 than in a member in Tier 4. This difference in the number of nodal forces involved

78

explains why the increase in the failure probability for Sequence 1 is smaller than that for Sequence 2.

In the perfectly correlated case (Case A.1, $\rho_c = 1.0$), sequence 1 has a higher failure probability than Sequence 2. However, as we decrease the correlation, the increase in failure probability of Sequence 2 is larger than that of Sequence 1. Finally, for Case A.5 ($\rho_c = 0.2$), the failure probability of Sequence 2 is larger than that of Sequence 1. At the system level, the sequences which contribute most significantly to the system failure probability include members from both Tier 3 and Tier 4. Hence, as expected, we find that the percentage increase in the system failure probability is larger than that for a sequence involving members primarily in Tier 3 (e.g., Sequence 1) and smaller than that for a sequence involving members in Tier 4 (e.g., Sequence 2).

As pointed out earlier, the change in failure probability away from the perfectly correlated assumption is significant only after a major drop in the nodal force correlation (e.g., below $\rho_c = 0.6$). If the sequences involving members in the topmost tier had dominated the system failure event, the change in the failure probability would have been more sensitive to the correlation level, and a significant increase in failure probability would have been caused by a smaller drop in correlation. Also, in our truss model, the internal member forces are influenced by several to many nodal forces, and hence, the effect of an increase in the nodal force cov (due to a decrease in correlation) is diminished because of averaging. In contrast, if we had a frame model, in which members could fail in bending, and we considered the effect of local loads (e.g., vertical loads on members in the splash zone), then there would have been less averaging for some members. If these local-force-dominated member failures contributed significantly to the system failure event, the system failure probability would have been more sensitive to the correlation level.

3.4 CALIBRATION

The open question now is what correlation pattern is realistic. In order to investigate if the additional computational effort to model the correlation is justified, we have followed an approximate procedure to calibrate our correlation model from the published results from the Ocean Test Structure (*Dean et al., 1979; Heideman et al., 1979*). This highly instrumented 20 x 40 x 120 ft. platform was installed in 66 ft. water depth in the Gulf of Mexico in November 1976 to evaluate wave-force calculation procedure.

The correlation scheme used in our parametric study modeled correlation between the nodal forces because of computation expediency. It is more natural to quantify the spatial correlation between y-direction (see Fig. 2.1) forces per unit length, S, at any two points on the structural members. Accordingly, we assumed a very simplified probabilistic model for the wave force (ignoring inertia force) per unit length at a point of the form:

$$S = c_1 \, \bar{C}_D \, f'(z) \, H^2 \, \varepsilon_i \, \phi_i \tag{3.7}$$

where, c_1 = a deterministic constant determined from density of water, time period of the wave, etc.

$\bar{C}_D$ = mean coefficient of drag force used in wave-force calculation

ε_i = uncertainty in local value of drag coefficient $C_{D_i} = \dfrac{C_{D_i}}{\bar{C}_D}$

ϕ_i = uncertainty in fluid kinematics (velocity square term) = $\dfrac{v^2_{i \, (actual)}}{v^2_{i \, (calculated)}}$

$f'(z)$ = function of depth for the decay of (squared) fluid velocity with depth

H = random wave height.

80

H, ε_i, and ϕ_i are independent random variables. We assumed that the error terms, ε and ϕ are unbiased. Their coefficients of variation are estimated to be: $\delta_\varepsilon = 0.25$ (*Heideman et al., 1979*) and $\delta_\phi = 0.30$ (for calculations based on Stokes Vth order theory) (*Dean et al., 1979*) from the OTS results. We further assumed the spatial correlation of ε and ϕ to be of the form:

$$\rho_{\varepsilon_i \varepsilon_j} = \exp\left\{ - \left(\frac{x_i - x_j}{r_{x\varepsilon}}\right)^2 - \left(\frac{z_i - z_j}{r_{z\varepsilon}}\right)^2 \right\} \qquad (3.8)$$

$$\rho_{\phi_i \phi_j} = \exp\left\{ - \left(\frac{x_i - x_j}{r_{x\phi}}\right)^2 - \left(\frac{z_i - z_j}{r_{z\phi}}\right)^2 \right\} \qquad (3.9)$$

The above models were calibrated analyzing the limited OTS results reported by *Dean et al., 1979* and *Heideman et al., 1979*. The x and z direction correlation lengths (r_x and r_z) were assumed to be equal in the absence of any information to the contrary. In particular, *Heideman et al., 1979*, reports a correlation coefficient of 0.5 between C_D values for a spatial separation of 40 ft. under the same wave. Assuming the spatial separation to be in the x-direction only, we estimate $r_{x\varepsilon} = 48$ ft. We further assume that $r_{z\varepsilon} = r_{x\varepsilon} = 48$ ft. Estimation of correlation lengths for the fluid kinematics term was more complicated. *Dean et al., 1979*, reports for two spatially separated piles, the variability of the local drag forces (at four vertical levels) and of the combined total drag forces. The variability reported was solely due to the uncertainty in the fluid (squared) velocity term. Since the total force is the sum of the lumped local forces, the total force cov is related to the covs and the correlation between the local forces. Appropriate correlation lengths (equal in x and z-directions) for

81

the velocity square term were selected by trial and error to match the reported local and total

drag force cov. The correlation lengths were estimated to be: $r_{x\phi} = r_{z\phi} = 50$ ft.
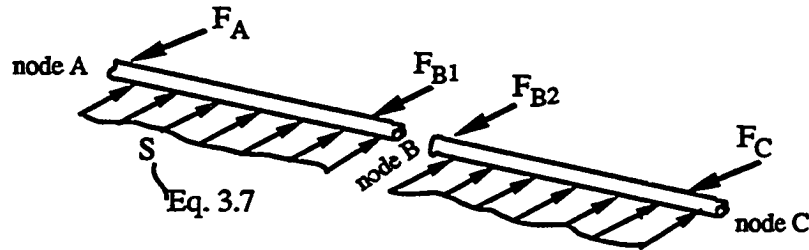
Fig. 3.1 Member End Reactions of Adjacent Members due to Distributed Wave Loading

In order to relate the above model for the correlation between local wave forces, S, to

the nodal wave forces, F_i, we proceeded as follows. We used the model in Equation 3.7 to

represent the local force per unit length at each point of two adjacent members AB and BC

at level 4 (=15 ft. elevation) of the jacket structure under study (Figs. 2.1 and 3.1). For

this (larger) jacket structure we used for the mean, cov, and correlation lengths of the error

terms ε and ϕ the same numerical values that were estimated for the (smaller) OTS

structure. We obtained the moments of and the correlations between the four member-end

reactions (F_A, F_{B1}, F_{B2}, and F_C, see Fig. 3.1) at nodes A, B, and C by integrating the

product of the load influence function and the spatial random wave-force process across the

lengths of the members AB and BC (Fig. 3.1). Because more than one member frames

into one node, one more level of averaging was needed to get the correlation between the

total nodal wave forces at nodes A, B, C (and extrapolated to D, see Fig. 2.1). We did this

approximately by assuming an intermediate model for correlation between the four member

end reactions at A, B, and C (due to members AB and BC) of the form:

82

$$\rho_{ij} = \rho_c' + (1 - \rho_c') \left[\exp \left\{ - \left(\frac{x_i - x_j}{r_x'} \right)^2 - \left(\frac{z_i - z_j}{r_z'} \right)^2 \right\} \right] \qquad (3.10)$$

A non-ergodic term ρ_c' is needed because, unlike ε and ϕ, the member end reactions

arise out of a common random variable, wave height H. We calibrated the above model,

i.e., estimated $\rho_c' = 0.51$, and $r_x' = 50$ ft. from the correlations between the four member

end reactions calculated before. Note that the point of action of the four nodal forces at

nodes, A, B, and, C (Fig. 3.1) have zero vertical separation and hence the correlation

between the forces could not be used to obtain an estimate for r_z'. As before in the absence

of any information to the contrary we assumed, $r_z' = r_x' = 50$ ft. (For the purpose of this

calibration we assumed that the distributed applied forces were due to concentrated forces

located at the member third points, following the triangular shape of the influence

function). The cov of each of the member end reactions was calculated to be 0.574.

Next, we extended the model to include forces from all the members framing into a

node. Using the calibrated model in Equation 3.10, and considering the relative mean

magnitude (but with equal cov = 0.574) of the member end reactions due to different

members framing in at nodes A, B, C and D (Fig. 2.1), we calculated the correlation

coefficients between total nodal forces at these nodes, and also the coefficients of variation

of the total nodal forces. We finally obtained the following crude correlation estimates:

$\rho_{F_A F_B} = 0.80$, $\rho_{F_A F_C} = 0.58$, $\rho_{F_A F_D} = 0.54$,

and also the covs:

$\delta_{F_A} = 0.558$, $\delta_{F_B} = 0.558$, $\delta_{F_C} = 0.558$, and $\delta_{F_D} = 0.558$.

83

For this relatively high level of correlation the cov of the total nodal forces, at nodes A, B, C, and D, were in fact numerically equal (up to three significant figures). We assumed the cov of the total nodal forces at each node of the jacket structure to be equal to 0.56.

Results

Finally we used the above correlations between the total nodal forces to roughly calibrate the model in Equation 3.3, and obtained: $\rho_c = 0.53$ and $r_x = 55$ ft. We further assumed that $r_z = r_x$, and that the variation in y direction is not significant, i.e., $r_y = 1000$ (large). For this calibrated correlation structure and the 0.56 value of the nodal force cov, we calculated the base shear cov, δ_B, to be 0.45.

If in the probabilistic modeling of base shear (by Equation 3.2) we had used $\alpha = 2$, (consistent with the local wave force per unit length modeling (by Equation 3.7) in our calibration study), we would have obtained for $\delta_{\Gamma_a} = 0.25$ and $\delta_H = 0.20$:

$$\delta_B = \sqrt{\delta_{\Gamma_a}^2 + \alpha^2 \delta_H^2} = 0.47$$

Note that the calculated value of δ_B is in fact somewhat smaller than 0.47. This is the result of the greater spatial averaging that takes place over this larger structure compared to the OTS structure (which was the basis of using $\delta_{\Gamma_a} = 0.25$). The additional averaging reduces the uncertainty on base shear given the wave height. In fact, the implied value of δ_{Γ_a} for this structure is equal to $\sqrt{0.45^2 - 2^2 \times 0.2^2} = 0.21$ rather than 0.25.

We finally reevaluated the system reliability. The mean nodal wave-force pattern and the mean base shear were kept the same as before. The correlation parameter values and the nodal force cov specified by the calibrated model are shown as Case G.2 in Table 3.4. The probability of system failure is 6.99×10^{-4}. For comparison, we show as Case G.1 the perfectly correlated case in which the base shear (and hence all the nodal force) cov is the same as the calibrated case, i.e., $= 0.45$. Finally the case G.3 corresponds to the perfectly

84

correlated case with base shear cov = 0.47 (for $\delta_{r_a} = 0.25$ with $\alpha = 2$). The more realistic correlation structure appears to increase the system probability of failure by about a factor of 3. But these results are based on the unrealistic assumption of Gaussian distribution of the nodal wave forces.

Table 3.4 Summary of System Reliability Analyses with Calibrated Correlation Model

Case #	ρ_c	r_x (ft.)	r_y (ft.)	r_z (ft.)	Nodal Force cov(δ)	P(MLM)	P(AFF)	P(MLS)	P(Sys. Failure)	System Factor
G.1	1.00	1	1	1	0.45	1.85e-3	3.62e-3	1.09e-4	1.91e-4	0.10
G.2	0.53	55	1000	55	0.56	2.79e-3	6.61e-3	3.52e-4	6.99e-4	0.25
G.3	1.00	1	1	1	0.47	2.33e-3	4.57e-3	1.71e-4	2.99e-4	0.13

3.5 EFFECT OF MODELING BY LOGNORMAL DISTRIBUTION

Lognormal distributions are skewed to the right and have fatter tails compared to normal distributions. Noting that the cov of the load is higher than that of the capacity, the most obvious effect of modeling load and capacity (resistance) variables by lognormal distributions instead of normal distributions (with the same mean and cov) would be an increase of probability of failure both at the member and the system level. Another effect of using lognormal distribution is that the member and system failure probabilities would be more sensitive to the load variability because the effective squared sensitivity on the nodal wave loads, α_L^2, is higher than that in the Gaussian case for the same load and resistance

cov[1] In our structure, if we fix the resistances at their mean values then the load at which

---

[1]Consider a simple load and resistance problem in which the mean load and resistance are μ_L and μ_R; the load and resistance c.o.v.s are δ_L and δ_R, and the failure criterion is L > R. If the random variables are normally distributed, then the square of the sensitivity to the load, α_L^2, is $(\mu_L\delta_L)^2/[(\mu_L\delta_L)^2+(\mu_R\delta_R)^2]$ and the square of the sensitivity to the resistance, α_R^2, is $(\mu_R\delta_R)^2/[(\mu_L\delta_L)^2+(\mu_R\delta_R)^2]$. In our case, for the critical members in Tiers 3 & 4, δ_L is larger than δ_R, but μ_R is larger than μ_L. The products $\mu_R\delta_R$ and $\mu_L\delta_L$ are about the same, and hence, $\alpha_R^2 \approx \alpha_L^2$. For the sequence and the system failure events, we have

85

the system fails is not very much higher than the load at first member failure. Hence, in the lognormal case where load effects dominates (i.e., have much higher sensitivity) the failure probability of the most likely to fail member (MLM) is expected to be of the same order as the failure probability of the system. This would result in higher system factors for the lognormal case.

Table 3.5 System Reliability Analyses with Lognormal Model

Case #	ρ_c	r_x (ft.)	r_y (ft.)	r_z (ft.)	Nodal Force cov(δ)	P(MLM)	P(AFF)	P(MLS)	P(Sys. Failure)	System Factor
H.1	1.00	1	1	1	0.45	8.24e-3	13.3e-3	3.76e-3	5.36e-3	0.65
H.2	0.53	55	1000	55	0.56	9.72e-3	23.1e-3	5.78e-3	11.5e-3	1.18

Results from system reliability analysis using lognormal model is summarized in Table 3.5. Cases H.1 and H.2 respectively correspond to cases with perfect correlation among the nodal forces and correlation specified by the calibrated model. These two Cases, H.1 and H.2, correspond to the Gaussian Cases G.1 and G.2 in Table 3.4 (i.e., with same mean values, coefficients of variation and correlation structure for the random variables) respectively. As expected, in the lognormal case, the probability of failure increased both at the member and the system level compared to the corresponding Gaussian cases for both levels of correlation. In the Gaussian case with perfect correlation between the nodal forces (Case G.1), for the most likely member failure, the (squared) sensitivity to the load, α_L^2, is

---

multiple member failures all of which involve the same load, and hence the sensitivity to the load is higher in these cases. If we have lognormal random variables, then $\sigma_{logL} \approx \delta_L$ and $\sigma_{logR} \approx \delta_R$; the (squared) sensitivity (in transformed log space) to the load, α_{logL}^2, is $(\delta_L)^2/[(\delta_L)^2+(\delta_R)^2]$, and to the resistance, α_{logR}^2, is $(\delta_R)^2/[(\delta_L)^2+(\delta_R)^2]$. Since δ_L is larger than δ_R, α_{logL}^2 is larger than α_{logR}^2. Hence at the member failure level, the (squared) sensitivity to the load is larger for the lognormal case than the Gaussian case. At the system level, the sensitivity to the load is also larger for the lognormal case than the Gaussian case but the difference is smaller because the sensitivity is already quite high in the Gaussian case.

86

0.58 (also, $\alpha_R^2 = 1 - \alpha_L^2 = 0.42$), and for the system failure, the sensitivity, α_L^2, to the load

is 0.89. For the corresponding perfectly correlated lognormal case (Case H.1), the sensitivity to the load, α_L^2, is 0.90 (also, $\alpha_R^2 = 1 - \alpha_L^2 = 0.10$), and for the system failure,

the sensitivity to the load is 0.98. These sensitivities compare to the Gaussian as expected. Also, as expected, the system factors are much larger in the lognormal case, i.e., the failure probability of the most likely to fail member is close to the system failure probability. Note that the system failure probability is still affected significantly more than the failure probability of the MLM when the correlation is reduced in the lognormal case. The effect of the realistic correlation structure is now about a doubling of the system failure probability.

To study the effects of lognormal modeling without the effects due to the obvious change in the absolute failure probability level, we carried out system reliability analyses for the lognormal model with the parameters adjusted such that the system failure probability for the perfectly correlated lognormal case (Case I.1, Table 3.6) is same as that of the corresponding Gaussian case (Case G.1, Table 3.4), i.e., about 1.9×10^{-4}. This was done by scaling down the mean nodal wave forces by approximately 35.5% and keeping all other mean values and covs the same. Case I.2 (Table 3.6) is the lognormal case with the same adjusted means as in Case I.1, but with the correlation structure and the nodal force cov specified by the calibrated model.(as in Case G.2). In general, the trends for the adjusted lognormal cases are the same for the as our earlier lognormal cases (Table 3.5), e.g., large system factors and high sensitivity to the load (in Case I.1, the squared sensitivity to the load, α_L^2, is 0.90, and for the system failure, the squared sensitivity to the load is 0.98).

Table 3.6 System Reliability Analyses with Adjusted Lognormal Model

Case #	ρ_c	r_x (ft.)	r_y (ft.)	r_z (ft.)	Nodal Force cov(δ)	P(MLM)	P(AFF)	P(MLS)	P(Sys. Failure)	System Factor
L1	1.00	1	1	1	0.45	3.78e-4	6.57e-4	1.27e-4	1.93e-4	0.50
I.2	0.53	55	1000	55	0.56	6.59e-4*	1.73e-3	3.33e-4*	7.09e-4	1.07

* most likely to fail member or sequence is different from the base case

Because the load effect is more dominant in the lognormal case, one would expect to see greater changes in failure probabilities with decreasing correlation between the nodal forces (and the accompanying increase in the nodal force cov) compared to the Gaussian case. In comparing results from Table 3.4 and Table 3.5, we see the contrary. However, if we compare the adjusted lognormal results in Table 3.6, we do see this effect. (Note that in the adjusted lognormal case the most likely to fail member is different for the $\rho_c = 0.53$ case from the $\rho_c = 1.0$ case. If we consider the same member for the $\rho_c = 0.53$ case that is most likely to fail in the $\rho_c = 1.0$ case, the failure probability is 5.9×10^{-4}). Note, however, that even for the first member failure event, where there is considerable increase in load sensitivity in the lognormal case compared to the Gaussian case, the failure probability increases by only a factor of about two with the decrease in correlation. This relatively mild change is the result of the spatial load averaging involved in the internal member forces, which reduces the impact of the change in the nodal force cov arising from the change in correlation level. This is further explored below.

88

Table 3.7 Effect of Distribution Type on Sequence Failure Probability

Case #	Distrb. Type	ρ_c	Sequence 1 (Tier 3 and 4)		Sequence 2 (Tier 4)		P(System Failure)
			P(1st. mem.)	P(seq.)	P(1st. mem.)	P(seq.)	
G.1	Normal	1.00	9.81e-4	1.09e-4	2.91e-4	0.49e-4	1.91e-4
G.2	Normal	0.53	21.7e-4	3.52e-4	9.42e-4	2.31e-4	6.99e-4
I.1	Lgnrm.	1.00	2.30e-4	1.27e-4	1.11e-4	0.83e-4	1.93e-4
I.2	Lgnrm.	0.53	6.59e-4	3.17e-4	5.05e-4	3.33e-4	7.09e-4

Table 3.7 contains failure probabilities, for two critical sequences, at two correlation levels for both the Gaussian and the adjusted lognormal model. Especially at the first-member failure, the sensitivity to the load is much higher in the lognormal case, and hence a decrease in correlation (with the accompanying increase in the nodal force cov) causes a greater change in failure probability than in the Gaussian case (factors of 3 to 5 versus 2). This is seen for the first member failures in both Sequences 1 and 2. On the other hand, because the load sensitivity to the system failure is similar for Gaussian and lognormal models, the changes in the system failure probability (due to a similar change in the correlation level) are of same order (a factor of 3) for both models. In both the Gaussian and the lognormal case, the change in correlation has a greater impact on Sequence 2 (which has members from Tier 4 and therefore involves less load averaging) than on Sequence 1 (which has members primarily in Tier 3). It is also interesting to note that for the case of perfect correlation, the failure probabilities of the two sequences, 1 and 2, are closer to each other in the lognormal case than in the Gaussian case. This is expected because the problem is load dominated in the lognormal case, and the loads required to cause failure of Sequences 1 and 2 (with member capacities at their mean values) are similar. Also, in both models, for perfect correlation, Sequence 1 has a higher probability of failure than Sequence 2. In the lognormal case (Table 3.7), because the failure probabilities for the two sequences at perfect correlation are similar, the greater increase of

89

failure probability (with decrease in correlation) for Sequence 2 leads to Sequence 2 being more important than Sequence 1 at the calibrated correlation level. In contrast, in the Gaussian case, the difference in failure probability of the two sequences at the perfectly correlated level is larger and even though Sequence 2 has a larger increase in failure probability for the same decrease in correlation, Sequence 1 is still more important than Sequence 2 at the calibrated correlation level.

The same behavior is seen for the most likely to fail member for the lognormal model (Table 3.6). The most likely member to fail member in the perfectly correlated case (Case I.1) has many nodal loads influencing its internal member force, and therefore its failure probability is less sensitive to the change in the correlation between nodal forces. Hence when we decrease the correlation to the calibrated level, there is a smaller increase in failure probability of the most likely to fail member than in many other members and some other member becomes the most likely to fail member.

3.6 SUMMARY

A framework to model the spatial correlation structure of nodal wave forces in system reliability analysis of offshore structures is presented.

Application of the framework to a fixed jacket structure modeled as a space truss shows that for a fixed base shear cov, the correlation level among the nodal wave forces has to decrease markedly before such drop in the correlation level has a significant effect on the failure probabilities. This is because the internal member forces are influenced by multiple nodal loads which causes spatial averaging and lessens the impact of the decrease in correlation.

The correlation for our jacket structure was estimated from measured wave force and kinematics data. Although the correlation due to local uncertainties appears to decay quite rapidly over space, the absolute correlation level remains high because of the high degree of common functional dependence of the nodal wave forces on the random wave height, H.

90

For the estimated correlation, it appears that the more accurate spatial stochastic modeling of the nodal wave forces may be only of marginal benefit for truss type behavior of steel jacket structures. For the most realistic cases the system failure probability may increase by a factor of 2 to 3, while the most-likely-to fail member failure probability is virtually unchanged, when compared to the fully correlated model customarily used in reliability practice. Nonetheless, depending on circumstances (e.g., with a more accurate structural model considering failure in bending due to local loads), even this relatively high common correlation may affect the member failure probabilities, and the more accurate spatial stochastic model may be necessary.

The calibration procedure outlined here is quite crude; further analyses of the wave-load data are needed before definite conclusions on the common correlation and the rate of decay can be made.

91

SYSTEM REDUNDANCY AND APPROXIMATE SYSTEM RELIABILITY ANALYSIS

In this chapter the reliability of near-ideal parallel structural systems is studied in order to understand and quantify the system factors influencing the overload capacity and the redundancy of realistic statically indeterminate structures. From a deterministic point of view, redundancy is the ability of the structure to withstand load beyond that causing the first member-failure event. In structural system reliability redundancy has been defined as the conditional probability of system failure given first failure of any member (*Cornell, 1987; Nordal et al., 1987; Paliou et al., 1987*). It is an inverse measure, i.e., a "more redundant" structure has a lower value for this measure.

In contrast to previous studies of ideal parallel systems (e.g., *Daniels,1945; Shinozuka and Itagaki, 1966; Hohenbichler and Rackwitz, 1983a; Guenard, 1984; Stahl and Geyer, 1985; Cornell, 1987; Rackwitz and Gollwitzer, 1988; Grigoriu, 1989;* etc.), the present study considers unbalanced parallel systems. In an unbalanced system, the ratio of mean member capacity to mean member force, i.e., the mean safety factor, is different for different members, both in the intact and in the potential damaged states of the structure. For an elastoplastic structure that is perfectly balanced (in the mean), the system effects, including overload capacity beyond the first member failure, are strictly due to the randomness in the capacity variables, i.e., they are probabilistic in origin. In contrast, for a more realistic (see Section 1.1.1) unbalanced structure, the system effects inducing redundancy are both deterministic and probabilistic in origin. A major question is how important these probabilistic effects remain in the presence of the deterministic effects associated with this lack of balance. In this study the effects of various parameters, such as the number of members, postfailure member capacity, excess design capacity, etc., are

92

investigated. Simple approximations are developed for estimation of the probability of failure of complex unbalanced systems. A Reduced Space Monte Carlo Simulation (also known as conditional expectation, see *Cornell, 1987; Karamchandani, 1987*) approach has been used for the reliability computations. This proved to be a very efficient technique for the present study.

Finally the findings from near-ideal parallel systems are applied to non-ideal redundant systems, in particular, to the fixed offshore structure studied in Chapters 2 and 3. Several simulation based accelerated system reliability analysis techniques for the fixed offshore structure are also investigated.

4.1 PROBABILISTIC AND DETERMINISTIC SYSTEM EFFECTS

For a statically indeterminate structure, failure of an individual member does not imply system failure , and usually (but not always) the ultimate capacity of the structure is larger than the load at which the first member failure occurs. The overload capacity of the system beyond the member-level (first failure) capacity, and hence the redundancy, depend not only on the degree of static indeterminancy, but also on the ability of the structure to provide alternate "load paths"[1] and the postfailure behavior (e.g., the ductility) of the individual members. In addition, the probability of system failure depends on the relative uncertainty of the load with respect to that of the member capacities, correlation between member capacities, and individual member failure probability levels. These are well studied issues for ideal parallel balanced systems, i.e., those with a common mean load-to-capacity ratio (e.g., *Cornell, 1987; Rackwitz and Gollwitzer, 1988*; etc.). These studies have led to many usef⁻ insights into the nature of structural system reliability. But, in addition, system   :s in reliability depend on how the real system deviates from this academic

---

[1] "Load path" here refers to the rather ill-defined but popular structural engineering notion of alternative "ways" a particular load may be delivered to the foundation. The term does not refer here to the relative rates by which various loads are raised to their final random values, as in Section 1.1.3.

93

ideal. A balanced multimember system with nonductile members may behave no better than a single element. If one or more redundant members are not so severely stressed (i.e., if there is unbalance), however, then they can perhaps absorb the effect of first member's failure and help the system sustain larger loads. The impact of these deviations from a balanced system is the focus of this study.

The common design practice to achieve sufficient safety entails, in effect, designing each member to a prescribed reliability level. The "weakest" of these members (i.e., the member with the largest individual probability of failure, which is usually, but not necessarily, the member with smallest mean factor of safety) is called the most-likely-to-fail (MLM) member. Because initial failure can occur in any of the several members, the probability that any first-member failure (AFF) occurs is greater than (or at least equal) to the probability of failure of the most-likely-to-fail member. This so-called "weakest link" or "series system effect" is an adverse system effect, in contrast to the redundancy effects, which are beneficial. Also, while the redundancy effect can be both probabilistic and deterministic in origin, the "series system effect" described above is purely probabilistic in origin, i.e., the "series system effect" arises from the uncertainties in the governing variables. The issue of categorization and quantification of these deterministic and probabilistic system effects is one of the subjects of this investigation. The choice of base parameters (e.g., coefficients of variation of load and capacities, most-likely-first-member failure level, etc.) have been motivated by our experience in system reliability analyses of offshore structures. Effects of systematic variation of other parameters (e.g., number of members, degree of unbalance, number of weak members, postfailure ductility level, etc.) on system behavior have been studied. One objective is to suggest simple approximate relationships that reflect observed patterns in this multidimensional parameter space.
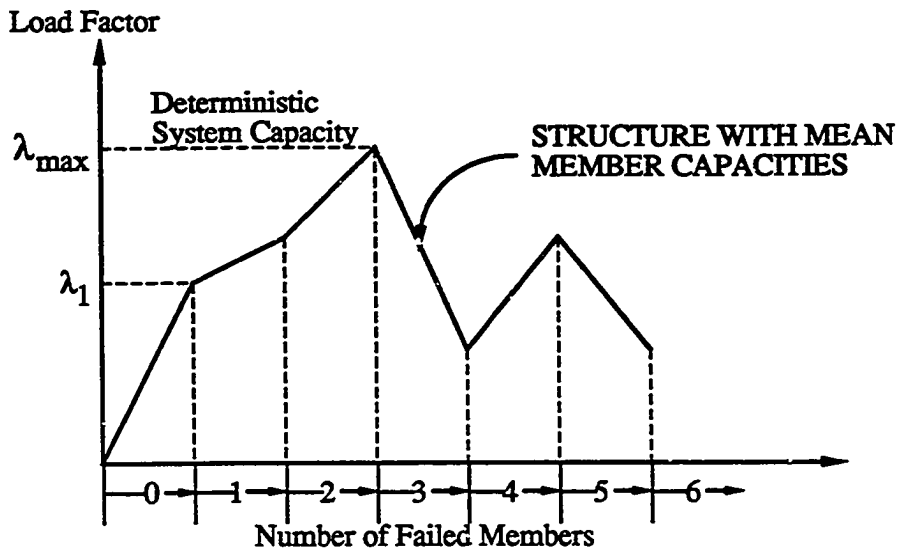
94

4.1.1 Deterministic Measures

Fig. 4.1 Static Pushover Test

For offshore jacket structures, deterministic system effects have been studied by static push-over analysis (e.g., *Lloyd and Clawson, 1983; Stewart et al., 1988;* etc.). The nodal design wave load pattern is increased proportionally (multiplying by a scale factor, say Λ) beyond failure of first member ($\Lambda = \lambda_1$) until the maximum load ($\Lambda = \lambda_{max}$) is reached (Fig. 4.1) in the structure with mean member capacities. In this work, λ_1 is defined as the deterministic first-failure capacity (DFFC) and λ_{max} is defined as the deterministic system capacity (DSC). A measure of system reserve strength is the ratio: $\lambda_{max} / \lambda_1$. We refer to this ratio as the deterministic system factor (DSF). DSF > 1 implies overload capacity beyond the first member failure, while DSF = 1 implies no deterministic "system back-up". The deterministic system factor depends on the ability of the structure to provide alternate load paths to carry the load in the event of a member failure, the degree of unbalance of the members, and postfailure capacities of the failed members. Usually the system capacity is measured by the "reserve resistance factor", which is the ratio of the ultimate capacity to the

95

design capacity of the structure (e.g., *Lloyd and Clawson, 1983 , Furuta et al., 1985; Feng and Moses, 1985; Frangopol et al., 1987;* etc.). But the design capacity is a code-specific quantity; hence the DSF is introduced here to measure the redundancy with reference to the load (and hence the capacity) at first-member failure.

For the reliability analysis here, postfailure member behavior is idealized as ductile, brittle, or semibrittle (Fig. 4.2) for truss type elements. Ductile members continue to carry their full force at failure while brittle members carry no force after failure. Semibrittle members carry a constant force equal to a fraction (η) of the force at failure in the failed state. Recent studies (e.g., *Cornell, De, Karamchandani, and Bjerager, 1988*) have verified the adequacy of this simple member model in representing realistic buckling members in larger systems. With such members in a balanced deterministic system, failure of one member implies failure of the system irrespective of the degree of statical indeterminancy, resulting in no deterministic back-up, i.e., DSF = 1. It is also possible that some unbalanced systems will have no deterministic back-up because of a lack of adequate ductility of the failed members.
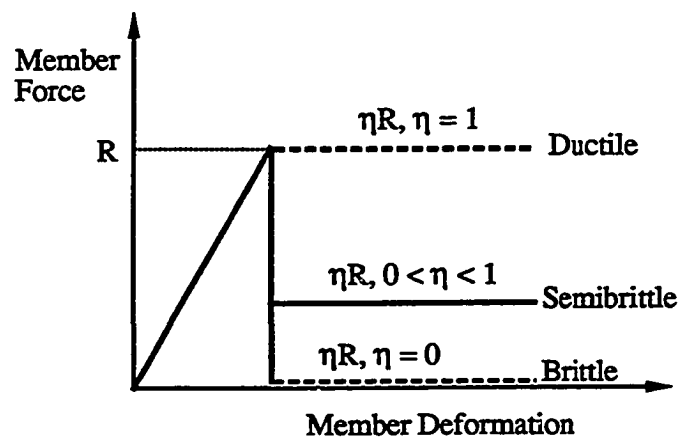

Fig. 4.2 Postfailure Behavior of Truss Members

96

4.1.2 Probabilistic Measures

In addition to the deterministic back-up, system effects are also probabilistic in origin. Probabilistic system redundancy measures have been used in recent reliability studies of offshore structures (e.g., *Paliou, Shinozuka, and Chen, 1987; Nordal, Cornell, and Karamchandani, 1987;* etc.). *Cornell (1987)* suggested and studied (for balanced systems) the following ratios of failure probabilities to measure the probabilistic system effects :

Complexity Factor $(C_0) = P\{AFF\}/P\{MLM\}$

Redundancy Factor $(R_0) = P\{$ System failure $\mid$ AFF $\} = P\{$System Failure$\}/P\{AFF\}$

Net system factor $(S_0) = P\{$System Failure$\}/P\{MLM\} = C_0 R_0$

The complexity factor, C_0, measures the adverse system effect on the "any first failure event" due to the presence of more than one failable member. This system effect is purely probabilistic in origin and is always present in both balanced and unbalanced multimember systems. C_0 is always equal to or greater than one and depends on the number of members, or more precisely, on the number of relatively weak (heavily stressed) members. C_0 is less than n, the number of such members; therefore it seldom exceeds a value of 2 to 5. C_0 is also inversely dependent on the stochastic dependence among the individual first-member-failure events. This degree of dependence in turn depends strongly on the relative uncertainty of the load with respect to that of the capacity, and usually relatively weakly on the correlation between the member capacities. For example, if the load variability (cov) is much larger than that of the member capacities, the chances are high that the individual member failure events will result from the common load being high, rather than individual member capacities being low. Hence, in this case the member failure events will be strongly dependent, even if the capacities are not. However, if the number of members and / or the correlation coefficients between the member capacities become large, C_0 can be affected significantly by the correlation between member capacities as well.

97

The redundancy factor, R_O, is the conditional probability of total system failure given at least one member has failed. It represents the redundancy of the intact system with respect to overloads. R_O is less than or equal to one. If the structure is statically determinate, R_O is equal to one. For a statically indeterminate structure, R_O will be shown below to depend strongly on the deterministic "back-up" as measured by the deterministic system factor, DSF. Given a nonzero deterministic back-up (i.e., DSF > 1), R_O is less than one. However, even for systems that have no deterministic back-up (DSF = 1, e.g., balanced systems), because of the probabilistic variation of the capacities, individual realizations of the system can be such that the load at system failure is larger than the load at any first-member failure, and R_O can then be less than one. This effect is more significant when the postfailure capacities (η) of members are high. Hence, a balanced system may possess probabilistic redundancy even in the absence of deterministic redundancy. The calculation of the redundancy factor involves evaluation of the probability of system failure considering all possible member failure sequences leading to the failure of the system. In contrast to C_O, R_O is strongly influenced by the postfailure behavior (η) of the members. The net system factor, $S_O = C_O R_O$, relates the probability of system failure directly to the probability of failure of the single most likely to fail (weakest) member. A net system factor less than one implies positive system benefit reflecting net redundancy (i.e., $R_O < \frac{1}{C_O}$) of the structural system whether deterministically or probabilistically induced.
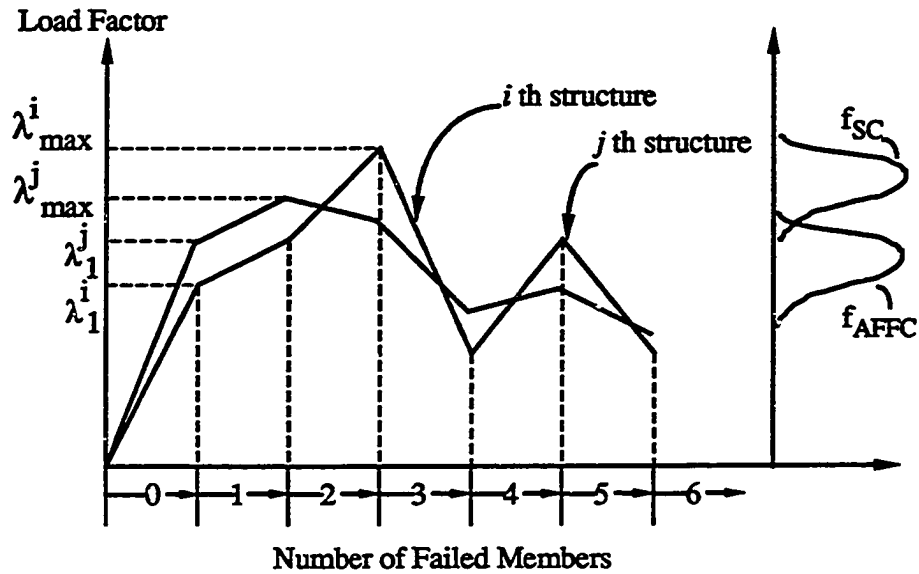
4.1.2.1 System Capacity as A Random Variable

For the case of reliability analysis of fixed offshore structures, in general, the problem is generally load driven, i.e., the uncertainty in load is much greater than that in capacity (e.g. load coefficient of variation (cov) ≈ 0.40 and member-capacity cov ≈ 0.1 to 0.13, see Chapter 2). Furthermore, if the load can be represented by a single random variable (e.g., a fully correlated spatial load pattern, i.e., a deterministic load pattern with random scale

98

factor) considerable computational advantage (in system reliability estimation) and insight can be gained by probabilistically characterizing the system capacity (SC) under the action of the specified deterministic load pattern. The system reliability can then be calculated as the probability that the load exceeds the system capacity. In the simplest case the system capacity may be characterized only by its mean E[SC]; it may be sufficient for the purpose of system failure probability estimation ($P_{sys} \approx P \{ L \geq E[SC] \}$), provided that the load sensitivity, α_L, is much larger than the capacity sensitivity, α_{SC} (see Chapter 3 for a discussion on load and capacity sensitivities). The accuracy of such an estimate will depend on the assumed probability distribution shape of the load and capacity variables (see Appendix II). An improvement of the estimate of failure probability can be achieved if the second moment characterization (cov) of system capacity is also sought. In general, the form of the probability distribution of the system capacity (SC) will be different from that of the individual member capacities because of the ordering and averaging involved in the calculation of system capacity from individual member capacities. However, as a first approximation it may be reasonable to adopt any convenient distribution shape and calculate the probability of system failure as:

$$P_{sys} = P \{ L \geq SC \} = \int_0^\infty [1 - F_L(r)] \, f_{SC}(r) \, dr = \int_0^\infty F_{SC}(l)] \, f_L(l) \, dl \qquad (4.1)$$

where, $F_L(\cdot)$ and $F_{SC}(\cdot)$ are the cumulative probability distribution functions of the load and system capacity respectively, and $f_L(\cdot)$ and $f_{SC}(\cdot)$ are the corresponding probability density functions.

Fig. 4.3 Static Pushover of Random Realizations of the Structure

In view of the discussion above, it is useful to characterize both the capacity at any-first-member failure (AFFC) and system capacity (SC) as random variables (Fig. 4.3). The term "system-level capacities" will be used here to imply both the any-first-member failure capacity (AFFC) and system capacity (SC). Their statistics can be estimated by simulating the structure and conducting static pushover tests (under the given deterministic load pattern) for each stochastic realization of the structure. In a deterministic static pushover analysis the structure, defined by mean capacities of its members, is subjected to the action of the load pattern with increasing magnitude. We define the resulting system capacity, λ_{max} (Fig. 4.1), as the deterministic system capacity (DSC). The resulting failure sequence is the so-called "mean-based sequence". If, however, such pushover tests are repeated for different random realizations of the structure (Fig. 4.3) the resulting any-first-failure capacity (Λ_1) and system capacity (Λ_{max}) will be random variables. The failure sequences for different random realizations of the structure, in general, will be different. Unlike probabilities of any first failure and system failure (and hence, C_0, R_0, and S_0), the

100

probabilistic description of AFFC and SC (when subjected to a specified deterministic spatial load pattern) depend only on the variability of the structural capacities but not on the variability of the load pattern magnitude.

A simple approximation for the mean system capacity, E[SC], will be suggested later. The covs of the system-level capacities are generally less than or equal to those of the individual member capacities due to the averaging and ordering involved in their calculation. The exact amount of reduction depends on parameters such as number of critical members, correlation between individual member capacities, number of potential failure sequences, etc. Simple determination of the system distribution or cov without simulation is seldom feasible. Exceptions are, for example, a structure with ductile members having only one possible plastic mechanism for failure (in which case the system capacity can be expressed as a linear combination of the individual capacities), or statically determinate structures with independent member capacities (for this "weak link problem", the cumulative probability distribution of the system capacity, $F_{SC}(\cdot)$, is given by: $F_{SC}(r)$ $= 1 - \prod_i [1 - F_i(r)]$, where, $F_i(\cdot)$ is the cumulative probability distribution of the i th member capacity). Results from a large number of different examples of different parallel unbalanced (statically indeterminate) structures, within the range of parametric variations suitable for fixed offshore jacket structures, indicates that the reduction of the system capacity cov, compared to the individual member capacity cov, is around 20 to 40% (e.g., see Table 4.2 for cases involving small correlation coefficient between member capacities).

The system factors (C_o, R_o, and S_o) introduced above measure the system effects (complexity and redundancy) with reference to member-level and system-level failure probabilities. The corresponding system factors quantifying the effects of complexity and redundancy on the system-level capacities (AFFC and SC) will be introduced here. Note that DFFC in the following definitions is the "deterministic first-failure capacity" introduced in Section 4.1.1.

101

$$\text{Capacity Reduction Factor Due to Complexity, } C_c = \frac{E[AFFC]}{DFFC}$$

$$\text{Capacity Increment Factor Due to Redundancy, } R_c = \frac{E[SC]}{E[AFFC]}$$

$$\text{Net System Factor on Capacity, } S_c = R_c C_c = \frac{E[SC]}{DFFC}$$

The "capacity system factors", C_c, R_c, and S_c, are independent of the variability (cov) of the load pattern magnitude. Otherwise, many other observations made about the system factors, C_o, R_o, and S_o are also applicable to the "capacity system factors". The capacity reduction factor due to complexity, C_c, measures the adverse "series system effect" on the system capacity at "any first-failure event" due to the presence of more than one failable member. This system effect is purely probabilistic in origin and is always present in both balanced and unbalanced multimember systems. Unlike C_o, C_c is always equal to or less than one. C_c depends inversely on the number of members, or more precisely, on the number of weak (heavily stressed) members. C_c will be shown to be positively dependent on the correlation between the member capacities and inversely dependent on the variability (cov) of the individual member-capacity variables.

The redundancy factor, R_c, represents the redundancy effect (both deterministically and probabilistically induced) on the system capacity of the intact system with respect to overloads. R_c, unlike R_o, is greater than or equal to one. If the structure is statically determinate, R_c is equal to one. For a statically indeterminate structure, R_c will be shown to depend strongly on the "deterministic system back-up" (indicated by the deterministic system factor, DSF). Given a nonzero "deterministic system back-up" (i.e., DSF > 1), R_c is greater than one. However, even for systems that have no deterministic back-up (DSF = 1, e.g., balanced systems), because of the probabilistic variation of the capacities, individual realizations of the system can be such that the load at system failure is larger than the load at any first-member failure, and R_c can then be greater than one. This is more

likely to happen when the postfailure capacity, η, of members is high, and certain to happen if the members are ductile ($\eta = 1$). Hence, a balanced system may have positive probabilistic redundancy effect on the system capacity (i.e., $R_c > 1$) even in the absence of deterministic redundancy (i.e., DSF =1). The calculation of R_c requires evaluation of the expected ultimate system capacity, E[SC], considering all possible member failure sequences leading to the failure of the system. In contrast to C_c, R_c is strongly influenced by the postfailure behavior (η) of the members. The net system factor, $S_c = C_c R_c$, relates the expected system capacity directly to the deterministic first (weakest member) failure capacity. A net system factor greater than one implies positive system benefit reflecting net redundancy (i.e., $R_c > \frac{1}{C_c}$) of the structural system whether deterministically or probabilistically induced. As will be shown later, a major part of the redundancy effect (and hence of the net system effects) is of deterministic origin. The effect of deterministically induced redundancy on the capacity can be quantified through the deterministic system capacity (DSC) or the deterministic system factor (DSF). Hence, it is advantageous to quantify the general system effects on the capacities instead of doing so on the failure probabilities.

4.1.3 Estimation of System Failure Probabilities and System-Level Capacities by Reduced Space Monte Carlo Simulation

Failure probabilities and system-level capacities for this study were estimated by a Reduced Space Monte Carlo simulation (e.g., *Cornell, 1987; Karamchandani, 1987*). This approach is very suitable for the preceding representation of the system-level capacities as random variables. In this approach the load variable L is removed, and k samples from the reduced space of capacity variables ($\underline{R}$) are simulated. For each realization of the capacity variables ($\underline{r}^{(i)}$) the system-level capacities, affc$^{(i)}$ and sc$^{(i)}$, are calculated. For the i th realization, the conditional probability of system failure, p$^{(i)}$, is calculated from the

103

probability distribution of the load, L (i.e., $p^{(i)} = (p_f | R = r^{(i)}) = P \{ L > sc^{(i)} \}$).

Because the load is characterized by a single random variable, the computation of $p^{(i)}$ is simple. The expected system capacity, E[SC], is estimated as the average of the calculated system capacities, $sc^{(i)}$, for each realization, and the failure probability, p_f, is estimated as the average of the conditional probabilities, $p^{(i)}$. The cov of the system capacity can also be estimated as follows:

$$E[\hat{SC}] = \frac{1}{k} \sum_{i=1}^{k} sc^{(i)} ; \qquad (4.2)$$

$$\hat{cov}[SC] = \frac{1}{E[\hat{SC}]} \sqrt{\frac{1}{k} \sum_{i=1}^{k} (sc^{(i)})^2 - E[\hat{SC}] * E[\hat{SC}]}$$

$$cov(E[\hat{SC}]) = \frac{1}{\sqrt{k}} \hat{cov}[SC]$$

where $cov(E[\hat{SC}])$ is an estimate of the uncertainty in the estimator of E[SC], and

$$\hat{p}_f = \frac{1}{k} \sum_{i=1}^{k} p^{(i)} ; \qquad cov(\hat{p}_f) = \frac{1}{\hat{p}_f} \frac{1}{\sqrt{k}} \sqrt{\frac{1}{k} \sum_{i=1}^{k} (p^{(i)})^2 - \hat{p}_f * \hat{p}_f} \qquad (4.3)$$

where $cov(\hat{p}_f)$ is an estimate of the uncertainty in the estimator of P_f.

Similarly, the expected any-first-member failure capacity, E[AFFC], and the corresponding probability of any-first-member failure, P{AFF}, can be estimated from the reduced space simulation results.

For a load driven problem, i.e., load sensitivity (α_L) >> capacity sensitivity (α_{SC}), p_f can be estimated through Equation 4.1 with a small cov of estimation from relatively few samples. For example, for lognormally distributed load and capacity variables with covs 0.40 and 0.10 respectively, a failure probability of the order 10^{-3} was estimated with covs of estimation 0.30, 0.15, 0.10, 0.04 and 0.03 from sample sizes 10, 40, 90, 550, and

104

1000 respectively. In contrast, using general Monte Carlo simulation, estimation of the same failure probability with a cov of estimation 0.30 would require about 10^4 samples. Each simulation in the reduced space approach yields some information about the estimate of p_f through $p^{(i)}$, whereas in general Monte Carlo simulation only few samples are considered hits (i.e., failed according to the performance function). For well behaved problems a cov of estimation between 0.3 and 0.1 is considered acceptable for reliability estimation, requiring from 10 to 90 simulations (for the range of covs and failure probability as stated in the example above). In this study for the lognormal case, however, a sample size of 1000 was used, because the purpose was to estimate the failure probability as accurately as possible for comparison between different cases with parametric variation. The cov of estimation, described above, is sensitive to the form of the probability distribution of the governing variables. A discussion of the effect of distribution shape (Lognormal vs. Normal) on the efficiency of reduced space Monte Carlo Simulation is given in Appendix II.

4.2 IDEALIZATION OF STRUCTURAL SYSTEMS

To quantify the general trends of the system factors, near-ideal parallel structural systems have been investigated. The systems are as shown in Fig.4.4b, but with an arbitrary number of members, n. For a general structure, the safety margin of the member i in the intact condition can be written as: $M_i^o = R_i - a_i^o L$, where a_i^o is the load influence coefficient for the member i in the intact structure due to the global load, L and R_i is the capacity of member i. For postfailure analysis we use the so-called "member replacement" method (see Section 1.1.2). After the failure of the member k the safety margin of the same member i can be written as: $M_i^k = R_i - a_i^k L + c_i^k \eta R_k$, where, ηR_k is the postfailure capacity of the failed member k, and c_i^k is the load influence coefficient for the

105

member i due to a pair of unit loads acting at the nodes corresponding to the failed member k in a structure where member k is considered removed (see *Karamchandani, 1987*).

a) Real Structure (Two Dominant Memmbers)   b) Idealized Parallel Structure
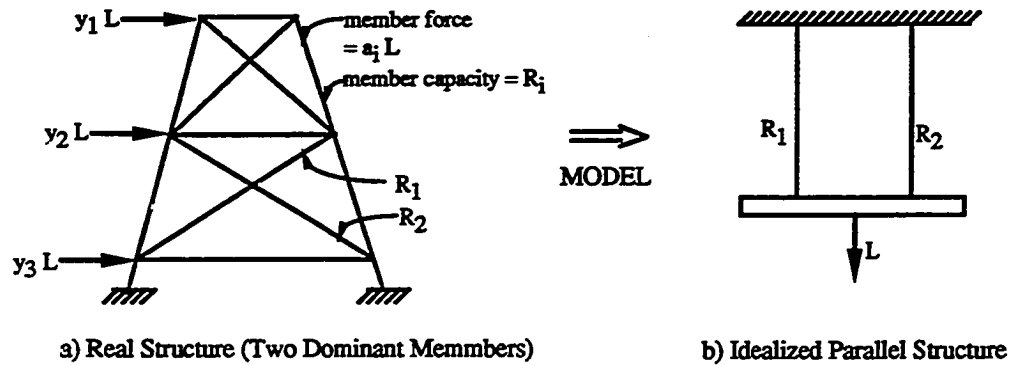
Fig. 4.4   Idealization of Statically Indeterminate Structure.

For a general structure, the member capacities and the influence coefficients vary from member to member, so observed trends of the system behavior are hard to generalize. Parallel structural systems have, in the past, been characterized by common member stiffness and by all the member capacities having the same mean and the coefficient of variation. This class of perfectly balanced systems has been studied by many investigators (e.g., *Daniels,1945; Hohenbichler and Rackwitz, 1983a; Guenard, 1984; Stahl and Geyer, 1985; Cornell, 1987; Rackwitz and Gollwitzer, 1988;* etc.).

Balanced structures represent behavior of real structures that are well optimized (i.e., perfectly proportioned) under a single load case (see Section 1.1.1). Offshore structures, in general, are unbalanced. One of the reasons for unbalance is that the diverse design requirements such as, loadout, transportation, launching, etc., require strengthening of certain members beyond that required by the inplace load condition. Often this implicitly provided unbalance has more pronounced "system effects" than an idealization of the balanced type might suggest.

106

In the study of parallel systems, unbalance can be introduced by unequal member capacities and / or unequal load influence coefficients. In this study, unbalance is simulated through unequal mean member capacities, keeping the load influence coefficients a_i^k the same for all the members. There can be a number of different possible ways that a general structure can redistribute the load given up by the failed member (e.g., load redistributed only to few adjacent members; load redistributed to a group of "weak" members or "strong" members only, etc.). For a proper parametric study involving different redistribution schemes many conditions need to be investigated. The present investigation is restricted to the simplest case of equal redistribution among the surviving members, i.e., where the influence coefficient c_i^k in a given damaged state is same for all members. This assumption is not true for a general system, and this should be kept in mind while generalizing conclusions from the near-ideal parallel systems studied here. For example, the redistribution due to the failure of a diagonal in an X-brace will be localized. On complete failure of an X-braced subsystem (both diagonals failed), however, the load is expected to be almost evenly redistributed among the surviving parallel braces.

Because there also is any number of different ways the capacities of the members can be unequal, we first restrict our attention to the case with two groups of members, called "weak" and "strong"; within each group all the members have the same mean capacity. This category of unbalanced systems will be referred to as the "binary-capacity system". (Balanced systems can be studied as special cases of the "binary-capacity" unbalanced systems with no "weak" members.) Subsequently, results from unbalanced systems with linear capacity gradient and finally with arbitrary capacity unbalance will be discussed.

4.3 SYSTEM BEHAVIOR OF BALANCED PARALLEL SYSTEMS

Balanced parallel structural systems are the simplest class of idealized structures that are of interest for studying system effects. This is also the starting point of the present

107

investigation. In a balanced (deterministic) structure with mean member capacities, all the members are stressed up to their limit at the time of first member failure and hence such a structure progressively collapses at the first failure load in spite of its high degree of static indeterminancy. The static pushover diagram of a balanced (deterministic) parallel structure with mean member capacities is as shown in Fig. 4.5. For the example shown in Fig. 4.5 it has also been assumed that the postfailure capacities (η) of all the members are the same. In the absence of deterministic system back-up (i.e., DSF = 1.0) the deterministic first failure capacity (DFFC = λ_1) is equal to the deterministic system capacity (DSC = λ_{max}).
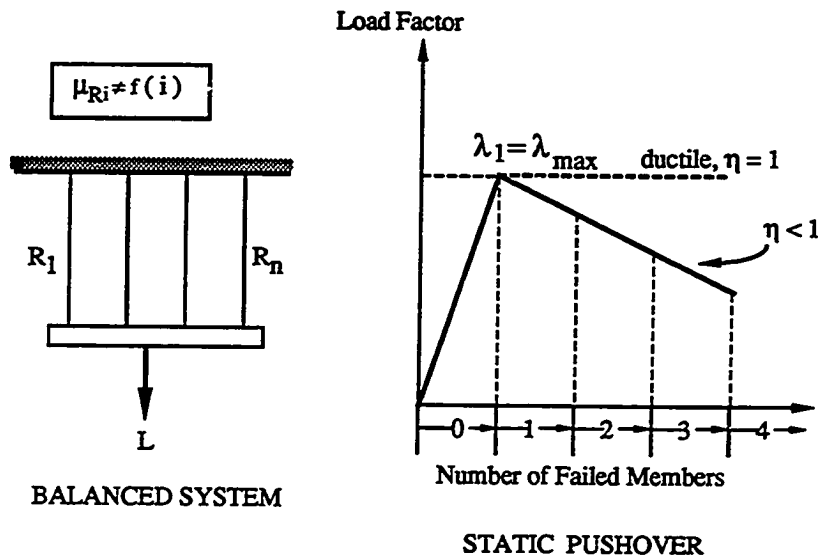
Fig. 4.5 Static Pushover Test of a Deterministic Balanced Parallel System

Given the safety factors of individual members equal in the mean, it is possible, however, that individual realizations of the structure will be unbalanced, i.e., some members will have capacities (noting that the load influence coefficients for parallel structural systems are equal) more than the mean while others will have capacities less than the mean member capacity. The system effects (such as C_0 or E [AFFC]) in a balanced

108

system are strictly due to these probabilistic variations of the capacity and load variables. Figs. 4.6 and 4.7 show the effects of variation of the number of members and the postfailure capacity (η) of individual members in a balanced parallel structure on the system factors, C_0, R_0, and S_0. In all the simulation cases, the mean capacity of the members are assumed to be unity. As the number of members increases, the mean value of the common load L, is increased to keep the most-likely-first (MLM) failure probability to a prescribed level of 1.3×10^{-3} (i.e., the reliability index $\beta = 3$). This is adopted as a basis for equality of comparison between cases with unequal numbers of members. Furthermore, the load and the individual member capacities are assumed to be lognormally distributed with covs $\delta_L = 0.4$ and $\delta_{R_i} = 0.1$ respectively; the individual member capacities are assumed to be equicorrelated, with a correlation coefficient, $\rho_{R_i R_j} = 0.3$. The choice of the above base parameters are motivated by experience in analyzing offshore jacket structures. The same base parameters are used for the subsequent study of unbalanced systems. Selected parametric variations around the base case parameters have been investigated. Furthermore, the effect of postfailure capacity is studied for $\eta = 1.0, 0.7,$ and 0.4. The postfailure compression capacity of a tubular truss member in an offshore jacket is often modelled as having $\eta = 0.4$, whereas the postfailure capacity for tension failure is given by $\eta = 1.0$.
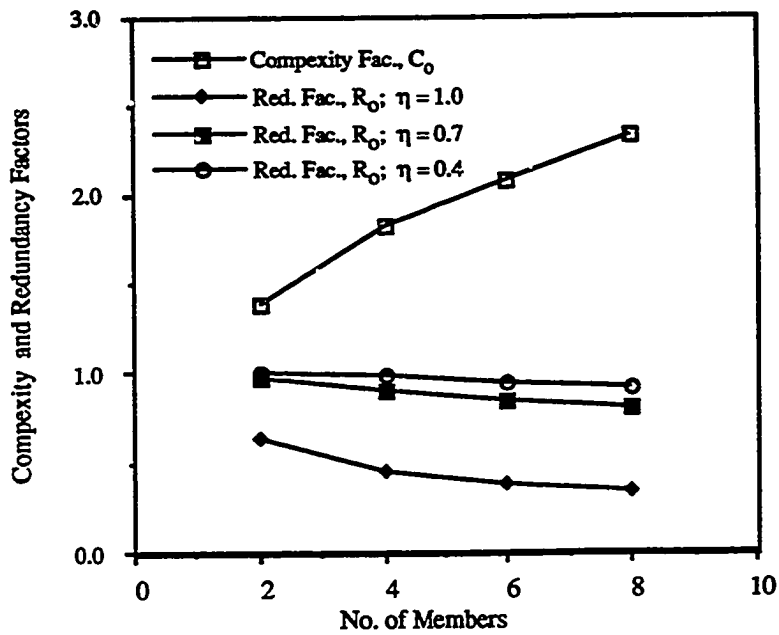
109

Fig. 4.6 Complexity and Redundancy Factors for Balanced Parallel Structures
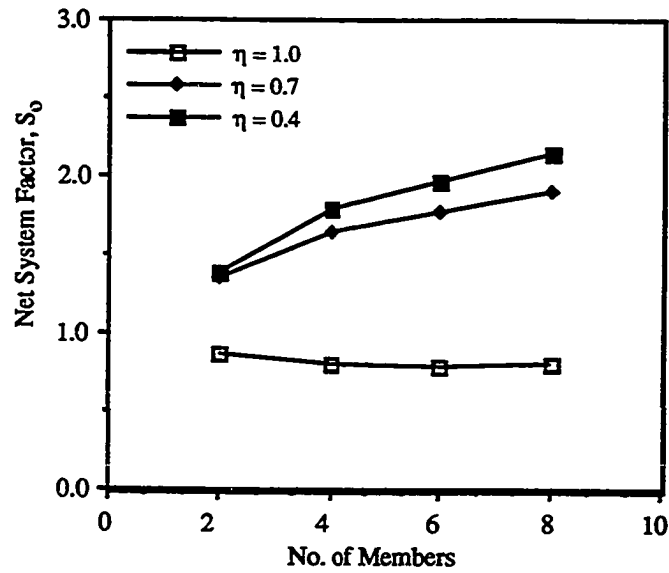

Fig. 4.7 Net System Factors for Balanced Parallel Structures

110

Fig 4.6 shows, as expected, the complexity factor, C_0, increases with the increase in the number of members (i.e., the number of potential failure initiators). Also note that unlike redundancy factors, the complexity factors are independent of the postfailure capacity (η) of individual members. Probabilistic redundancy for balanced systems, as measured by the redundancy factor, R_0, can be neglected (i.e., $R_0 \approx 1.0$) unless the members are ductile ($\eta = 1.0$). Fig 4.7 shows that for balanced parallel structures with nonductile members ($\eta < 1$), the complexity effect on the system failure probability dominates over the redundancy effect resulting in a net adverse system effect (i.e., $S_0 > 1$). A slight overall system benefit (i.e., $S_0 < 1$) is gained if the members are ductile.

The stochastic dependence among the member failure events (measured by the correlations between individual member safety margins) is influenced by the relative variability of the load and capacity variables and by the degree of the correlation between individual member capacities. The effects of parametric variations of the cov of the safety margin of individual members in the intact structure and the correlation between the safety margins on the system factors, C_0, R_0, and S_0, are well documented in *Cornell, 1987*. Some qualitative conclusions from *Cornell, 1987* are as follows. For highly correlated safety margins (i.e., the variability (cov) of the common load is much greater than the member-capacity variability and / or the member capacities are very highly correlated) the system effect vanishes. On the other hand, in general, for the case of independent safety margins (seldom realizable in practical situations because of the presence of the common load random variable in all the safety margins), balanced structures exhibit adverse system effect (i.e., $C_0 > \frac{1}{R_0}$), unless the members are ductile. The system factors are also sensitive to the failure probability level (and / or the equal safety factor) of individual members.

In the present study, the emphasis is on quantifying the system effects in terms of the "capacity system factors". As will be shown later, the capacity system factors of balanced

111

structures are useful in understanding and in approximately estimating system-level capacities of unbalanced structures.

For any stochastically realized structural system the system capacity is greater than or equal to its first failure capacity, by definition. Hence, $E[SC] \geq E[AFFC]$. For a general system, the difference between $E[SC]$ and $E[AFFC]$ will depend on redundancy, both deterministically and probabilistically induced. For the case of balanced parallel systems the entire redundancy is probabilistically induced. This probabilistic redundancy is very small unless the structural members are ductile. Consider simulating parallel systems which are balanced in the mean. Each realization of the structure will be unbalanced. However, because the mean capacity of each member is the same and their covs relatively small, the member capacities will be quite close to each other. Hence all the members will be stressed almost to their limit at the time of first failure. Therefore, unless the members are ductile, the chance of the structure withstanding the load given up by the first failed member and manifest a system capacity larger than the first-failure capacity is small. It follows then that for nonductile balanced systems we expect, $E[SC] \approx E[AFFC]$.

Given that the probabilistic redundancy is small, the dominating system effect in balanced parallel systems is the "adverse series system effect" or complexity. As a consequence, for a balanced parallel system $E[SC] \leq DFFC$ (or, $E[SC] \leq DSC$, since for balanced systems $DSF = 1$, i.e., $DFFC = DSC$), where the equality sign holds for ductile systems ($\eta = 1.0$) and in the trivial case when the number of members = 1.

Some typical simulation results (based on 1000 samples) for balanced parallel systems are shown in Table 4.1. The individual member capacities are assumed to be lognormally distributed with mean = 1 unit, cov $\delta_{R_i} = 0.1, 0.2$, and common correlation ($\rho_{R_iR_j}$, $i \neq j$) as reported. Two common member ductility levels given by $\eta = 0.4$ and 1.0 are considered. Compared to the complexity factor, C_0 (and hence S_0) the capacity reduction factor due to complexity, C_c (and hence S_c) have relatively stronger dependencies on the correlation of member capacities because the load variability in the case of the latter does not play a role.

112

Higher correlation coefficient cases reported below are only of theoretical interest because the member capacities are not expected to be highly correlated in the case of jacket structures.

Selected results from Table 4.1 are presented graphically (Figs. 4.8.1 through 4.10). The capacity reduction factor due to complexity, C_c, continues to depend on the number of members (i.e., on the number of potential failure initiators), cov of the individual capacities (Fig. 4.9), and the correlation between individual member capacities (Fig. 4.10). R_c for balanced systems with nonductile members came consistently close to 1.0, implying E[SC] $\approx$ E[AFFC]. As expected, the net system factor on capacity, S_c, for ductile systems is close to one, because E[SC] = DSC = DFFC for ductile balanced structures. For nonductile systems, among all the factors, C_c, R_c, and S_c, only C_c is independent of the postfailure capacity measure η. Hence for nonductile systems, it is simplest to quantify results on the complexity measure C_c and approximate $R_c \approx 1.0$ (and hence $S_c \approx C_c$). This approximation makes it possible to estimate simply the expected system capacity of a more general redundant structure whose individual members may have different postfailure capacities.

113

Table 4.1 Capacity System Factors of Balanced Parallel Structures
(Lognormal model for member-capacity variables)

| # of Mem.	$\rho_{R_iR_j}$	δ_{R_i}	C_c	$\eta = 0.4$		$\eta = 1.0$	
				R_c	S_c	R_c	S_c
2	0.0	0.1	0.943	1.000	0.943	1.060	0.999
4	"	"	0.899	1.003	0.901	1.114	1.001
6	"	"	0.878	1.007	0.884	1.140	1.000
8	"	"	0.865	1.011	0.875	1.156	1.000
2	0.3	"	0.952	1.000	0.952	1.050	0.999
4	"	"	0.916	1.001	0.917	1.094	1.002
6	"	"	0.898	1.004	0.901	1.115	1.001
8	"	"	0.886	1.007	0.892	1.129	1.000
2	0.6	"	0.963	1.000	0.963	1.037	0.999
4	"	"	0.937	1.000	0.937	1.070	1.002
6	"	"	0.923	1.001	0.924	1.085	1.002
8	"	"	0.913	1.002	0.915	1.095	1.000
2	0.9	"	0.981	1.000	0.981	1.018	0.999
4	"	"	0.969	1.000	0.969	1.034	1.002
6	"	"	0.962	1.000	0.962	1.042	1.002
8	"	"	0.956	1.000	0.956	1.046	1.000
2	0.3	0.2	0.904	1.004	0.9077	1.104	0.998
4	"	"	0.838	1.018	0.853	1.199	1.004
6	"	"	0.805	1.032	0.830	1.246	1.003
8	"	"	0.784	1.042	0.817	1.276	1.004

114
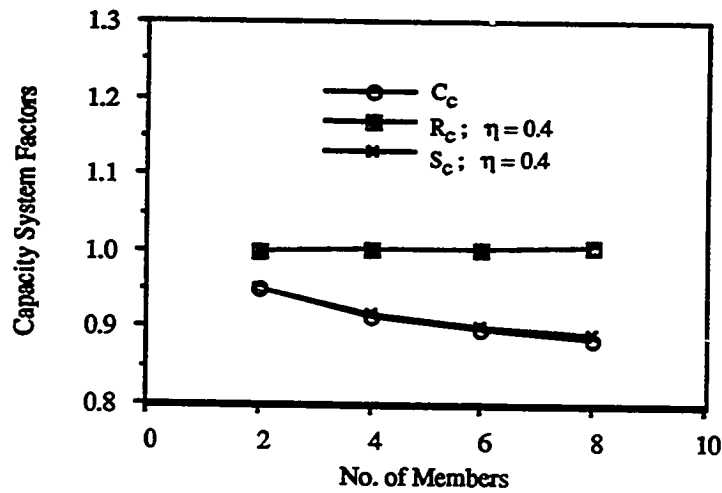
Fig. 4.8.1 Capacity System Factors for Balanced Parallel Structures; $\eta = 0.4$

(Table 4.1; $\delta_{R_i} = 0.1$; $\rho_{R_iR_j} = 0.3$)
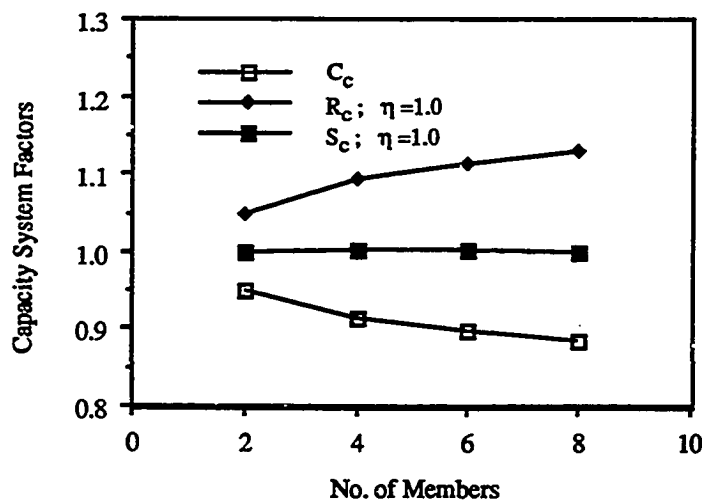
Fig. 4.8.2 Capacity System Factors for Balanced Parallel Structures; $\eta = 1.0$

(Table 4.1; $\delta_{R_i} = 0.1$; $\rho_{R_iR_j} = 0.3$)

115
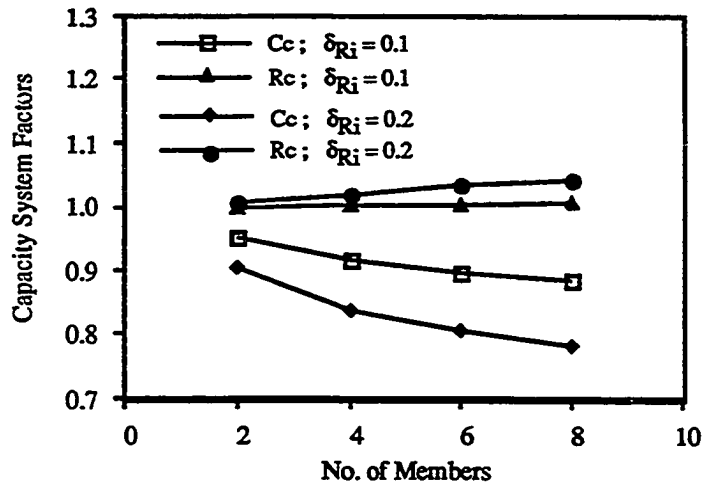
Fig. 4.9 Capacity System Factors of Balanced Parallel Structures;
Parametric Variation of the Member-Capacity COV
(Table 4.1; $\rho_{R_iR_j} = 0.3$; $\eta = 0.4$)
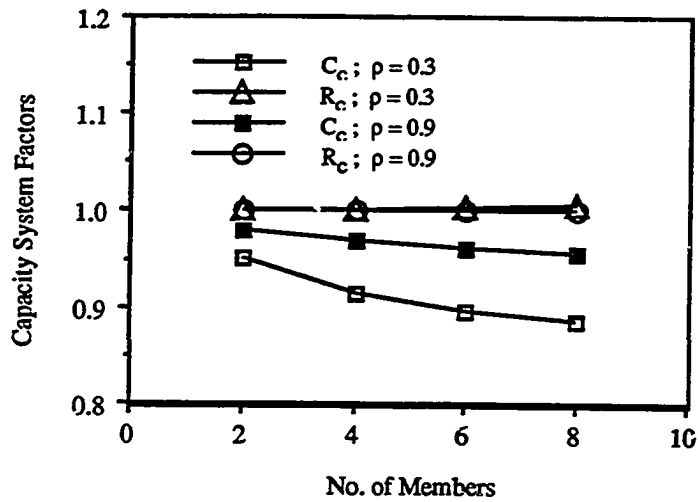
Fig. 4.10 Capacity System Factors of Balanced Parallel Structures;
Parametric Variation of the Correlation between Member capacities
(Table 4.1; $\delta_{R_i} = 0.1$; $\eta = 0.4$)

116

In addition to results of expected system capacity, E[SC], and expected any first failure capacity, E[AFFC], coefficients of variation of the system-level capacities are also of interest (see Section 4.1.2.1). Accordingly, simulation estimates (from 1000 samples) of the covs of system-level capacities (AFFC and SC) of balanced parallel structures for the lognormal distribution model of the member-capacity variables are reported in Table 4.2. Note that the cov (AFFC) is independent of the postfailure capacity of the members. The covs of the system-level capacities depend on the common cov of the individual member-capacity variables and (inversely) on the common correlation between the member-capacity variables. As in Table 4.1, the higher values of the member-capacity correlation are reported for theoretical understanding only. As expected the cov of the system-level capacities get closer to the common member-capacity cov as the correlation increases. The expected values and covs of the system-level capacities appear sensitive to the correlation between the member-capacity variables. However, such variations in capacity may or may not be significant in estimating system-level failure probabilities. In particular, for offshore jacket structures the load variability is much greater than the capacity variability, and hence the problem is "load driven". In addition if the upper tail of the probability density function of the load variable decays slowly (e.g., lognormal) the system failure probabilities will be insensitive to small changes in system capacity parameters; this implies the member-capacity correlations have to be very large before they can begin to influence the system-level failure probabilities.

117

Table 4.2 COV of System-Level Capacities for Balanced Structures

(Lognormal model for member-capacity variables)

# of Mem.	$\rho_{R_iR_j}$	δ_{R_i}	δ(AFFC)	δ(SC)	
				$\eta = 0.4$	$\eta = 1.0$
2	0.0	0.1	0.082	0.082	0.070
4	"	"	0.068	0.065	0.048
6	"	"	0.066	0.058	0.041
8	"	"	0.063	0.051	0.035
2	0.3	"	0.087	0.087	0.080
4	"	"	0.080	0.079	0.069
6	"	"	0.078	0.074	0.065
8	"	"	0.077	0.071	0.063
2	0.6	"	0.093	0.093	0.089
4	"	"	0.089	0.089	0.084
6	"	"	0.088	0.087	0.082
8	"	"	0.088	0.086	0.081
2	0.9	"	0.099	0.099	0.098
4	"	"	0.097	0.097	0.096
6	"	"	0.097	0.097	0.096
8	"	"	0.098	0.098	0.097
2	0.3	0.2	0.174	0.171	0.160
4	"	"	0.159	0.149	0.138
6	"	"	0.154	0.140	0.130
8	"	"	0.152	0.133	0.125

4.4 SYSTEM BEHAVIOR OF UNBALANCED PARALLEL SYSTEMS

4.4.1 Parallel Structures with Two Capacity Levels ("Binary-Capacity Systems")

Unbalance can be simulated in many different ways. All systems investigated here, are assumed to redistribute the load given up by the failed members equally among the surviving members. In the simplest class of unbalanced parallel structures studied here,

118

only two different levels of member capacities are considered. Within each group, all members have the same mean capacity. All capacities in the two group, weak and strong, have the same coefficient of variation. The capacities are also assumed to be equicorrelated. In all the simulations the (common) mean capacity of the weak members is assumed to be unity. As in the case of balanced parallel structures, as the number of members increases, the common load L, is increased to keep the most-likely-first failure (MLM) probability to a prescribed level of 1.3×10^{-3}. The amount of unbalance is characterized by the "excess capacity" and the "degree of unbalance". The base case is a balanced system with a net capacity of $n\mu_{Rw}$, where n = the total number of members and μ_{Rw} = the mean weak member capacity = 1 unit. If we want to study the effect of strengthening the system by x % excess capacity, we may do so by distributing the "excess capacity" equally among all the members (resulting in a balanced case with higher DFFC and lower P{MLM} compared to the base case), or among a specified number of members, n_S (= number of "strong members", $n_S \leq n$) members. We will refer to the remaining n_w (= $n - n_S$) members as "weak members". The degree of unbalance, r, is the ratio of mean capacities of the strong members (μ_{Rs}), to that of the weak members (μ_{Rw}). Hence it follows:

$$\text{excess capacity in \%, } x = \frac{n_S (\mu_{Rs} - \mu_{Rw})}{n \, \mu_{Rw}} * 100$$

$$\Rightarrow \quad \text{degree of unbalance, } r = \frac{\mu_{Rs}}{\mu_{Rw}} = 1 + \frac{x}{100} * \frac{n}{n_S} \tag{4.4}$$

Under deterministic static pushover analysis (Fig. 4.11) the weak members fail simultaneously at load $L_w = n \, \mu_{Rw}$. The load at which the strong members fail is given by: $L_S = n_S \, \mu_{Rs} + \eta \, n_w \, \mu_{Rw}$. The binary system will have "deterministic system back-up", i.e., L_S will be larger than L_w only if $r > (n-\eta \, n_w) / n_S$. The deterministic system factor, DSF, is given by:

119

$$DSF = \frac{L_s}{L_w} = \frac{n_s \, r + n_w \, \eta}{n} \qquad \text{when } L_s > L_w \qquad (4.5)$$

$$= 1 \qquad \text{otherwise}$$

For a given excess capacity of x% and n, n_s, and hence n_w, the degree of unbalance (r) and the deterministic system factor (DSF) can be calculated using Equations 4.4 and 4.5.
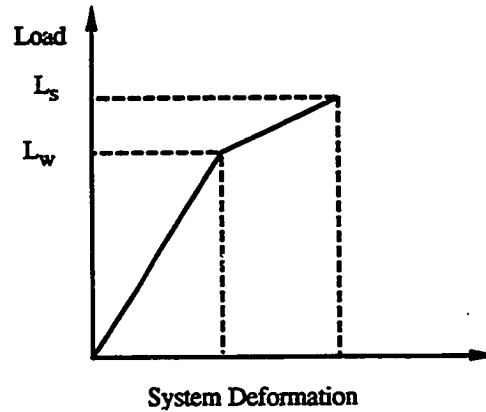
Fig. 4.11 Static Pushover Diagram of a Deterministic Binary System

Lognormal models are adopted for both the load and capacity variables. The coefficients of variation for load and capacity are adopted as 0.4 and 0.1 respectively. The capacities are modeled as equicorrelated with a correlation coefficient 0.3. The following parameters are varied during the study. The total number of members, n, is varied between 2 and 8. For each n, all possible cases of unbalance (i.e., n_s and n_w, given $n = n_s + n_w$) are investigated for excess capacities: 10%, 30%, and 60%. Furthermore, the effect of postfailure capacity is studied for $\eta = 1.0, 0.7,$ and 0.4.

The "base" balanced parallel system is a special case of the binary-capacity system with all members weak ($n = n_w$ and $n_s = 0$) and no excess capacity. The case corresponding to all strong members (i.e., $n_s = n$) is also a balanced case where all individual members have higher capacity and reliability compared to the base case.

120

Results from the parametric study of binary parallel structures are presented below (Table 4.3 and Figs. 4.12.1 through 4.18.2). In all the graphs results for different possible combinations of the number of weak members for each given total number of members (and hence of the number of strong members) are shown. In some cases (e.g., system failure probability of ductile member systems), however, the results are independent of the variation of the n_S or n_W for a given total number of members, n. The results of deterministic measures for the parametric variations are presented first.

Deterministic System Capacity

Table 4.3 presents the normalized deterministic system capacity (= DSC / n) for representative cases for different excess capacities and member postfailure capacities. The normalizing factor used is the total number of members, n. Because the deterministic (mean) capacity of the weak members in the study is assumed to be 1 unit, deterministic first failure capacities (DFFC) of the binary unbalanced systems are equal to n. Hence for binary unbalanced systems, the deterministic system factor, DSF, is equal to the normalized deterministic system capacity. However, for the special (balanced) case of n_W = 0 (or n_S = n), the deterministic (mean) capacity of the each member is given by: 1+ x / 100, where x% excess capacity is distributed equally among the members of the base balanced structure. Hence, the normalized deterministic system capacity for the balanced case of n_W = 0 is equal to 1 + x / 100, and not equal to its DSF which is 1 for balanced systems.

Also note that the normalized deterministic system capacity for ductile systems is independent of n, n_W, or n_S and is given by: 1 + x / 100 (Equations 4.4 and 4.5).

121

Table 4.3 Normalized Deterministic System Capacity

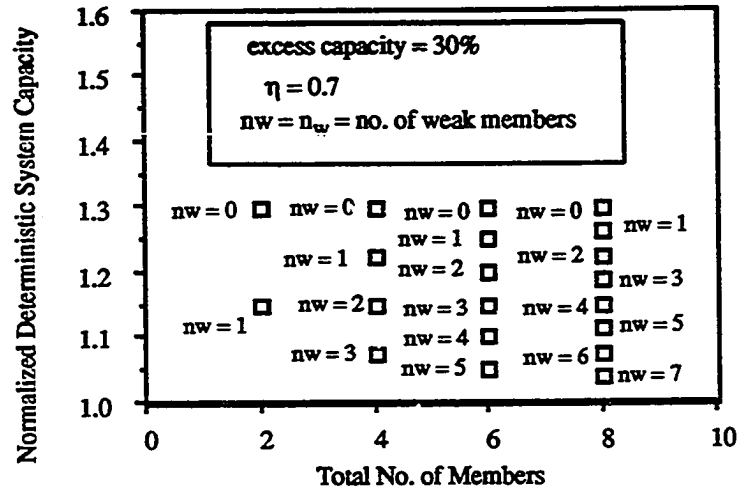(Various excess capacity , x%, and postfailure capacity, η)

# of Mem. n	# of Weak Mem. n_w	# of Strong Mem. n_s	Normalized Deterministic System Capacity; DSC/n			
			$x = 10\%$ $\eta = 0.4$	$x = 30\%$ $\eta = 0.4$	$x = 30\%$ $\eta = 0.7$	$x = 60\%$ $\eta = 0.4$
2	0	2	1.10	1.30	1.30	1.60
"	1	1	1.00	1.00	1.15	1.30
4	0	4	1.10	1.30	1.30	1.60
"	1	3	1.00	1.15	1.23	1.45
"	2	2	1.00	1.00	1.15	1.30
"	3	1	1.00	1.00	1.08	1.15
6	0	6	1.10	1.30	1.30	1.60
"	1	5	1.00	1.20	1.25	1.50
"	2	4	1.00	1.10	1.20	1.40
"	3	3	1.00	1.00	1.15	1.30
"	4	2	1.00	1.00	1.10	1.20
"	5	1	1.00	1.00	1.05	1.10
8	0	8	1.10	1.30	1.30	1.60
"	1	7	1.03	1.23	1.26	1.53
"	2	6	1.00	1.15	1.23	1.45
"	3	5	1.00	1.08	1.19	1.38
"	4	4	1.00	1.00	1.15	1.30
"	5	3	1.00	1.00	1.11	1.23
"	6	2	1.00	1.00	1.08	1.15
"	7	1	1.00	1.00	1.04	1.08

122
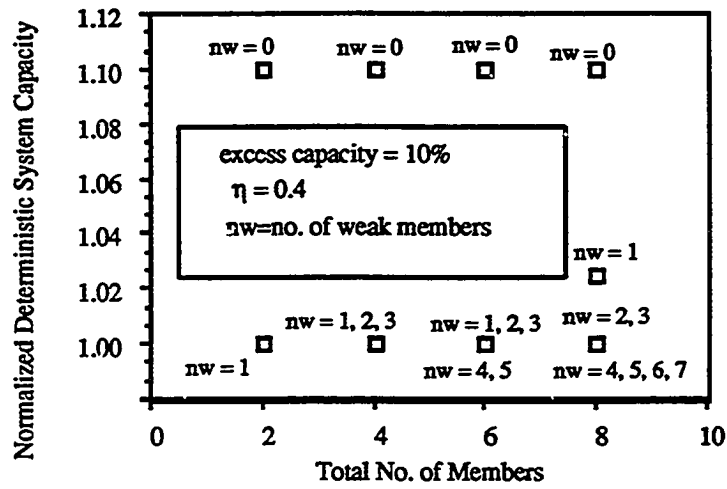
Fig. 4.12.1 Normalized Deterministic System Capacity
(Excess Capacity = 10%; postfailure capacity, $\eta = 0.4$)
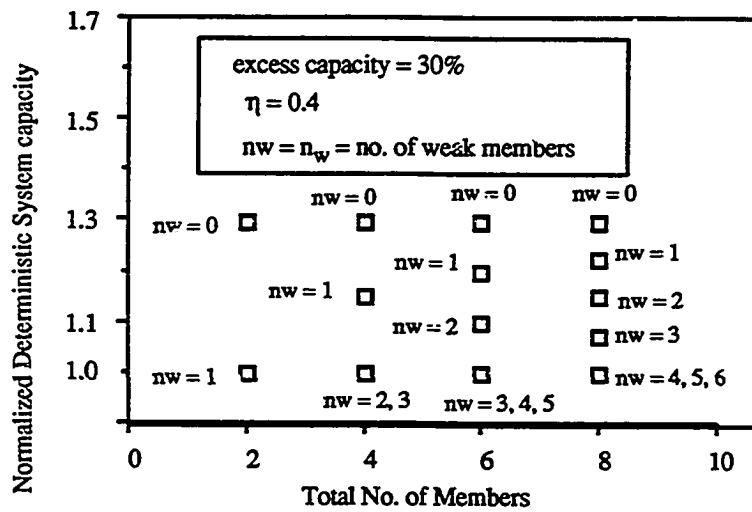
Fig. 4.12.2 Normalized Deterministic System Capacity
(Excess Capacity = 30%; postfailure capacity, $\eta = 0.4$)

123

Fig. 4.12.3 Normalized Deterministic System Capacity
(Excess Capacity = 30%; postfailure capacity, η = 0.7)

Figs. 4.12.1 through 4.12.3 are plots from data shown in Table 4.3. For nonductile binary parallel systems the deterministic system capacity is largest when the excess capacity is distributed equally among all the members, even though the resulting balanced structure (with n_W = 0) will have no deterministic system back-up (i.e., DSF = 1). Table 4.3.and Fig. 4.12.1 show that for a small excess capacity of 10% and a low ductility given by η = 0.4; among all the unbalanced cases (i.e., $0 < n_W < n$), only one case (n =8; n_W =1) has normalized deterministic system capacity (and hence DSF) greater than 1.0. Table 4.3 and Figs. 4.12.2.through 4.13.3 show the positive system benefit of increasing the amount of excess capacity and / or the postfailure capacity of the members.

Probability of System Failure

Figs. 4.13.1 through 4.13.4 below show the effect of variations of the excess capacity (and hence the level of unbalance) and the common member-ductility level (η) on the

124

probability of system failure for binary parallel structures. For nonductile structures (Figs. 4.13.1 and 4.13.2), the probability of system failure for a given excess capacity increases with the number of members (i.e., number of potential failure initiators) in the system. For a given total number of members of the structure, the system reliability depends on how evenly the excess capacity is distributed among the members, i.e., lower the number of "weak" members the better.

One interesting observation: *to maximize the reliability the best way to distribute the excess capacity to a balanced system is to do so evenly among all the members. The resulting balanced structure will have no "deterministic back-up" (i.e., DSF = 1) and very small probabilistic redundancy implying $R_O \approx 1.0$.*

In contrast, having all the excess capacity in just one "strong" member may (depending on other parameters, such as, n, η, and excess capacity x) imply an improvement in the redundancy measures, DSF and R_0, but as shown in Fig 4.11.1 the improvement in system reliability compared to the base case (balanced structure with no excess capacity) will be marginal. On the other hand, the balanced parallel structure with the specified excess capacity will have an overall improvement in all the individual member reliabilities (in particular, in the reliability of the weakest, i.e., MLM member) and in the deterministic first member failure capacity, DFFC compared to the base case structure with no excess capacity. This in turn will result in an improvement of the system reliability and deterministic system capacity, DSC in spite of poor redundancy measures (i.e., DSF =1 and $R_0 \approx 1.0$). The probability of system failure increases as the excess capacity is distributed among fewer and fewer members. This was observed at different ductility levels and for different amounts of excess capacity of nonductile systems. The variation of the system failure probability with n_w or n_s (for a given n) decreases with increasing ductility (η). For fully ductile members, such variations with the number of strong members, n_s, are negligible. This is because the expected system capacity of a ductile system is independent of n_s, for a given n, while the change in the cov of the system

125

capacity with n_S is so small (especially relative to the load cov) that the system failure probability remains effectively unchanged. For example for a six member ductile system with 30% excess capacity, the estimated covs (from 1000 samples) of the system capacity for $n_S = 6$ and $n_S = 3$ are 0.0649 and 0.0651(the individual member capacities are equicorrelated with a common correlation coefficient of 0.3 and have a common cov of 0.10) respectively.
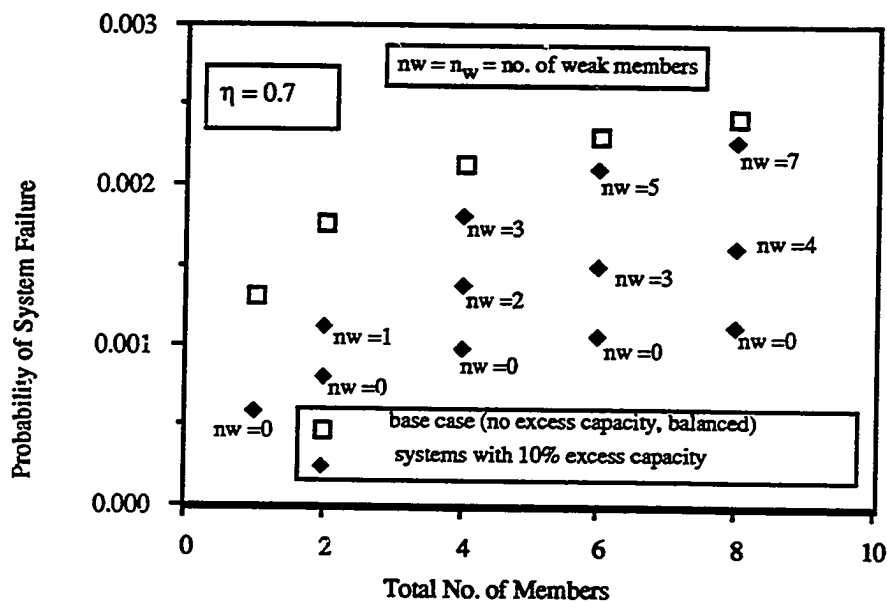
Fig. 4.13.1 Effect of Excess Capacity and its Distribution among the
Members on Probability of Binary-System Failure
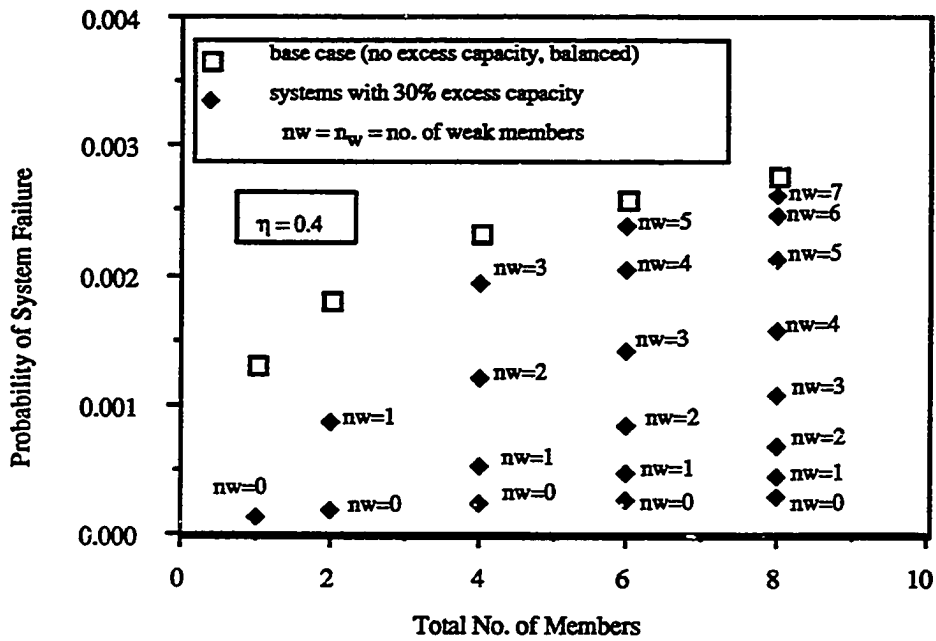(Excess capacity = 10%; postfailure capacity $\eta = 0.7$)

126

Fig. 4.13.2 Effect of Excess Capacity on Probability of Binary-System Failure

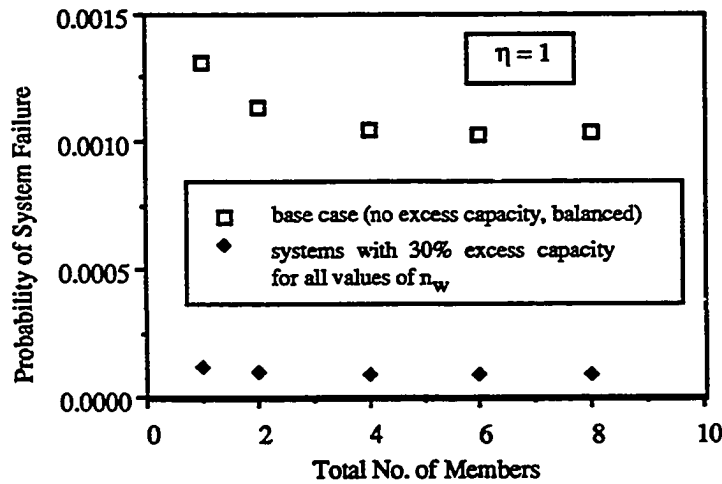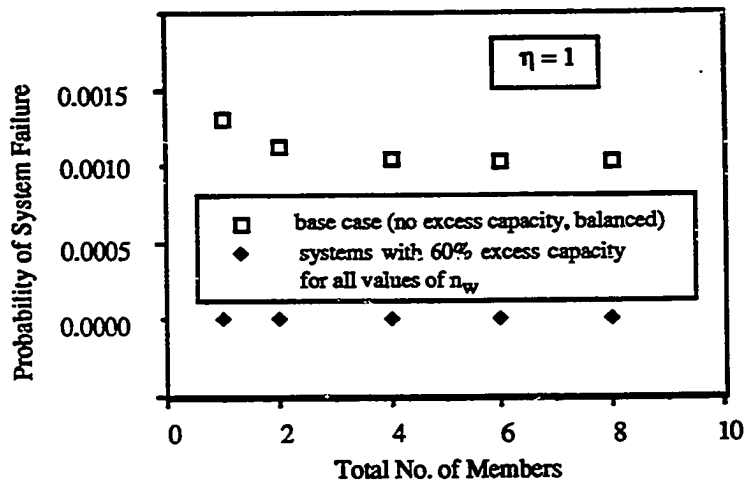(Excess capacity = 30%; postfailure capacity η = 0.4)

Fig. 4.13.3 Ductile Systems: Effect of Excess Capacity on

Probability of Binary-System Failure

(Excess capacity = 30%; postfailure capacity η =1.0)

127

Fig. 4.13.4 Ductile Systems: Effect of Excess Capacity on
Probability of Binary-System Failure
(Excess capacity = 60%; postfailure capacity η =1.0)

Complexity Factor. C_o

Figs. 4.14.1 through 4.14.3 below show the effect of three levels of excess capacity on
the complexity factor, C_o. We conclude from Figs. 4.13 2 and 4.14.3 that the complexity
factor for a binary system with high degree of unbalance (e.g., excess capacity = 30% or
60%) may be approximated from a balanced system with number of members equal to the
number of weak members in the unbalanced system. This was found true for cases with
excess capacity as low as 10%, except for cases with the number of weak members n_w = 1
(Fig. 4.14.1). Fig 4.14.1 also shows that for 10% excess capacity and n_w = 1, the
complexity factor increases with the total number of members. For all the cases
investigated, the complexity factors of binary systems were found to be independent of the
total number of members and dependent only on the number of weak members, except for
the cases with a single weak member. For a very small degree of unbalance this
observation will not hold, because then even the strong members (having mean capacities

128

close to that of weak members) may contribute to the any-first-member failure probability. For the same reason, the extension of this rule to non-binary-capacity systems (e.g., systems with a linear member-capacity gradient or arbitrary capacity variation of each member, etc.) is not straightforward.
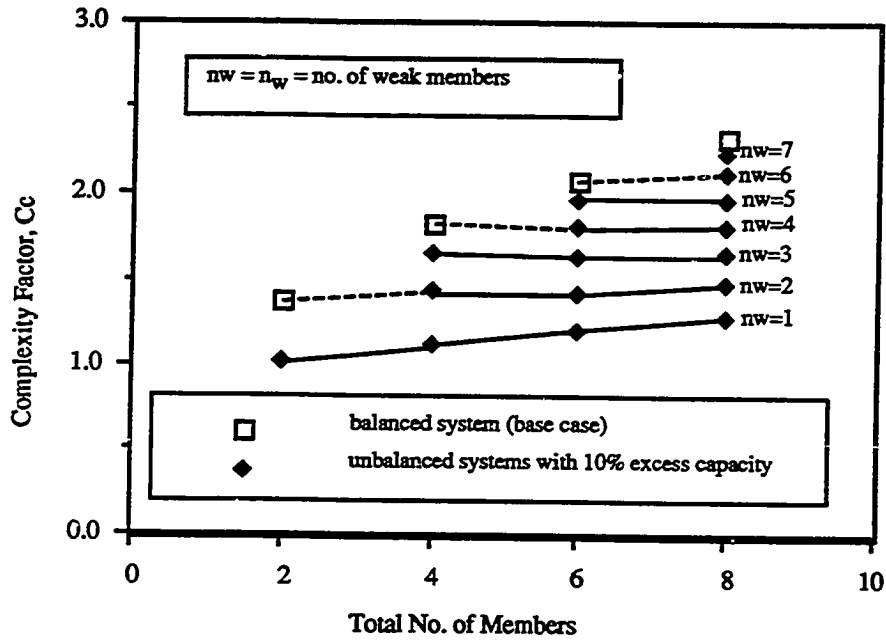

Fig. 4.14.1 Complexity Factor, Co, of Unbalanced Binary Systems; (Excess Capacity = 10%)
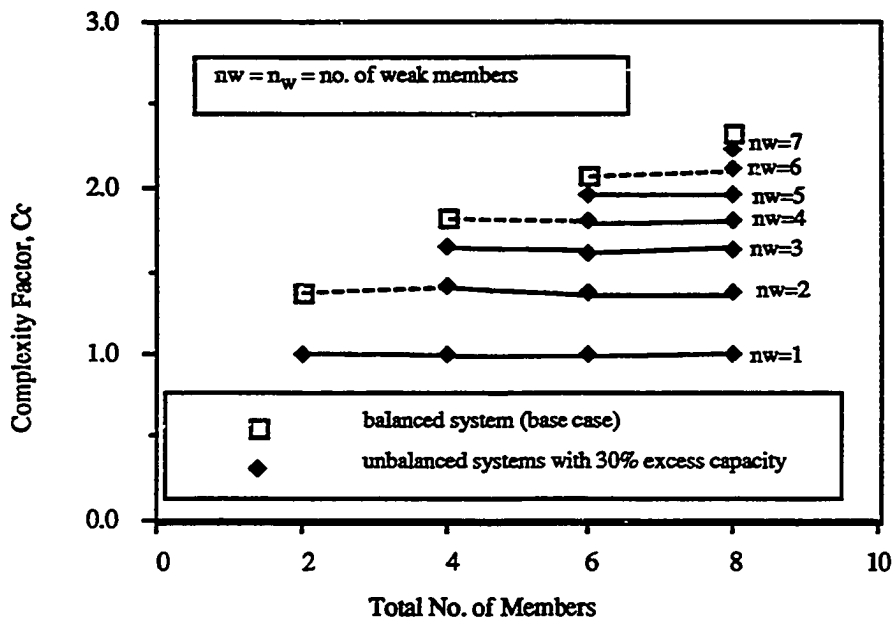
129

Fig. 4.14.2 Complexity Factor, C_0, of Unbalanced Binary Systems; (Excess Capacity = 30%)

Fig. 4.14.3 Complexity Factor, C_0, of Unbalanced Binary Systems; (Excess Capacity = 60%)
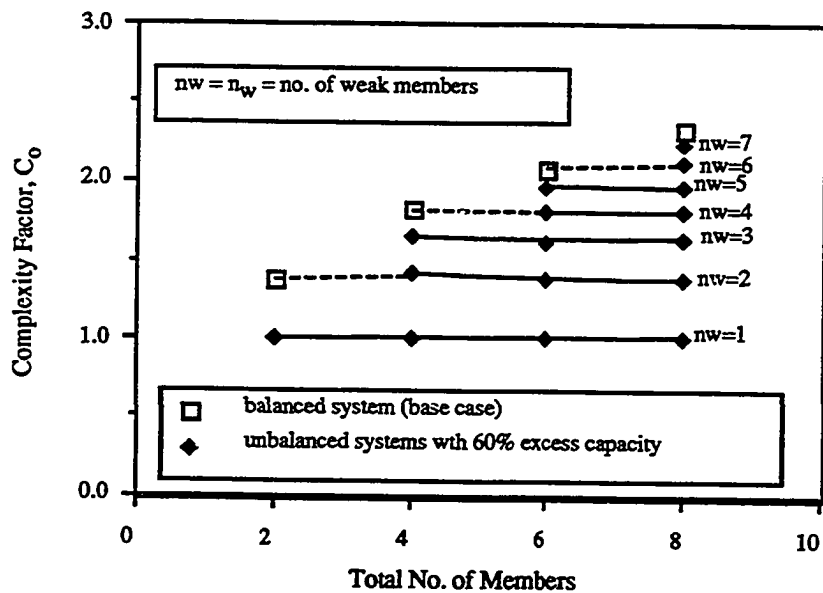
130

Redundancy Factor, R_o

Figs. 4.15.1 through 4.16.4 below show the redundancy factor of binary systems for various levels of excess capacity and member postfailure capacity. Figs. 4.15.1 and 4.15.2 show that for higher ductility levels ($\eta = 0.7, 1.0$), the redundancy factor, R_o, is a weak function of both the total number of members, n and of the number of weak members, n_w, but a strong function of the amount of excess capacity, x, and hence of the "deterministic system back-up" (see Table 4.3 and Figs. 4.12.1 through 4.12.3). Therefore, for systems with high ductility ($\eta \geq 0.7$), we suggest that the redundancy factor may be approximated by that of a simple two member ($n = 2$; $n_w = n_s = 1$) unbalanced system with the same excess capacity. Redundancy factors for the cases with $\eta = 0.4$ were found to be relatively more sensitive to the number of weak members, n_w, for a given total number of members, n (Fig. 4.15.2, Figs. 4.16.2 through 4.16.4). A close-up plot for η =0.7 with excess capacity = 30% is shown in Fig. 4.16.1 for the purpose of comparison.
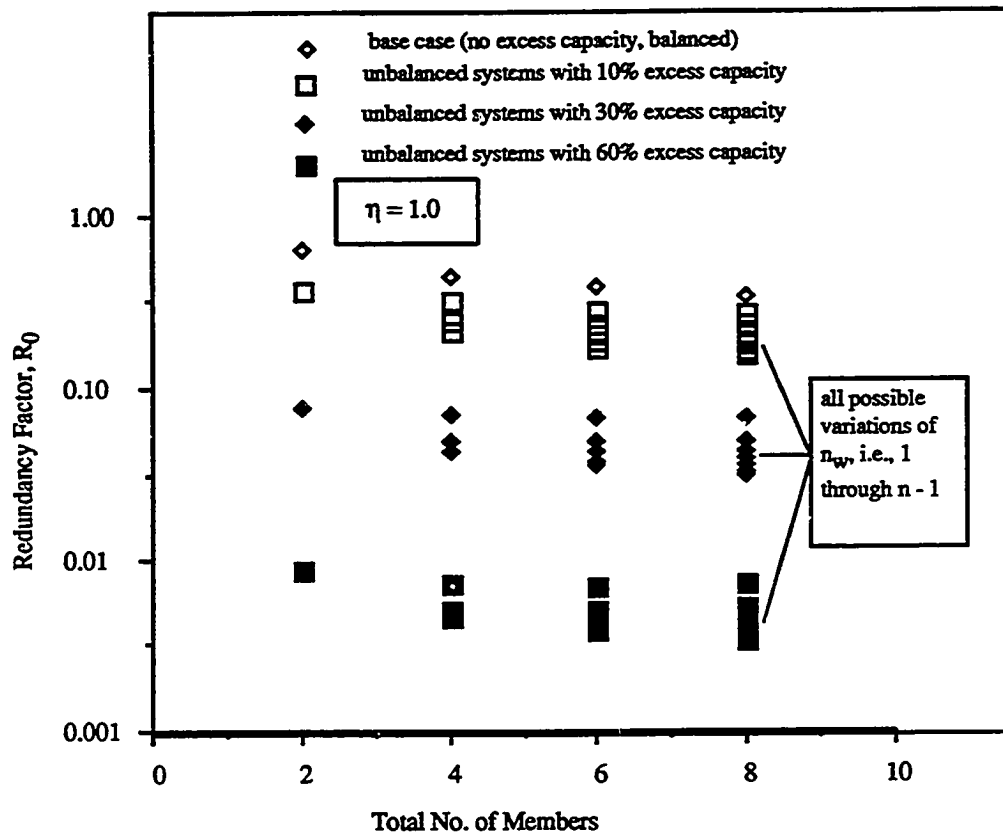
131

Fig. 4.15.1 Redundancy Factor, R_O, for Binary Systems, $\eta = 1.0$

The figure legend reads:

◇ base case (no excess capacity, balanced)
☐ unbalanced systems with 10% excess capacity
◆ unbalanced systems with 30% excess capacity
■ unbalanced systems with 60% excess capacity

$\eta = 1.0$

all possible variations of n_w, i.e., 1 through n - 1

Axis labels: Redundancy Factor, R_O (vertical); Total No. of Members (horizontal)
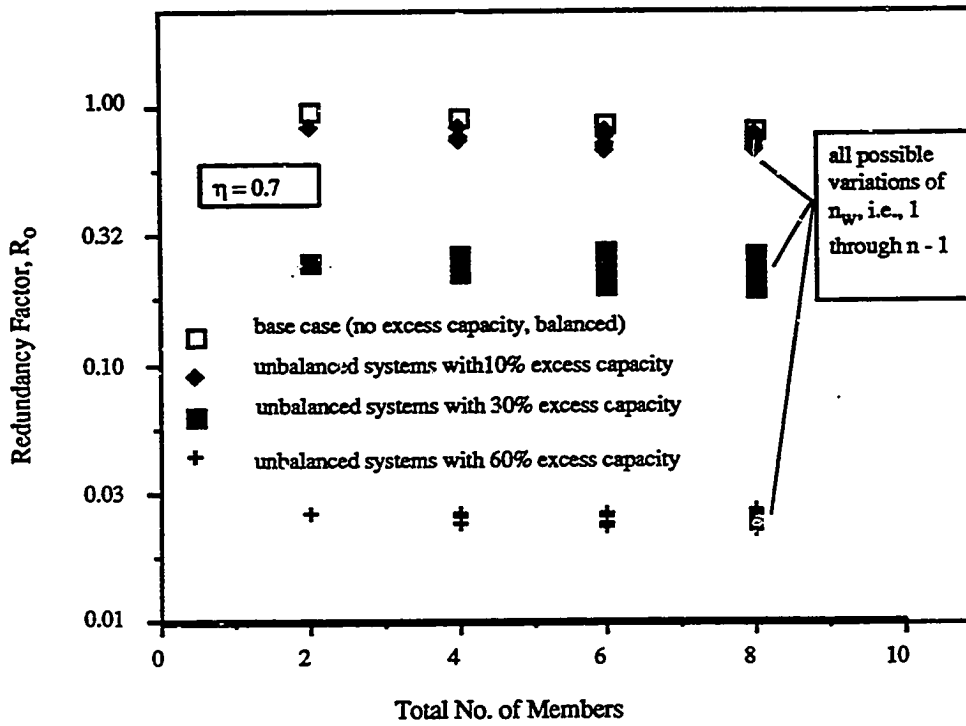
132

Fig. 4.15.2 Redundancy Factor, R_O, for Binary Systems, $\eta = 0.7$
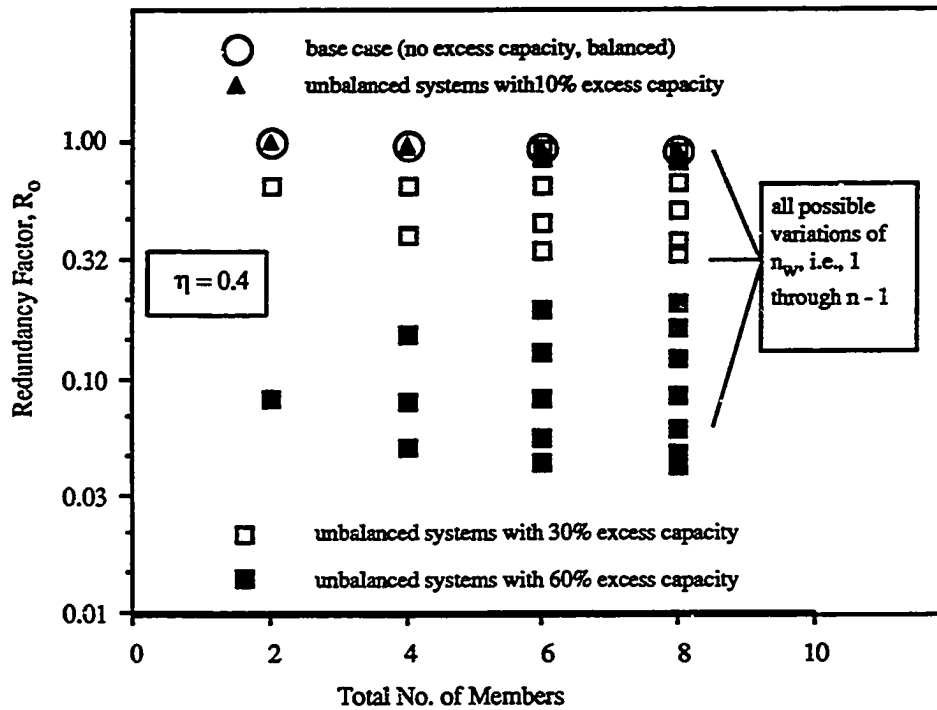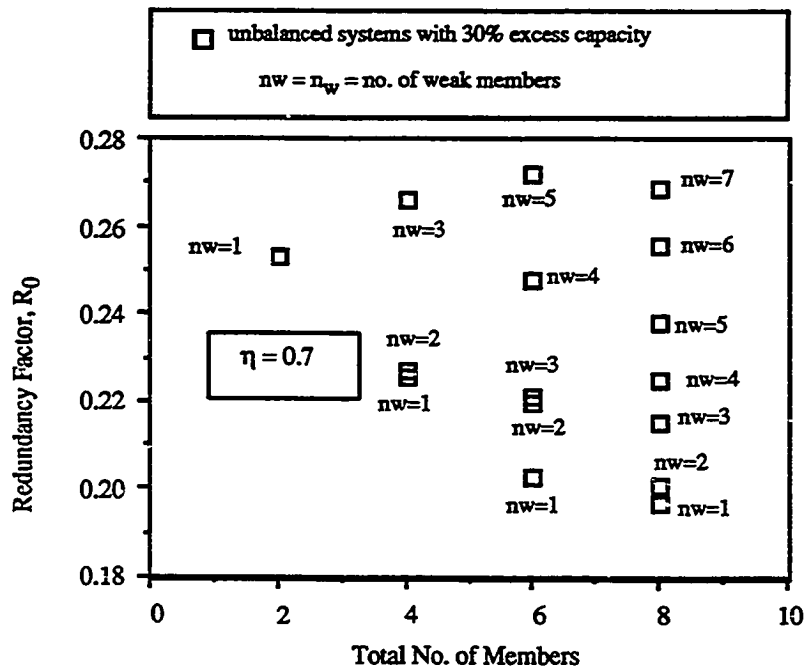
133

Fig. 4.15.3 Redundancy Factor, R_o, for Binary Systems, $\eta = 0.4$

134

Fig. 4.16.1 Redundancy Factors For Binary Systems, $\eta = 0.7$
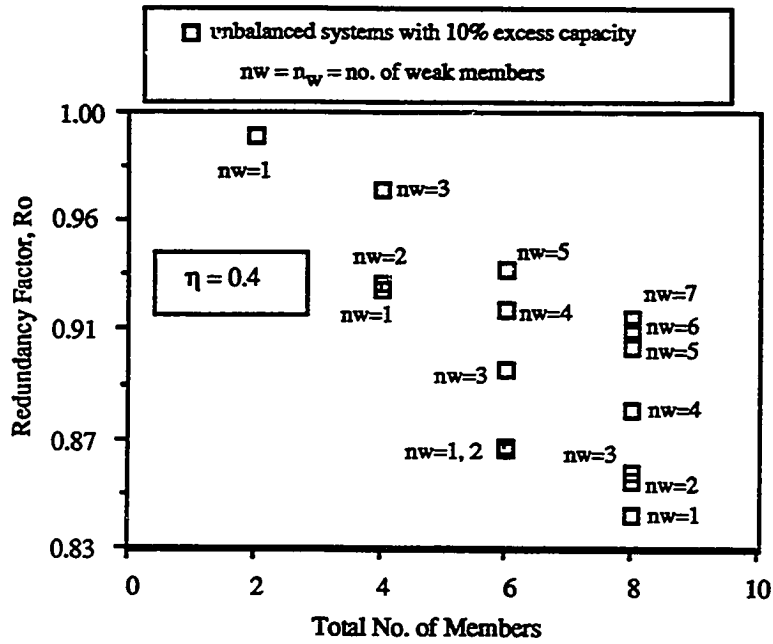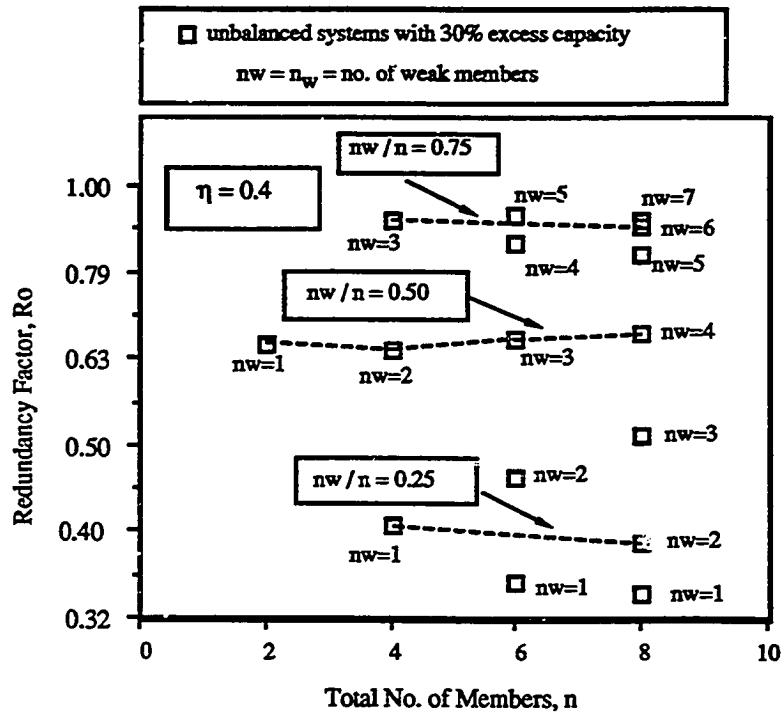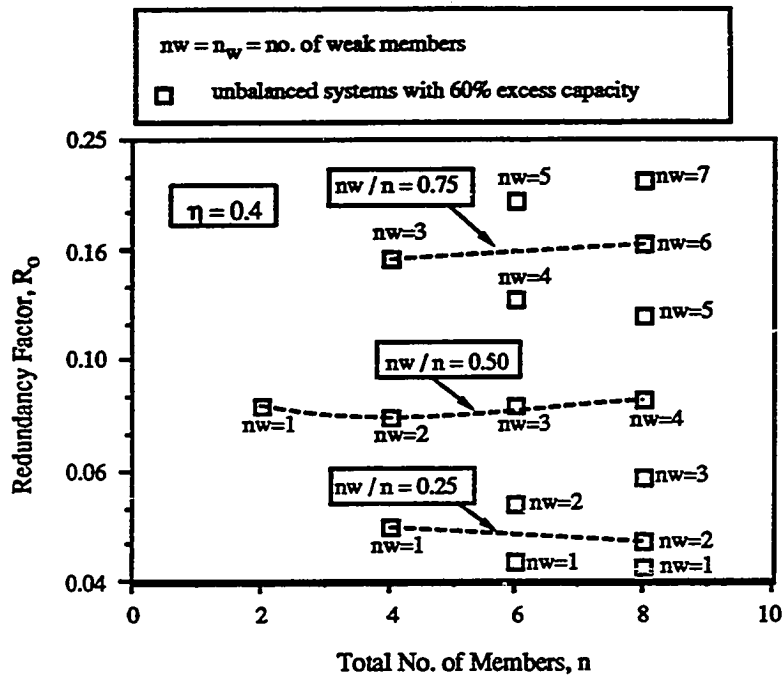(Excess Capacity = 30%)

135

Fig. 4.16.2 Redundancy Factors For Binary Systems, $\eta = 0.4$
(Excess Capacity = 10%)

136

Fig. 4.16.3 Redundancy Factor, R_O, For Binary Systems, $\eta = 0.4$
(Excess Capacity = 30%)

137

Fig. 4.16.4 Redundancy Factor, R_0, For Binary Systems, $\eta = 0.4$
(Excess Capacity = 60%)

For systems with low level of ductility (e.g., $\eta = 0.4$), and high excess capacity ($x = 30\%$ and 60%) the redundancy factor, R_0, was found to depend on the ratio of the number of weak members to the total number of members (Figs. 4.16.3 and 4.16.4). This pattern was not observed either for high ductility (e.g., $\eta = 0.7$, Fig. 4.16.1) or for low excess capacity (e.g., $x = 10\%$, Fig. 4.16.2). R_0 continues to depend strongly on the amount of excess capacity. For a general unbalanced binary system, with low ductility and high excess capacity, we suggest that R_0 may be approximated from the simplest unbalanced system with the same n_w / n ratio.

For unbalanced systems with no deterministic back-up (DSF = 1, or more precisely, r $\leq (n - \eta\, n_w) / n_s$, see Equation 4.5, e.g., all cases with 10% excess capacity in Fig. 4.16.2

138

except the case with $n = 8$ and $n_w = 1$ which has a DSF close to but greater than 1), R_0 may be estimated to be equal to 1.0.

These simplifying rules are suggested primarily to gain insight into the system behavior of unbalanced systems. We found that the complexity factors of unbalanced binary parallel structures could be related to the behavior of balanced systems. For highly unbalanced structures manifesting strong deterministic system back-up, the redundancy factor dominates (i.e., $R_0 << \frac{1}{C_0}$) and R_0 is a strong function of the excess capacity. Recall that one of the main objectives of this investigation is to find out when the redundancy effects due to deterministic unbalance are much greater than those due to the probabilistic effects. It appears from Figs. 4.15.1 through 4.15.3 that at 10% excess capacity the deterministic effects are comparable to the probabilistic effects and this is consistent with the 0.10 cov of the individual member-capacity variables. Figs. 4.15.1 through 4.15.3 show that for excess capacity of 30% or larger the deterministic effects dominate over the probabilistic effects. In view of this importance of the deterministically induced system back-up, the further studies of the unbalanced system behavior focused on the system-level capacities (rather than system-level failure probabilities) which can be related to the deterministic system back-up as measured by the deterministic system capacity, DSC, or the deterministic system factor, DSF.

Expected System Capacity, E[SC]

Figs. 4.17 through 4.18.2 show the normalized expected system capacity (= E[SC] / n), obtained from 1000 simulations for each case, for various excess capacities and member ductility levels. Normalized deterministic system capacities (DSC / n) are also shown.

139
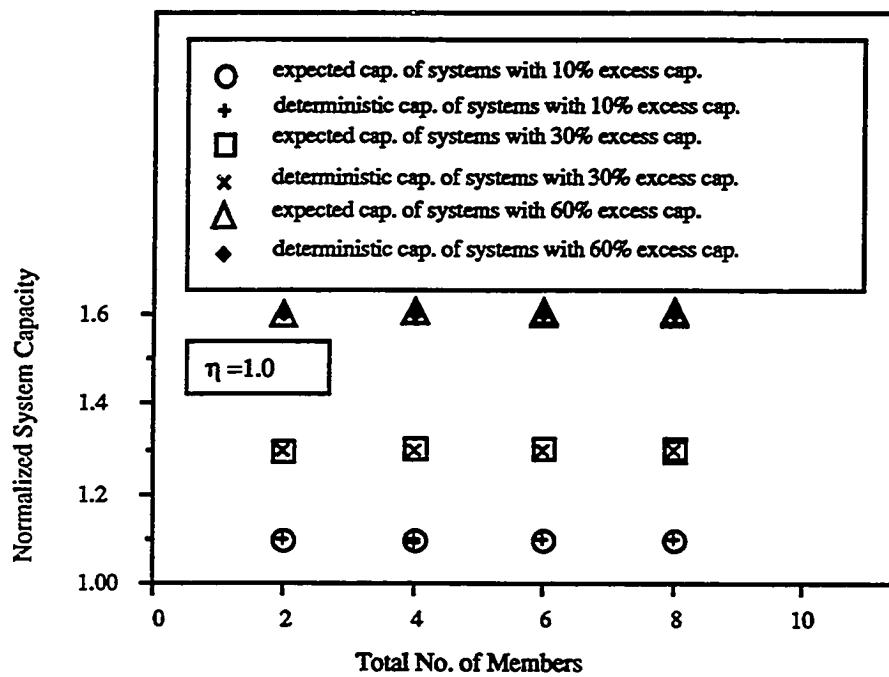
Fig. 4.17 Expected System Capacity of Ductile Binary Systems

140
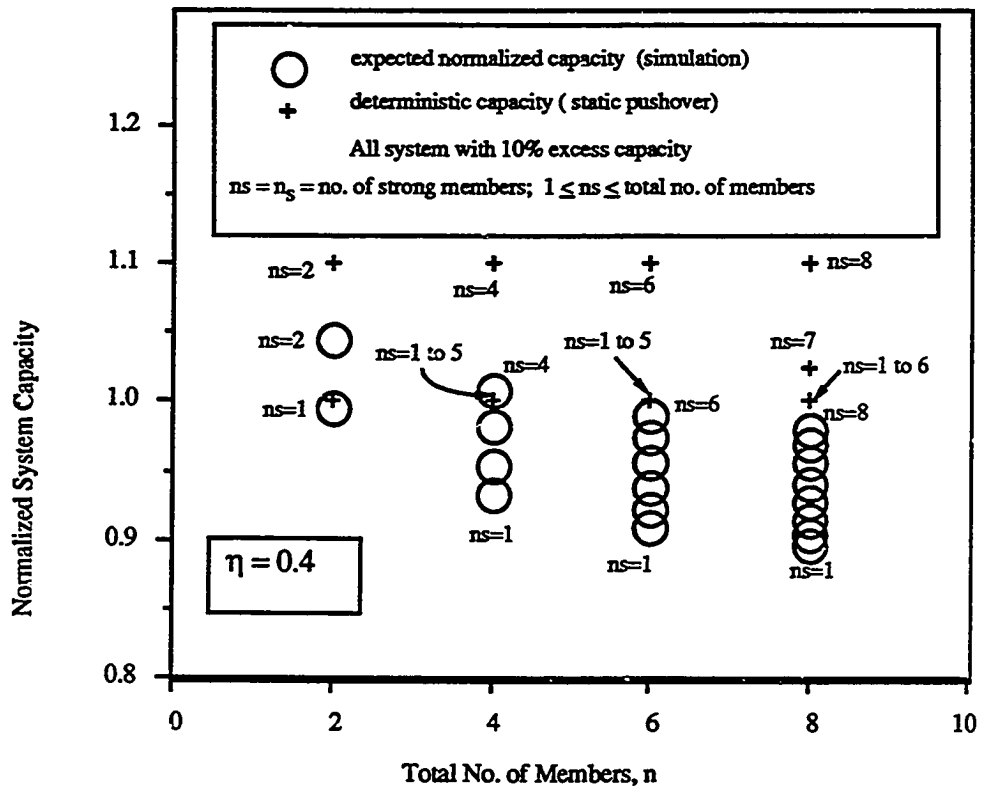
Fig. 4.18.1 Expected System Capacity of Nonductile Binary Systems
(Excess capacity = 10%; postfailure capacity η = 0.4)

141
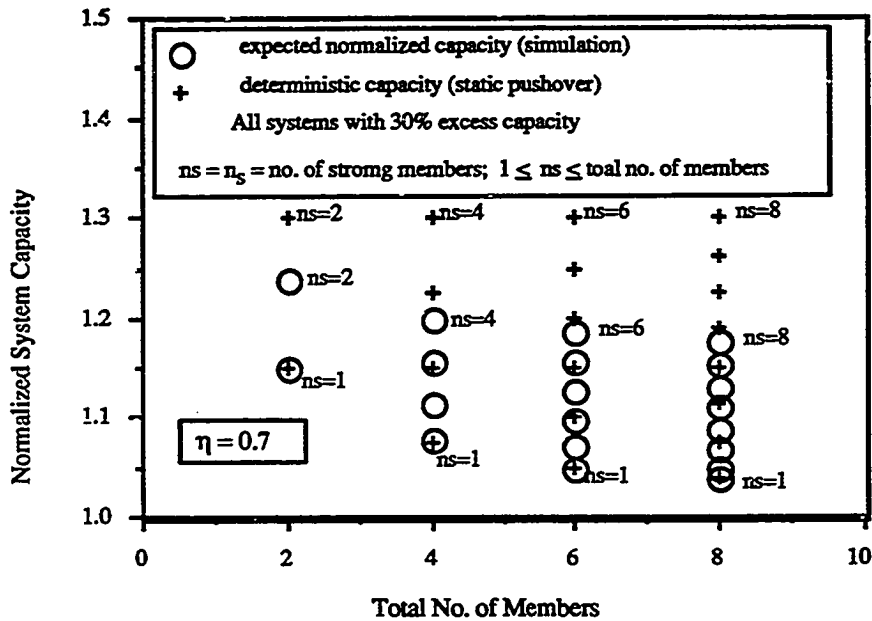
Fig. 4.18.2 Expected System Capacity of Nonductile Binary Systems
(Excess capacity = 30%; postfailure capacity η = 0.7)

Results in Fig. 4.17 confirm our earlier observation that for fully ductile systems, the (normalized) expected system capacity, E[SC], is equal to the (normalized) deterministic system capacity, DSC, which is independent of n, n_w, and n.

Figs. 4.18.1 and 4.18.2 show that for other binary unbalanced systems the expected system capacity is smaller than or equal to the corresponding deterministic system capacity. This implies that for binary parallel systems the reduction of system capacity from the deterministic level (DSC) due to complexity is greater than the increment due to redundancy of probabilistic origin. This observation was relatively more significant in the cases reported in Fig. 4.18.1, where most of the cases have no or little deterministic system back-up (i.e., DSF ≈ 1, see Table 4.3). All the cases reported in Fig. 4.18.2 have nonzero deterministic system back-up due to higher excess capacity and ductility. While the same

142

trend, namely E[SC] ≤ DSC, is observed in Fig. 4.18.2, the dominance of complexity effects over probabilistic redundancy effects are muted compared to the cases with no or negligible deterministic back-up (Fig. 4.18.1). One observation: among the cases reported in Fig. 4.18.2 (note, DSF > 1 for all cases, see Table 4.3), the expected system capacity is closest to the deterministic system capacity when all the excess capacity is distributed to one member, i. e., $n_S = 1$.

A set of rules for approximately estimating the expected system capacity of a binary system is given below. The rules have been motivated by the preceding observations.

Rule 1: *For fully ductile systems the expected system capacity is equal to the deterministic system capacity.*

Rule 2: *For nonductile unbalanced binary-capacity systems with deterministic system back-up (DSF > 1), the studies show that the expected system capacity, E[SC], may be approximated from that of a balanced system using the following rule: (i) assume all weak members have failed and estimate their deterministic residual capacity (= $\eta\, n_w\, \mu_{Rw}$); (ii) estimate the expected capacity of the set of strong members from the E[SC] of a balanced system with number of members equal to n_S; (iii) estimate the E[SC] of the unbalanced system by adding the deterministic residual capacity of the weak members to the E[SC] of the strong members.*

Rule 3: *The nonductile binary parallel system without deterministic system back-up (i.e., DSF ≤ 1; the static pushover diagram is similar to that of balanced systems as shown in Fig. 4.5) behaves much like a balanced system with the number of members equal to the number of weak members in the unbalanced system (n_w). The expected system capacity of an unbalanced binary system may be approximated by scaling the E[SC] of this equivalent balanced system by the ratio of the total number of members, n, to the number of the weak members, n_w. An example will follow.*

143

These rules are presented here primarily to add insight into the behavior of unbalanced systems. E[SC] for any binary-capacity unbalanced system with or without deterministic back-up can be estimated from E[SC] of an equivalent balanced system. Later on these rules will be extended for non-binary systems. E[SC] of representative balanced systems can be generated easily through simulation (Table 4.1).

The following examples illustrate the use of the approximating rules for E[SC] of binary-capacity nonductile systems.

Example 4.1: Binary System with Deterministic Back-up

Excess capacity, $x = 30\%$; $\eta = 0.7$ (all members); number of members, $n = 8$; no. of weak members, $n_w = 6$; no. of strong members, $n_s = 2$; common correlation between member capacities, $\rho_{R_iR_j} = 0.30$; cov $(R_i) = 0.10$; $\mu_{R_w} = 1.0$; $R_i \sim$ lognormal. Hence, from Equation 4.4, degree of unbalance, $r = 2.2$, i.e., $\mu_{R_s} = 2.2$ units, and from Equation 4.5, deterministic system factor, DSF $= 1.075$.

i) Deterministic residual capacity of "pre-failed" weak members $= 6 \times 0.7 \times 1 = 4.2$

ii) No. of members in the equivalent balanced system $= n_s = 2$

For, an equivalent balanced system with $n = 2$, $C_c = 0.952$ (Table 4.1)

Assume, $R_c \approx 1.000$ (exact result from simulation for $\eta = 0.7$ is 1.001)

Therefore, $S_c \approx C_c = 0.952$ (exact result from simulation for $\eta = 0.7$ is 0.953)

Approximate expected capacity of strong members $= 2 \times 0.952 \times 2.2 = 4.190$

iii) Approximate E[SC] of the unbalanced system $= 4.200 + 4.190 = 8.390$

Simulation results: estimated E[SC] $= 8.397$ and estimated cov of SC $= 0.068$

For a cov of member capacity $= 0.10$, the cov of the system capacity was observed to lie between 0.06 and 0.09. For fully correlated member capacities the cov of the system capacity is exactly equal to that of the member capacity. The cov of the system capacity decreases with increasing ductility (η) and increasing number of strong members, n_s. If the load sensitivity is large compared to the system capacity sensitivity, the system failure

144

probability can be approximated by the probability of the load exceeding the approximate E[SC], i.e., neglecting the variability of the system capacity (see Section 4.1.2.1). For example, under the lognormal model of load and individual member-capacity variables, for a system capacity (not lognormal) with E[SC] = 8.397 and cov= 0.068, and a lognormal load with mean = 2.585 and cov= 0.4, the probability of system failure was observed to be 6.96×10^{-4} in direct simulation (Equation 4.3). The probability of the load exceeding a constant level of system capacity given by 8.390 is 5.80×10^{-4}, which is a satisfactory approximation of the true probability, 6.96×10^{-4}. In general (exceptions in the case of general redundant structures will be noted later on), the approximate E[SC] calculated from Rule 2 (also Rule 3) is less than the true E[SC], because the probabilistic redundancy is neglected. This approximation would result in overprediction of the probability of system failure. Then again, if the variation (cov) of system capacity is neglected, as above, the system failure probability would be underestimated. These two approximations would introduce errors in opposite directions but they may not exactly cancel each other. The final error would strongly depend on the assumed distribution model of load and capacity variables (see Appendix II).

Also if the reduced space Monte Carlo simulation is carried out only partially, i.e., in order to characterize only the first two moments (mean and cov) of the system capacity (Equation 4.2), the probability of system failure could be computed as: $P_{sys} = P \{ L \geq SC \}$ (Equation 4.1). In particular, for the lognormal model the system failure probability can be calculated to be 6.99×10^{-4}, which is close to that obtained from direct simulation (Equation 4.3). For a further discussion on this approach, the reader is referred to Appendix II.

Example 4.2: Binary System without Deterministic Back-up

Excess capacity, x = 30%; η = 0.4 (all members); number of members, n = 6; no. of weak members, n_w = 4; no. of strong members, n_s = 2; common correlation between

145

member capacities, $\rho_{R_iR_j} = 0.30$; cov $(R_i) = 0.10$; $\mu_{R_w} = 1.0$; $R_i \sim$ lognormal. Hence, from Equation 4.4, degree of unbalance, $r = 1.9$, i.e., $\mu_{R_s} = 1.9$ units, and from Equation 4.5, deterministic system factor, DSF = 1.0 (more precisely, $L_s / L_w = 0.9$, per Equation 4.5)

No. of members in the equivalent balanced system = $n_w = 4$

For, an equivalent balanced system with n = 4, $C_c = 0.916$ (Table 4.1)

Assume, $R_c \approx 1.000$ (exact result from simulation for $\eta = 0.4$ is 1.001, Table 4.1)

Therefore, $S_c \approx C_c = 0.916$ (exact result from simulation for $\eta = 0.4$ is 0.917)

Approximate E[SC] of the unbalanced system = 6 x 0.916 = 5.496

Simulation results: estimated E[SC] = 5.572 and estimated cov of E[SC] = 0.074

The approximation of E[SC] is less accurate in the case without deterministic system back-up compared to the case with deterministic system back-up. This is because the presence of excess capacity is totally neglected unless it results in deterministic system back-up. In reality, the excess capacity distributed among the strong members in the case without deterministic back-up will create probabilistic redundancy which is not accounted for. In contrast, for the case with deterministic system back-up, the approximating rule considers the equivalent balanced system members with capacity equal to that of the strong members. Typically, nonductile balanced systems have negligible probabilistic redundancy $(R_o \approx 1)$.

The procedure to estimate the system failure probability from E [SC] is as described in Example 4.1.

4.4.2 Parallel Structures with More General Capacity Distribution

In this section a more general class of unbalanced parallel structures is studied. The capacities are not restricted to only two groups, "strong" and "weak". In particular, capacities were specify to vary linearly for one group of simulations, and later were allowed to vary "randomly" (within reasonable limits with specified excess capacity) for

146

another group. Hence, the conclusions drawn from the following study are applicable to a more general class of unbalanced parallel systems. The assumption of equal redistribution of the load given up by the failed members among the surviving members is retained. Applicability of the conclusions made from the study of this restricted class of parallel structures to more general non-parallel structures (without equal redistribution) will be addressed subsequently.

As before, lognormal models are adopted for both the load and capacity variables. The coefficients of variation for load and capacity are adopted as 0.4 and 0.1 respectively. The capacities are modeled as equicorrelated with a correlation coefficient 0.3. The mean capacity of the weakest member in the system is taken as 1 unit. As in the case of balanced and binary-capacity parallel structures, as the number of members increases, the common load L, is increased to keep the most-likely-first (MLM) failure probability to a prescribed level of 1.35×10^{-3}. The following parameters are varied during the study. The total number of members, n, is varied between 2 and 8. Unless otherwise noted, the postfailure capacities of individual members are given by $\eta = 0.4$. The excess capacity was varied between 2% to 60%. The linear variation in mean member capacities is given by: $\mu_{R_i} = 1 + 2 * \frac{x}{100} * \frac{(i - 1)}{(n - 1)}$, where μ_{R_i} is the mean capacity of the i th member. The following plots show both the deterministic and the probabilistic system behavior of nonductile non-binary parallel structures.

147
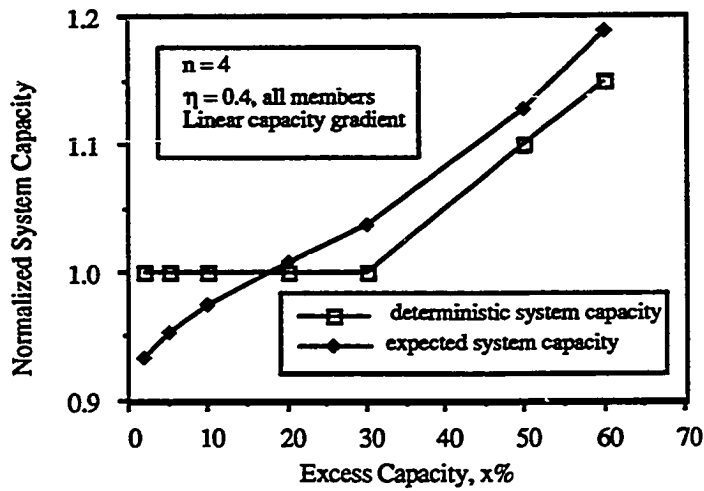
Fig. 4.19.1 Normalized Deterministic and Expected System Capacities for Different Excess Capacities (No. of Members = 4)
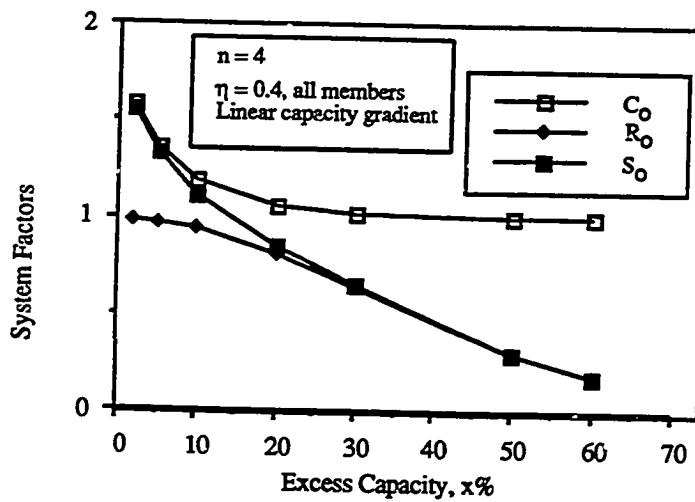
Fig. 4.19.2 System Factors for Different Excess Capacities
(No. of Members = 4)

148
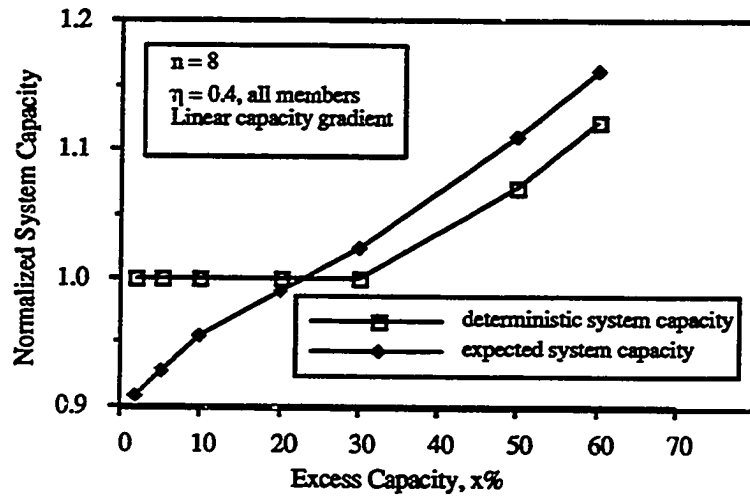
Fig. 4.20.1 Normalized System Capacity for Different Excess Capacities
(No. of Members = 8)
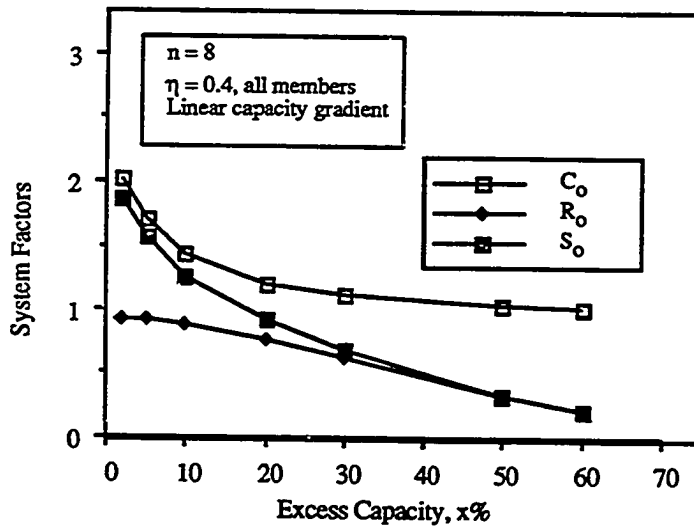
Fig. 4.20.2 System Factors for Different Excess Capacities
(No. cf Members = 8)

149
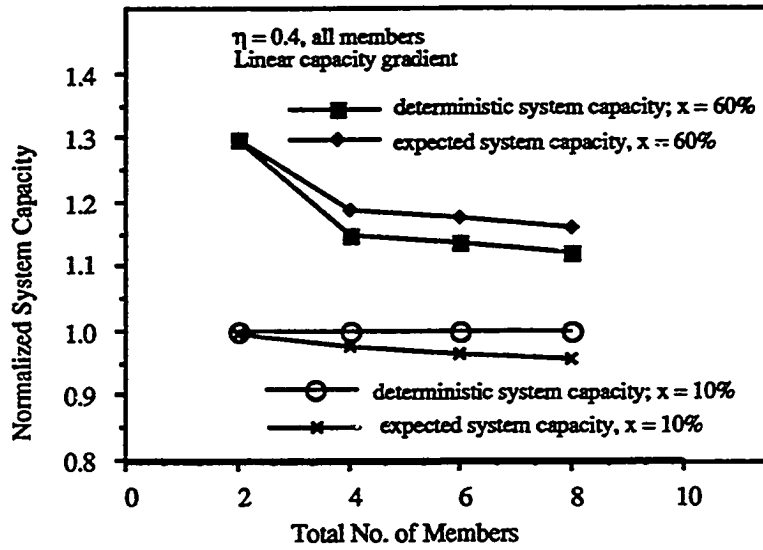
Fig. 4.21.1 Normalized Deterministic and Expected System Capacities
for Two Levels of Excess Capacity
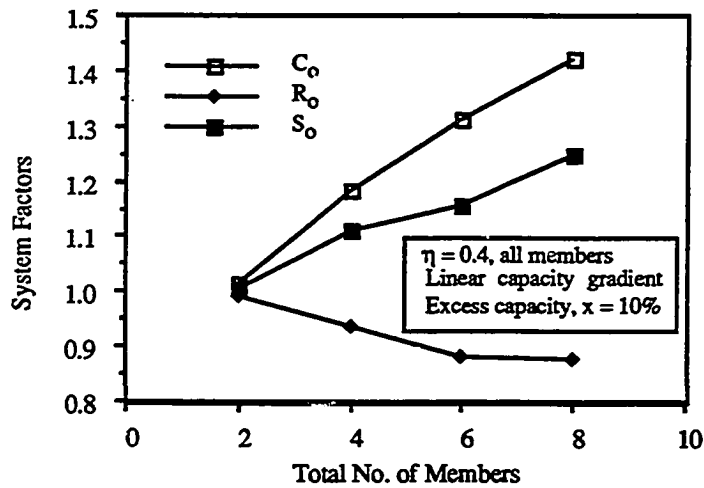
Fig. 4.21.2 System Factors for 10% Excess Capacity

150
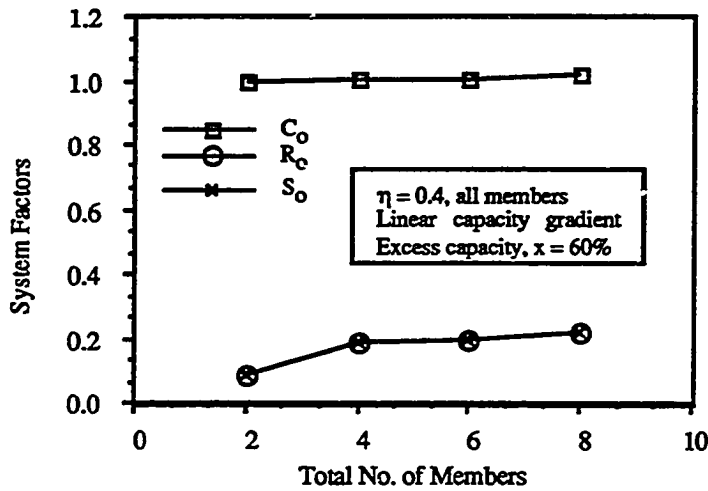
Fig. 4.21.3 System Factors for 60% Excess Capacity

Figs. 4.19.1 through 4.23.3 show representative cases with parametric variations in the level of excess capacity and in the number of members. The system capacities are normalized with respect to the number of members as in the case of binary-capacity systems. For nonductile binary systems, the expected system capacity, E[SC] was observed to be less than the corresponding deterministic system capacity, DSC (Figs.4.18.1 and 4.18.2). However for linear capacity systems with high excess capacity and / or low number of members, we observe that the E[SC] is greater than the DSC (Figs. 4.19.1, 4.20.1, and 4.21.1). The complexity effect dominates over the probabilistic redundancy effect only when the amount of excess capacity (and hence the unbalance) is low (Figs. 4.19.2, 4.20.2, 4.21.2, and 4.21.3) and the dominance increases with the increase in the number of members in the linear capacity system (Fig.4.21.2). The beneficial effect of the excess capacity on the expected system capacity and on the net system factor, S_o, can be seen with increasing excess capacity, even though the

151

deterministic system capacity becomes available only when the excess capacity crosses a certain threshold for given total number of members and the postfailure capacity of the members (Figs. 4.19.1 through 4.20.2). The net positive probabilistic system effect on both the system capacity and the probability of system failure (i.e., $E[SC] > DSC$, $S_0 < 1$, etc.) was observed even before the structure could manifest deterministic system back-up (i.e., when DSF = normalized deterministic system capacity = 1). Also in all cases of linear capacity systems with deterministic system back-up, the $E[SC]$ was observed to be greater than the DSC, but the reverse (i.e., that $E[SC] > DSC$ implies DSF >1) is not true. Such an observation is not true for the previously investigated binary systems.

Accelerated Estimation of Expected System Capacity

In the following we generalize the rules for estimating the expected system capacity from binary systems to non-binary systems. It will be seen that, as in the case of binary systems, the approximate $E[SC]$ calculated from the proposed rule is less than the corresponding DSC. Hence, for the cases where the $E[SC]$ is greater than the DSC, DSC is a better approximation to the true $E[SC]$ than the approximate $E[SC]$ calculated using the rule. (The procedure to identify the cases where the $E[SC]$ is expected to be greater than DSC will be discussed). The proposed rule will be tested for general parallel systems, e.g., linear capacity and arbitrarily varying member-capacity systems. The rules are also applicable to balanced and binary-capacity systems as special cases.

152
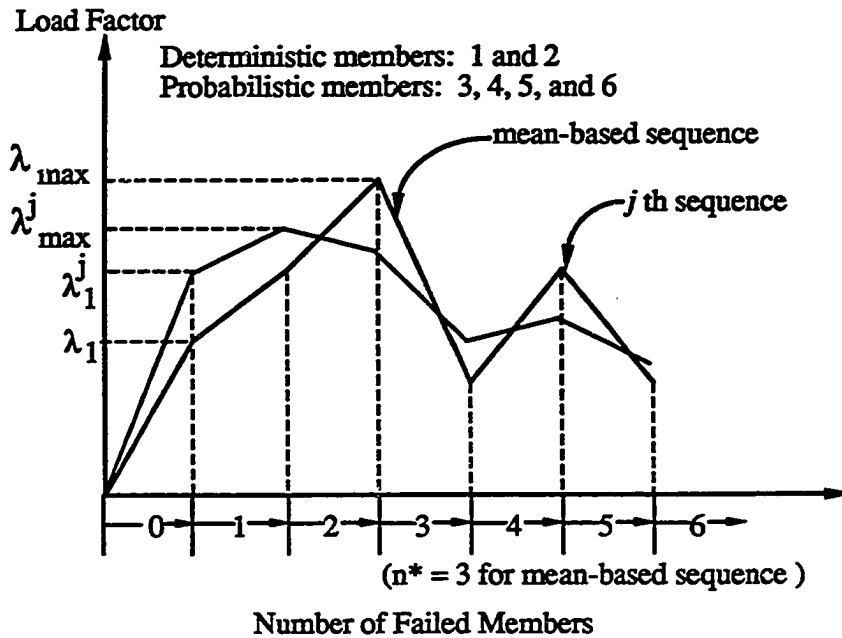
Fig. 4.22 Member Classification for General Parallel Structures

For non-binary parallel systems, the redundancy, and hence, the system factors continue to depend on the deterministic back-up. Unlike the binary system, the number of members in a non-binary-capacity system, can not be divided into two distinct groups, "weak" and "strong". Instead the members may be divided into two groups, which we will refer to as "deterministic" and "probabilistic". The basis for this division lies in the static pushover diagram of the structure with mean member capacities. Such a static pushover diagram is shown in Fig. 4.22. In addition to the mean-based sequence, Fig. 4.22 also shows the failure sequence in a static pushover test of an arbitrary random realization of the structure. Consider the member in the mean-based sequence whose failure leads a decrease in the applied load away from the maximum value attained, i.e., away from DSC. Let us call this member the "critical member"; in the ordered sequence of member failures, 1, 2, 3, ..., n, let n^* denote this critical member. The members $1, 2, 3, ..., (n^*-1)$ are classified as "deterministic" members, whereas, the members $n^*, (n^*+1), ..., n$ are classified as

153

"probabilistic" members. Let n_d and n_p be the numbers of the deterministic and the probabilistic members respectively. If the system has no deterministic system back-up (i.e., DSF = 1.0 and n* = 1), then all the members are probabilistic, i.e., $n_d = 0$ and $n_p =$ n. The following steps are proposed to approximately estimate the expected system capacity for any parallel system (binary or non-binary, with or without deterministic system back-up)

 i) *Calculate the residual capacity of deterministic members :*

 $$[SC]_{det.} = \sum_{k=1}^{k=n_d} \eta_k \, \mu_{R_k}$$

 ii) *Estimate capacity of probabilistic members:* $[SC]_{prob.} = n_p \, C_c \, \mu_{R_{(n*)}}$

 where, C_c is the capacity reduction factor due to complexity for the "equivalent balanced system"(an approximate procedure to calculate the number of "equivalent balanced members" for parallel structures is to follow later).

 iii) *Approximate E[SC] of the unbalanced system is given by:*

 Approx. E[SC] = $[SC]_{det}$ + $[SC]_{prob}$

The above rule has been suggested on the basis of simulation results of general parallel systems with non-binary capacity and was observed to behave satisfactorily even when applied to parallel systems with different combinations of member postfailure capacity, η_k, within a parallel system (e.g., some members semibrittle while others are ductile, etc.). In the proposed approach of estimating E[SC], the deterministic system capacity, DSC (which is based on the static pushover failure sequence of the structure with mean member capacities), is reduced to account for a limited amount of probabilistic system effect (complexity only). Note that the "approximate E[SC]" $\leq$ DSC, where the equality holds for C_c =1.0. In other words, the system capacity of the mean-based failure sequence is reduced because of the presence of two or more likely-to-fail members at the time of failure of the critical member. Also, for the mean-based sequence "probabilistic redundancy" is

154

neglected ($S_c \approx C_c$) resulting in an increase of the estimate of the system failure probability. In principle, there will be many failure paths because more than one member is likely to fail in the intact state and in the subsequent damaged states of the structure. The system failure is a "weak-link" problem where the failure of any of the possible sequences constitutes system failure. With increasing general unbalance (e.g., increasing excess capacity with linear capacity variation), the failure path based on the mean sequence becomes dominant, i.e., more likely than other possible failure paths. In the case of binary unbalance, however, any of the members within a group (first weak and then strong) may fail at each state of the structure increasing the complexity effect. This is reflected in a limited way (at least for the "probabilistic" members at the time of failure of the critical member) in the proposed approximation scheme both for binary and non-binary systems.

Implicit in the approach is the assumption that the system capacity calculated for the mean-based failure sequence is representative of the capacity (on the average) from all possible sequences. This means that either the sequences starting with different initial failures (e.g., j th sequence in Fig. 4.22 which begins with a relatively strong member with a lower probability of failure in the intact structure, but the resulting system capacity, λ_{max}^j,

is less than DSC) do not yield very different system capacities from DSC (at least on the average), or that the probabilities of occurrence of the sequences which do manifest very different system capacities ("rogue" paths) are small compared to that of the mean-based sequence. The postfailure capacity levels of failed members play an important role in determining the ultimate capacity and also the failure path because of redistribution of the loads given up by the failed members. In simulated case studies for parallel systems, where the excess capacity (and hence the unbalance) was distributed in many possible ways (e.g., binary and non-binary including arbitrarily / randomly distributed capacities) and postfailure capacities randomly selected, the existence of "rogue paths" was not evident.

155

It is also important to appreciate the level of errors in the estimate of system capacities required to cause a significant difference in the system failure probability estimate. As discussed in Appendix II, for lognormal model of the load variable, the tail of the distribution decays very slowly and hence a large difference in system capacity is required for any appreciable change in the failure probability estimate. For example, for a lognormal load with cov = 0.4, a reduction of 15% in the estimation of system capacity (in the mean) corresponds to an increase of failure probability (initial level of 1.3×10^{-3}) of roughly 3.5 times. (In contrast, a normal tail decays faster (exponentially) and for the same reduction of the mean system capacity with normally distributed load, the probability of failure will increase by roughly an order of magnitude). In regular structures, it is difficult to find failure paths that not only have ultimate capacity very different from the mean path but also are likely to occur. It is possible to construct pathological examples of parallel systems (with carefully chosen capacity gradient and the combination of brittle and ductile members) where "rogue paths" exist, but even in this case the probability of occurrence of the "rogue paths" are not expected to be significant enough to create appreciable differences in the probability of system failure. Consider qualitatively a binary-capacity system where the common mean capacity of the "strong" members is r times more than the common mean capacity of the "weak" members. Furthermore, assume that the weak members are ductile and the strong members are brittle. The static pushover failure sequence of the mean structure will consist of failure of "weak" ductile members first and and "strong" brittle members later. Now, let us consider two group of possible failure paths, namely, ones starting with ductile members failing first and the others with brittle members failing first. The sequences with brittle members failing first will manifest system capacities lower than the sequences with ductile members failing first, because of the absence of postfailure capacity of the brittle members. The higher the degree of unbalance, r, larger is the reduction of the system capacity for the brittle group ("rogue" paths) compared to the ductile group. However, the higher the degree of unbalance, the lower is the probability of

156

occurrence of the brittle group ("rogue" paths) because then the weaker ductile members are even more likely to fail first.

The proposed approximation for estimation of expected system capacity is based on the observed behavior of unbalanced parallel structures with truss type semibrittle members and equal "load redistribution" assumption. We will attempt later in this work to apply the findings to more general truss type "non-parallel" structural systems (i.e., with unequal load redistribution) assuming the absence of any "significant" rogue path. However, the implementation of the procedure (to be described shortly) for calculating the number of equivalent members for non-parallel structures will be relatively complicated compared to the parallel structural systems (i.e., equal redistribution). In the case of general redundant systems (i.e., non-parallel systems with unequal redistribution of loads from failed members), we expect the DSC to be representative of the system capacity (i.e., no "rogue paths"). As a first approximation (i.e., neglecting the probabilistic variation of member capacities) a "semi-probabilistic" estimate of system failure probability is given by the probability of the load exceeding the constant level of DSC. It will be shown later that for the offshore jacket structure studied in Chapter 2 and 3, the semi-probabilistic estimate is close to the system failure probability obtained by a full probabilistic analysis considering other than mean-based failure paths. Finally one could also calculate system failure probability assuming that the system capacity has a convenient probability distribution with mean equal to the DSC and cov equal to the 70% (i.e., assuming an approximate reduction of 30% based on simulation results, e.g., Table 4.2) of the individual member capacities.

Equivalent Balanced System for "Probabilistic" Members

As in the case of binary-capacity systems, an "equivalent balanced parallel system" is needed for the probabilistic members for the purpose of estimation of capacity reduction factor due to complexity, C_c. At the time of failure of the critical member in an unbalanced structure, the complexity effect depends on the number of potential failure initiators which

157

in turn depends on the level of unbalance among the surviving (probabilistic) members. In the special case of a balanced system, all the members are probabilistic and all members are equally likely failure initiators. For the case of a binary-capacity system with deterministic back-up, the strong members are the only potential failure initiators because the weak members are considered failed before the failure of the critical member. In the case of a binary system with no deterministic back-up, while all the members are probabilistic, only the weak members are potential failure initiators at that stage (intact condition) unless the difference in capacity between weak and strong members is so small that even the strong members contribute significantly to the union event of failure of any (i.e., at least one) first member. Extension of a similar procedure to non-binary systems is not straightforward because the mean capacities of the members vary arbitrarily.

A few empirical approaches to determine the "number of equivalent balanced" members, which yield exact results for the balanced and the binary-capacity systems, as special cases, were investigated. The complexity effect on the capacity of probabilistic members depends on (i) the relative marginal member failure probability levels at the load at which the critical member (n*) fails and (ii) the correlation between the member capacities. Let us assume that these two factors are separable and that the correlation effect can be taken care of by using simulation results of appropriately correlated equivalent balanced members (e.g., Table 4.1). We propose an approximation for the number of equivalent members (n_{eq}) as follows:

$$n_{eq} = \frac{\sum_{i=n^*}^{n} P_i}{P_{n^*}} \tag{4.6}$$

where, $P_i = \text{Prob.}\{R_i < E[R_{n^*}]\}$, and $i = n^*, (n^*+1), \ldots, n$.

Note, $E[R_{n^*}]$ is defined as the load level (in member-capacity units) at which the critical member fails in the mean structure. n_{eq} will, in general, be a non-integer, and the corresponding C_c will have to be obtained from interpolation of simulation results of balanced systems with integer number of members (Table 4.1). For probabilistic members

158

with increasing unbalance, Equation 4.6 predicts decreasing n_{eq} as desired. However, experience with simulations from non-binary parallel systems indicate that Equation 4.6 consistently overpredicts n_{eq} in the sense that a lower number for the equivalent members would have resulted in a better prediction of the capacity reduction factor due to complexity, C_c. Because higher n_{eq} implies lower C_c, this results in slight underprediction of E[SC] in the approximating rule given before. It was found that for non-binary parallel systems with deterministic system back-up, for $n_{eq} \leq 1.8$ the complexity effects are small resulting in deterministic system capacity, DSC $\leq$ true E[SC] (i.e., from simulation). As pointed out before, the approximate E[SC], calculated from the rules given above, is always less than DSC, and hence, DSC is a better estimate of the true E[SC] provided that the "complexity effects" are small. In general, for a redundant structure in an intermediate damaged state at the time of failure of the critical member, the level of balance is not likely to be high (i.e., $n_{eq} < 1.8$ for the "corresponding parallel system"), and hence DSC may be used as a satisfactory estimate of E[SC] unless the system has "rogue paths". For $n_{eq} >$ 1.8, it is advisable to use the approximating rule for E[SC] using C_c for the corresponding balanced system. Note that, n_{eq} is a measure of the complexity effect only for the potential multiple member-failure events at the time of failure of the critical member in the mean-based sequence. In addition, a structure with deterministic system back-up may be well balanced in the intact condition in the sense that it has multiple failure paths which manifest system capacities comparable to that of the mean-based sequence. Because these multiple failure paths manifest system capacities (and hence probabilities of occurrence) comparable to the mean-based sequence they are not "rogue" paths according to our definition. The existence of the multiple failure-path events of comparable failure probabilities of occurrence in a well balanced structure induce complexity effects that are not accounted for in the above rule based estimation of the expected system capacity. For such a balanced structure reduced space Monte Carlo simulation can still be used to obtain mean and cov of the system capacity.

159

Following are some examples of the application of the proposed rule for general parallel systems.

Example 4.3 <u>Non-Binary Parallel System, Lognormal Model</u>

Number of members, n = 8;

postfailure capacity, η = 0.40 (all members);

common correlation between member capacities, $\rho_{R_iR_j}$ = 0.30;

cov of individual member capacity (R_i) = 0.1 (all members)

The mean member capacities (randomly selected within a range) and the loads at failure of each member in a static pushover analysis of the mean structure are as follows:

Table 4.4 Static Pushover Test; Example 4.3

Member	Mean Capacity	Load at Failure
1	1.000	8.000
2	1.102	8.111
3	1.130	7.621
4	1.218	7.382
5	2.041	9.944
6	2.413	9.836
7	2.836	9.234
8	2.932	7.628

The critical member number, n* = 5 and the deterministic system capacity (DSC) = 9.944. The approx. E[SC] can be calculated as follows:

i) Deterministic members: 1, 2, 3, and 4; probabilistic members: 5, 6, 7, and 8.

Residual capacity of prefailed deterministic members:

$$[SC]_{det} = \sum_{k=1}^{k=4} \eta_k \, \mu_{R_k} = 0.4 \times (1.000 + 1.102 + 1.130 + 1.218) = 1.780$$

160

ii) No. of members in the equivalent balanced system $= n_{eq} = \dfrac{\sum\limits_{i=5}^{8} P_i}{P_5} = 1.10$

For, an equivalent balanced system with $n = 1.10$, $C_c = 0.998$ (by interpolation, Table 4.1)

Assume, $R_c \approx 1.000$

Therefore, $S_c \approx C_c = 0.998$

Approx. expected capacity of prob. members, $[SC]_{prob} = n_p\ C_c\ \mu_{R_{(n^*)}}$

$$= 4 \times 0.998 \times 2.041 = 8.147$$

iii) Approximate $E[SC]$ of the unbalanced system $= 1.780 + 8.147 = 9.927$

Since $n_{eq} < 1.8$, $DSC = 9.944$ is a better estimate of true $E[SC]$

Simulation results: estimated $E[SC] = 10.160$ and estimated cov of $SC = 0.076$

The procedure to estimate the system failure probability from $E[SC]$ is as described in Example 4.1.

Example 4.4 Non-Binary Parallel System, Normal Model

Number of members, $n = 8$;

postfailure capacity, $\eta = 0.40$ (all members);

common correlation between member capacities, $\rho_{R_iR_j} = 0.30$;

cov of individual member capacity $(R_i) = 0.1$ (all members)

The mean member capacities (linearly increasing for a given excess capacity of 60%) and the loads at failure of each member in a static pushover analysis of the mean structure are as follows:

161

Table 4.5 Static Pushover Test; Example 4.4

Member	Mean Capacity	Load at Failure
1	1.000	8.000
2	1.171	8.600
3	1.343	8.926
4	**1.514**	**8.977**
5	1.686	8.754
6	1.857	8.257
7	2.029	7.486
8	2.200	6.440

The critical member number, $n^* = 4$ and the deterministic system capacity (DSC) = 8.977. The approx. E[SC] can be calculated as follows:

i) Deterministic members: 1, 2, and 3; probabilistic members: 4, 5, 6, 7, and 8.

Residual capacity of prefailed deterministic members:

$$[SC]_{det} = \sum_{k=1}^{k=3} \eta_k \, \mu_{R_k} = 0.4 \times (1.000 + 1.171 + 1.343) = 1.406$$

ii) No. of members in the equivalent balanced system $= n_{eq} = \dfrac{\sum_{i=5}^{8} P_i}{P_5} = 1.39$

For, an equivalent balanced system with $n = 1.39$, $C_c = 0.982$ (by interpolation, Table 4.1)

Assume, $R_c \approx 1.000$

Therefore, $S_c \approx C_c = 0.982$

Approx. expected capacity of prob. members, $[SC]_{prob} = n_p \, C_c \, \mu_{R_{(n^*)}}$

$$= 5 \times 0.982 \times 1.514 = 7.430$$

iii) Approximate E[SC] of the unbalanced system $= 1.406 + 7.430 = 8.836$

Since $n_{eq} < 1.8$, DSC = 8.977 is a better estimate of true E[SC]

Simulation results: estimated E[SC] = 9.293 and estimated cov of SC = 0.070

The procedures outlined above for approximately estimating the expected system capacity and for calculating n_{eq} are appropriate for parallel systems.(i.e., with equal load redistribution); it is, however, feasible to extend the procedures to treat unequal load redistribution by considering "equivalent parallel systems", i.e., parallel systems with the member capacities normalized by the respective load influence coefficients in the intact and in the "critical" states of the structure. This was not implemented in this work. In the following, however, we explore the applicability of some of the general insights gained from parallel structures to a non-parallel redundant structure.

4.5 APPROXIMATE SYSTEM RELIABILITY ANALYSIS OF AN OFFSHORE JACKET STRUCTURE

In this section the applicability of the mean-sequence-based approximation for the expected system capacity (and for the subsequent system failure probability estimation) of a non-parallel redundant structure is investigated. The computational efficiency in using the reduced space Monte Carlo simulation approach to estimate the system reliability for this non-ideal structure is also demonstrated.

The structure analyzed is an eight-leg fixed offshore jacket in 140 feet of water modeled as a space truss. The same jacket structure was analyzed in Chapter 2 and 3 using failure path methods. The structure was analyzed under the static monotonic application of gravity and wave loads. The wave load was characterized by a deterministic load pattern (corresponding to the position of a regular "most-likely-to-cause-failure" wave when the base shear is maximum) scaled by the total lateral load (base shear) which is considered random. The nodal wave forces are fully correlated spatially, and hence are characterized by a single random variable, the base shear. Details of the wave load and the structural model is as described in Chapter 2. In brief, the lifetime maximum applied base shear is lognormally distributed with mean = 2361 kips and cov = 0.40. The individual member

163

capacities are assumed to be independent lognormals with cov = 0.10 for tension failure and cov = 0.13 for compression failure. The failure probability of the most-likely-to-fail member, P(MLM) = 2.72 x 10^{-3}. The criterion of system failure, as used in this study, is a major loss (50% reduction) of global stiffness. The stiffness is measured by the increase in deflection at the center of the deck due to an unit increase in load.

4.5.1 Results from Reduced Space Monte Carlo Simulation

Number of simulation = 60

Probability of any-first-member failure, P(AFF) = 4.03 x 10^{-3}; cov of estimation = 0.15

Probability of system failure, P_{sys} = 1.58 x 10^{-3}; cov of estimation = 0.08

Expected system capacity, E[SC] = 6987 kips; cov of estimation = 0.009;

Estimated cov of system capacity = 0.07

The above probability of system failure was obtained by averaging the probability of failure for each stochastic realization of the structure (using Equation 4.3). If instead the probability of system failure is calculated as, P_{sys} = Prob.{L > SC}, using Equation 4.1, under the assumption that the system capacity is also lognormal with mean and cov as estimated above, we have, P_{sys} = 1.53 x 10^{-3}, which is close to the result obtained by direct simulation.

The results obtained from the failure path approach, as reported in Chapter 2 (Table 2.8.2, Case F) are as follows:

P(AFF) = 4.66 x 10^{-3}

P_{sys} = 1.29 x 10^{-3}

The close agreement between results obtained from the simulation and that from the "failure path approach" validates using the "failure path" method which requires several approximations both in the enumeration of the component failure events making up the failure sequences and also in the computation of probability of those events. Information

164

about critical component failure events can also be obtained from simulation by sensitivity analyses requiring very little additional computational effort (*Karamchandani et al., 1988*).

4.7.2   Mean-Sequence-Based Approximate Analysis
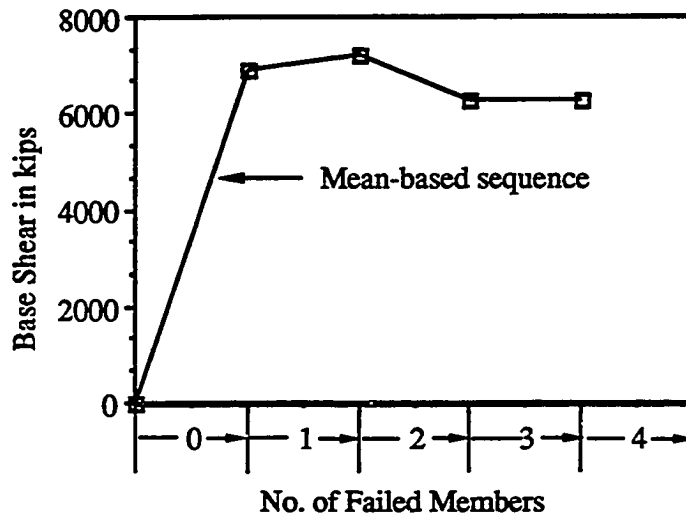
Fig. 4.23 Mean-Based Static Pushover Diagram of the Offshore Jacket

Fig. 4.23 shows results of a static pushover test of the offshore jacket structure under study. The member capacities have been assumed at their mean capacity. The jacket looses more than 50% of its intact global stiffness (see Section 2.4.3) on failure of the 4th member, and hence is considered failed according to the adopted system failure criterion. The "mean-based sequence" and the total lateral load (base shear) at failure of each member are as follows:

165

Table 4.6 Static Pushover Test; Offshore Jacket Structure

No. of Failed Members	Failed Member No.[1]	Base Shear in kips
1	+151[2]	6923
2	+141	7240
3	+160	6281
4	+192	6257

The deterministic system capacity is 7240 kips. This maximum system capacity is attained just before failure of member 141, which is the critical member. The procedure to calculate the equivalent number of balanced members, n_{eq}, using Equation 4.6 was not implemented. However, the mean-load-to-capacity ratios of the different surviving members just before the failure of member 141 was significantly unbalanced, making the member 141 the by far the most likely failure initiator in the mean sequence. Hence, the complexity effect at that stage can be neglected and DSC = 7240 kips can be taken as an estimate of the expected system capacity, E[SC]. Note, that unlike the unbalanced systems in Examples 4.3 and 4.4, the approximate E[SC] is overpredicted when compared to the true (i.e., simulated) E[SC]. Our earlier experience while using "failure path method"(Chapter 2 and 3) rules out existence of any significant "rogue path". This leaves us only with the possibility of having high complexity effect at the first member failure event (and to a lesser extent during subsequent member failure events) which are neglected in the approximate approach. This seems to be the case because the jacket was designed for the inplace load condition only without the benefit of extra strengthening for other operational and installation requirements. This resulted in a balanced behavior of the jacket at least during the first member failure event. However, because the DSC is not significantly different from the true E[SC], the estimate of probability of system failure can

---

[1]Refer to Appendix I for details of the structural model.
[2]Plus sign denotes failure of member in compression.

.

166

still be satisfactorily estimated as, $P_{sys} \approx \text{Prob.}\{L > DSC\} \approx 9.64 \times 10^{-4}$. The estimate of P_{sys} can be improved by assuming the system capacity is lognormally distributed with a mean $\approx DSC = 7240$ and $cov = 0.09$ (70% of compression capacity cov of individual members; in the absence of simulation results this is assumed as a first approximation on the basis of results reported in Table 4.2) and is calculated as, $P_{sys} = \text{Prob.}\{L > SC\} = 1.26 \times 10^{-3}$, using Equation 4.1. However, for a normally distributed load it would be necessary to characterize the mean and cov of system capacity from reduced space simulation (see Appendix II). Also, during system reliability estimation of new structural designs it is prudent to avoid using the system capacity based on the mean sequence, especially since the reduced space simulation is so efficient.

The reduced space Monte Carlo simulation technique is easy to implement with any available structural non-linear analysis program to carry out the static pushover analysis. In cases where the load can be characterized by a single random variable, this is a preferred method to estimate system reliability.

4.6   SUMMARY

In order to understand better the system reliability of realistic statically indeterminate structures, the system behavior of simple classes of unbalanced structures has been studied. Probabilistic measures of systems effects have been provided. For a number of cases, these system factors can be approximated from the corresponding (well-studied) balanced systems and simple unbalanced systems using rules developed from observations made of the results. The rules also provide insights into system reliability of more general unbalanced systems.

Deterministic and probabilistic measures of "system effects" have been proposed. In particular, probabilistic measures of "systems effects" have been provided in terms of "expected system-level capacities" and the resulting "complexity" and "redundancy"

factors. The capacity based "system factors" have the advantage of not being dependent on the load variability.

The dependence of the probabilistic system factors on the deterministic system factor has also been investigated. In the cases studied it appears that the deterministic system effects dominate over the probabilistic system effects once the amount of unbalance is greater than the variability (cov) of the member-capacity variables.

Efficient use of reduced space Monte Carlo simulation (also known as conditional expectation) techniques in system reliability analysis has been demonstrated. Application of these findings in accelerated system reliability assessment of practical structures, in particular, a fixed offshore jacket structure, has been demonstrated.

The findings in this study are based on our analysis of structures with two-state (semibrittle) truss members. Further investigation is recommended for truss type structures with multi-state (postfailure) member model. Also more work is needed to generalize to conclusions for frame type structures.

A SHORT-TERM EXTREME SEA-STATE MODEL FOR OFFSHORE STRUCTURAL RELIABILITY ANALYSIS

A new model for statistically characterizing observed, irregular, processes is presented in this chapter. The model is based on a "multivariate" random variable characterization of the random process suitable for use in efficient reliability computation, e.g., FORM / SORM, and in general purpose methods such as Monte Carlo simulation (MCS). Although the model is restricted to at least semi-narrow banded time histories, it does not make any a priori assumption regarding the Gaussianity of the time series. It does, however, decompose the process into harmonic components facilitating the application of "Airy" or modified ("stretching", e.g., *Wheeler, 1969*) "Airy" kinematics for irregular gravity waves. Hence it is attractive for characterizing the skewed wave elevation processes observed in shallow water and / or in extreme (storm) sea states (see *Spidsoe et al., 1986*). In this work the application of the proposed model is demonstrated by analyzing a 34.13 min. long wave-elevation record collected during hurricane Camille. The model is evaluated by comparing the results with currently available other Gaussian and non-Gaussian results. In addition, calculation of response statistics such as the probability distribution of extreme base shear of a pile, the spatial correlation of sets of drag forces at different locations, etc., is demonstrated.

5.1 INTRODUCTION AND BACKGROUND

One of the common assumptions used in modeling a short-term sea state is that the observed sea surface elevation for short periods of time is a realization of a Gaussian stationary random process (e.g., *Borgman, 1972; Sarpkaya and Isaacson, 1981; Madsen et al., 1986*). Under the Gaussian hypothesis the stationary random process is completely

characterized by its spectral density function. The area under the energy spectrum (power spectral density) is equal to the mean square value of the stationary random process. The spectral density function is the Fourier transform of the autocorrelation function of the process. Hence the spectral density function completely defines the zero-mean process within the "second moment" context (i.e., variances, and correlations of the suite of random variables describing the process at any set of instants of time) as is required for Gaussian distributions. In practice some analytical expression is often adopted for the spectral density function (e.g., the Pierson-Moskowitz spectrum). Typically long-term distributions of the parameters characterizing the wave spectral density (e.g., significant wave height , peak spectral period, etc.) are available relating the short-term wave spectral model to the long-term wave statistics. Within the "short-term", the statistics of the extreme value of the process are often derived using the assumption that the process is narrow banded. For a linear system the response to Gaussian input is also Gaussian. The linear system is characterized by its frequency transfer functions and the spectral density of the response is then calculated by simple frequency domain multiplications. The various short-term extreme response statistics are calculated under the assumption that the resulting Gaussian response is also narrow banded, although several correction factors are available for departure from narrow bandedness (e.g.,*Vanmarcke, 1975; Winterstein and Cornell, 1985*). For calculation of response statistics of non-linear systems, often an equivalent linear transfer function is sought so that the computational efficiency of the linear spectral method can be retained (e.g., linearization of the Morison drag force, see *Borgman, 1972; Sarpkaya and Isaacson, 1981*).

In view of the importance of the wave-load variability in system reliability analysis of offshore structures (see Chapter 4), a framework for modeling short-term extreme sea states retaining the non-Gaussian characteristics is of particular interest. It is often observed during extreme sea states that the crest heights in general tend to be higher than the associated trough heights. This results in positive skewness of the wave elevation

170

process. The Gaussian process in contrast has zero skewness. As the spectral representation suggests, the Gaussian stationary random process can be interpreted as a superposition of an infinite number of harmonic components with frequencies $-\infty < \omega < \infty$; the random amplitudes of the sinusoidal components at different frequencies are independent and statistically specified by the spectral density function, while their phases are independent and have uniform distributions between 0 and 2π. The observed positive skewness in the wave surface elevation process in extreme sea states suggests that the component harmonic oscillations of the irregular wave surface are perhaps "phase locked" producing "constructive interference" under the crests and "destructive interference" under the troughs. Several researchers have studied the behavior of the phase spectrum of surface gravity waves, although considerable complications arise due to the need to "unwrap" and "detrend" the phase spectrum (*Read and Sobey, 1987*). Phase wrapping refers to the modulo 2π operations on the phase angles; this will be further discussed below. Phase trend arises because a shift in time origin of the wave record produces a "saw-tooth" variation of the "principal phase" contributing to the random appearance of the phase spectrum. The magnitude of the "saw-tooth" variation depends on the amount of time shift and the frequency of the component.

Anticipating its application to static structural reliability problems, in this work a radically different model has been investigated that discretizes the irregular record into individual "waves" and captures their statistical properties in a "multivariate" format. In addition to thecretically retaining the non-Gaussian characteristics of the random process, the model has a format suitable for efficient calculation of wave kinematics and response statistics.

5.2 "MULTIVARIATE" MODEL OF AN EXTREME SEA STATE

In the proposed model, an observed wave elevation record is discretized on a "wave-by-wave" basis. The discretization algorithm used in this study is described in Appendix

171

III. To facilitate the decomposition of the "waves" of primary interest, certain "waves" which are of small intensity were not considered, i.e., they were "disqualified". The criteria used in this study for disqualification of "waves" are described in Appendix III. Each qualified "wave" is expressed as a linear superposition of a finite number (say, three to five) of sinusoidal components by discrete Fourier transform. As Fig. 5.1 shows just three components represent an actual observation very well. In all that follows this number (only three components) will be used.
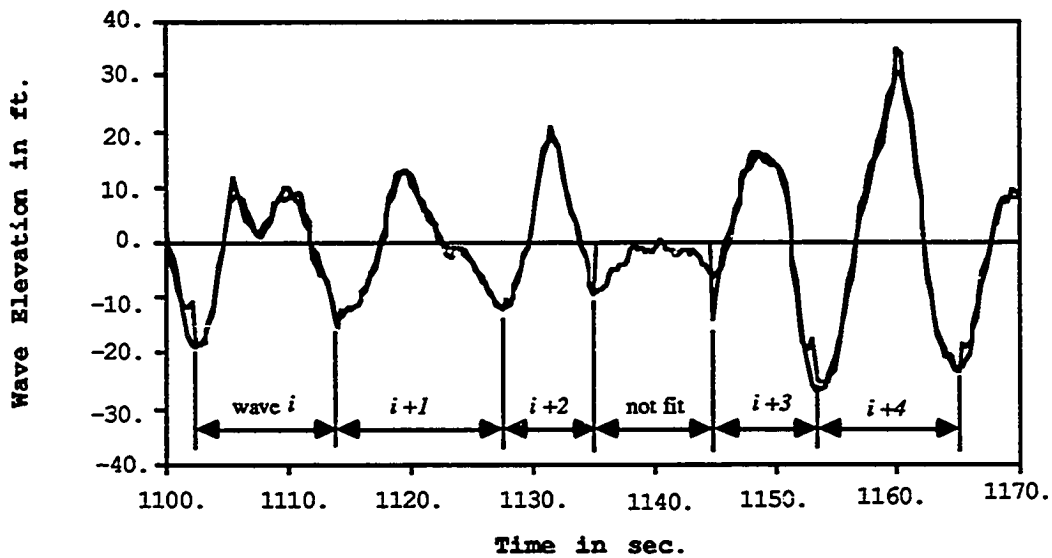
Fig. 5.1 Original Time Series and "Wave-by-Wave" Sets of Superposed Sums of Three Sinusoidal Waves: A Partition of Camille Record

It can be seen from Fig. 5.1 that the individual "waves" have been discretized from trough to trough. The maximum disagreement between the parent time series and the superposed time series occurs at the points of discretizations, i.e., at the troughs. It can be shown that for a regular Airy wave passing over a fixed pile, the maximum drag force occurs when the wave crest is at the pile and the maximum inertia force occurs when a wave node (zero wave elevation) is at the pile. Therefore, the total wave force reaches its

172

maximum at a location where the wave elevation is positive, the precise location being determined by the relative importance of the drag force and the inertia forces. Hence, discretization at the troughs ensures that the points of maximum disagreement between the actual time series and the modeled time series occur at points away from the points of primary interest in this study.

The observed record is usually given in terms of wave surface elevation at equal time intervals, Δt (e.g., the Camille record analyzed contains elevations recorded every 0.25 sec.). Each qualified trough-to-trough "wave" is then characterized by a vector of eight random variables: the fundamental period which is the trough-to-trough length of the "wave", a zero-frequency component which is the average surface elevation within the "wave" (Equation 5.2.1), and three pairs of cosine and sine wave amplitudes (i.e., corresponding to one fundamental and two harmonic components). The last six variables are obtained by discrete Fourier Transform of the "wave" data which essentially gives the least square fit of three sinusoidal components to the mean removed surface elevation data within the "wave" (Equations 5.2.2 and 5.2.3). The sine and cosine amplitudes of each sinusoidal component define the amplitude and the phase of the component. For the jth "wave" let T_f^j be the fundamental trough-to-trough period in sec. The corresponding fundamental frequency is given by $\omega_f^j = 2\pi / T_f^j$ in rad/sec. The surface elevation, x_t^j, of the jth wave at time t (with time origin at the leading trough and discretized at $t = 0$, Δt, $2\Delta t$, $\cdots$) is then expressed as:

$$x_t^j = a_0^j + \sum_{i=1}^{3} \{ \ a_i^j \cos(i*\omega_f^j*t) + b_i^j \sin(i*\omega_f^j*t) \ \} \tag{5.1}$$

where, the zero-frequency component, a_0^j, and the three pairs of cosine and sine wave amplitudes $(a_i^j, b_i^j; i = 1, 2, \text{ and } 3)$ for the jth "wave" are given by:

173

$$a_0^j = \bar{x} = \frac{1}{n_j} \sum_t x_t^j \tag{5.2.1}$$

$$a_i^j = \frac{2}{n_j} \sum_t (x_t^j - \bar{x}) \cos(i*\omega_f^j*t); \qquad \text{for } i = 1, 2, \text{ and } 3 \tag{5.2.2}$$

$$b_i^j = \frac{2}{n_j} \sum_t (x_t^j - \bar{x}) \sin(i*\omega_f^j*t); \qquad \text{for } i = 1, 2, \text{ and } 3 \tag{5.2.3}$$

where, x_t^j refers to the data points in the discrete time series at time, $t = 0, \Delta t, 2\Delta t, \ldots$,

$(n_j - 1)\Delta t$ in the jth "wave", and $n_j = \dfrac{T_f^j}{\Delta t}$ is the number of time series data points in the jth

"wave".

From analysis of all qualified "waves" a total of n_q (where n_q = number of qualified "waves" in the time series obtained as a result of discretization of the record) sets of the eight random variables are observed. Statistics are collected in the form of eight sets of first four marginal moments, i.e., mean μ, standard deviation σ, skewness coefficient α_3, and kurtosis coefficient α_4 (e.g.,Table 5.2.1), plus an 8 x 8 matrix of pair-wise correlation coefficients (e.g., Table 5.3.1). The correlations between the amplitudes of the harmonic cosine and sine components of the "waves" are related to the so called "phase locking" of non-Gaussian records. This effect will be more explicit in an alternative form of the Equation 5.1 given as:

$$x_t^j = a_0^j + \sum_{i=1}^{3} R_i^j \cos(i*\omega_f^j*t + \phi_i^j) \tag{5.3}$$

where three $R_i^j = \sqrt{(a_i^j)^2 + (b_i^j)^2}$ and $\tan \phi_i^j = \dfrac{-b_i^j}{a_i^j}$ (for $i = 1, 2, \text{ and } 3$) describe the

amplitudes and the phases of the fundamental and two harmonic components of the "wave" j. In this form "phase locking" would be related to non-zero correlation between the Φ_i

174

variables. In this representation (Equation 5.3), the phase angles calculated by any coded trigonometrical algorithm are in the range $-\pi$ to π and are termed the principal phases. In other words, phase angles are circular data (see *Mardia, 1972*) and are "wrapped" because of the modulo 2π operation. To avoid the complications associated with estimating the marginal statistics and correlations of a mixed set of circular (e.g., phase angles) and linear (e.g., amplitudes) data, the representation of the surface elevation process in the form given by Equation 5.1 was used in characterizing the "waves", i.e., statistics were collected on the amplitudes of sine and cosine waves, a_i^j and b_i^j, which are linear variables. As a result,

no direct physical correspondence between the correlation coefficients of the phases and the correlation coefficients of the amplitudes of cosine and sine components could be established. However, it is expected that the correlation matrix used in this scheme will capture the "phase locking" indirectly.

By analyzing correlation between the random variables characterizing the adjacent "wave" segments, "lag-1 correlation" statistics for the vector of 8 random variables (e.g., Table 5.4.1) are also estimated. Typically only a smaller subset of all qualified "waves" are such that the adjacent (leading or following) "waves" are also qualified. The "lag-1 correlation" coefficients are evaluated from this smaller sample size. These correlation coefficients are of interest in characterizing the "persistence" of wave amplitudes and shapes. In addition the use of these "wave-to-wave" correlation data to improve the estimation of the extreme response has been explored in this study.

A framework that characterizes the random variables in terms of the first four marginal moments and the pair-wise correlation structure of the random variables is presented in Appendix IV. This framework implicitly assigns a joint probability distribution consistent with the available (incomplete) information in the form of a transformation between the standard uncorrelated Gaussian space and the space of the physical random variables so that FORM / SORM analysis or Monte Carlo simulations can be conveniently carried out.

175

5.3 EXTREME RESPONSE STATISTICS

The short-term extreme sea state is implicitly characterized by the joint probability probability density function, f_Y $(y; \theta)$ of the eight characteristic random variables, Y, in terms of the observed statistics, θ, (marginal moments and correlation coefficients) of the characteristic variables which are the parameters of the distribution. This representation provides statistical definition of an arbitrary qualified "wave" during the short-term sea state.

Let R be any response quantity due to any qualified "wave". The general equation for the response can be written as: $r = r$ (z, y), where the additional variables z (such as current, force coefficient in Morison equation, etc.) can either be deterministic or random. In the demonstrations to follow we have assumed z to be deterministic for clarity. The probability, P_{1q}, that the response, R, exceeds a given threshold, r_0, in an arbitrary qualified "wave" can be evaluated as the probability of failure (using FORM / SORM or Monte Carlo simulation) for the limit-state function: $g(z, y) = r_0 - r$ (z, y). P_{1q} can also be interpreted as the mean outcrossing rate of the response for the threshold, r_0, per qualified "wave". The mean outcrossing rate, P_1', per *any* "wave" (qualified or unqualified) can be estimated as $P_1' = \frac{n_q}{n_t} P_{1q}$, where n_q and n_t are the numbers (or expected numbers) of qualified and total "waves" respectively within the duration of the short-term process analyzed. Similarly an estimate of the mean outcrossing rate, P_{1T}, per unit time can be estimated as $P_{1T} = \frac{n_q}{T} P_{1q}$, where T is the duration of the short-term process analyzed.

The probability distribution of the extreme value of the response during a short-term period is of interest in design and "time-integrated" reliability analysis . Under the Bernoulli process approximation, the events of the response exceeding a certain threshold during qualified "waves" are considered independent from event to event. Hence, the

176

cumulative distribution of the extreme value of the response, R_T in the short-term process in n_q qualified "waves" is given by:

$$F_{R_T}(r_0) = \text{Prob.} \{\text{no outcrossing of the threshold, } r_0, \text{ in } n_q \text{ qualified "waves"}\}$$

$$= [\text{ Prob.} \{R_i < r_0 \}]^{n_q}; \quad i = 1, 2, 3, \dots, n_q$$

$$= [1 - P_{1q}]^{n_q}; \text{ since all the qualified waves are identically distributed}$$

$$\approx \exp(-n_q P_{1q}); \text{ for small } P_{1q} \tag{5.4.1}$$

Alternatively Equation 5.4.1 can be expressed either in terms of the number of total "waves", n_t or the duration of the short-term process, T. Using the corresponding mean outcrossing rates, P_1' and P_{1T} respectively, we obtain the following two equivalent forms of Equation 5.4.1.

$$F_{R_T}(r_0) = \text{Prob.} \{\text{no outcrossing of the threshold, } r_0, \text{ in } n_t \text{ total "waves"}\}$$

$$\approx \exp(-n_t P_1'); \text{ for small } P_1' \tag{5.4.2}$$

$$F_{R_T}(r_0) = \text{Prob.} \{\text{no outcrossing of the threshold, } r_0, \text{ in duration T}\}$$

$$\approx \exp(-T P_{1T}); \text{ for small } P_{1T} \tag{5.4.3}$$

In general the results of extreme response statistics obtained using Equation 5.4 are of acceptable accuracy because the independence assumption of the threshold crossing events is reasonable for the higher thresholds that influence the extreme value statistics. This will be demonstrated later.

However, using the "multivariate" framework established above it is possible to improve upon the independence assumption of the Bernoulli process. In particular, a

177

Markovian assumption of one-step memory process can be used. The cumulative distribution function of the extreme response in this case is given by:

$F_{R_T}(r_0) =$ Prob.{no outcrossing of the threshold, r_0, in time T or in n_t "waves"}

$\quad =$ Prob.{ $(R_1 < r_0) \cap (R_2 < r_0) \cap (R_3 < r_0) \cap \ldots\ldots \cap (R_{n_t} < r_0)$ }

$\quad = P[R_1 < r_0] * P[R_2 < r_0 \mid R_1 < r_0] * P[R_3 < r_0 \mid (R_1 < r_0) \cap (R_2 < r_0)]\ldots\ldots$

$\quad = P[R_1 < r_0] * P[R_{i+1} < r_0 \mid R_i < r_0]^{(n_t-1)}$

$\quad = [1 - P_1'] * [1 - P_{2|1c}']^{(n_t-1)}; \quad$ where $P_{2|1c}' = P[R_{i+1} \geq r_0 \mid R_i < r_0]$

$\quad \approx [1 - P_{2|1c}']^{n_t}; \quad\quad$ for high thresholds

$\quad \approx \exp(-n_t P_{2|1c}'); \quad\quad$ for small $P_{2|1c}'$ $\hfill (5.5)$

$P_{2|1c}'$ is the probability that the response due to the following "wave" exceeds the threshold, r_0, given that the response due to the preceding "wave" does not exceed the threshold, r_0. Note that $P_{2|1c}'$ is the modified mean outcrossing rate per *any* "wave", qualified or unqualified.

Now, $P_{2|1c}' = P[R_{i+1} \geq r_0 \mid R_i < r_0]$

$\quad = \dfrac{P[R_{i+1} \geq r_0 \cap R_i < r_0]}{P[R_i < r_0]}$

$\quad = \dfrac{P[R_{i+1} \geq r_0] - P[R_{i+1} > r_0 \cap R_i > r_0]}{P[R_i < r_0]}$

$\quad = \dfrac{P_1' - P_{12}'}{1 - P_1'}; \quad$ where $P_{12}' = P[R_{i+1} > r_0 \cap R_i > r_0]$

$\quad \approx P_1' - P_{12}' \hfill (5.6)$

178

Hence, from Equation 5.5 we have,

$$F_{R_T}(r_0) \approx \exp(-n_t P'_{2|1c})$$

$$= \exp\{-n_t (P'_1 - P'_{12})\}$$

$$= \exp\{-n_q (P_{1q} - \frac{n_t}{n_q} P'_{12})\} \qquad (5.7)$$

Typically, the thresholds of interest for extreme response statistics are high enough so that the joint exceedance of the threshold from adjacent "waves" (i.e., ith and $i + 1$ th "waves") are possible only when both the adjacent "waves" are qualified. Hence, we have the following relationship between P'_{12}, the joint threshold exceedance probability per *any* wave and P_{12q}, the joint threshold exceedance probability per qualified "wave":

$P'_{12} = \frac{n_q}{n_t} P_{12q}$; note that $\frac{n_q}{n_t}$ is the relative frequency of occurrence of a qualified "wave".

Hence, Equation 5.7 can be written as:

$$F_{R_T}(r_0) \approx \exp\{-n_q (P_{1q} - P_{12q})\} \qquad (5.8)$$

For process with high "wave-to-wave" "persistence", such as in very narrow banded seas or perhaps (to be studied below) in very high seas, the threshold crossings may occur in clusters causing P_{12q} to be comparable to P_{1q} and hence reducing the probabilities of exceeding r_0 in any period. If P_{12q}, however, is small compared to P_{1q}, Equation 5.8 reduces to Equation 5.4 which was derived on the basis of the assumption of independence of the threshold exceedance events. Note that under the independent assumption, $P_{12q} = (P_{1q})^2$ which is $\ll P_{1q}$ for high r_0.

The probability, P_{12q}, that the response, R, exceeds a given threshold, r_0, in an arbitrary qualified "wave" and also in the following "wave" which is qualified, can be evaluated as the probability of *system* failure (using FORM / SORM based system

179

reliability methods or Monte Carlo simulation) for a parallel system with two component events, $R_i > r_0$ and $R_{i+1} > r_0$. Both the components have the same limit-state function: $g(z, y) = r_0 - r(z, y)$. The eight sea-state variables, y, in each of the two component events are modeled by different sets of random variables (Y_i and Y_{i+1}). Each of these two sets of variables (Y_i and Y_{i+1}) have the same marginal statistics and correlation among themselves (e.g., ρ described by Tables 5.2.1 and 5.3.1). The correlations between the vectors Y_i and Y_{i+1} are described by the lag-1 correlation statistics of the adjacent "waves" (e.g.,Table 5.4.1).

In this study the primary objective is to demonstrate the efficiency of the proposed "multivariate" representation of the extreme sea state in calculation of distribution of extreme response quantities, such as base shear of a pile, wave height, etc. To evaluate the proposed "multivariate" model we also calculate the crest mean outcrossing rates and the extreme crest elevation statistics for which Gaussian and simple non-Gaussian results are readily available. Following are some known Gaussian and non-Gaussian results used in this study for the purpose of comparison.

For the Gaussian process $X(t)$, the mean outcrossing rate corresponding to a threshold level x is given by the following well known result (e.g., *Vanmarcke, 1975*):

$$v_x = v_0 \exp \{-u^2/2\} \tag{5.9}$$

in which $u = x/\sigma_x$, for a zero mean Gaussian process, $X(t)$, and v_0 is the zero-upcrossing rate given by:

$$v_0 = \frac{1}{2\pi} \sqrt{\frac{m_2}{m_0}} \tag{5.10}$$

where m_2 and m_0 are respectively the second spectral moment and the area under the power spectral density of the process. For a Poisson approximation of the threshold

180

outcrossing events, the cumulative distribution of X_T, the extreme value of the process in duration T, is given by:

$$F_{X_T}(x) = \text{Prob.}\{\text{ no outcrossing of the threshold x in time T}\} \approx \exp\{-v_x T\} \qquad (5.11)$$

The mean outcrossing rate, v_x, for the threshold x, is also available for a class of non-Gaussian processes if the higher marginal moments, e.g., skewness and kurtosis coefficients of the random process are available. A non-Gaussian process, X(t), can be related to a standardized Gaussian Process, U(t), through a functional transformation of the form $X = T(U)$ (Equations A.IV.1 and A.IV.2 in Appendix IV) using Hermite polynomials such that the specified marginal moments match (see *Winterstein, 1987; Winterstein et al., 1989*). Because the above transformation relates the actual non-Gaussian process, X(t), to an underlying standard Gaussian process, U(t), at each point in time, including the times at which the peaks occur, Equation 5.9 for the mean outcrossing rate of a threshold x can be expressed as *(Winterstein et al., 1989)*:

$$v_x = v_0 \exp\{-u^2/2\} = v_0 \exp[-\{T^{-1}(x)\}^2/2] \qquad (5.12)$$

An improvement of the mean outcrossing rates for lower thresholds and / or "narrow bandwidths" of the process spectrum is also available to account for the fact that the threshold exceedance events under the above mentioned conditions may happen in "clusters" when the independence of the outcrossing events is no longer valid. An improved mean outcrossing rate is given by *(Vanmarcke, 1975)*:

$$v_x = v_0 \exp\{-u^2/2\}[1 - \exp\{-\sqrt{2\pi}\,\delta\,u\}] \qquad (5.13)$$

181

in which, the bandwidth parameter, $\delta = \sqrt{1 - \dfrac{m_1^2}{m_0 \, m_2}}$, where m_i is the ith spectral

moment of the random process.

5.4 DESCRIPTION OF THE WAVE DATA ANALYZED

The applications of the proposed "multivariate-sequence" model of an extreme sea state have been demonstrated by analyzing a 34.13 min. long time series data of wave surface elevation during hurricane Camille at a 348.7 ft. deep location in the Gulf of Mexico (obtained from Dr. Charles Petrauskas, Chevron Oil Field Research Company). The data were recorded at a time interval of 0.25 sec. The estimates of the first four marginal moments, mean, standard deviation, skewness coefficient, and kurtosis coefficient for the elevation data points (after removal of mean; no linear trend was present in the data) are shown in Table 5.1.1. The estimated skewness is 0.27 which implies non-Gaussianity of the time series. The objective of this representation of the irregular sea surface is to retain such non-Gaussian characteristics. The raw periodogram of the surface elevation process calculated from 8192 data points and the corresponding power spectral density / wave energy spectrum (obtained by smoothing the raw periodogram by a "moving average window" consisting of 27 data points) are shown in Figs. 5.2 and 5.3 respectively.

In order to study the behavior of the "wave-by-wave" discretization of the random process and the resulting "multivariate" representation, two simulated Gaussian time series, referred to here as "Gauss1" and "Gauss2" respectively, have also been analyzed. Both Gauss1 and Gauss2 are 34.13 min. long zero mean Gaussian time series with time intervals of 0.25 sec. which were simulated by superposing 4096 sinusoids with amplitudes corresponding to the 4096 "non-redundant" ordinates of the periodogram of the Camille time series (Fig 5.2) and phases selected randomly between zero and 2π. The only difference between the two time series, Gauss1 and Gauss2, is that two different sets of simulated phases were used in their generation. As a result both Gauss1 and Gauss2 have

182

the same second moment characterization (i.e., same wave energy spectrum) as that of the Camille time series (Figs. 5.2 and 5.3). The estimates of the first four marginal moments, mean, standard deviation, skewness coefficient, and kurtosis coefficient, for the elevation data points for Gauss1 and Gauss2 are shown in Table 5.1.1 along with that of the Camille data. The skewness and kurtosis coefficients for Gaussian variables are 0.0 and 3.0 respectively. While the estimated skewness coefficients for Gauss1 and Gauss2 is very close to zero, the estimates of the kurtosis coefficients for Gauss1 and Gauss2 deviate slightly from 3.0. This deviation is perhaps due to the increased statistical uncertainty associated with estimating higher marginal moments from a finite sample size. Also, the simple marginal moment based estimator used in the calculation of kurtosis coefficients is biased. It is usual practice to "taper" the data in the time domain (e.g., by a cosine bell taper window affecting 5% to 10% of the data at both ends of the time series) to prevent "leakage". The "leakage" in the spectral analysis of a time series of finite length (i.e., tapered by a boxcar window) is caused by the "sidelobes" that are associated with the Fourier transform of the boxcar (see *Bloomfield, 1976*). An unfortunate side effect of tapering the data is the reduction of the root mean square (standard deviation for the zero mean process) of the process. For this comparative study it is desirable to have the second moment characteristics of the simulated Gaussian time series, in particular the rms, match that of the original Camille time series, and hence no tapering was done to the Camille data to obtain the periodogram and the spectrum (Figs. 5.2 and 5.3). However, the length of the time series is sufficiently long and accordingly no significant presence of the "sidelobes" in the spectrum can be seen (Fig. 5.3). The estimates of the spectral moments for Camille, Gauss1, and Gauss2 are shown in Table 5.1.2. The calculated energy spectrum of Gauss1 and Gauss2 and hence their spectral moments were found to be in close agreement to the corresponding estimates for Camille data as expected.

183

Table 5.1.1 Marginal Moments of Time Series: Camille, Gauss1 and Gauss2

Time Series	Mean (ft.)	Std. Dev. (ft.)	Skewness Coeff.	Kurtosis Coeff.
Camille	0.00	10.75	0.27	3.34
Gauss1	0.00	10.75	-0.03	3.13
Gauss2	0.00	10.75	-0.01	3.13

Table 5.1.2 Spectral Moments of Time Series: Camille, Gauss1 and Gauss2

Time Series	m_0 (ft^2)	m_1 (ft^2/sec)	m_2 (ft^2/sec^2)	m_3 (ft^2/sec^3)	m_4 (ft^2/sec^4)
Camille	115.67	70.84	58.27	118.51	735.37
Gauss1	115.65	70.85	58.28	118.52	735.44
Gauss2	115.67	70.84	58.28	118.51	735.32
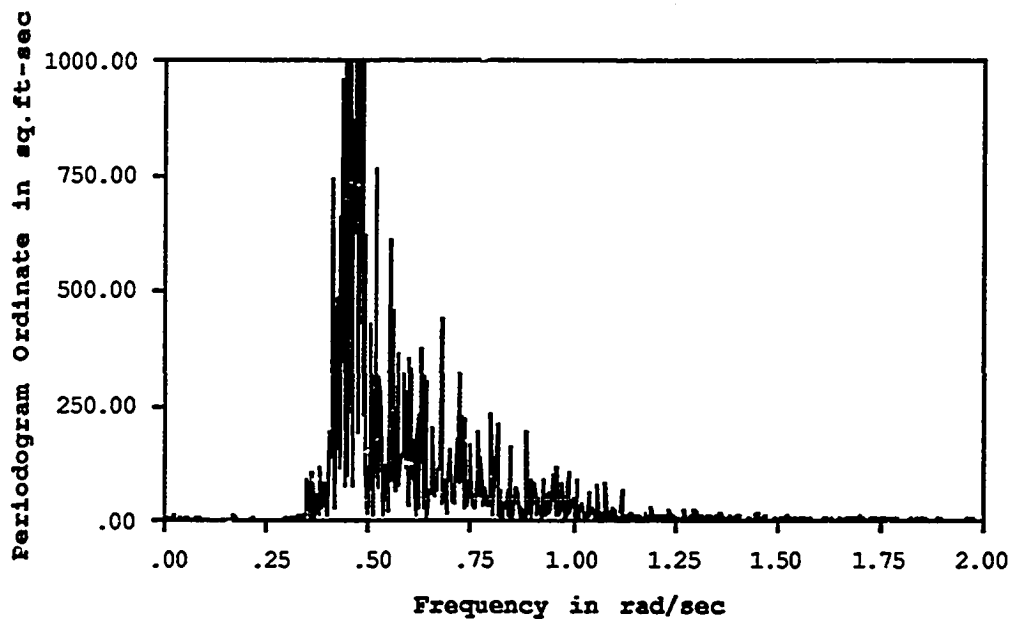
Fig. 5.2 Periodogram of Camille Time Series (34.13 min.; 8192 Points)

184
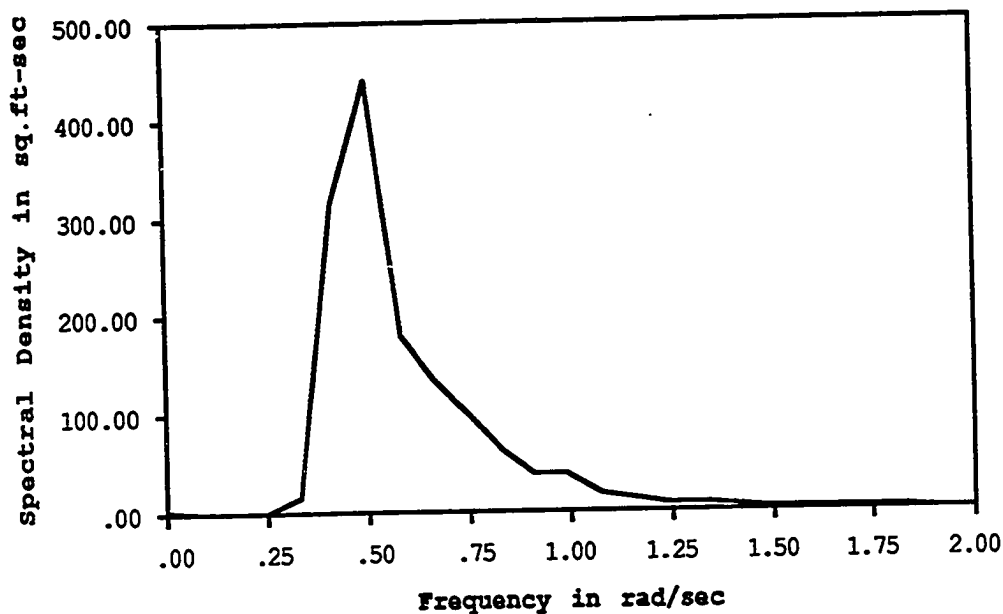
Fig. 5.3 Wave Energy Spectrum of Camille Time Series

5.5 RESULTS AND DISCUSSION

All the three 34.13 min. long time series, Camille, Gauss1, and Gauss2, were discretized (see Appendix III for the discretization algorithm used in this study) in the "wave-by-wave" form. The summary of the estimates of marginal moments and pair-wise correlation coefficients including "lag-1 correlation" coefficients for the variables characterizing the "waves" (Section 5.2) are presented in Tables 5.2.1 through 5.4.3. Table 5.5 summarizes the number of qualified and the total number of "waves" obtained as a result of discretization of the time series of Camille, Gauss1, and Gauss2. Figs 5.4.1 shows the profile of the "wave" with mean value of the characteristic variables corresponding to the Camille sea state (2nd column, Table 5.2.1). Fig. 5.4.2 shows the components (i.e., zero-frequency component, fundamental and two harmonics) of the same "mean wave". From Fig. 5.4.2 it can be seen that the intensity of the "wave" follows the

185

magnitude of the variable A_1, which is the amplitude of the first (fundamental) cosine wave (component).

Table 5.2.1 First Four Marginal Moments of Eight Characteristic Random Variables 34.13 min. of Hurricane Camille Wave Elevation Data

Random Variable	Mean	Standard Deviation	Skewness Coeff.	Kurtosis Coeff.
Time Period (sec.), T_f	10.82	2.37	-0.11	2.06
Zero-Freq. Comp.(ft), A_0	0.70	1.76	0.76	6.22
1st. cosine Amp. (ft), A_1	-12.55	5.81	-0.56	3.38
1st. sine Amp. (ft), B_1	-0.12	6.05	-0.17	2.89
2nd. cosine Amp. (ft), A_2	-1.31	2.92	-0.43	4.07
2nd. sine Amp. (ft), B_2	0.43	3.29	0.52	5.05
3rd. cosine Amp. (ft), A_3	-0.30	1.13	0.24	3.48
3rd. sine Amp. (ft), B_3	-0.05	1.46	-0.15	2.47

Table 5.2.2 First Four Marginal Moments of Eight Characteristic Random Variables 34.13 min. of Gauss1 Wave Elevation Data

Random Variable	Mean	Standard Deviation	Skewness Coeff.	Kurtosis Coeff.
Time Period (sec.), T_f	10.91	2.33	-0.14	2.15
Zero-Freq. Comp.(ft), A_0	0.51	1.36	0.42	3.16
1st. cosine Amp. (ft), A_1	-12.14	6.17	-0.65	3.64
1st. sine Amp. (ft), B_1	0.01	5.17	-0.06	2.42
2nd. cosine Amp. (ft), A_2	-2.16	2.63	-0.49	3.15
2nd. sine Amp. (ft), B_2	-0.02	2.96	-0.24	3.51
3rd. cosine Amp. (ft), A_3	-0.47	1.05	-0.17	3.42
3rd. sine Amp. (ft), B_3	0.08	1.43	0.28	2.78

186

Table 5.2.3 First Four Marginal Moments of Eight Characteristic Random Variables 34.13 min. of Gauss2 Wave Elevation Data

Random Variable	Mean	Standard Deviation	Skewness Coeff.	Kurtosis Coeff.
Time Period (sec.), T_f	11.04	2.53	-0.18	1.98
Zero-Freq. Comp.(ft), A_0	0.57	1.47	0.38	3.30
1st. cosine Amp. (ft), A_1	-12.63	5.35	-0.61	3.46
1st. sine Amp. (ft), B_1	1.35	5.91	-0.27	3.13
2nd. cosine Amp. (ft), A_2	-2.30	2.92	-0.67	3.34
2nd. sine Amp. (ft), B_2	-0.11	5.37	0.22	3.69
3rd. cosine Amp. (ft), A_3	-0.40	1.13	-0.38	4.61
3rd. sine Amp. (ft), B_3	-0.01	1.65	-0.03	3.14
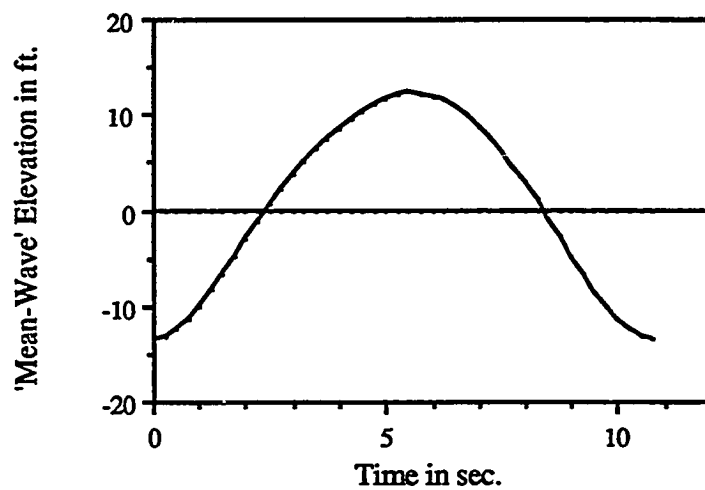
Fig. 5.4.1 Profile of "Wave" with Mean Value of the Characteristic Variables; Camille Sea State

187
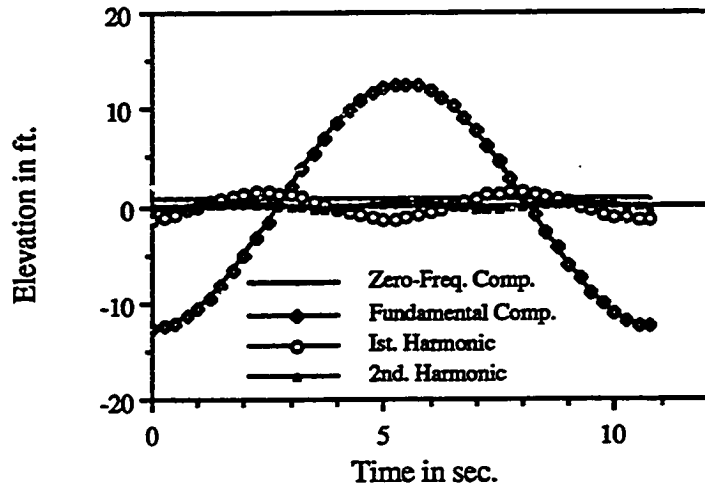
Fig. 5.4.2 Components of the "Mean Wave"; Camille Sea State

Table 5.3.1 Symmetric Correlation Coefficient Matrix of Eight Characteristic Variables 34.13 min. of Hurricane Camille Wave Elevation Data

	T_f	A_0	A_1	B_1	A_2	B_2	A_3	B_3
T_f	1.00				.			
A_0	-0.22	1.00						
A_1	-0.01	-0.40	1.00					
B_1	-0.06	0.04	0.25	1.00				
A_2	-0.45	0.18	-0.33	0.10	1.00			
B_2	0.07	0.18	-0.18	-0.23	0.04	1.00		
A_3	-0.06	-0.06	-0.08	0.11	-0.22	0.13	1.00	
B_3	-0.05	0.16	0.05	0.25	0.24	0.16	-0.05	1.00

188

Table 5.3.2 Symmetric Correlation Coefficient Matrix of Eight Characteristic Variables
34.13 min. of **Gauss1** Wave Elevation Data

	T_f	A_0	A_1	B_1	A_2	B_2	A_3	B_3
T_f	1.00							
A_0	-0.24	1.00						
A_1	-0.05	-0.27	1.00					
B_1	0.03	-0.10	0.01	1.00				
A_2	-0.46	0.09	-0.27	0.16	1.00			
B_2	-0.13	0.05	0.07	-0.19	0.00	1.00		
A_3	-0.10	0.07	-0.10	0.13	-0.12	0.12	1.00	
B_3	-0.02	-0.03	0.12	0.09	-0.01	0.39	0.13	1.00

Table 5.3.3 Symmetric Correlation Coefficient Matrix of Eight Characteristic Variables
34.13 min. of **Gauss2** Wave Elevation Data

	T_f	A_0	A_1	B_1	A_2	B_2	A_3	B_3
T_f	1.00							
A_0	-0.29	1.00						
A_1	-0.02	-0.13	1.00					
B_1	0.13	0.10	0.06	1.00				
A_2	-0.47	-0.03	-0.23	-0.06	1.00			
B_2	-0.04	-0.07	0.01	-0.28	0.00	1.00		
A_3	-0.17	0.00	0.06	-0.03	-0.06	0.22	1.00	
B_3	-0.04	0.05	0.15	0.24	0.02	0.33	0.27	1.00

189

Table 5.3.4 Summary of Selected[1]Correlation Coefficients of Three Time Series

	Camille	Gauss1	Gauss2
$T_f - A_0$	-0.22	-0.24	-0.29
$T_f - A_2$	-0.45	-0.46	-0.47
$T_f - A_3$	-0.06	-0.10	-0.17
$A_0 - A_1$	-0.40	-0.27	-0.13
$A_0 - A_2$	0.18	0.09	-0.03
$A_0 - B_2$	0.18	0.05	-0.07
$A_0 - B_3$	0.16	-0.03	0.05
$A_1 - B_1$	0.25	0.01	0.06
$A_1 - A_2$	-0.33	-0.27	-0.23
$A_1 - B_2$	-0.18	0.07	0.01
$B_1 - A_2$	0.10	0.16	-0.06
$B_1 - B_2$	-0.23	-0.19	-0.28
$B_1 - B_3$	0.25	0.09	0.24
$A_2 - A_3$	-0.22	-0.12	--0.06
$A_2 - B_3$	0.24	-0.01	0.02
$B_2 - A_3$	0.13	0.12	0.22
$B_2 - B_3$	0.16	0.39	0.33
$A_3 - B_3$	-0.05	0.13	0.27

---

[1]The correlation coefficients whose absolute values are greater than 0.15 for at least one of the three time series, Camille, Gauss1, and Gauss2, are selected for Table 5.3.4.

190

Table 5.4.1 "Lag-1 Correlation" Coeff.Matrix of Eight Characteristic Variables
34.13 min. of Hurricane Camille Wave Elevation Data

Lag-0 / Lag-1	T_f	A_0	A_1	B_1	A_2	B_2	A_3	B_3
T_f	0.16	0.08	-0.13	-0.10	-0.23	-0.03	-0.08	0.04
A_0	0.12	-0.35	-0.02	-0.54	-0.13	0.17	0.03	-0.21
A_1	-0.13	0.17	0.32	0.27	0.27	0.10	-0.11	0.37
B_1	-0.08	0.34	-0.24	0.02	0.29	0.09	-0.02	0.06
A_2	-0.02	0.10	-0.08	-0.10	-0.02	0.24	0.16	-0.14
B_2	0.09	-0.20	-0.09	-0.28	-0.34	-0.19	-0.04	-0.39
A_3	0.02	0.13	-0.23	0.13	0.12	-0.34	-0.07	0.07
B_3	0.00	0.20	-0.37	-0.25	0.06	0.20	0.06	-0.18

Table 5.4.2 "Lag-1 Correlation" Coeff. Matrix of Eight Characteristic Variables
34.13 min. of Gauss1 Wave Elevation Data

Lag-0 / Lag-1	T_f	A_0	A_1	B_1	A_2	B_2	A_3	B_3
T_f	0.17	0.22	-0.17	-0.04	-0.10	-0.10	0.07	-0.01
A_0	0.17	-0.32	0.11	-0.35	-0.10	0.06	-0.11	0.03
A_1	-0.32	0.05	0.50	0.20	0.16	0.20	0.14	0.27
B_1	-0.00	0.50	-0.30	0.12	0.09	-0.06	0.09	-0.17
A_2	-0.01	-0.02	-0.04	0.09	0.04	0.10	0.16	-0.00
B_2	0.10	-0.17	-0.13	-0.09	-0.11	-0.11	0.02	-0.05
A_3	0.13	-0.00	-0.17	0.07	0.10	-0.14	-0.19	-0.04
B_3	0.06	-0.12	-0.13	-0.03	-0.04	-0.22	-0.08	-0.12

191

**Table 5.4.3 "Lag-1 Correlation" Coeff. Matrix of Eight Characteristic Variables
34.13 min. of Gauss2 Wave Elevation Data**

Lag-0 \ Lag-1	T_f	A_0	A_1	B_1	A_2	B_2	A_3	B_3
T_f	0.21	0.25	-0.18	0.05	-0.13	-0.06	-0.00	-0.03
A_0	0.10	-0.25	0.09	-0.34	0.03	-0.03	0.06	-0.00
A_1	-0.10	0.11	0.31	0.24	0.27	0.08	-0.01	0.33
B_1	0.22	0.36	-0.03	0.38	-0.16	-0.25	-0.04	0.09
A_2	-0.26	-0.08	0.01	-0.12	0.15	0.16	0.16	0.16
B_2	-0.03	-0.01	-0.43	-0.14	0.13	-0.08	-0.27	-0.27
A_3	-0.14	0.05	-0.04	-0.03	0.10	-0.11	-0.01	-0.13
B_3	-0.04	0.11	-0.36	0.04	0.13	-0.27	-0.09	-0.08

Table 5.5 Number of Total and Qualified "Waves" in "Wave-by-Wave" Representation

	Camille	Gauss1	Gauss2
Total # of "Waves"	191	196	189
# of Qualified "Waves"	148	164	149

Trends are difficult to detect in the estimated marginal moments and correlation coefficients of the characteristic random variables in the "wave-by wave" representation for Camille, Gauss1, and Gauss2. In studying the tables one should remember that the difference between the parameters estimated for Gauss1 and Gauss2 is an indication of the extent of sample-to-sample variability (Gauss1 and Gauss2 being samples of the same Gaussian stationary process). In addition it should be remembered that there is higher statistical uncertainty in estimating higher marginal moments.

192

Note that, even when the parent process is Gaussian there is no reason why the eight characteristic variables will be Gaussian themselves. Certainly the first two variables, T_f and A_0 need not be Gaussian even for Gaussian processes because of the nature of the discretization algorithm used in this study (see Appendix III). The other variables, e.g., A_i and B_i, the amplitudes of cosine and sine waves, have non-linear functional dependence on the time period, T_f, and the zero-frequency component, A_0 (Equations 5.2.2 and 5.2.3). Also note that even though the process is zero mean, the mean of the zero-frequency component A_0 is non-zero. Results from more time series are required to make definitive conclusions about the trends in the parameter statistics; in the following, however, we discuss the pattern, or lack of it, in the limited number of cases presented in the tables above. Comparing the marginal statistics of the characteristic variables from Tables 5.2.1 through 5.2.3 we see that the zero-frequency component A_0 has a higher mean and positive skewness for Camille sea state compared to the Gaussian sea states, Gauss1 and Gauss2. This is not unexpected because higher incidences of the zero-frequency components tend to make the process skewed. The skewness of the discretized "wave" train will be examined in more detail later in this section. It should also be noted that the "qualifying process" (Appendix III) keeps only the "waves" with relatively higher intensity thereby systematically modifying the statistics, viz-a-viz the underlying process. This is the main reason we study in this section two other Gaussian time series, Gauss1 and Gauss2 subjected to the same discretization and qualifying process.

It is not surprising that the first and second marginal statistics of the fundamental time period and the amplitudes of the component sine and cosine waves are not significantly different in Camille, Gauss1, and Gauss2. The three time series have the same spectral density function; the mean square amplitudes, $E\{A_i^2 + B_i^2\}$, for i =1, 2, and 3, are specified by the common spectral density function, even though the corresponding phases are not. We expect the correlation coefficient matrix (Tables 5.3.1 through 5.3.3) of the

characteristic variables to capture the "phase locking" for non-Gaussian processes indirectly, even though it is difficult to interpret the physical significance of the correlation coefficients with regard to "phase locking" expect for a few cases.

In Table 5.3.4 we present a comparison of the selected correlation coefficients with relatively high magnitude (i.e., absolute value > 0.15) between the three time series. Not withstanding the effect of sample to sample variability, we observe some similarity of the correlation coefficients of Gauss1 and Gauss2 compared to the non-Gaussian series Camille (Table 5.3.4). For example, we observe that the negative correlation coefficient between the variables A_0 and A_1, $\rho_{A_0 A_1}$, is higher in absolute value for Camille than that of Gauss1 or Gauss2. Because the mean value of A_1 is negative, the high negative correlation for Camille indicates that the zero-frequency component A_0 tends to be higher for bigger "waves" and this tendency is greater for Camille compared to Gauss1 or Gauss2; this at least partially is responsible for the skewness in the discretized and qualified "waves". For the so-called phase locking we should be looking for trends primarily in the correlation coefficients of the amplitudes of the fundamental with that of the first harmonic, i.e., $\rho_{A_1 A_2}$, $\rho_{A_1 B_2}$, $\rho_{B_1 A_2}$, and $\rho_{B_1 B_2}$. In particular, A_1 is by far the largest and hence most influential among the eight characteristic variables; hence the correlation coefficients involving A_1 are of particular interest. In Table 5.3.4 we observe that the correlation coefficient $\rho_{A_1 B_2}$ and to a lesser extent the correlation coefficient $\rho_{A_1 A_2}$ have higher absolute values for Camille compared to the Gaussian sea states Gauss1 and Gauss2. However, physical significance are difficult to establish for such results. Also the magnitude of the correlation coefficient $\rho_{A_1 B_1}$ is larger in Camille than in Gauss1 and Gauss2. There are also some correlation coefficients which are comparable for all the three time series. More time series need to be analyzed in order to make statistically significant conclusions. The lag-1 correlation results (Tables 5.4.1 through 5.4.3) do not display any significant difference in trend between the three time series studied. We note that there is moderate positive correlation between the A_1 variables of the adjacent "waves" for all three

194

time series as expected for a non-broad banded process. Next we evaluate the results obtained from application of the "multivariate" sea-state model in response statistics calculations.

In particular we evaluate the "multivariate wave-by-wave" model by comparing below the results obtained in calculating the statistics of crest elevation. The crest elevation or crest height is defined as the maximum wave surface elevation. For a given sea state characterized by $f_X(\underline{y}; \underline{\theta})$, the limit-state function corresponding to a threshold exceedance r_0, is given by : $g(\underline{y}) = r(\underline{y}) - r_0$; where $r(\underline{y})$ is the maximum surface elevation in the "wave" for which the characteristic variables are given by $\underline{y}$. The results for crest response statistics presented in Figs. 5.5 through 5.8 are based on calculation of probability of failure using "axis-orthogonal simulation". Axis-orthogonal simulation (AOS) uses information about the limit-state surface around the "design" (most likely to fail) point , obtained by a FORM analysis. It is aimed at simulating a correction to the FORM result (*Hohenbichler and Rackwitz, 1988; PROBAN-2: Users Manual, 1989*). The reliability calculations for this study were carried out using PROBAN, a general purpose software package for probabilistic analysis. Rather unusual results were obtained by the FORM, SORM, and AOS computational methods. A discussion on the accuracy of failure probability results obtained by different computation methods (e.g., FORM, SORM, MCS, and AOS) is given in Appendix V. In the following we further demonstrate how such efficient reliability solution methods become available with the "multivariate" sea-state model under investigation.

The following plots for the crest mean outcrossing rates (Figs. 5.5 and 5.6) and the cumulative distribution function (CDF) of the extreme crest height in 34.13 min. (Fig. 5.7 and 5.8) are based on the AOS results.
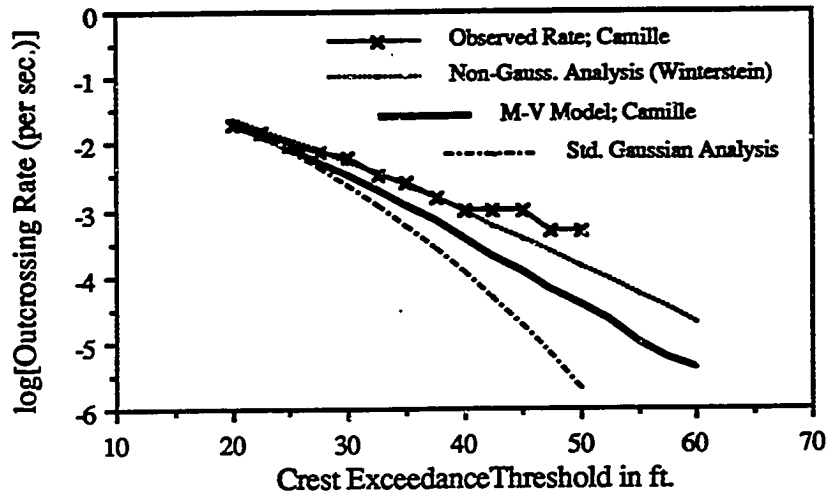
Fig. 5.5 Crest Outcrossing Rate : Camille Time Series; Various Alternative Methods
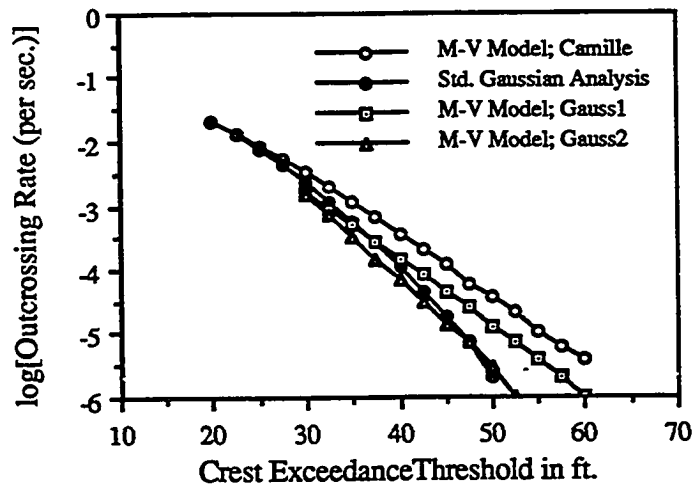

Fig. 5.6 Crest Outcrossing Rate : Camille and Simulated Gaussian Time Series
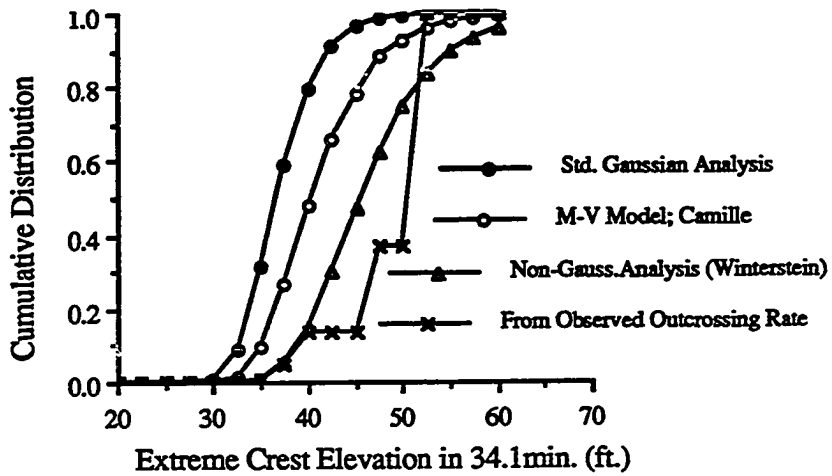
196

Fig. 5.7 CDF of Extreme Crest Height in 34.13 min. : Camille Time Series; Various Alternative Methods
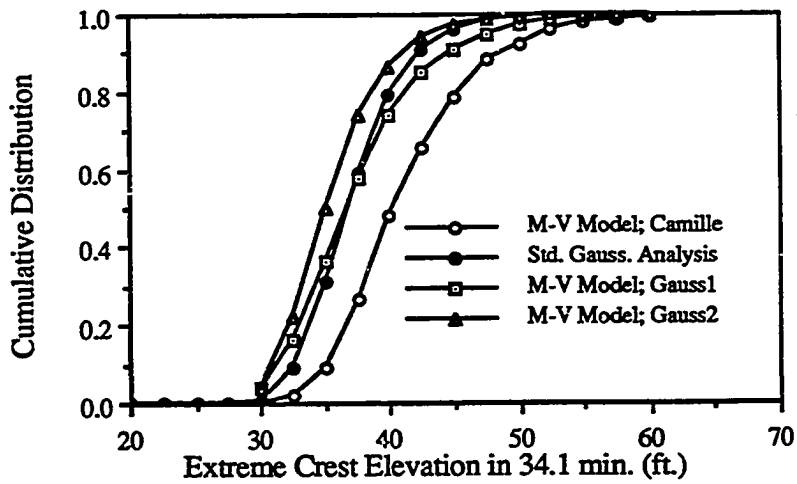

Fig. 5.8 CDF of Extreme Crest Height in 34.13 min. : Camille and Simulated Gaussian Time Series

197

As expected, the plots for crest mean outcrossing rates (Fig. 5.5) for the Camille data show that the Gaussian estimate (Equation 5.9) is lower than the "observed" rate, i.e., the relative frequency of the crest level exceedance in the non-Gaussian (positive skewness, see Table 5.1.1) Camille time series. Note, that the estimates of the mean outcrossing rate obtained from the observed rate have large statistical uncertainty for higher threshold values, because the observed events for the higher thresholds are increasingly fewer in number. In general, the simple non-Gaussian mean outcrossing rates (Equation 5.12) are in very good agreement with the directly observed outcrossing results for the lower range of thresholds for which the observed rates are meaningful. The proposed "multivariate" model using "wave-by-wave" representation yields better agreement than the Gaussian model, but it does not do as well as the simple non-Gaussian model in matching the outcrossing rates. In contrast to the "multivariate" sea-state model, the simple non-Gaussian analysis uses the higher moments of the underlying process directly and is able to predict the mean outcrossing rates closer to the observed values. In order to understand the reasons for the possible shortcomings of the "multivariate" model we will examine later the skewness of discretized and qualified "wave" trains for Camille, Gauss1, and Gauss2. Also, the accuracy of the failure probability computation in the "multivariate" model could not be ascertained for higher threshold values because verification by Monte Carlo simulation is very expensive to carry out for higher thresholds where the failure probability is in the range of 10^{-5} and smaller (see Appendix V).

Fig 5.6 shows the crest mean outcrossing rates obtained from the multivariate model of Camille, Gauss1, and Gauss2. Note that the multivariate sea-state model parameters were estimated from 34.13 min. long samples (Tables 5.2.1 through 5.3.3). Also shown is the Gaussian estimate (Equation 5.9) which corresponds to the second moment properties of the time series (same for Camille, Gauss1, and Gauss2 and estimated from 34.13 min. long samples, see Table 5.1.2). Before comparing the multivariate model estimates of the mean outcrossing rates of the three sea states and the corresponding Gaussian results, it is

198

worthwhile to examine the uncertainty associated with the estimation of mean outcrossing rates from a time series of finite length. For a Poisson process approximation of the crest threshold exceedance events in time it can be shown that the one standard deviation error band on the estimate of the mean outcrossing rate, $\mathring{v}_x$, is given by: $\mathring{v}_x \pm \sqrt{\dfrac{\mathring{v}_x}{T}}$. In other words the cov of estimation of the mean outcrossing rate is $\dfrac{1}{\sqrt{\mathring{v}_x T}}$ Using the crest mean outcrossing rate estimates from Equation 5.9, the covs of estimation of the mean outcrossing rates for thresholds of 30, 35, 40, and 50 ft. are calculated to be 0.5, 0.9, 2.1, and 15.6. Also note that the mean outcrossing rates in Fig. 5.6 have been plotted in log scale. In view of the discussion above we can conclude from Fig. 5.6 that for crest thresholds up to 40 ft., the mean outcrossing rates estimated from the multivariate models of the Gaussian series Gauss1 and Gauss2 follow the theoretical results (Equation 5.9) well and are significantly lower than that obtained from the multivariate model of the non-Gaussian sea-state Camille.

The cumulative distribution functions (CDF) of the extreme crest elevation in 34.13 min. shown in Figs. 5.7 and 5.8 were calculated from the corresponding outcrossing rates (including the observed outcrossing rate) under the assumption of independence of crest exceedance events (Equation 5.4). The observed extreme crest elevation in the 34.13 min. long Camille record is 51.63 ft. The CDF results follow the pattern dictated by the corresponding outcrossing rates.

As mentioned previously the "wave" discretization and qualifying process introduces certain statistical bias viz-a-viz the underlying process. We present below a study of the effects of "qualifying" (and associated discretization) and "modeling" (using the sum of superposed components in lieu of the original wave elevation data) on the marginal process moments of Camille, Gauss1, and Gauss2. In addition we also present the marginal moments of three simulated (Monte Carlo simulation) samples of "wave" trains (each with the number of "waves" equal to the number of qualified "waves" in 34.13 min.)

199

corresponding to each of Camille, Gauss1, and Gauss2 sea states. In Tables 5.6 and 5.7 "modeling" refers to the replacing the original surface elevation by the sum of superposed sinusoids.

Table 5.6 Effects of "Qualifying" and "Modeling" on Marginal Moments

Description of Time Series	Mean (ft.)	Std. Dev. (ft.)	Skewness Coeff.	Kurtosis Coeff.
Camille, Original T = 34.13 min., n_t = 191	0.00	10.75	0.27	3.34
Camille, qualified but before "modeling" T = 26.70 min., n_q = 148	0.62	11.53	0.16	2.95
Camille, qualified and "modeled" T = 26.70 min., n_q = 148	0.62	11.46	0.18	2.83
Gauss1, Original T = 34.13 min., n_t = 196	0.00	10.75	-0.03	3.13
Gauss1, qualified but before "modeling" T = 29.81 min., n_q = 164	0.44	11.20	-0.11	2.97
Gauss1, qualified and "modeled" T = 29.81 min., n_q = 164	0.44	11.10	-0.06	2.84
Gauss2, Original T = 34.13 min., n_t = 189	0.00	10.75	-0.01	3.13
Gauss2, qualified but before "modeling" T = 27.41 min., n_q = 149	0.47	11.59	-0.09	2.82
Gauss2, qualified and "modeled" T = 27.41 min., n_q = 149	0.47	11.49	-0.03	2.65

Table 5.6 shows that the discretization and qualifying process increases the mean and variance and apparently decreases the skewness and kurtosis coefficients of the elevation process compared to the underlying original process (Camille, Gauss1, or Gauss2). The "modeling" operation has no apparent statistically significant effects on the mean, standard

200

deviation, skewness, or kurtosis coefficients. See results below for sampling variability indications.

Table 5.7 Marginal Moments of Simulated "Wave" Trains From "Multivariate" Model

Description of Time Series	Mean (ft.)	Std. Dev. (ft.)	Skewness Coeff.	Kurtosis Coeff.
Camille Sea state; Simulated Series #1 $n_q = 148$, T = 26.63 min.	0.34	11.12	0.17	2.66
Camille Sea state; Simulated Series #2 $n_q = 148$, T = 26.11 min.	0.45	11.13	0.17	3.00
Camille Sea state; Simulated Series #3 $n_q = 148$, T = 27.34 min.	0.52	11.81	0.13	2.87
Gauss1 Sea state; Simulated Series #1 $n_q = 164$, T = 29.90 min.	0.41	10.57	-0.06	2.53
Gauss1 Sea state; Simulated Series #2 $n_q = 164$, T = 29.98 min.	0.35	11.00	-0.08	2.59
Gauss1 Sea state; Simulated Series #3 $n_q = 164$, T = 28.85 min.	0.63	11.54	-0.07	2.80
Gauss2 Sea state; Simulated Series #1 $n_q = 149$, T = 26.55 min.	0.57	11.53	-0.13	2.32
Gauss2 Sea state; Simulated Series #2 $n_q = 149$, T = 27.65 min.	0.53	11.25	-0.05	2.41
Gauss2 Sea state; Simulated Series #3 $n_q = 149$, T = 26.53 min.	0.65	11.46	-0.11	2.38

The results of three time series simulated for each of the sea states show sample-to-sample variability in the case of each sea state. The sampling variabilities are expectedly high for skewness and especially for kurtosis. To understand the ability of the "multivariate" model to simulate representative "waves", it is necessary to compare the results of Table 5.7 with the results of the corresponding qualified and modeled "wave" trains reported in Table 5.6. Results from Camille, Gauss1, and Gauss2 sea states taken

201

together, show that, within the sampling variability, the multivariate model apparently reproduced the qualified process well.

The results above indicate the loss of some skewness in the qualifying scheme and this explains why the multivariate model mean outcrossing results are not as accurate as the mean outcrossing results calculated by simple non-Gaussian analysis which uses the marginal moments of the underlying process directly. However, the multivariate model aims to preserve more information than mere marginal moments of the process and in particular about the shapes of the qualified waves which might be critical for certain response calculation. In the following we demonstrate the calculation of few other response statistics.

The statistics of the extreme wave height in a given short-term period can be estimated by assuming that in the limit-state function, $g(\underline{y}) = r(\underline{y}) - r_0$, where $r(\underline{y})$ is the difference between the maximum and the minimum wave elevations in the "wave" in which the characteristic variables are given by $\underline{y}$. As in the case of the crest limit-state function, the outcrossing probability of different wave-height thresholds could be estimated by axis-orthogonal simulation with relatively small (compared to MCS) cpu time. The cumulative distribution functions of the extreme wave height in three different time periods, 34.13 min., 1 hour, and 3 hours, for the Camille sea state are shown in Fig.5.9. The CDF is calculated from the corresponding mean outcrossing rates under the assumption of the independence of the height threshold exceedance events (Equation 5.4). The observed extreme value of the wave height in the 34.13 min. long Camille record is 74.38 ft.
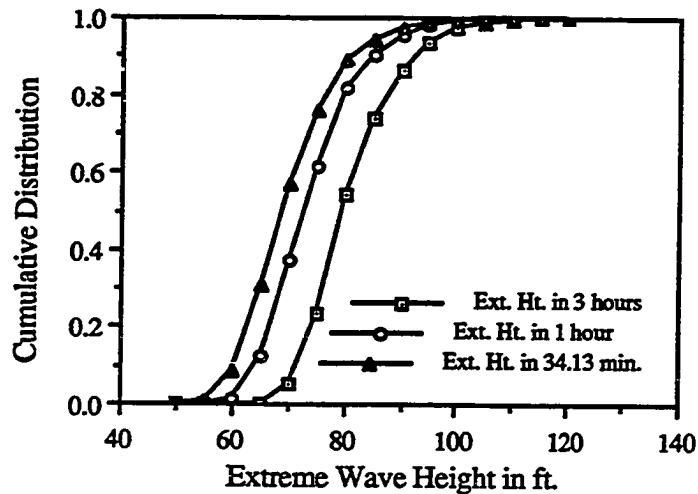
202

Fig. 5.9 CDF of Extreme Wave Height for Camille Time Series

Next the calculation of statistics of the extreme base shear (due to Morison drag force only) on a pile during a short-term interval (3 hours) is demonstrated. The limit-state equation used for outcrossing probability calculations is of the form: $g(\underline{y}) = r(\underline{y}) - r_0$; where $r(\underline{y})$ is the maximum base shear (in this demonstration due to drag force only) of a pile in the "wave" for which the characteristic variables are given by $\underline{y}$. Inclusion of the inertia force in the framework is straightforward. For this example it was assumed that the diameter of the pile is 6 ft. and that the pile is located in a water depth of 348.7 ft. The first step in calculating the wave force on a pile is to calculate the water particle kinematics (only horizontal velocity is required for calculation of the horizontal drag force on a vertical pile) under the wave. At present no theoretically rigorous method exists for calculating the kinematics in the trough-to-crest region in irregular gravity waves (see *Sobey, 1989*). The most common approach adopted for irregular waves (well suited for the representation of the "waves" adopted in the proposed extreme sea-state model) is to consider the irregular wave as a superposition of a finite number of regular Airy waves. However, straightforward linear superposition of the kinematics of the component Airy waves under

203

the crest result in erroneously high water particle velocities due to the high frequency component waves (see *Sobey, 1989*). In response, in this study we use an engineering solution to the problem known as "Wheeler Stretching" (*Wheeler, 1969*), where an empirical modification of the "depth-decay" function is used in calculation of the component Airy wave kinematics. Recent tank test results show that the Wheeler stretching gives a reasonable agreement with the measurement in the surface zone and much better agreement than the linear theory (*Torum and Skjelbreia, 1989*). In principle any other wave kinematics solution can easily be implemented in the limit-state function to calculate the resulting base shear on the pile. The next step in the calculation of the base shear is to calculate the force per unit length along the length of the pile for the calculated wave kinematics field. The force per unit length (due to drag force only) is calculated along the pile using Morison equation with a drag force coefficient of 0.6. The drag force is maximum when the "wave" crest is located at the pile. Finally the base shear is obtained by integrating the drag force per unit length up to the crest elevation. In this demonstration, no uncertainty in the drag force coefficient and in the modeling uncertainty in predicting fluid kinematics were included. However, if the probability distributions of such uncertainties ($\underline{Z}$) are known they can easily be incorporated in the limit-state function in the form: $g(\underline{y}) = r(\underline{z}, \underline{y}) - r_0$.

For the base shear limit-state equation it was found that the axis-orthogonal simulation was cpu intensive to carry out. For demonstration of the application of "multivariate" sea-state framework in calculating extreme base shear statistics, the reliability computations were carried out using FORM. For a discussion on the accuracy of the probability computation see Appendix V.
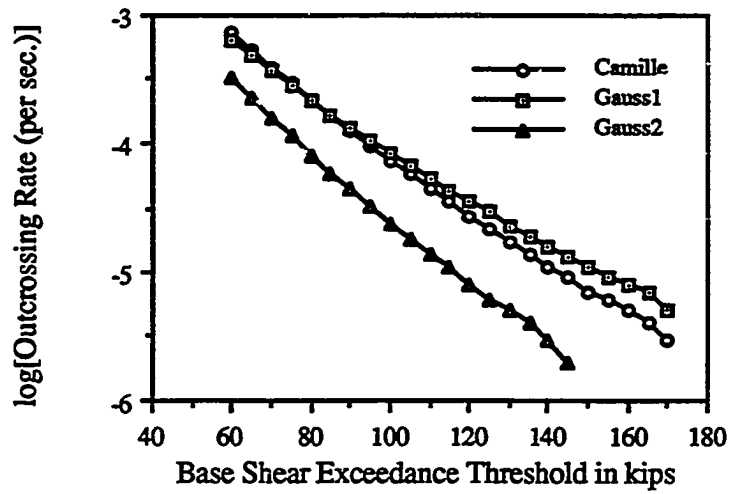
Fig. 5.10 Base Shear Outcrossing Rate :
Camille and Simulated Gaussian Time Series
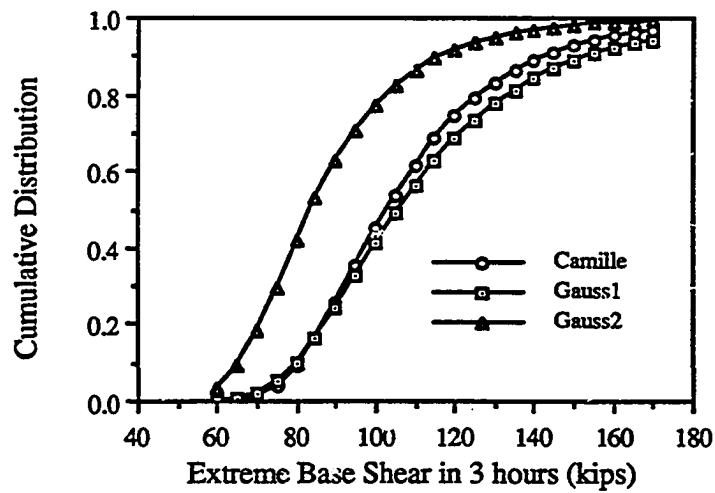
Fig. 5.11 CDF of Extreme Base Shear in 3 hours:
Camille and Simulated Gaussian Time Series

205

Fig. 5.10 shows the base-shear mean outcrossing rates for the multivariate model based on statistics from the Camille, Gauss1 and Gauss2 sea-elevation time series. Simple Gaussian (Equation 5.9) and non-Gaussian (Equation 5.12) mean outcrossing rates for the base shear are not available because, unlike the case of the crest height, the corresponding process statistics (spectral moments, base shear mean, standard deviation, skewness coefficient, and kurtosis coefficients) for the base shear are not available. Time domain solutions are expensive; this is a motivation for seeking alternative methods of analysis. Fig. 5.11 shows the calculated CDF of the extreme base shear in 3 hours for the corresponding mean outcrossing rates shown in Fig. 5.10. It is interesting to note that the plot for non-Gaussian Camille time series lies between the plots of Gaussian time series, Gauss1 and Gauss2 (Figs. 5.10 and 5.11). Both for the crest height (Figs. 5.6 and 5.8) and the base shear the Camille results are close to that of Gauss1, although in the case of crest height the results of Camille do not lie below those of Gauss1. This difference between the crest height and base shear outcrossing results is not surprising, because the base shear response is dependent not only on the crest elevation but also on the profile of the "wave" through the kinematics.

The median of the 3 hour extreme base shear for Camille sea state was found to be 102.9 kips.by linear interpolation of CDF values in Fig.5.11. The 3 hour extreme base shear cov = 0.28 was estimated from the CDF results. Note, the cov of the extreme base shear calculated here is due solely to the "wave"-to-"wave" variations within the stationary sea state characterized by the sea-state variables, $\underline{\theta}$, estimated from the Camille data.

As a byproduct of the FORM (note even the AOS simulation requires FORM results as starting points) calculations for various response threshold outcrossing probabilities, we obtain the values of the characteristic variable, $\underline{y}$, for which the "failure" ($g(\underline{Y}) < 0$) is most likely to occur. This point in the multidimensional characteristic variable space is known as the "design" point and it corresponds to the point on the failure surface closest to the origin of the transformed standard normal space (see *Madsen et al., 1986*).

206

Figs. 5.12 and 5.13 show "design" "waves" for various threshold exceedance events for crest height and base shear respectively. Tables 5.8 and 5.9 show the corresponding "design" point values of the characteristic variables and some derived parameters (e.g., ratio of the amplitudes of the fundamental and the 1st harmonic components, etc.) of the "design wave". The results shown in Fig. 5.12, Fig. 5.13, Table 5.8, and Table 5.9 are for the Camille sea state.

Fig. 5.12 "Design Waves" for Various Crest Threshold Exceedance Events

Table 5.8 Design Point and Characteristics of "Design Waves"
for Various Crest Threshold Exceedance Events

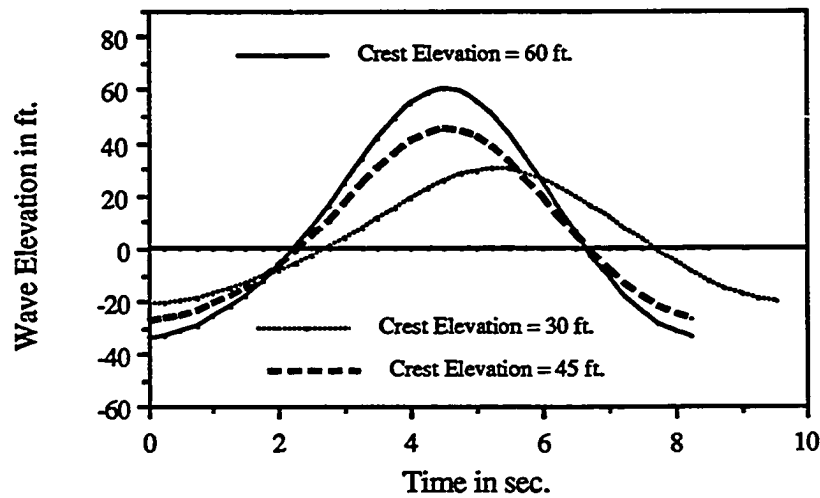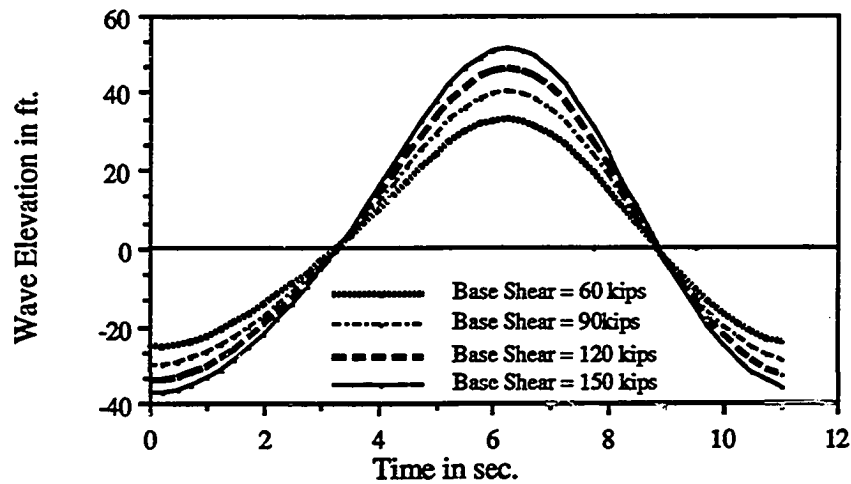| Variables / Parameters of "Design Wave"	Crest Threshold = 30 ft.	Crest Threshold = 45 ft.	Crest Threshold = 60 ft.
Time Period (sec.), t_f	9.89	8.62	8.55
Zero-Freq. Comp.(ft), a_0	2.43	4.94	7.84
1st. cosine Amp. (ft), a_1	-24.68	-35.17	-45.83
1st. sine Amp. (ft), b_1	-3.89	-4.77	-6.25
2nd. cosine Amp. (ft), a_2	1.54	3.55	4.60
2nd. sine Amp. (ft), b_2	1.88	2.54	3.61
3rd. cosine Amp. (ft), a_3	-0.49	-0.52	-0.49
3rd. sine Amp. (ft), b_3	-0.12	0.05	0.07
$\dfrac{\text{Amp. of Fundamental Comp.}}{\text{Zero-Freq. Comp.}}$	10.28	7.18	5.90
$\dfrac{\text{Amp. of Fundamental Comp.}}{\text{Amp. of 1st.Harmonic Comp.}}$	10.28	8.13	7.92

Fig. 5.13 "Design Waves" for Various Base Shear Threshold Exceedance Events

208

Table 5.9 Design Point and Characteristics of "Design Waves"
for Various Base Shear Threshold Exceedance Events

Variables / Parameters of "Design Wave"	Base Shear Thres.=60k	Base Shear Thres.=90k	Base Shear Thres.=120k.	Base Shear Thres.=150k.
Time Period (sec.), t_f	11.27	11.30	11.35	11.39
Zero-Freq. Comp.(ft), a_0	1.83	2.32	2.74	3.12
1st. cosine Amp. (ft), a_1	-27.52	-33.17	-38.03	-42.34
1st. sine Amp. (ft), b_1	-6.73	-8.05	-8.87	-9.42
2nd. cosine Amp. (ft), a_2	0.98	1.56	2.02	2.40
2nd. sine Amp. (ft), b_2	2.81	3.49	3.96	4.29
3rd. cosine Amp. (ft), a_3	-0.35	-0.32	-0.31	-0.29
3rd. sine Amp. (ft), b_3	-0.42	-0.48	-0.51	-0.52
$\frac{\text{Fundamental Amp.}}{\text{Zero-Freq. Comp.}}$	15.48	14.71	14.25	13.90
$\frac{\text{Fundamental Amp.}}{\text{1st.Harmonic Amp.}}$	9.51	8.93	8.78	8.82

The "design wave" profiles for crest thresholds (Fig. 5.12) show substantial positive skewness as expected. In contrast, the base shear is maximized when the wave height is maximized and hence the "design waves" for the base shear thresholds (Fig.5.13) are more symmetrical. It is also interesting to note that the positive zero-frequency components are relatively high for the crest threshold exceedance "design waves" (Table 5.8) compared to the base shear exceedance "design waves" (Table 5.9) with comparable a_1, the first cosine amplitudes.

All the extreme response statistics presented above have been calculated based on the assumptions of the Bernoulli / Poisson process (e.g., independence of the outcrossing events). Next we explore the improved estimation of extreme response statistics (Equation 5.8) by using the Markov process assumption of one-step memory. Recall from Section 5.3 that calculation of the improved mean outcrossing rate ($P_{1q} - P_{12q}$, in Equation 5.8) requires calculation of P_{12q}, the joint threshold exceedance probability, i.e., the probability that the response exceeds a given threshold, r_0, in an arbitrary qualified "wave" and also in

209

the following "wave" (which is also qualified). Choice of the limit-state functions for the response and the probability characterization of the sea state using lag-1 correlation coefficients have been discussed in Section 5.3. Also recall that P_{1q} is the response threshold outcrossing (or exceedance) probability of an individual qualified "wave". Figs. 5.14 and 5.15 show in log scale P_{1q} and P_{12q}, the individual and joint exceedance probabilities for various thresholds for the crest-height and shear-force limit-state functions. The results presented in Figs. 5.14 ad 5.15 are based on probability computation by FORM (see Appendix V for a discussion on the accuracy of FORM calculations). Figs. 5.14 and 5.15 show that for both the cases of crest height and shear force the joint threshold exceedance probability is a few orders of magnitude less than the individual threshold exceedance probability at all thresholds of interest for extreme response statistics. This suggests that the independence assumption for the outcrossing events at thresholds of interest is a reasonable one; hence the use of Equation 5.4 in calculation of extreme response statistics is justified. An alternative way of taking into the account the possibility of threshold exceedance in successive waves (i.e., clustering of outcrossing events) is given for a Gaussian process by Equation 5.13 (*Vanmarcke, 1975*). For the crest threshold exceedance the spectral moments of the underlying surface elevation process are available (Table 5.1.2). The bandwidth parameter δ in Equation 5.13 was calculated to be 0.505. For this value of δ and for the crest outcrossing thresholds of interest (i.e., between 30 and 60 ft.) Equation 5.13 yields the mean outcrossing rates very close to those calculated by Equation 5.9 where clustering effects are neglected. This further confirms our finding from the "multivariate" sea-state model that the joint crest threshold exceedance probability is small compared to the individual crest threshold exceedance probability. The following results are shown for the Camille sea state. Results from Gauss1 and Gauss2 also showed large difference in magnitude between the joint and individual probability of response threshold exceedance.
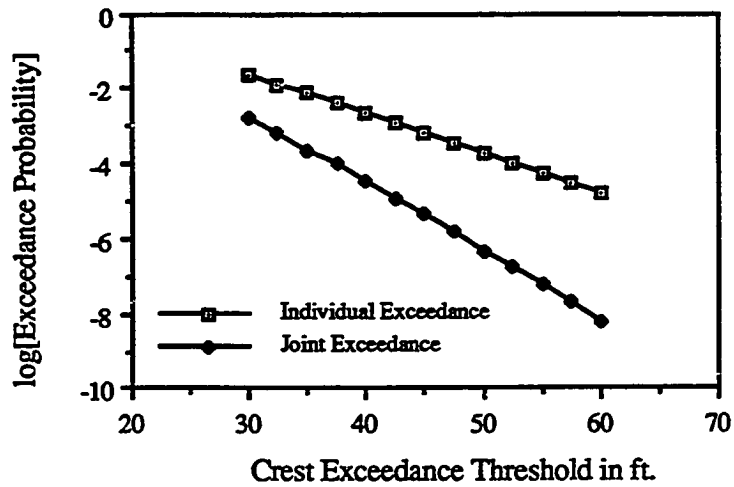
Fig. 5.14 Individual and Joint Probability of Crest Threshold Exceedance for any Qualified "Wave"; Camille Sea State
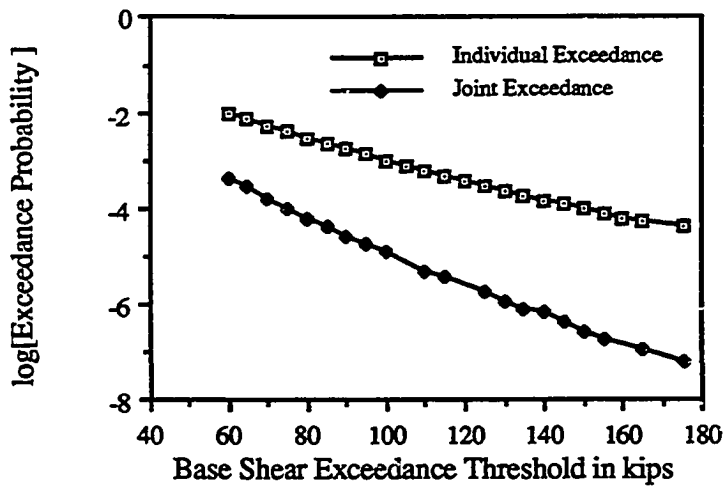
Fig. 5.15 Individual and Joint Probability of Base Shear Threshold Exceedance for any Qualified "Wave"; Camille Sea State

211

Finally we demonstrate the application of the "multivariate" sequence model of the extreme sea state in the calculation of the spatial correlation of sets of drag forces per unit length at different locations on two adjacent piles. This demonstration is motivated by the need for a systematic way of incorporating spatial uncertainties in kinematics, force coefficients, etc., in calculation of the spatial correlation of the nodal wave forces (see Chapter 3). As in the demonstration of the framework in extreme base shear statistics calculation, the uncertainty due to the drag force coefficient and modeling errors in predicting wave kinematics are neglected in this demonstration calculation of the spatial correlation coefficients between drag forces. However, the framework is general enough to estimate spatial correlation for various response quantities (e.g., nodal forces due to drag as well as inertia) taking into account the uncertainties due to force coefficients and / or wave kinematics should such information become available.
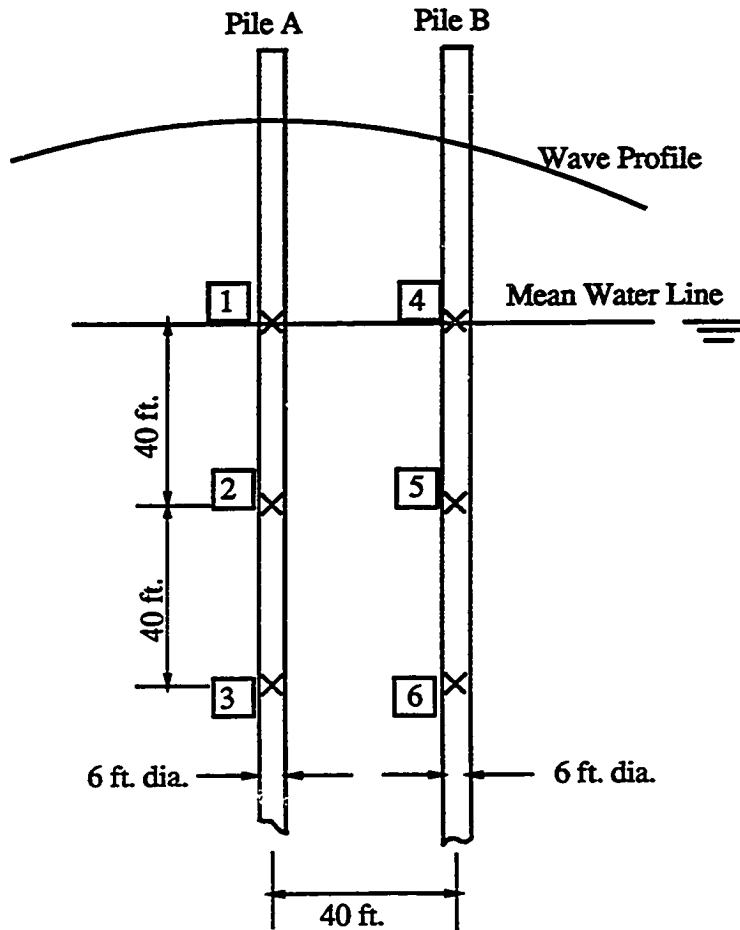
Fig. 5.16 Spatial Locations for Calculation of Drag Force Spatial Correlation

Fig. 5.16 shows the position of the six points on the two adjacent piles located 40 ft. apart in the direction of wave travel in 348.7 ft. of water depth. Drag forces per unit length (using Morison Equation) at each of the six points were simulated (Monte Carlo simulation) 10000 times (although 50 - 100 simulations would yield second moment estimates with acceptable cov of estimation) using individual "waves" generated according to the probability characteristics of the Camille sea state. Table 5.10 shows the correlation coefficients between the drag forces (per unit length) at the six locations estimated from the simulation. In Table 5.10, F_i represents the drag force per unit length at point i, (i =1, 2, ..., 6; see Fig 5.16). Selected results from Table 5.10 are shown in Figs. 5.17 and 5.18.

213

Table 5.10 Symmetric Correlation Coefficient Matrix
between Drag Forces Per Unit Length

	F_1	F_2	F_3	F_4	F_5	F_6
F_1	1.00					
F_2	0.77	1.00				
F_3	0.58	0.95	1.00			
F_4	0.65	0.83	0.74	1.00		
F_5	0.63	0.95	0.95	0.84	1.00	
F_6	0.51	0.91	0.98	0.71	0.96	1.00
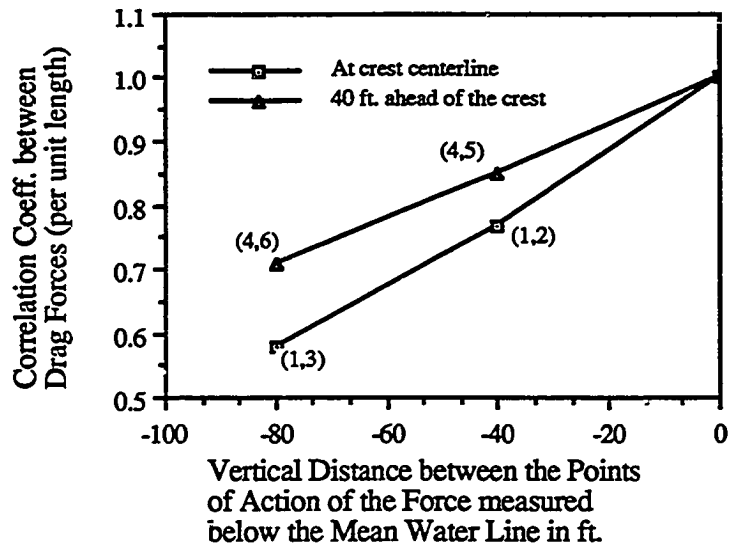
Fig. 5.17 Variation of Drag Force Spatial Correlation in Vertical Direction

214
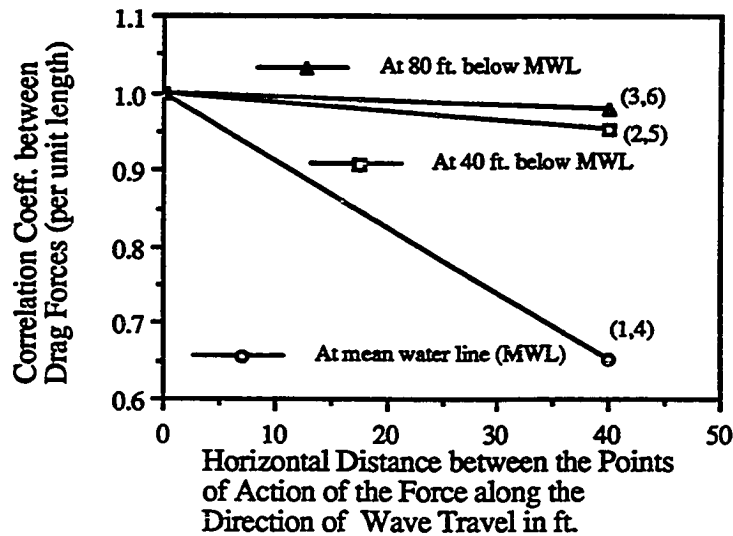
Fig. 5.18 Variation with Depth of the Drag Force Spatial Correlation in the Horizontal Direction

The correlation coefficients reported in Table 5.10 are due to "wave-to-wave" variation with the extreme sea state characterized by the Camille data. In contrast, the spatial correlation coefficients between nodal wave forces modeled in Chapter 3 by the parametric equation of the isotropic "squared exponential decay" type (Equation 3.3) include the uncertainties in the force coefficients and uncertainties in wave kinematics modeling. Results in Table 5.10 indicate that at least for the "wave-to-wave" variability the spatial correlation between the drag forces per unit length at different points cannot be expressed in a form similar to Equation 3.3 because the decay of the correlation is dependent not only on the spatial separation of the points of action of the drag force but also on the position of the points in the wave field (i.e., distance from crest, position relative to the mean water line etc. However, the proposed framework is a more systematic way of incorporating all spatially varying uncertainties compared to the calibration of the parametric model (Equation 3.3) as carried out in Chapter 3.

215

5.6 SUMMARY

A new model to characterize short-term extreme sea states has been presented and its application in calculating the statistics of extreme response has been demonstrated. The model has been evaluated by comparing extreme crest height statistics obtained from the proposed framework with known Gaussian and non-Gaussian results. This "multivariate" model of the extreme sea state is conceptually attractive because it makes the efficient reliability solution methods, such as FORM and SORM, available for estimating statistics of response (due to a class of random processes). The use of this model in calculation of response statistics such as the probability distribution of extreme base shear of a pile, the spatial correlation of sets of drag forces at different locations, etc., has been demonstrated.

The sensitivity of the results with respect to the "wave-by-wave" discretization scheme (see Appendix III) for irregular records needs to be evaluated. In particular the discretization and qualification process introduces statistical bias (e.g., reduction of skewness) viz-a-viz the underlying process. It would be interesting to compare the multivariate statistics (e.g., shapes of "mean waves", "design waves", etc.) as the qualifying wave crest elevation threshold increases. (Such qualification for Gaussian processes results in Slepian processes). By qualifying only large "waves" it is possible to get statistics more representative of the extreme "waves". However, there would be fewer "waves" qualifying; this would increase the statistical uncertainty of estimation of the sea-state parameters.

Hence, work is needed in quantifying the effects of statistical uncertainty in estimating the parameters of the "multivariate" model.

The focus here is on maximum static response prediction, but the model might also be used to simulate elevation and forces for dynamic response prediction (at least for lower frequency effects). Extension to short-crested seas might be possible, but would probably be inefficient. It is expected that in the future through analysis of similar extreme sea-state data, parameters of this multivariate-sequence model of a short-term sea state can be

216

functionally related to the long-term sea-state distribution parameters such as, significant wave heights, average zero-up crossing periods, etc., as well as to water depth. At present, this idea is presented as a research tool for better understanding and characterization of load processes. The methodology also demonstrates diverse application of both the component and the system FORM / SORM reliability techniques.

217

CHAPTER 6

CONCLUSIONS

The application of system reliability methodology for offshore structural problems have been investigated. The work carried out can be categorized in three interrelated areas: wave-load modeling, study of system behavior, and system reliability analysis framework.

The wave-load variability is significantly greater than the variability of the capacity parameters at least for the truss type behavior of offshore jacket structures studied in this work and this tends to obscure the probabilistic "system effects". In response, improvement of wave-load modeling for system reliability analysis has been investigated.

The current practice of wave-load modeling for failure path based system reliability analysis consists of using a fixed spatial pattern of nodal forces (corresponding to the position of a regular design wave with respect to the structure when the base shear is maximum) scaled by a random intensity factor. In Chapter 2 the structural system reliability analysis when the spatial force pattern changes as the load increases under increasing wave height is considered. The so-called "fragility approach" to systems analysis, wherein the reliability of the system is obtained for each of a set of increasing wave heights, is demonstrated. The method is applied to analyze a fixed offshore jacket in 140 feet of water and designed for a 100-year (63 foot) wave. In this case study, the inclusion of wave slamming forces on the deck at higher wave heights led to an increase of the system failure probability by an order of magnitude. The change of the relative importance of different member-failure sequences with wave loads corresponding to different wave heights is studied. In particular, inclusion of slamming forces on deck substantially changes the relative importance of failure sequences (i.e., different members are part of the critical sequences when slamming is included). Results from simplified "fixed-pattern" analyses were calibrated against "fragility" analysis. While computationally

218

much simpler, the fixed-pattern approach can work well only if the "appropriate" wave pattern is used. An approximate procedure to obtain the "appropriate" wave-load pattern is outlined in Chapter 2. A comparison of the member-level and system-level failure probabilities is presented in terms of factors measuring different system effects.

The wave-load spatial patterns adopted for both the "fixed pattern " and the "wave-fragility" approaches are deterministic, i.e., the nodal wave forces are fully correlated. Common functional dependence of the nodal wave forces on the wave height results in a high level of correlation among the nodal wave forces. Realistically, however, local variations due to the irregular wave elevation, uneven marine growth on the structure, and local uncertainties in wave kinematics and force prediction result in less than this implied perfect correlation among the nodal wave forces. Given the importance of the load aspects of the problem the question arises as to what the effects of the typical (fully correlated) nodal force assumption are on system reliability assessments.

In Chapter 3, an analytical form is assumed for the spatial distribution of correlation between nodal wave forces. The parameters of the correlation model include a base (non-ergodic level) correlation and rates of decay in each of the three dimensions in space. A framework is developed for the probabilistic description of nodal wave forces, consistent with the prescribed correlation structure and the available information on the base shear distribution. Application of the framework to the space truss model of the previously studied fixed offshore jacket shows that for a fixed base shear cov, the correlation level among the nodal wave forces has to decrease markedly before such drop in the correlation level has a significant effect on both the member-level and system-level failure probabilities. This is because the internal member forces are influenced by multiple nodal loads which causes spatial averaging and lessens the impact of the decrease in correlation. Calibration from limited published data indicates that although the correlation due to local uncertainties appears to decay quite rapidly over space, the absolute correlation level remains high because of the high degree of common functional dependence of the nodal

219

wave forces on the random wave height, H. Hence unless future work suggests much lower spatial correlation than we now estimate, it appears that the wave-load representation by a deterministic pattern scaled by a scalar random variable can be satisfactorily used in system reliability analysis for global truss type behavior of jacket structures. The investigation also clarifies issues dealing with spatial averaging involved in the base shear (the chosen global load intensity random variable) and suggests when the commonly adopted estimates of load variability have to be be reduced (or increased) in system reliability calculations.

To develop deeper understanding of the system reliability of realistic statically indeterminate structures, the system behavior of simple classes of "unbalanced" (i.e., mean safety factor different for different members) structures have been studied in Chapter 4. Probabilistic measures of "systems effects" have been provided in terms of "expected system-level capacities" and the resulting "complexity" and "redundancy" factors. For a number of cases, these system factors can be approximated from the corresponding well studied "balanced" systems and simple "unbalanced" systems using rules developed from the results of the study. The rules also provide insights into system reliability of more general unbalanced systems. The deterministic system effect is quantified in terms of the "deterministic system capacity" and the resulting "deterministic system factor". The dependence of the probabilistic system factors on the deterministic system factor has also been investigated. In the cases studied it appears that the deterministic "system effects" dominate over the probabilistic "system effects" once the amount of unbalance is greater than the variability (cov) of the member capacity variables. Efficient use of reduced space Monte Carlo simulation (also known as conditional expectation) techniques in system reliability analysis has been demonstrated. Application of these findings in accelerated system reliability assessment of practical structures, in particular, a fixed offshore jacket structure under wave loading, has been successfully demonstrated. This efficient method of simulation based analysis was possible because the wave-load variability dominates over

220

the structure capacity variability and because the wave load could be represented by a single random variable (Chapter 3).

In view of the importance of the load variability in system reliability analysis, a new model for statistically characterizing narrow banded random processes is presented and explored in Chapter 5. The model is based on a "multivariate" random variable characterization of the random process suitable for use both in efficient reliability computation, e.g., FORM / SORM and in general purpose methods such as Monte Carlo simulation. This model does not make any assumption regarding the Gaussianity of the random process and hence is attractive for characterizing the wave elevation process in an extreme (storm) sea-state which is often non-Gaussian. Moreover, the response of nonlinear hydro-mechanical systems (e.g., those involving the drag force) becomes non-Gaussian, even if the input wave process is Gaussian. In this work the application of the proposed model has been demonstrated by analyzing a 34.13 min. long wave-elevation record collected during hurricane Camille. The model has been evaluated by comparing the results with other currently available Gaussian and non-Gaussian results. In addition, calculation of response statistics, e.g., probability distribution of extreme base shear of a pile, spatial correlation of sets of drag forces at different locations, etc., have been demonstrated. The focus in this work is on the maximum static response prediction, but the model might also be used to simulate elevation and forces for dynamic response prediction (at least for lower frequency effects). Extension to short crested seas might be possible, but would probably be inefficient. It is expected that in the future through analysis of similar extreme sea-state data, parameters of this multivariate-sequence model of a short-term sea state can be functionally related to the long-term sea-state distribution parameters such as, significant wave heights, average zero-up crossing periods, etc. At present, this idea is presented as a research tool for better understanding and characterization of load processes. The methodology also demonstrates diverse application of both the component and the system FORM / SORM reliability techniques.

221

Taken together, the experience from this work suggests that at least for the wave over-load problem of the space truss model of the fixed offshore structures, the variability (cov) of the load will continue to dominate over the capacity variability (cov). Better force prediction models and reduced statistical uncertainty through increased data collection are not expected to change the relative importance of the load and capacity variability. Furthermore, if the upper tail of the probability distribution of the wave load decays slowly (e.g., as in the lognormal distribution) then as shown in Chapter 4, a satisfactory "semi-probabilistic" estimate of the system failure probability is given by the probability of the load exceeding the mean (or mean-based) level of the deterministic system capacity. An improved estimate of the system failure probability can be obtained by characterizing the system capacity as a random variable using either the efficient reduced space Monte Carlo simulation method or the capacity-only-based system factors.

The most important future application of system reliability will perhaps be in assessing the system capacity of damaged structures. The ability of an offshore structure to manifest residual system reliabilities under different possible exogenous failure scenarios with quantifiable probabilities of occurrence (e.g., supply vessel collision, impact due to dropped heavy objects, riser failure impacts, construction defects, and even perhaps fatigue failures) can be expressed as a "robustness" measure of the design (see *Cornell, 1987*). In this regard, the use of <u>expected</u> system-level capacities and capacity-only-based system factors proposed in Chapter 4 will be useful. Short of explicit system reliability analysis, the expected system capacities can be quantified under the expected wave loading, for each damaged scenario. Recall that, the capacity based system factors are not dependent on the load variability. Furthermore experience in Chapter 4 suggests that, given the relatively small variability of the member capacities, it is possible to get a good estimate of the system-level capacities from relatively few simulations, obviating the necessity of using specialized system reliability techniques. Also, system-level capacities can be estimated

222

using any state-of-the-art nonlinear postfailure structural analysis method without the restrictions imposed by the classical system reliability framework.
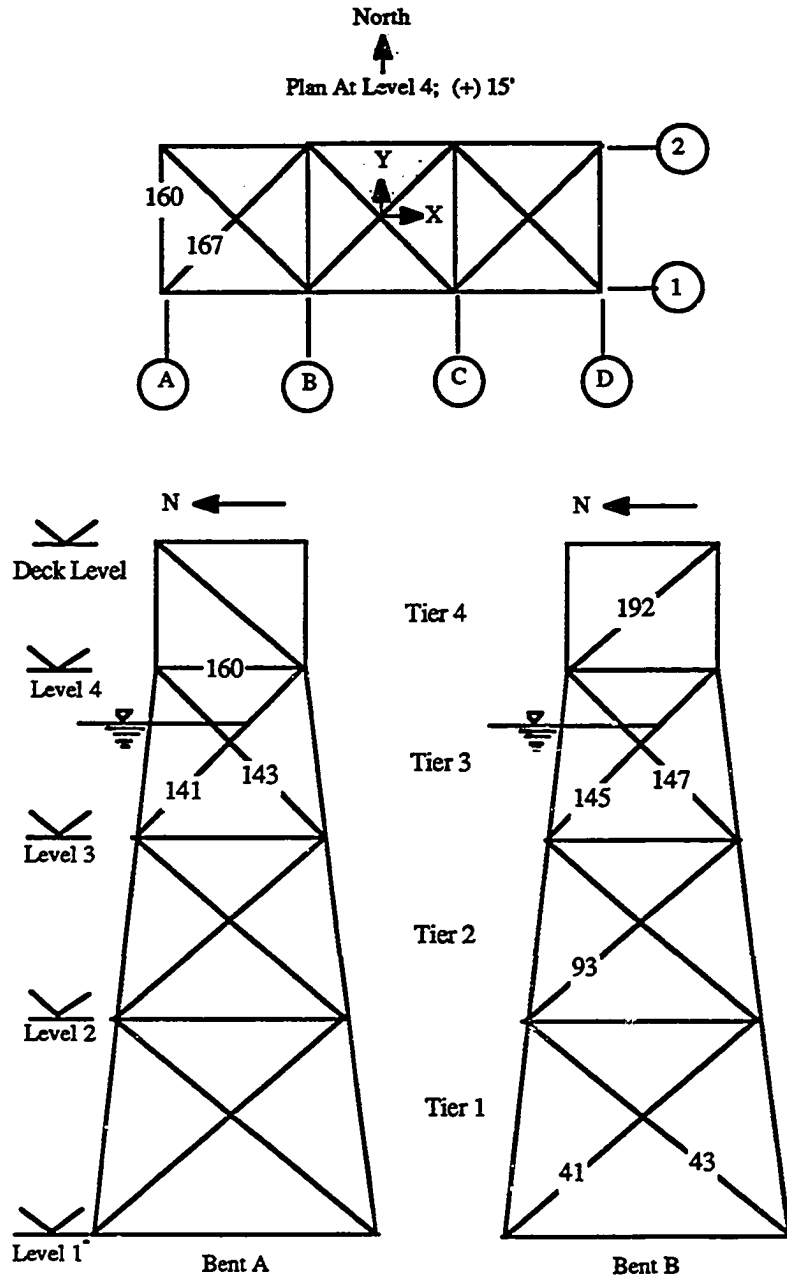
The relative importance of the load and capacity variability will be different for other classes of offshore structural problems not studied here. For example, for fixed offshore structures failing under fatigue and fracture, the uncertainties on the capacity (or the material side) and on the wave height to local stress analysis factor (see, *Wirsching, 1984*) will dominate. The wave load causing fatigue failure over a large number of moderate sea states will have reduced variability because of averaging. Also for floating structures with continuous hulls, the inertia dominated wave load can be predicted more accurately (i.e., with smaller analysis uncertainty of predicting the wave load given the wave height) than the drag dominated wave loads on a fixed offshore structures while the capacity variability associated with postfailure behavior of complex stiffened hulls is expected to be higher. The system reliability approach used in this work is expected to find application in other offshore problems.

Finally, it is noted that the system reliability methods used in this work are dependent on simplified postfailure behavior model of individual members. Finite element reliability methods (FERM, e.g., *Liu and Der Kiureghian, 1988; Holm, 1990;* etc.) are being developed which treat the system failure (defined in terms of a global response measure) as a component problem. The success of such an approach will depend on the system failure surface being smooth. Our experience, however suggests the existence of multiple failure modes of comparable marginal probability of occurrence whose safety margins are less than fully correlated. This is an indication that the FORM / SORM failure probability results obtained for a component equivalent to the most-likely-to-occur failure mode will result in a poor approximation of the system failure probability. Hence, the challenge in using FERM for system reliability lies in identifying and treating multiple failure modes (e.g., using different starting points in the search algorithm for FORM / SORM

calculations, see *Bjerager, 1989b*). The advantage of FERM in using advanced structural

analysis necessitates a closer examination of the preliminary observation made above.

224

STRUCTURAL MODEL IDENTIFYING MEMBERS IN TYPICAL FAILURE SEQUENCES

North

Plan At Level 4; (+) 15'

Bent A

Bent B

225

N ←—   Tier 4

N ←—

Tier 3

Tier 2

Tier 1

Bent C

Bent D

226
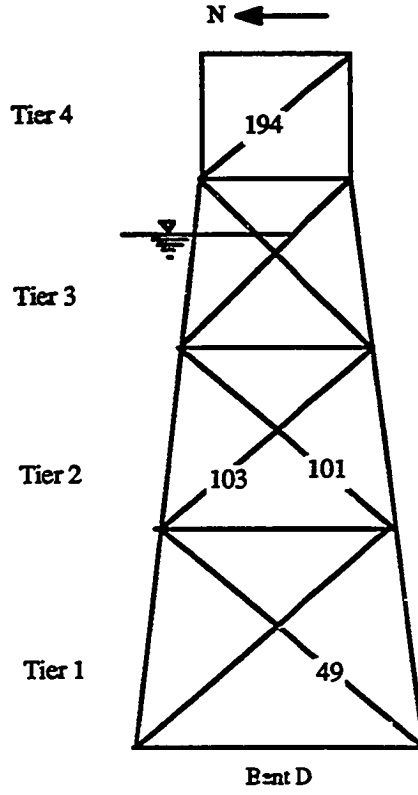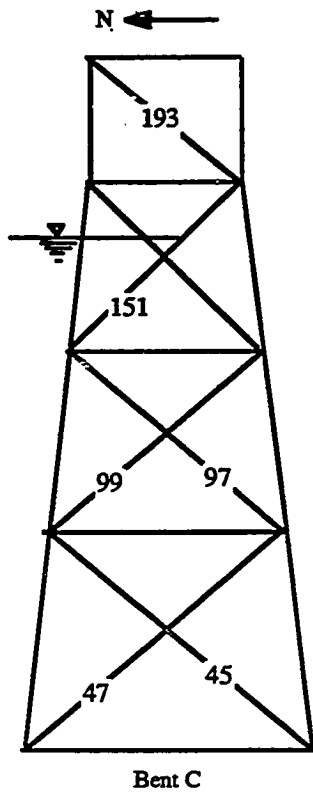
EFFECT OF DISTRIBUTION SHAPE (LOGNORMAL VS. NORMAL) ON APPROXIMATE ESTIMATION OF SYSTEM FAILURE PROBABILITY

The efficiency of "reduced space Monte Carlo simulation" in the estimation of system-level capacities and system-level failure probabilities depends on the assumed shape of probability distribution of the governing random variables. Also the suitability of using first or second moment characterization of the system-level capacities in the approximate estimation of system-level failure probabilities (e.g., by Equation 4.1) depends on the form of the probability distribution of the variables. In Chapter 4, the lognormal model has been used. If, in contrast, the normal distribution model is assumed for the load and the member-capacity variables, the load and capacity sensitivities (α_L and α_{SC} respectively) will be very close to one another even though the load cov (≈ 0.4) is much larger than the individual member capacity cov (≈ 0.10). The sensitivity in the normal model is proportional to the standard deviation of the variables, instead of the cov, which is the case in the lognormal distribution. Because the mean capacity is larger than the mean load, the standard deviations of load and capacity and hence the load and capacity sensitivities are comparable. Looking from another angle, the normal tail of the load distribution decays faster than the lognormal case, and hence p_i ($= p_f \mid \underline{R} = \underline{r}^{(i)}$), used in Equation 4.3, has a higher variance. This makes the normal-model reduced space Monte Carlo simulation inefficient compared to the lognormal model. For example, for normally distributed load and capacity variables with covs 0.40 and 0.10 respectively, a failure probability of the order 10^{-3} was estimated with covs of estimation 0.30, 0.15, 0.10, 0.04 and 0.03 from sample sizes 100, 400, 900, 5500, and 10000 respectively. Compared to the lognormal

227

case, the number of simulations required for the normal model to achieve comparable accuracy (Section 4.1.3) is about 10 times higher.

The simulation also yields estimates of the moments of any first failure capacity (AFFC) and system capacity (SC) (e.g., Equation 4.2). Unlike the case of estimation of failure probabilities, the accuracy of estimation of the expected system capacities is not sensitive to the assumed distribution shape (i.e., normal or lognormal). This is because, for the given small cov of the individual member-capacity variables there is not much difference between the normal and lognormal distribution at least in the first and second moment characterization. The cov estimates of system-level capacities were found to be almost identical for the normal and the lognormal case. Accuracy of the estimation of cov depends on higher marginal moments (implicitly assumed in the distribution shape). However, in general, satisfactory estimation of statistics up to the second moment for the system-level capacities can be obtained by simulation from few samples even in the case of normal distribution.

Instead of using direct simulation of failure probabilities, as in Equation 4.3, the system failure probability can alternatively be estimated as: $P_{sys} = P \{ L \geq SC \}$, using Equation 4.1. This would require an approximation on the distribution shape of the system capacity, as discussed in Section 4.1.2.1.

"WAVE-BY-WAVE" DISCRETIZATION
OF AN IRREGULAR RECORD

The "multivariate" extreme sea-state model presented in Chapter 5 is based on collecting statistics of discrete "wave" segments of the an irregular wave record from a presumed stationary sea state. A general irregular record realized from a relatively wide banded process (i.e., with contributions from a wider range of frequencies) is much more difficult to discretize than an irregular record from a narrow banded process. The "wave cycles" with well defined crests and troughs get increasingly difficult to identify as the process becomes more and more wide banded. It is possible to discretize the "waves" in any number of ways; no claim of superiority is made for the particular discretization scheme presented here except that they fulfil some basic requirements which will be stated later.

First we describe the particular discretization (trough-to-trough "waves") scheme used in the study reported in Chapter 5 (see Fig. 5.1 for an example of discretization).

1. Define a crest threshold equal to 75% of the rms value of the process.

2. Moving forward in the time axis locate the first zero (mean water line) downcrossing.

3. Locate the next crest threshold upcrossing on the time series.

4. Locate the trough as the point of minimum surface elevation between the zero downcrossing point (step 2) and the crest threshold upcrossing (step 3).

5. Define a "primary wave" between two successive troughs. The trough leading in time is referred to as the "leading primary trough" and the trough trailing in time is referred to as the "trailing primary trough". Note that the "leading" event is closer to the time origin than the "trailing" event on the time axis in a time series plot.

229

6. If the trough-to-trough time period of the "primary wave" is between t_{high} (= 15 sec.) and t_{low} (= 5 sec.), the "primary wave" is considered qualified, i.e., included for the purpose of estimating the statistics of the characteristics variables of the "multivariate" sea-state model. The discretization scheme then proceeds to look for the next "wave". The choice of t_{high} and t_{low} is discussed later.

7. If the time period is less than t_{low} then the "primary wave" is considered disqualified, i.e., no superposed sinusoids are fitted and hence no statistics are collected from these "waves" (see Fig. 5.1)

8. If the trough-to-trough time period of the "primary wave" is greater than t_{high} then we look for the first "secondary" trough leading (in time) the first crest threshold upcrossing point in the "primary wave". A secondary trough should at least be below the mean water line and be a local minimum among four adjacent (two leading and two trailing) data points. If such a secondary trough can be located then the segment between the "leading primary trough" and the secondary trough is disqualified. If the resulting "wave" between the secondary trough and the "trailing primary trough" has a time period less than t_{high} then the resulting "wave" is considered qualified and the discretization scheme continues.

    If on the other hand, no secondary trough is located in the "primary wave" that leads the crest threshold upcrossing point, or the resulting "wave" after the previous truncation has a time period greater than t_{high}, we look for a "second secondary trough" which is the nearest to and trailing the first crest outcrossing point in the "primary wave". This secondary trough should also at least be below the mean water line and be a local minimum among four adjacent (two leading and two trailing) data points. If such a secondary trough is located in the trailing part of the "primary wave", the segment between the secondary trough and the trailing primary trough is disqualified and the resulting "wave" between the leading trough (either the "first secondary trough" in the leading part of the "primary wave" or the

230

"leading primary trough" depending on whether such a secondary trough was located or not) and the "second secondary trough" is considered qualified whether or not the resulting time period is less than t_{high}. Similarly the "primary wave" that has no secondary trough on either the leading or the trailing side, is also considered qualified even though its time period is greater than t_{high}. Hence a limited number of qualified "waves" may have time periods greater than t_{high}.

Because the fundamental time period itself is a random variable (Section 5.2) characterizing the discretized "waves", the other characteristic variables (a_0, a_i, b_i, $i = 1, 2$, and 3; see Equations 5.2.1 through 5.2.3) are sensitive to the time period and hence to the discretization algorithm. In contrast, in the Fourier analysis, recall that the spectral density ordinates are determined at equi-spaced discrete Fourier frequencies which are determined by the length of the time series and the resulting spectral density curve is not sensitive to the length of the record provided that the record is sufficiently long. In the "multivariate" model it is desirable not to have the time period vary in a wide range so that in the statistics calculation of the fundamental or any (first or second) harmonic amplitudes, the sample values of the component sine and cosine amplitudes could all represent observations corresponding to less overlapping time period ranges. In other words, due to our thinking in the lines of Fourier analysis we try to avoid lumping all amplitude observations from a wide frequency range even though they may represent the fundamental or any particular harmonic component of the analyzed "waves". What consequences this overlapping has, if any at all, have not been investigated. In any case, for this study we artificially force the fundamental time periods of the "waves" within a band given by t_{high} and t_{low} (steps 6, 7, and 8). Some limited number of "waves" with time periods greater than t_{high} are also included when no secondary troughs are located within them (see step 8) because these "waves" are "truly" big "waves" which in general are of interest for reliability calculations. The time band used in this study (5 sec. to 15 sec.) is centered around 10 sec. because the

231

average time period (corresponding to centroidal frequency of the energy spectrum) of Camille was found close to 10 sec.

The choice of the crest threshold ($= 75\%$ of the process rms) should also satisfy certain requirements. The choice facilitates elimination of "small waves" which pose a problem of identification and are frequently associated with fundamental time periods below t_{low}. Yet the choice permits inclusion of all "waves" which are likely to produce extreme response in the range of interest for statistics calculation.

A visual inspection of the discretized time series, Camille, Gauss1, and Gauss2, confirmed that the discretization algorithm includes all the "waves" of interest. It is expected that the resulting statistics of the characteristic variables will also be able to simulate representative "waves" for reliability calculations.

CORRELATED NON-GAUSSIAN MODELS BASED ON HIGHER MARGINAL MOMENTS FOR RELIABILITY APPLICATIONS

A framework is presented here that statistically characterizes the random variables in terms of the first four marginal moments and the pair-wise correlation structure of the random variables. The marginal distribution of each (scalar) random variable is implicitly modeled by a transformation (between the random variable, X, and the standard Gaussian variate, U) using Hermite polynomials such that the specified marginal moments match. Following the Nataf model (see *Der Kiureghian and Liu, 1986*) the physical (in general, non-Gaussian) variables are transformed into <u>correlated</u> standard Gaussian variables. For example, consider a pair of random variables (X_i, X_j) whose marginal distributions are either known or modeled implicitly from the specified marginal moments. Let ρ_x be the correlation coefficient between the pair X_i, X_j. The random variables X_i and X_j are first mapped into standard (i.e., zero mean and unit standard deviation) Gaussian variables, U_i and U_j. Hence, $U_k = \Phi^{-1} [F_{X_k} (x_k)]$; $k = i, j$. The "equivalent Gaussian correlation", ρ_u, (correlation between U_i and U_j) that produces the desired correlation, ρ_x, between the pairs of physical (non-Gaussian) variables is estimated here in closed form (using Hermite expansion method) from either full marginal distributions or a limited number of moments. These estimates are found to agree well with exact results for ρ_u (see *Winterstein, De, and Bjerager, 1989*), which require iterative use of double integration over the joint Gaussian density (*Der Kiureghian and Liu, 1986*).

This framework implicitly assigns a joint probability distribution consistent with the available (incomplete) information in the form of a transformation between the standard

uncorrelated Gaussian space and the space of the physical random variables so that FORM / SORM analysis or Monte Carlo simulations can be conveniently carried out.

Hermite Model for Marginal Distributions :

Instead of directly estimating the marginal distribution of the random variable, X_i, from its marginal moments (e.g., mean μ, standard deviation σ, skewness $\alpha_3 = \dfrac{E[(X_i - \mu)^3]}{\sigma^3}$, and kurtosis $\alpha_4 = \dfrac{E[(X_i - \mu)^4]}{\sigma^4}$), let us consider the functional transformation, $X_i = T_i$ (U_i), that relates X_i to a standard Gaussian variate U_i. For the case where the cumulative distribution function, $F_{X_i} (\cdot)$ is known, recall that $T(.) = F_{X_i}^{-1} [\Phi (\cdot)]$.

Now the transformation $T (\cdot)$ can be expressed through a four moment Hermite model (see *Winterstein, 1987; Winterstein, De, and Bjerager, 1989*) as follows. Note that for the case of $\alpha_4 < 3$ an inverse transformation of the form $U_i = T^{-1} (X_i)$ is recommended.

$$\alpha_4 > 3: \quad X_i (U_i) = \mu + \kappa\sigma [U_i + c_3 (U_i^2 - 1) + c_4 (U_i^3 - 3 U_i)] \qquad (A.IV.1)$$

$$\alpha_4 < 3: \quad U_i (X_i) = Y_i - c_3(Y_i^2 - 1) - c_4 (Y_i^3 - 3 Y_i); \quad Y_i = 6c_3c_4 + (X_i - \mu) / (\kappa\sigma) \qquad (A.IV.2)$$

The coefficients in the above equations are given (*Winterstein, 1987;* reproduced here from *Winterstein, De, and Bjerager, 1989*) in Table A.IV.1 below.

Table A.IV.1 Hermite Series Coefficients

Case	c_4	c_3	κ
$\alpha_4 > 3$	$[(6\alpha_4 - 14)^{1/2} - 2] / 36$	$\alpha_3 / 6(1 + 6c_4)$	$(1 + 2c_3^2 + 6c_4^2)^{-1/2}$
$\alpha_4 < 3$	$(\alpha_4 - 3) (35 - 9\alpha_4) / 192$	$\alpha_3 / 6(1 + 24c_4)$	$(1 + 10c_3^2 + 42c_4^2)^{-1/2}$

234

Correlation Mapping :

The binormal probability density can be expressed in terms of the Hermite polynomials as follows (*Winterstein, 1987*):

$$\phi_2\,(u_i,\,u_j,\,\rho_u) = \phi(u_i)\,\phi(u_j)\sum_{n=0}^{\infty}\frac{\rho_u^n}{n!}\,He_n(u_i)\,He_n\,(u_j) \qquad\qquad (A.IV.3)$$

where, the Hermite polynomials are given by $He_n(z) = (-1)^n\,\exp(z^2)\dfrac{d^n}{dz^n}[\exp(-z^2)]$; in particular, $He_0(z) = 1$, $He_1(z) = z$, $He_2(z) = z^2 - 1$, $He_3(z) = z^3 - 3z$, and $He_4(z) = z^4 - 6z^2 + 3$, etc. (see *Winterstein, 1987*) and $\phi(z) = (2\pi)^{-1/2}\exp(-z^2/2)$ is the standard normal probability density function. It can be readily shown that the Hermite polynomials, $He_n(U)$ for $n = 1, 2, 3, \dots$ have mean $= 0$, variance $= n!$, and are uncorrelated (i.e., orthogonal) with each other.

Hence,

$$E[X_i\,X_j] = \int_{-\infty}^{\infty}\int_{-\infty}^{\infty} T_i(u_i)\,T_j(u_j)\,[\,\phi(u_i)\,\phi(u_j)\sum_{n=0}^{\infty}\frac{\rho_u^n}{n!}\,He_n(u_i)\,He_n\,(u_j)\,]\,du_i\,du_j$$

$$= \sum_{n=0}^{\infty}\frac{\rho_u^n}{n!}\,t_{in}\,t_{jn};\ \text{where,}\ t_{kn} = \int_{-\infty}^{\infty} T_k(u)\,He_n(u)\,\phi(u)\,du\ ;\ \text{for}\ k = i, j$$

The coefficients t_{kn} can be evaluated by numerical integration if the transformations, $T_k(\cdot)$, $k = i, j$, are available either through the full marginal distributions or the moment based Hermite models (Equations A.IV.1 and A.IV.2) for the variables X_i and X_j.

Now, noting that $t_{k0} = E[X_k]$, we have:

$$\text{COVARIANCE } [X_i, X_j] = E[X_i\,X_j] - E[X_i]\,E[X_j] = \sum_{n=0}^{\infty} \frac{\rho_u^n}{n!}\, t_{in}\, t_{jn} - t_{i0}\, t_{j0}$$

$$= \sum_{n=1}^{\infty} \frac{\rho_u^n}{n!}\, t_{in}\, t_{jn}$$

$$\text{Hence, } \rho_x = \frac{\text{COV}[X_i, X_j]}{\sigma_{x_i}\,\sigma_{x_j}} = \sum_{n=1}^{\infty} \frac{t_{in}\, t_{jn}}{n!\,\sigma_{x_i}\,\sigma_{x_j}}\, \rho_u^n \qquad\qquad \text{(A.IV.4)}$$

The contribution from the higher order terms in Equation A.IV.4 decrease rapidly. Satisfactory results can be obtained by truncating the series at n = 3, in which case the "equivalent" Gaussian correlation, ρ_u, can be obtained in close form as a solution of a cubic equation. Truncation errors are greatest for $|\rho|$ near 1 and highly non-Gaussian cases, in which case the coefficient of ρ_u^n in Equation A.IV.4 decays slowly with n, and it

is advisable to retain higher order terms. Nonetheless, full distribution results are quite accurate for various Gumbel, lognormal, and beta pairs, although the latter two models become quite non-Gaussian for larger values of their coefficient of variation as shown in *Winterstein, De, and Bjerager, 1989.*

236

APPENDIX V

ACCURACY OF PROBABILITY COMPUTATION IN "MULTIVARIATE SEQUENCE" WAVE MODEL

The threshold outcrossing probabilities of the response (e.g., crest height, wave height, base shear, etc.) calculated for the "multivariate" wave model in Chapter 5 varied appreciably depending on the probability computation method (e.g., FORM, SORM, Monte Carlo simulation, axis-orthogonal simulation, etc.) used. In this appendix examples of this discrepancy are discussed.

In general, for the performance functions analyzed in this study (e.g., crest elevation, base shear on a pile, and wave height), it was noted that the probabilities of failure (outcrossing rate per qualified "wave") obtained by SORM (using a "curvature-fitted"[1] hyperparaboloid approximation of the failure surface at the "design" point) were 40 to 60% lower than those obtained by FORM. Monte Carlo simulation (MCS) results were obtained only for lower levels of threshold exceedance where the outcrossing probabilities are large (in the range of 10^{-2} to 10^{-3}). For these lower threshold outcrossing events where the outcrossing probabilities are large, the MCS results with acceptable accuracy (e.g., cov of estimation ≤ 0.3) could be obtained using reasonable cpu time (e.g., 100 to 200 cpu sec.in a Vax 8650 computer with a floating point accelerator board). For these lower thresholds it was observed that MCS failure probabilities were even 30 to 60% higher than the FORM results. Hence, more accurate MCS results are closer to FORM than SORM ("curvature-fitted" hyperparaboloid) results.

For the case of crest limit state function it was found that the axis orthogonal simulation results matched closely to the Monte Carlo simulation results at least for the lower levels of

---

[1]The "curvature-fitted" hyperparaboloid is determined by matching its curvatures at the apex to the principal curvatures of the failure surface at the "design" point.

237

threshold exceedance for which the MCS results are available. Furthermore, reliable estimates (small cov of estimation) of the crest outcrossing probabilities by AOS required relatively small cpu time (compared to MCS) even for higher thresholds where the failure probabilities are small (in the range of 10^{-5}) although AOS requires increasingly higher cpu time for estimation of the failure probability with acceptable accuracy at higher thresholds. The AOS results are available only for individual (not joint) exceedance probability of crest thresholds. For the base shear performance function AOS did not yield outcrossing probabilities with acceptable covs for reasonable cpu time especially at higher thresholds. Table A.V.1 shows a few examples of outcrossing probabilities (P_f and their covs of estimation for MCS and AOS) per wave cycle obtained by different computation methods for the Camille sea state.

Table A.V.1 Example Results of Outcrossing Probability Estimates
from Alternative Methods

Limit-State	FORM P_f	SORM curvature-fitted P_f	MCS P_f (cov of est.)	AOS P_f (cov of est.)
Crest Thres. = 30 ft.	0.0224	0.0126	0.0531 (0.10)	0.0440 (0.06)
Crest Thres. = 50 ft.	1.66×10^{-4}	8.02×10^{-5}	5.00×10^{-4} (0.41)	5.28×10^{-4} (0.23)
Base Shear = 50 kips	0.0180	0.0090	0.0315 (0.124)	0.043 (0.202)

It was observed that the difference between FORM and SORM ("curvature-fitted") results could be substantially reduced if the variable t_f, the time period of the "waves" is treated as a deterministic variable, say at its mean point. Furthermore, it was noted that the "design" point and hence the FORM / SORM results, especially for higher threshold outcrossing events, are sensitive to the starting point of the optimization algorithm that attempts to locate the "design" point. These observations suggest that the failure surface

238

has multiple minima (i.e., in terms of distances from the origin of the standard normal space) and or noise that pose obstacles in estimating the outcrossing probability accurately. In the absence of the means to plot projections of the failure surface, the true nature of the failure surface and hence the cause of the discrepancy between failure probability results from different methods could not be fully ascertained. Also the AOS results for crest threshold exceedance events (where the agreements were satisfactory compared to the MCS results, at least for the lower thresholds) were found to be unusually sensitive to the starting seed of the simulation.

An alternative method for approximating the failure surface by fitting a hyperparaboloid at discrete points around the "design" point is available (*Der Kiureghian et al., 1987*). The "point-fitting" method is known to be less sensitive to noise in the failure surface and hence we investigated if the "point-fitted" SORM calculations for the limit-state functions used in this study would yield accurate results. However, at present, the "point-fitted" SORM option is not available in PROBAN, the software used in reliability calculations for this study. The "point-fitted" SORM option is available in CALREL, a general purpose structural reliability analysis program. However, at present, the option to characterize random variables through higher marginal moments using Hermite polynomials (as used in this study, see Chapter 5 and Appendix IV) is not available in CALREL (*CALREL User Manual, 1989*). Hence, for the purpose of evaluating the feasibility of using the "point-fitted" SORM, we modeled the characteristic variables of the Camille sea state by a jointly normal distribution with mean, standard deviation, and correlation-coefficient matrix specified in Tables 5.2.1 and 5.3.1. The outcrossing probabilities were computed for three low crest thresholds for which Monte Carlo simulations could be carried out using reasonable cpu time. The g-function, corresponding to a crest threshold r_0 is given by: $g(\underline{y}) = r(\underline{y}) - r_0$; where $r(\underline{y})$ is the maximum elevation in the "wave" for which the characteristic variables are given by $\underline{y}$. Elevations at discrete time steps during the duration of the time period (the first characteristic variable) are given by Equation 5.1. For the sake

239

of comparison the same problems (i.e., crest outcrossing rates for the jointly normal characteristic variables of the Camille sea state) were solved by PROBAN. The results are summarized in Table A.V.2 and A.V.3 below.

Table A.V.2 Comparison of Crest Outcrossing Probabilities Using FORM, SORM ("Curvature-Fitted" and "Point-Fitted" Hyperparaboloids), and Monte Carlo Simulation; CALREL Results

Crest Threshold ft.	FORM P_f	SORM curvature-fitted P_f	SORM point-fitted P_f	MCS P_f (cov of est.)
30.0	18.4×10^{-3}	8.74×10^{-3}	29.9×10^{-3}	34.3×10^{-3} (0.05)
32.5	9.74×10^{-3}	4.09×10^{-3}	14.5×10^{-3}	17.7×10^{-3} (0.05)
35.0	4.40×10^{-3}	1.72×10^{-3}	6.89×10^{-3}	8.29×10^{-3} (0.05)

Table A.V.3 Comparison of Crest Outcrossing Probabilities Using FORM, SORM ("Curvature-Fitted" Hyperparaboloids), and Monte Carlo Simulation; PROBAN Results

Crest Threshold ft.	FORM P_f	SORM curvature-fitted P_f	MCS P_f (cov of est.)
30.0	18.4×10^{-3}	8.69×10^{-3}	34.1×10^{-3} (0.05)
32.5	9.42×10^{-3}	4.01×10^{-3}	17.9×10^{-3} (0.05)
35.0	4.39×10^{-3}	1.68×10^{-3}	8.01×10^{-3} (0.05)

The results in Tables A.V.2 and A.V.3 show the same pattern of relative discrepancy between FORM, "curvature-fitted" SORM, and Monte Carlo simulation results as previously reported in Table A.V.1. Hence it appears that the previously suspected "noise" in the failure surface is not due to the nonlinear Hermite transformation, because the characteristic variables for the examples reported in Tables A.V.2 and A.V.3 were modeled

240

by jointly normal distributions. It is seen in Table A.V.2 that the "point-fitted" curvature results are in very good agreement with the Monte Carlo Simulation results at least for the lower crest threshold exceedance events studied here.

An accurate SORM capability for the limit-state functions used in this study would greatly enhance the applicability of the proposed framework. It is expected, that more robust optimization schemes will be available for locating the "design" point and efficient methods will be available for accurate computation of the failure probability

241

REFERENCES

AMERICAN PETROLEUM INSTITUTE: *API Draft Recommended Practice for Planning, Design, and Constructing Fixed Offshore Platforms*, A preliminary release of API RP 2A - LRFD draft, American Petroleum Institute, Dallas, Texas, USA, May, 1989.

ANG, A.H.-S. and TANG, W.H.: *Probability Concepts in Engineering Planning and Design*, Vol. II, John Wiley and Sons, New York, 1984.

ANG, A.H.-S. and MA, H.-F.: "On the Reliability of Structural Systems", *Proceedings of the Third International Conference on Structural Safety and Reliability*, ed. T. Moan and M. Shinozuka, Trondheim, Norway, June, 1981.

ANG, A.H.-S., and AMIN, M.: "Reliability of Structures and Structural Systems", *Journal of the Engineering Mechanics Division*, ASCE, Vol. 94, No. EM2, pp. 671-691, April, 1968.

AUGUSTI, G., BARATTA, A., and CASCIATI, F.: *Probabilistic Methods in Structural Engineering*, Chapman and Hall, London, 1984.

BARLOW, R.E.and PROCHAN, F.: *Statistical Theory of Reliability and Life Testing*, Holt, Reinhart and Winston, 1975.

BEA, R.G., PAWSEY, S.F., and LITTON, R.W.: "Measured and Predicted Wave Forces on Offshore Platforms", *Proceedings of the Offshore Technology Conference*, OTC Paper No. 5787, Houston, Texas, May, 1988.

BJERAGER, P.: "Probability Computation Methods in Structural and Mechanical Reliability", *Mechanics of Probabilistic and Reliability Analysis*, ed. W.K. Liu and T. Belytschko, Elme Press International, Lausanne, Switzerland, February, 1989a.

BJERAGER, P.: "Introduction to Structural System Reliability", Lecture Notes for the course, *Structural Reliability: Methods and Applications*, University of California, Berkeley, April 27-29, 1989b.

BJERAGER, P., WINTERSTEIN, S., and CORNELL, C. A.: "Outcrossing Rates by Point Crossing Methods", *Probabilistic Engineering Mechanics*, ASCE, ed. P.D. Spanos, pp. 533-536, 1988a.

BJERAGER, P., LOSETH, R., WINTERSTEIN, S., and CORNELL, C. A.: "Reliability Method for Marine Structures under Multiple Environmental Load Processes", *Proceedings of the Fifth International Conference on the Behavior of Offshore Structures*, Vol. 3, BOSS '88, The Norwegian Institute of Technology, Trondheim, Norway, 1988b.

BJERAGER, P.: *Plastic Systems Reliability By LP and FORM*, Report No. 368, pp. 1-17, Department of Structural Engineering, The Technical University of Denmark, Lyngby, Denmark, December, 1987.

242

BJERAGER, P., OLESEN, R., and MADSEN, H.O.: "System Reliability of Offshore Jacket Structures by Ideal Plastic Analysis", *Proceedings of the Marine Structural Reliability Symposium*, SNAME, USA, October, 1987.

BJERAGER, P., KARAMCHANDANI, A. and CORNELL, C. A.: "Failure Tree Analysis in Structural System Reliability", *Proceedings of the Fifth International Conference on Applications of Statistics and Probability in Soil and Structural Engineering*, Vancouver, Canada, 1987.

BJERAGER, P.: *Reliability Analysis of Structural Systems*, Report No. 183, Series R, Department of Structural Engineering, Technical University of Denmark, Lyngby, Denmark, 1984.

BLOOMFIELD, P.: *Fourier Analysis of Time Series: An Introduction*, John Wiley & Sons, 1976.

BORGES, J.F. and CASTANHETA, M.: *Structural Safety* , Laboratorio Nacional de Engenharia Civil, Lisbon, 1972.

BORGMAN, L.E.: "Statistical Models for Ocean Waves and Wave Forces", *Advances in Hydroscience*, Vol. 8, pp. 139-181, 1972.

CALREL: User Manual (by P-L. Liu, H-Z. Lin, and A. Der Kiureghian), Report No. UCB/SEMM - 89/18, Department of Civil Engineering, University of California, Berkeley, USA, 1989.

CHAN, H.Y. and MELCHERS, R.E.: "Reliability of Complex Structures Under Wave Loads", *Proceedings of the Fifth International Conference on Application of Statistics and Probability in Soil and Structural Engineering*, ICASP, Vancouver, Canada, 1987.

CORNELL, C.A., DE, R.S., KARAMCHANDANI, A., and BJERAGER, P.: *Enhanced Failure-Path Based Structural System Reliability*, Offshore Structural System Reliability Joint Industry Project Report to Amoco Production Company, C. Allin Cornell, Inc., Portola Valley, California, USA, 1988.

CORNELL, C. A.: *Offshore Structural Systems Reliability*, A Report to Amoco Production Company for the Joint Industry Project Participants, C. Allin Cornell, Inc., Portola Valley, California, USA, 1987.

DANIELS, H.E.: "The Statistical Theory of the Strength of Bundles of Threads", *Proceedings of the Royal Society (London)*, Series A, Vol. 183, pp. 405-435, 1945.

DEAN, R.G., LO, J-M. and JOHANSSON, P.I.: "Rare Wave Kinematics Vs. Design Practice", *Proceedings of the Specialty Conference, Civil Engineering in the Oceans IV*, Volume II, ASCE, September, 1979.

DER KIUREGHIAN, A.: "Thoughts on Research Needs in Structural Reliability ", Presented at the *National Science Foundation Workshop on Research Needs for Application of System Reliability Concepts and Techniques in Structural Analysis, Design and Optimization*, University of Colorado, Boulder, USA, September 1988.

DER KIUREGHIAN, A., LIN, H.-Z., and HWANG, S.J.: "Second-Order Reliability Approximations", *Journal of Engineering Mechanics*, ASCE, Vol. 113, No. 8, pp. 1208-1225, 1987.

DER KIUREGHIAN, A. and LIU, P-L.: "Structural Reliability Under Incomplete Probability Information", *Journal of Engineering Mechanics*, ASCE, Vol. 112, No. 1, pp. 85-104, January, 1986.

DITLEVSEN, O. and BJERAGER, P.: "Methods of Structural Systems Reliability", *Structural Safety*, Vol. 3, pp. 195-229, 1986.

DITLEVSEN, O.: "Narrow Reliability Bounds for Structural Systems", *Journal of Structural Mechanics*, Vol. 7, No. 4, pp. 453-472, December, 1979.

FENG, Y.S. and MOSES. F.: "Optimum Design, Redundancy, and Reliability of Structural Systems", *Computers and Structures*, Vol. 24, No. 2, 1986.

FRANGOPOL, D.M., GOBLE, G.G., TRAUTNER, J.J., and SCHOLFIED, M.M.: "Redundancy Evaluation of Existing Bridges", *Bridges and Transmission Line Structures, Proceedings of the Sessions at Structures Congress '87 related to Bridges and Transmission Line Structures*, ed. L. Tall, ASCE, 1987.

FREUDENTHAL, A.M. and GAITHER, W.S.: "Design Criteria for Fixed Offshore Structures", *Proceedings of the First Annual Offshore Technology Conference*, OTC Paper No. 1058, Houston, USA, May, 1969.

FURUTA, H., SHINOZUKA, M., and YAO, J.T.P.: "Probabilistic and Fuzzy Representation of Redundancy in Structural Systems", Presented at the *First International Fuzzy Systems Associated Congress*, Palma de Malorca, Spain, July, 1985.

GRIGORIU, M.: "Expected Failure Time of Fiber Bundle Systems Subject to Gaussian Load Processes", Presented at the *Fifth International Conference on Structural Safety and Reliability*, ASCE, San Fransisco, 1989.

GUENARD, Y.F.: *Application of System Reliability Analysis to Offshore Structures*. Report No. RMS-1, Reliability of Marine Structures Program, Dept. of Civil Engineering (Formerly, Report No. 71, John A. Blume Earthquake Engineering Center), Stanford University, California, USA, 1984

GUERS, F., DOLINSKI, K., and RACKWITZ, R.: "Probability of Failure of Brittle Redundant Structural Systems in Time", *Structural Safety*, Vol. 5, pp. 169-185, 1988.

HARBITZ, A.: "Efficient and Accurate Probability of Failure Calculation by use of the Importance Sampling Technique", *Proceedings of the Fourth International Conference on Applications of Statistics and Probability in Soil and Structural Engineering*, Firenze, Italy, 1983.

HARDING, S.J. and BANON, H.: "Reliability of TLP Tethers Under Maximum and Minimum Lifetime Loads", *Proceedings of the 21st Offshore Technology Conference*, OTC Paper No. 5935, Houston, USA, May, 1989.

244

HARING, R.E., OLSEN, O.A. and JOHANSSON, P.I.: "Total Wave Force and Moment Vs. Design Practice", *Proceedings of the Specialty Conference, Civil Engineering in the Oceans IV*, ASCE, Volume II, September, 1979.

HAVER, S.: Lecture Notes for the course, *Ocean Waves and Wave Induced Response*, Department of Civil Engineering, Stanford University, Stanford, California, Spring Quarter, 1989.

HAVER, S. AND NYHUS, K.A.: "A Wave Climate Description for Long Term Response Calculations", *Proceedings of the Fifth International Offshore Mechanics and Arctic Engineering Symposium*, Vol. 4, ASME, 1986.

HEIDEMAN, J.C., OLSEN, O.A., and JOHANSSON, P.I.: "Local Wave Force Coefficients", *Proceedings of the Specialty Conference, Civil Engineering in the Oceans IV*, ASCE, Volume II, September, 1979.

HOHENBICHLER, M. and RACKWITZ, R.: "Improvement of Second-Order Reliability Estimates by Importance Sampling", *Journal of Engineering Mechanics*, ASCE, Vol. 114, No. 12, pp. 2195-2199, 1988.

HOHENBICHLER, M., GOLLWITZER, S., KRUSE, W., and RACKWITZ, R.: "New Light on First- and Second-Order Reliability Methods", *Structural Safety*, Vol. 4, pp. 267-284, 1987.

HOHENBICHLER, M. and RACKWITZ, R.: "Reliability of Parallel Systems under Imposed Uniform Strain", *Journal of Engineering Mechanics Division*, ASCE, Vol. 109, No. 3, pp. 896-907, June, 1983a.

HOHENBICHLER, M. and RACKWITZ, R.: "First-Order Concepts in System Reliability", *Structural Safety*, Vol. 1, pp. 177-188, 1983b.

HOHENBICHLER, M. and RACKWITZ, R.: "Non-Normal Dependent Vectors in Structural Reliability", *Journal of Engineering Mechanics Division*, ASCE, Vol. 107, No. 3, pp. 1127-1238, June, 1981.

HOLM, C. A.: *Reliability Analysis of Structural Systems Using Nonlinear Finite Element Methods*, Doctoral Thesis, Division of Structural Mechanics, The Norwegian Institute of Technology, Trondheim, Norway, 1990.

KARAMCHANDANI, A.: *New Methods in System Reliability*, Ph.D. Dissertation, Department of Civil Engineering, Stanford University, Stanford, California, USA, to be published in 1990.

KARAMCHANDANI, A., BJERAGER, P., and CORNELL, C.A.: "Methods to Estimate Parametric Sensitivity in Structural Reliability Analysis", *Probabilistic Engineering Mechanics*, ASCE, ed. P.D. Spanos, pp. 164-167, 1988.

KARAMCHANDANI, A.: *Structural System Reliability Analysis Methods*, Report No. 83, John A. Blume Earthquake Engineering Center, Stanford University, California, USA, 1987.

KARAMCHANDANI, A., GUENARD, Y.F., and ORTIZ, K.: *SHASYS a Software Package for Component and System Reliability Analysis*, Report No. 78, John A. Blume Earthquake Engineering Center, Stanford University, California, USA, 1986.

245

LARABEE, R.D. and CORNELL, C.A.: "Upcrossing Rate Solution for Load Combinations", *Journal of the Structural Division*, ASCE, Vol. 105, No. ST1, pp. 125-132, January, 1979.

LIN, H.-Z. and DER KIUREGHIAN, A.: "A Topology Variational Method for Reliability Analysis of Structural Systems", Presented at the *Fifth International Conference on Structural Safety and Reliability*, ASCE, San Fransisco, 1989.

LIU, P.-L. and DER KIUREGHIAN, A.: "Reliability of Geometrically Nonlinear Structures", *Probabilistic Engineering Mechanics*, ASCE, ed. P.D. Spanos, pp. 164-167, 1988.

LLOYD, J.R. and CLAWSON, W.C.: "Reserve and Residual Strength of Pile Founded Offshore Platforms", *Proceedings of an International Symposium, The Role of Design, Inspection, and Redundancy in Marine Structural Reliability*, National Academic Press, pp.157-196, November, 1983.

MADSEN, H.O.: "Reliability of Offshore Structures", Lecture Notes for the course, *Structural Reliability: Methods and Applications*, University of California, Berkeley, April 27-29, 1989.

MADSEN, H.O., KRENK, S., and LIND, N.C.: *Methods of Structural Safety*, Prentice-Hall, Inc., USA, 1986.

MARDIA, K.V.: *Statistics of Directional Data*, Academic Press, Inc., USA, 1972.

MARSHALL, P.: "Risk Evaluations for Offshore Structures", *Journal of the Structural Division*, ASCE, Vol. 95, No. ST12, Proc. Paper 6981, pp. 2907-2929, December, 1969.

MARSHALL, P. and BEA, R.G.: "Failure Modes of Offshore Platforms", *Proceedings of the First International Conference on the Behavior of Offshore Structures*, BOSS '76, The Norwegian Institute of Technology, Trondheim, Norway, 1976.

MELCHERS, R.E.: *Structural Reliability: Analysis and Prediction*, Ellis Horwood Series in Civil Engineering, Halsted Press, England, 1987.

MELCHERS, R.E. and TANG. L.K.: "Dominant Failure Modes in Stochastic Structural Systems", *Structural Safety*, Vol. 2, pp. 127-142, 1984.

MOSES, F.: *Development of Preliminary Load and Resistance Design Document for Fixed Offshore Platforms*, API-PRAC Project 85-22, Final Report to the American Petroleum Institute, Dallas, Texas, USA, 1986.

MOSES, F. and RASHEDI, M.R.: "The Application of System Reliability to Structural Safety", *Proceedings of the Fourth International Conference on Applications of Statistics and Probability in Soil and Structural Engineering*, Firenze, Italy, 1983.

MOSES, F. and YAO, J.T.P.: "Safety Evaluation of Building and Bridges", *Proceedings of the Symposium, on Structural Design, Inspection, and Redundancy*, Williamsburg, Virginia, USA, November, 1983.

246

MOSES, F.: *Guidelines for Calibrating API RP2A for Reliability Based Design*, API-PRAC Project 80-22, Final Report to the American Petroleum Institute, Dallas, Texas, USA, 1981.

MOSES, F. and STAHL, B.: "Reliability Analysis Format for Offshore Structures", *Proceedings of the 10th Offshore Technology Conference*, OTC Paper No. 3046, Houston, USA, May, 1978.

MUROTSU, Y., OKADA, H., IKEDA, Y., and MATSUZAKI, K.: "On the System Reliability of Semisubmersible Platforms", *Proceedings of the Third International Conference on Practical Design of Ships and Mobile Units*", PRADS '87, Trondheim, Norway, 1987.

MUROTSU, Y., OKADA, H., YONEZAWA, M., and KISHI, M.: "Identification of Stochastically Dominant Failure Modes in Frame Structures", *Proceedings of the Fourth International Conference on Applications of Statistics and Probability in Soil and Structural Engineering*, Firenze, Italy, 1983.

MUROTSU, Y., OKADA, H., YONEZAWA, M., and TAGUCHI, K.: "Reliability Assessment of Redundant Structures", *Proceedings of the Third International Conference on Structural Safety and Reliability*, ed. T. Moan and M. Shinozuka, Trondheim, Norway, June, 1981.

NORDAL, H., CORNELL, C.A., and KARAMCHANDANI, A.: "A Structural System Reliability Case Study of an Eight-leg Steel Jacket Offshore Production Platform", *Proceedings of the Marine Structural Reliability Symposium*, SNAME, USA, October, 1987.

OLUFSEN, A. and BEA, R.G.: "Loading Uncertainties In Extreme Waves", Presented at *the Fifth International Conference on Structural Safety and Reliability*, ASCE, San Fransisco, 1989.

PALIOU, C., SHINOZUKA, M., and CHEN, Y.-N.: "Reliability Analysis of Offshore Structures", *Proceedings of the Marine Structural Reliability Symposium*, SNAME, USA, pp. 143-157, October, 1987.

PROBAN-2: Users Manual, A.S Veritas Research, Norway, 1989.

RACKWITZ, R. and GOLLWITZER, S.: "On the Reliability of Daniels Systems", *Proceedings of the National Science Foundation Workshop on Research Needs for Application of System Reliability Concepts and Techniques in Structural Analysis, Design, and Optimization*, University of Colorado, Boulder, USA, September, 1988.

RASHEDI, M.R. and MOSES, F.: *Studies on Reliability of Structural Systems*, Report No. R-83-3, Department of Civil Engineering, Case Western Reserve University, Cleveland, Ohio, USA, 1983.

READ, W.W. and SOBEY, R.J.: "Phase Spectrum of Surface Gravity Waves", *Journal of Waterway, Port, Coastal, and Ocean Engineering*, ASCE, Vol. 113, No. 5, pp. 507-522, September, 1987.

247

ROSENBLATT, M.: "Remarks on a Multivariate Transformation", *The Annals of Mathematical Statistics*, Vol. 23, pp. 470-472, 1952.

SARPKAYA, T. and ISAACSON, M.: *Mechanics of Wave Forces on Offshore Structures*, Van Nostrand and Reinhold Company, USA, 1981.

SHINOZUKA, M. and ITAGAKI, H.: "On the Reliability of Redundant Structures", *Proceedings of the Fifth Reliability and Maintainability Conference, Annals of Reliability and Maintainability*, Vol. 5, Academic Press, New York, pp. 605-610, July, 1966.

SHINOZUKA, M.: "Basic Analysis of Structural Safety", *Journal of Structural Engineering*, ASCE, Vol. 109, No. 3, pp. 721-740, , 1983.

SIMONS, J.W. and POWELL, G.H.: *Solution Strategies for Statically Loaded Nonlinear Structures*, Report No. UCB/EERG - 82/22, Earthquake Engineering Research Center, College of Engineering, University of California, Berkeley, California, USA, 1982.

SPIDSOE, N., BRATHAUG, H.P., and SKJASTAD, O.: "Nonlinear Random Wave Loading on Fixed Offshore Platforms.", *Proceedings of the Offshore Technology Conference*, OTC Paper No. 5101, Houston, Texas, May, 1986.

STAHL, B and GEYER, J.F.: "Ultimate Strength Reliability of Tension Leg Platform Tendon Systems", *Proceedings of the 17th Offshore Technology Conference*, Houston, Texas, pp. 151-162, May, 1985.

STEWART, G., EFTHYMIOU, M., and VUGTS, J.H.: "Ultimate Strength and Integrity Assessment of Fixed Offshore Platforms", *Proceedings of the Fifth International Conference on the Behavior of Offshore Structures*, Vol. 3, BOSS '88, The Norwegian Institute of Technology, Trondheim, Norway, 1988.

THOFT-CHRISTENSEN, P. and BAKER, M.J.: *Structural Reliability Theory and its Application*, Springer-Verlag, West Germany, 1982.

THOFT-CHRISTENSEN, P. and MUROTSU, Y.: *Application of Structural Systems Reliability Theory*, Springer-Verlag, West Germany, 1986.

TORUM, A. and SKJELBREIA, J.E.: "Irregular Water Wave Kinematics", *Water Wave Kinematics* (Proceedings of the NATO ARW Conference, Molde, Norway, 1989), ed. A. Torum and O.T. Gudmestad, Kluwer Academic Publishers, 1989.

TVEDT, L.: "Second Order Reliability by an Exact Integral", *Proceedings of the 2nd. Working Conference on Reliability and Optimization of Structural Systems, IFIP*, London, Sept.1988. (Proceedings published by Springer-Verlag in their series called *'Lecture Notes in Engineering'*)

VENEZIANO, D., GRIGORIU, M., and CORNELL, C.A.: "Vector-Process Models for System Reliability", *Journal of Engineering Mechanics Division*, ASCE, Vol. 103, No. EM3, pp. 441-460, 1977.

VANMARCKE, E.H.: *Random Fields, Analysis and Synthesis*, The MIT Press, Massachusets Institute of Technology, Cambridge, Massachusetts, USA, 1984.

VANMARCKE, E.H.: "On the Distribution of the First-Passage Time for Normal Stationary Random Processes", *Journal of Applied Mechanics*, ASME, Vol. 42, pp. 215-220, March, 1975.

WEN, Y.K. and CHEN, H.-C.: *System Reliability under Time Varying Loads: I, Journal of the Engineering Mechanics*, ASCE, Vol. 115, No. 4, pp. 808-823, 1989.

WEN, Y.K. and CHEN, H.-C.: *System Reliability under Time Varying Loads: II, Journal of the Engineering Mechanics*, ASCE, Vol. 115, No. 4, pp. 823-839, 1989.

WEN, Y.K.: "Approximate Methods for Nonlinear Time-Variant Reliability Analysis", *Journal of Engineering Mechanics*, ASCE, Vol. 113, No. EM3, pp. 1826-1839, May, 1987.

WEN, Y.K. and CHEN, H.-C.: "On Fast Integration for Time Variant Structural Reliability", *Probabilistic Engineering Mechanics*, ASCE, Vol. 2, No. 3, pp. 156-162, 1987.

WEN, Y.K. and CHEN, H.-C.: *System Reliability under Multiple Hazards*, Report No. UILU-ENG-86-2007, Department of Civil Engineering, University of Illinois, Urbana-Champaign, USA,1986.

WEN, Y.K.: "Statistical Combination of Extreme Loads", *Journal of the Structural Division*, ASCE, Vol. 103, pp. 1079-1093, May, 1977.

WINTERSTEIN, S.R., DE, R.S., and BJERAGER, P.: "Correlated Non-Gaussian Models in Offshore Structural Reliability", Presented at the *Fifth International Conference on Structural Safety and Reliability*, ASCE, San Fransisco, 1989.

WINTERSTEIN, S.R.: *Moment-Based Hermite Models of Random Vibrations*, Report No. 219, Series R, Department of Structural Engineering, Technical University of Denmark, Lyngby, Denmark, 1987.

WINTERSTEIN, S.R. and CORNELL, C.A.: "Energy Fluctuation Scale and Diffusion Models", *Journal of Engineering Mechanics* , ASCE, Vol. 111, No. 2, February, 1985.

WIRSCHING, P.: "Fatigue Reliability for Offshore Structures", *Journal of Structural Engineering*, ASCE, Vol. 110, No. 10, October, 1984.

WU, Y.-L. and MOAN, T.: "A Structural System Reliability Analysis of Jacket Using an improved Truss Model", Presented at the *Fifth International Conference on Structural Safety and Reliability*, ASCE, San Fransisco, 1989.